The University Of Sheffield.

OPTIMISATION OF THE GEOMETRY OF THE DRILL BIT AND PROCESS PARAMETERS FOR CUTTING HYBRID COMPOSITE/METAL STRUCTURES IN NEW AIRCRAFTS

OZDEN ISBILIR

Thesis submitted to the University of Sheffield in partial fulfillment of the requirements for the degree of doctor of philosophy

DEPARTMENT OF MECHANICAL ENGINEERING

THE UNIVERSITY OF SHEFFIELD

OCTOBER 2012

The University Of Sheffield.

OPTIMISATION OF THE GEOMETRY OF THE DRILL BIT AND PROCESS PARAMETERS FOR CUTTING HYBRID COMPOSITE/METAL STRUCTURES IN NEW AIRCRAFTS

O ISBILIR

Thesis submitted to the University of Sheffield in partial fulfillment of the requirements for the degree of doctor of philosophy

DEPARTMENT OF MECHANICAL ENGINEERING

THE UNIVERSITY OF SHEFFIELD

OCTOBER 2012

Abstract

Owing to their desirable strength-to-weight characteristics, carbon fibre reinforced polymer composites have been favorite materials for structural applications in different industries such as aerospace, transport, sports and energy. They provide a weight reduction in whole structure and consequently decrease fuel consumption. The use of lightweight materials such as titanium and its alloys in modern aircrafts has also increased significantly in the last couple of decades. Titanium and its alloys offer high strength/weight ratio, high compressive and tensile strength at high temperatures, low density, excellent corrosion resistance, exceptional erosion resistance, superior fatigue resistance and relatively low modulus of elasticity. Although composite/metal hybrid structures are increasingly used in airframes nowadays, number of studies regarding drilling of composite/metal stacks is very limited. During drilling of multilayer materials different problems may arise due to very different attributes of these materials. Machining conditions of drilling such structures play an important role on tool wear, quality of holes and cost of machining.

The research work in this thesis is aimed to investigate drilling of CFRP/Ti6Al4V hybrid structure and to optimize process parameters and drill geometry. The research work consist complete experimental study including drilling tests, in-situ and post measurements and related analysis; and finite element analysis including fully 3-D finite element models. The experimental investigations focused on drilling outputs such as thrust force, torque, delamination, burr formation, surface roughness and tool wear. An algorithm was developed to analyse drilling induced delamination quantitatively based on the images. In the numerical analysis, novel 3-D finite element models of drilling of CFRP, Ti6Al4V and CFRP/Ti6Al4V hybrid structure were developed with the use of 3-D complex drill geometries. A user defined subroutine was developed to model material and failure behaviour of CFRP. The effects of process parameters on drilling outputs have been investigated and compared with the experimental results. The influences of drill bit geometries have been simulated in this study.

DEDICATED TO MY FAMILY

Acknowledgement

"Learn from yesterday, live for today, hope for tomorrow.
The important thing is not to stop questioning"

-Albert Einstein

Hopefully the end…, but not doing research! It is difficult to believe that four years in Ph.D. have flown away so fast. Now it is the time to pack everything and also brings the memory back in my life in the UK. It is difficult to express my feelings right now as they are complicated. After having a long and tough time, I feel like a free bird in the sky after finishing my research. I am quite happy to finalize my study and going back to my country for my further life and research. However, at the same time I feel unhappy since Sheffield has become my second home and difficult to leave. I appreciated quite much and would like to express my kindest gratitude to all who have been supporting me; my family, my friends, colleagues and well-wishers during the period here. I am not good to express my feelings, but I will try to do my best with few sentences as all of them are fully deserved by heart.

First off all, I would like express my deep gratitude to my supervisor Dr. Elaheh Ghassemieh for giving me this wonderful opportunity to carry out my research at the Department of Mechanical Engineering in the University of Sheffield. I would like to thank her for everlasting interest, valuable guidance and endless encouragement throughout the project as being my main supervisor. I deeply acknowledge your contribution to my academic progress during my research.

I would like to acknowledge greatly the Ministry of National Education of the Republic of Turkey for financially supporting my whole Ph.D. study in the UK, including my tuition fees, monthly stipend and all other expenses. I am grateful to Airbus for the provision of materials in experiments and to Advanced Manufacturing Research Centre (AMRC) at University of Sheffield for the access to the machining facilities.

I am thankful to my dear friends Mr. Rahul Murali Cadambi, Mr. Akin Atas and Mr. Emin Yusuf Avan for being a good support throughout the whole period of research. I appreciated for your kind help and helpful discussions provided at all times here. Thanks to Rahul for his warm friendship and spending wonderful times in conference visits in Belfast and Cambridge. I also wish to thank all the members from Department of Mechanical Engineering and all my friends in other departments from the University of Sheffield.

Many thanks to my dear friends, namely Ms. Hatice Karpuzoglu and Mrs. Turkan Cakici for your support by accepting to be my guarantor at the beginning of my funding. I started to this wonderful experience with your help. I would like to present my deepest gratitude to my friend Mr. Abdullah Tazebay for your invaluable help in those days.

I would like to thank and dedicate this whole work to my great family. Their motivation, support, care, endless love and affection at all times have made me able to reach this stage of research. I especially would like to thank my mother for endless support and love since the first day of my life. Last but not least, I would like to share my deepest and warmest feelings with my dearest wife Edyta. Thanks a lot for your great support, care, motivation and love here. Thanks for being with me patiently all these years of my research.

OZDEN ISBILIR

Table of Contents

List of Figures

List of Tables

Nomenclature

Abbreviation	Definiton
CFRP	Carbon Fibre Reinforced Composite
GFRP	Glass Fibre Reinforced Composite
UD	Unidirectional
FEM	Finite Element Model
FEA	Finite Element Analysis
CZE	Cohesive Zone Element
VCE	Virtual Ccrack Extension
HSS	High Speed Steel
HSS-Co	High Speed Steel-Cobalt
PCD	Polycrystalline Diamond
WC	Tungsten Carbide
BUE	Built-up-edge
CBN	Cubic Boron Nitride

Symbol	Unit	Definition
A	MPa	Initial Yield Strength at Room Temperature
A_{nom}	mm^2	Nominal Hole Area
A_{max}	mm^2	Damaged Area (Including Hole Area)
B	-	Hardening Coefficient
C	-	Strain Rate Coefficient
C_D		Stiffness Matrix After Damage Initiation in Composite
C_m	-	Stiffness Matrix
C_p	(J/kg.°K)	Specific Heat Capacity
D	-	Damage Variable
d_{fb}	-	Fibre Damage Variable
d_m	-	Matrix Damage Variable

D_{max}	Mm	Maximum Damage Diameter
D_{nom}	mm	Nominal Hole Diameter
d_S	-	Shear Damage Variable
$d_1 - d_5$	-	Johnson-Cook Failure Model Parameters
E	GPa	Young's Modulus
F	mm/min	Feed Rate
F_A	-	Alternative Delamination Factor
F_D	-	Conventional Delamination Factor
F_{fb}^T	-	Hashin Failure Criterion in Fibre Tension Mode
F_{fb}^C	-	Hashin Failure Criterion in Fibre Compression Mode
F_m^T	-	Hashin Failure Criterion in Matrix Tension Mode
F_m^C	-	Hashin Failure Criterion in Matrix Compression Mode
G	GPa	Shear Modulus of an Isotropic Material
$G_{12,13,23}$	GPa	Shear Moduli Components of an Orthotropic Material
$G_{n,s,t}$	N/mm	Energy Release Rates in Normal and Shear Directions
$G_{n,s,t}^C$	N/mm	Critical Energy Release Rate in Normal and Shear Directions
K	(W/m.°K)	Thermal Conductivity
$K_{nn,ss,tt}$		Traction-Separation Stiffness Coefficients in Normal and Shear Directions
K_B	mm	Crater Wear
L_C	mm	The Characteristic Length of an Element
n	-	Strain Hardening Coefficient
m	-	Thermal Softening Coefficient
P	MPa	Pressure Stress
S	rpm	Spindle Speed
T	K	The Current Temperature
T_m	K	The Melting Temperature
T_{rf}	K	The Reference Environment

T_0	mm	Nominal thickness of a Ply
V_B	mm	Flank Wear
W_D	-	Failure Initiation Criterion
A	-	Energy Release Rate Coefficient in normal Direction
B	-	Energy Release Rate Coefficient in 1st Shear Direction
Γ	-	Energy Release Rate Coefficient in 2nd Shear Direction
Δ	mm	Separation of Cohesive Surfaces
ε	-	Strain of an Isotropic Material
$\varepsilon_{11,22,33}$	-	Strain Components of Orthotropic Material in Normal and Transverse Directions
$\varepsilon_{n,s,t}$	-	Strain of Cohesive Elements in Normal and Shear Directions
$\dot{\bar{\varepsilon}}$,	s^{-1}	The Equivalent Plastic Strain Rate
$\dot{\bar{\varepsilon}}_0$	s^{-1}	The Reference Strain Rate
$\bar{\varepsilon}^{pl}$	-	Equivalent Plastic Strain
$\bar{\varepsilon}^{pl}_f$	-	Equivalent Plastic Strain at Failure
P	(kg/m3)	Density
Σ	MPa	Flow Stress Prior to Damage Initiation
σ_u	MPa	Ultimate Strength
σ_y	MPa	Yield Strength
$\bar{\sigma}$	MPa	Effective Flow Stress after Damage Initiation
$\sigma_{11,22,33}$	MPa	Stress Components of an Orthotropic Material in Normal and Transverse Directions
$\sigma_{11}^{f,T}$	MPa	Tensile Strength in Fibre Direction
$\sigma_{11}^{f,C}$	MPa	Compressive Strength in Fibre Direction
$\sigma_{22}^{f,T}$	MPa	Tensile Strength in Transverse Direction
$\sigma_{22}^{f,C}$	MPa	Compressive Strength in Transverse Direction

$\sigma_{33}^{f,T}$	MPa	Tensile Strength in Normal Direction
$\sigma_{33}^{f,C}$	MPa	Compressive Strength in Normal Direction
$\sigma_{n,s,t}$	MPa	Stress of Cohesive Elements in Normal and Shear Directions
$\sigma^{0}{}_{n,s,t}$	MPa	Strength of Cohesive Elements in Normal and Shear Directions
τ_{12}^{f}	MPa	In-Plane Shear Strength
$\tau_{13,23}^{f}$	MPa	Out-Of-Plane Shear Strength
υ	-	Poisson Ratio
μ	-	Friction Coefficient
$\bar{u}_{f}^{pl}$	mm	The Equivalent Plastic Displacement at Failure

List of Publications

List of Journal Papers and Conference Proceedings

1. Ozden ISBILIR and Elaheh GHASSEMIEH, "Delamination and wear in drilling of carbon-fiber reinforced plastic composites using multilayer TiAlN/TiN PVD-coated tungsten carbide tools", Journal of Reinforced Plastics and Composites 31 (10) 2012 p:717-727

2. Ozden ISBILIR and Elaheh GHASSEMIEH, "Finite Element Analysis of Drilling of Carbon Fibre Reinforced Composites", Applied Composite Materials, 19 (3-4) 2012, p. 637-656

3. Ozden ISBILIR and Elaheh GHASSEMIEH, "Finite Element Analysis of Drilling of Titanium Alloy", Procedia Engineering, 10 2011, p: 1877-1882

4. Ozden ISBILIR and Elaheh GHASSEMIEH, "Finite Element Simulation of Drilling of Carbon Fibre Reinforced Composite/Titanium Stack", Proceeding of the 17th UK National Conference on Computational Mechanics in Engineering, 2009

5. Ozden Isbilir, Elaheh Ghassemieh, "Evaluation of drilling process in Ti6Al4V using 3D FE simulation International Journal of Machining and Machinability of Materials (IJMMM), 2012, Proof accepted and in Press.

6. Ozden ISBILIR and Elaheh GHASSEMIEH, "Numerical investigation of the effects of drill geometry on drilling induced delamination of carbon fiber reinforced composites", Composites Part A, 2012, Under Review

7. Ozden ISBILIR and Elaheh GHASSEMIEH, "3D numerical modelling of drilling of carbon fiber reinforced plastic composites", The Journal of Composite Materials, 2012, Under Review

8. Ozden ISBILIR and Elaheh GHASSEMIEH, "Tool life and quality of hole in drilling of Ti6Al4V using TiAlN coated tungsten carbide drill", International Journal of Industrial Engineering & Production Research, 2012, Under Review

9. Ozden ISBILIR and Elaheh GHASSEMIEH, "Comparative study of tool life and hole quality in drilling of CFRP/titanium stack using coated carbide drill", Machining Science and Technology, 2011, Under Review

List of Conference Presentations

1. Ozden ISBILIR and Elaheh GHASSEMIEH, "Finite Element Analysis of Drilling of Titanium Alloy", 11th International Conference on the Mechanical Behaviour of Materials, 5-9 June 2011, Milano, Italy, Oral Presentation

2. Ozden ISBILIR and Elaheh GHASSEMIEH, "Finite Element Analysis of Drilling of Aerospace Hybrid Structures", Deformation and Fracture of Composites (DFC-11) & Structural Integrity and Multi-scale Modelling (SI-5), 12-15 April 2011, Queens College, Cambridge, Oral Presentation

3. Ozden ISBILIR and Elaheh GHASSEMIEH, "Effect of Tool Wear on Hole Quality in the Drilling of Carbon Fibre Reinforced Composites, International Conference on Manufacturing of Advanced Composites (ICMAC 2011), 22-24 March 2011, BELFAST, NORTH IRELAND, Oral Presentation

4. Ozden ISBILIR and Elaheh GHASSEMIEH, "Finite Element Analysis of Delamination in the Drilling of Carbon Fibre Reinforced Plastic Composites", International Conference on Manufacturing of Advanced Composites (ICMAC 2011), 22-24 March 2011, BELFAST, NORTH IRELAND, Poster Presentation

5. Ozden ISBILIR and Elaheh GHASSEMIEH, "Finite Element Simulation of Drilling of Carbon Fibre Reinforced Composite/Titanium Stack", The 17th UK National Conference on Computational Mechanics in Engineering, 6th-8th April 2009, Nottingham, Oral Presentation

Chapter 1

General Introduction

Owing to their desirable strength-to-weight characteristics, carbon fibre reinforced polymer (CFRP) composites have been favorite materials for structural applications in different industries such as aerospace, transport, sports and energy. They provide a weight reduction in whole structure and consequently decrease fuel consumption. The use of lightweight materials such as titanium, aluminium and their alloys in modern aircrafts has also increased significantly in the last couple of decades. Titanium and its alloys offer high strength/weight ratio, high compressive and tensile strength at high temperatures, low density, excellent corrosion resistance, exceptional erosion resistance, superior fatigue resistance and low modulus of elasticity [1-3]. Particularly the use of titanium and its alloys are widespread in new aircrafts. For example, titanium is the primary structure of F-22 Fighter and Boeing 787 by 39% and 14% in weight, respectively [4]. CFRPs are used increasingly in form of stack with metals such as aluminium and/or titanium to optimize the weight/strength ratio. Assembly of these materials generally requires high number of rivets or bolts [5].

Composites components are produced to near-net shape, however machining operations are often needed for assembly requirements. Among several machining processes, drilling is one of the most common methods due to the need for holes to assemble different components with rivets or bolts. Despite the fact that composite materials, particularly carbon fibre reinforced plastics (CFRP) have attractive physical and mechanical properties, machining of these materials is complex, challenging and considerably distinct from cutting metals. This is mainly due to the heterogeneous structure which involves extremely abrasive reinforcement and heat sensitive matrix particularly in plastic composites [6]. Due to the structure of CFRPs, it is difficult to reach a desirable hole quality and to provide a desirable tool life in

drilling these materials. Several types of damages can be introduced during drilling such as delamination, fibre pull-out, matrix softening/melting, stress concentration, micro cracks and excessive tool wear. Studies [7-10] show that these defects influence service life of composites. Different researchers [11-15] indicated that most of these problems occur due to selection of non optimized process parameters, tool geometry and cutting tool material.

Titanium and its alloys have excellent physical and mechanical properties and it makes them one of the most attractive materials for aerospace design engineers. However, they are difficult to machine. Tool wear mechanisms in drilling of titanium are totally different from the wear mechanism present in drilling of CFRP. One of the most important reasons is low thermal conductivity of titanium. Concentrated heat at tool-workpiece interface could increase temperature of cutting edges over 1000 ºC easily in dry conditions. Consequently this high cutting temperature increases the wear rate and decreases the tool life substantially [16]. In addition, titanium has strong affinity to many tool materials at elevated temperatures. Chemically active workpiece can react with tool materials very rapidly during machining process which will result in chipping, accelerated tool wear and premature tool life [17]. Higher chemical affinity to tool materials can also lead to microwelding, called built-up-edge (BUE), on cutting tool throughout cutting process. This mechanism may result in a sudden tool failure. Furthermore, titanium maintains its hardness and strength at high temperatures, thus cutting forces and stresses on cutting edges will be higher due to insignificant softening of this material. This can cause high tool wear. Tool wear in drilling of titanium alloy is also very sensitive to the drilling process parameters [18]. Increasing feed rate and/or cutting speed increases tool wear. A small change in cutting speed could cause a very large change in the tool wear rate [19]. Another difficulty in drilling of titanium alloys is producing holes without burrs. It is estimated that 30% of machining cost is due to deburring operations in manufacturing of titanium components [17]. Due to these difficulties, machining of titanium is difficult and the material removal rate is low. Although drilling of titanium has been widely utilized in industry, research publications are limited on this subject.

Although composite/metal stacks are increasingly used in airframes nowadays, number of studies regarding drilling of composite/metal stacks is very limited. During drilling of multi-layer materials different problems may arise due to very different attributes of these materials. Machining conditions of drilling such structures plays an important role on tool wear and quality of holes. Different machining properties are required for different optimal machining conditions of each material [20-21]. Having materials with different modulus of elasticity will cause varied deformation which results in difficulties in drilling of holes with small diameter tolerances. Excessive heating caused by drilling of titanium induces a number of holes quality problems in CFRP such as softening of matrix and damaged surface roughness due to hot titanium chips [20-21]. In machining of multi-layer materials, wear of cutting tools is more complicated compared to machining of single material. Having different nature of wear mechanisms can accelerate the wear rate of the cutting tool [20-21].

1.1 Research Motivation

The objective of this research is to investigate the drilling mechanisms of carbon fibre reinforced composites and titanium alloy separately and together in a stack form to overcome the technical difficulties mentioned above and to achieve better machinability with the use of experimental and numerical technologies. Increasing the productivity and minimizing the workpiece defects are the main purpose of the study. For this reason both experimental and numerical approaches are utilized in this study. Particularly, FE analysis of drilling of CFRP and CFRP/metal stacks has not been studied extensively, so the possible advantages become one of the research goals of this research. The research will be pursued in the following directions:

Experimental investigation of drilling of CFRP: to investigate effects of drilling parameters on drilling outputs including thrust force, torque, delamination, tool wear, surface roughness and effect of tool wear on thrust force, torque, delamination and surface roughness by selecting appropriate drill geometry and drilling conditions.

Experimental investigation of drilling of Ti-6Al-4V: to investigate effects of drilling parameters on drilling outputs including thrust force, torque, burr formation, tool wear, surface roughness and effect of tool wear on thrust force, torque, burr formation and surface roughness by selecting appropriate drill geometry and drilling conditions.

Experimental investigation of drilling of CFRP/Ti-6Al-4V: to investigate effects of drilling parameters on drilling outputs including thrust force, torque, delamination, burr formation tool wear, surface roughness and effect of tool wear on thrust force, torque, delamination, burr formation and surface roughness by selecting appropriate drill geometry and drilling conditions based on the results of drilling of CFRP and Ti-6Al-4V separately.

Finite element modeling of drilling process of CFRP: to simulate and validate drilling process of CFRP by using Lagrangian FE codes by utilisation of a 3-D complex tool geometry, to investigate the effects of cutting parameters on the drilling outputs and to optimize drill geometry by using FE analysis.

Finite element modeling of drilling process of Ti-6Al-4V: to simulate and validate drilling process of Ti-6Al-4V by using Lagrangian FE codes with the use of 3-D complex drill geometry, to investigate the effects of cutting parameters on the drilling outputs and to optimize drill geometry by using FE analysis.

Finite element modeling of drilling process of CFRP/Ti-6Al-4V: to simulate and validate drilling process of CFRP/Ti-6Al-4V by using Lagrangian FE codes with the use of 3-D complex drill geometry, to investigate the effects of cutting parameters on the drilling outputs and to optimize drill geometry by using FE analysis.

1.2 Outline of Thesis

The research work described in this thesis comprises of drilling experiments of CFRP, Ti-6Al-4V, CFRP/Ti-6Al-4V stack; characterisation and measurements of workpiece and tool defects; a novel 3-D finite element analysis of drilling CFRP, Ti-6Al-4V, CFRP/Ti-6Al-4V including 3-D complex tool geometry and 3-D material failure models; and optimisation of process

parameters and tool geometry to minimize workpiece defects and increase productivity.

Chapter 2 presents a brief literature survey on composites and titanium alloys. Brief information on advantages, limitation and applications of these materials is presented in this chapter. A detailed review on machining and drilling of laminated fibre reinforced composites and titanium alloy and their alloy has been addressed. Machinability of these materials, cutting mechanisms, workpiece defects including delamination and burr formation and tool defects are discussed in detail in this chapter.

Chapter 3 outlines the details of experimental work carried out in this research. Details on the workpiece and tool materials used for in this research are described in detail. Details of the conditions of experimental drilling tests, in-situ and off-line measurements and characterisations are outlined in this chapter. The experimental methodology used in this research is given detail in this chapter.

Chapter 4 outlines the details of numerical methodology in this research. The components of numerical models; stress analysis, progressive failure analysis, material degradation rules are explained in a framework in for CFRP and Ti-6Al-4V. The meso-level modeling of CFRP is performed for intra-laminar and inter-laminar level to model workpiece defect.

Chapter 5 draws the details of finite elements analysis of drilling of the materials. The entire finite element model of drilling including type of analysis and solution, physical and geometrical details of workpiece and cutting tools, mesh attributes, boundary and loading conditions are introduced. The codes of constitutive and failure models of materials outlined in numerical methodology in Chapter 4 are utilized in finite element models.

Chapter 6 discusses drilling of laminated carbon fibre reinforced composites carried out experimentally and performed numerically. To understand machinability and increase productivity, the effects of process parameters on drilling outputs are outlined by experimentally and numerically. Brief information on some of the literature survey is addressed. It gives an insight to possible mechanisms in workpiece and tool defects. Based on the

success of FE analysis, the performances of different tool geometries on drilling of CFRP are simulated. Two different numerical approaches are compared and the advantages of the novel FE models are shown.

Chapter 7 consists of the results of the numerical and experimental analysis of drilling of Ti-6Al-4V. The influences of process parameters on thrust force, torque, burr formation, and surface roughness are discussed. Some information on the literature is addressed. Some of the insight into experimental studies carried out on the influences on tool wear on thrust force, torque, burr formation and surface roughness are given. The performance of step drill geometries with various stage ratios are investigated in FE analysis. The advantages of FE models are shown and possible difficulties regarding to the tool wear and chip formation has been discussed.

Chapter 8 discusses the results of the analysis of drilling of CFRP/Ti-6Al-4V. A novel FE analysis of drilling of CFRP/Ti-6Al-4V stack is debated in this chapter. The chapter gives some of the insight into studies carried out experimentally and numerically for both materials. The effects of cutting parameters on various outputs are investigated. Detailed comparisons are carried out with the results outlined in Chapter 6 and 7. Similar to the drilling of CFRP and titanium alloy in previous chapters, the influences of step drill on drilling of materials are investigated via finite element analysis.

Chapter 2

Literature Review

2.1 Composite Materials

Composite materials are composed of two or more distinct constituents separated by a distinct interface. In order to be called a composite material, the material must satisfy the following criteria:

- It must be composed of two or more physically and/or chemically distinct constituents.

- The constituents must be present in reasonable proportions.

- The characteristics of the new material must not be determined completely by any of the constituents alone.

The matrix is the constituent which is continuous and generally present in greater quantity in the composite material. The main objective of the matrix is to enclose and bind the reinforcement, protect it from environment and provide an effective load distribution to the reinforcement. In the majority of the applications, the properties of the matrix are weaker comparing to reinforcement constituent.

The reinforcement is the second constituent in a composite material and embedded in the matrix. It is generally stronger and stiffer material than the matrix. The main purpose of the reinforcement is to carry the load. The properties of the reinforcement and the effectiveness of the composite material are dependent on the quantity, shape and the type of the reinforcement

material. The reinforcement material can be metallic, ceramic, or organic. The commonly used reinforcements in polymer matrix composites are glass, carbon, or aramid fibres. In addition to matrix and reinforcement there can be some other materials such as fillers and additives for different purposes.

Composites can be categorized according to matrix and reinforcement. The first classification can be made according to the matrix material; *polymer matrix, metal matrix and ceramic matrix based composites*. The second classification can be made according to the shape of the reinforcement form; *particulate, discontinuous fibre, and continuous fibre reinforced composites*.

2.1.1 Advantages and Limitations

The properties of composite materials, such as stiffness or strength, may not be greatly different from monolithic materials. However, as the specific strength (strength-to-weight ratio) and specific stiffness (stiffness-to-weight ratio) are considered, composite materials generally outperform those materials [22]. Significant improvements in strength and stiffness can be obtained in the fibre reinforcement direction. In addition to improving structural properties, composites have greater properties in corrosion resistance, fatigue resistance, thermal insulation, conductivity, and acoustic insulation than traditional metals [23-24]. Composite materials are generally tailored; therefore designing with composite material may result in a reduction in the complexity of tooling and assembly comparing to traditional materials. The significant weight reduction in structural parts would lead remarkable fall in the service and operation costs.

Advanced composite materials are superior to traditional metals; however there are disadvantages of these materials as well. Although the complexity of tooling and assembly might be simple, the manufacturing costs are higher than metals. The high costs of constituent materials, lack of high

productivity and strong dependency on skilled labour can be the prominent reasons. Moreover material data and analysis tools are also limited due to being relatively new and complex material comparing to traditional engineering materials. Storage of these materials is also required extra care.

2.1.2 Applications in Aerospace & Aircraft Industries

Each industry seeks desirable features from materials that the engineering parts are required. Composite materials are known to be able to satisfy multiple requirements in part design and material optimisation. Particularly carbon fibre reinforced polymer composites have proven to be flexible and adaptable material for many applications, including aerospace, aircraft, automotive, marine, construction, and sports industries. For instance, high specific strength and high specific stiffness are required under wide range of structural and thermal loads. Carbon reinforced polymer composites generally offer high specific strength and high specific stiffness which makes them attractive for aircraft industry. A negative coefficient of thermal expansion of carbon fibres takes attention of designers in aerospace industry where the structures are subjected to wide range of temperature [25].

Material performance is one of the major criteria in military aircrafts therefore composite materials have been used extensively even though the high material costs. Carbon fibre reinforced polymer composites have been used on its own or together with metals in the primary structures as well as secondary structures of military aircrafts such as wings, stabilizers, radomes, rudders and various doors [22-23, 26-27].

After the applications and success of composites in military aircrafts, the civil aircraft industry realized the importance of composite materials. Although the cost analysis is a major factor as well as performance in the commercial

aircrafts, the utilisation of composites components has been reached 50% of total weight of new Boeing aeroplane, 787 Dreamliner [28-29] . Various interior components, doors, radomes, wing and stabilizer components, tail and elevator panels and entire fuselage of aeroplane are produced from different composite materials recently [22, 27].

2.2 Titanium Alloys

Titanium exists in the earth about 0.6 % and it is fourth most abundant metal after aluminum, iron, and magnesium. Titanium is a relatively lightweight, corrosion resistant structural material. Pure titanium can be strengthened drastically by alloying and heat treatment in some of its alloys. Titanium and its alloys advantages can be listed as good strength to weight ratio, relatively low density, low coefficient of thermal expansion, low coefficient of thermal conductivity, good corrosion resistance, good toughness, low heat treating temperature for hardening and ability to retain its hardness and strength at high temperatures. Not surprisingly, these properties depend on the alloy and heat treatment.

Ti-6Al-4V is one of titanium alloy which combines excellent properties and good producibility that makes it the most widely used titanium alloy. Ti-6Al-4V is a alpha-beta titanium alloy and contain both alpha and beta phases at room temperature. It can typically used up to 400-500 ˚C and mechanical properties are retained without significant loss. Ti-6Al-4V can be also heat treated [30].

2.2.1 Advantages and Disadvantages

As mentioned, titanium and its alloys have superior properties such as high strength to weight ratio, high compressive and tensile strength, relatively low density, high fatigue resistance in air and seawater, and exceptional corrosion resistance [18-19, 31-32]. High specific strength, good fatigue resistance and creep life, and good fracture toughness make titanium and its alloys a must-have material for aerospace applications. Titanium's corrosion

resistance is based on the formation of a stable, protective oxide layer. This behaviour makes an advantage for various applications including chemical processing and surgical implants.

However, Ti has been classified as difficult-to-machine material due to some of these properties [19]. Among these reasons thermal conductivity is one of the major. Since the workpiece cannot remove the generated heat in machining, the heat tends to concentrate on the cutting tool and causes excessive cutting temperatures [18]. This would result in accelerated tool wear and consequently short tool life. Another disadvantage of titanium is its strong affinity to many tool materials [17, 32]. This would cause to diffusion and built-up-edge and lead to increase in wear rate. Moreover, titanium and its alloys generally maintain their hardness and strength at high temperatures, which required high cutting forces and energy, thus reducing their machinability [18]. This can lead to excessive tool wear.

2.1.1 Applications

The primary application of titanium and its alloys takes place in the aerospace industry. The usage of Ti is widespread in most military and commercial aircrafts. For example, titanium is the primary structure of F-22 Fighter and Boeing 787 by 39% and 14% in weight, respectively [33]. Ti is also used for many parts in jet engine components, such as blades, discs, rotors, casings, bolts; and for many structural and non-structural applications in aircraft including wing boxes, fuselage frames, brake components, gear beams, bolts, floor support structure, pipes, clips and brackets [30, 34].

In addition to aerospace industry, there are many application areas of titanium and its alloys. Chemical and petrochemical processing industries, paper industry, marine industry and energy industry can be examples of titanium applications due to corrosion resistance [18, 30-31, 35]. Vessels, pumps, fractionation columns, storage tanks in chemical industry, offshore oil platforms components, submarine components are made from titanium alloys.

Biomedical applications take advantages of commercially pure titanium's inertness and resistance to corrosion in the human body [30, 36-37]. Implantable

pumps and components for artificial hearts, hip and knee implants can be some examples of these applications.

Due to various specifications, titanium and its alloys are also used in machinery industries such as coating on cutting tools, tubes and control instruments [30].

2.3 Drilling of Composites

Although composite components are produced to near-net shape, machining is often needed to fulfil tolerance requirements for the assembly needs. Among machining processes, drilling is one of the most frequently used to make holes for assemblies of different parts with screws, rivets and bolts [38]. Several non-traditional drilling applications, such as laser-beam [39-42], water-jet [43-44], ultrasonic [45-47], and electrical discharge machining [48], have been reported for the drilling of composites. Nevertheless, conventional drilling continues to be used widely for practical purposes. To ensure high strength and load capacity in the assemblies, damaged-free and precise holes must be obtained.

Some characteristics of composite laminates such as non-homogeneity, anisotropy, highly abrasive and hard reinforced fibres, and coexistence of hard abrasive fibres with soft matrix, make composites components difficult to machine [24, 49]. The most frequent drilling induced defects are delamination, fibre pull-out, inter-laminar cracking or thermal damages in addition to other minor damages [50-52]. These damages can affect not only the load carrying capacity of laminated parts but also strength and stiffness, fatigue life and long term performance of the composite structure, thus reliability [53-54]. Rapid tool wear can be a significant factor on the extent of damage due to the very abrasive fibres [55]. Moreover, it increases the number of tool changes which affects the production cycle and the final cost.

Several investigations have been carried out to understand drilling of composite materials better. This subsection will review mechanical drilling processes of composites. It consists various aspects, namely cutting forces, tool

damage, hole quality and numerical approaches by taking into account of process parameters, tool geometry, tool material and coolant.

2.3.1 Cutting Forces

Thrust force and torque are one of the important data in drilling operations therefore they have been subject matter of a number investigation in drilling of composite materials. The relations between machining parameters, cutting tool geometry, wear, delamination and thrust force and torque have been studied by a number of researchers and summarized below.

The induced thrust force and torque throughout drilling of laminated composites depend on machining parameters, namely cutting speed or spindle speed, feed rate. Chen [56] investigated the cutting forces in drilling of composite and stated that damage can be avoided by the proper selections of tool geometry and cutting parameters.

Most of the researchers found that the influence of feed rate on the thrust force and torque is dominant in drilling of composites whereas effect of spindle speed on the same outputs is unnoticeable [13]. The higher feed rate causes greater amount of thrust force and torque. El-Sonbaty et al [57] studied the drilling of GFRP and noticed that the effect of cutting speed on thrust force is negligible, however torque increased with the increasing cutting speed. However, in another study a slight decrease in thrust force and torque has been observed with the increased cutting speed due to higher temperatures produced by the increased heat generation in drilling of composite [58].

Drill geometry is another factor which affects induced thrust force and torque in drilling of composites. The effect of the drill diameter on thrust force and torque was investigated in drilling of GFRP [57, 59]. Results showed that thrust force and torque increased with drill diameter due to the increase in the shear area. Some investigators observed that thrust force increased significantly with the increase in point angle in drilling of composites [56, 60]. The effect of special drill geometry on cutting forces has been investigated in drilling of composites [61-62]. The authors suggested special drill bits to obtain lower thrust force during drilling of CFRP and GFRP.

The effects of wear via number of drilled holes on thrust force and torque were investigated in drilling of composites. A remarkable increase has been observed in cutting forces with increased wear [63-68]. It was also found that the rate of increase in thrust force was higher at the early stages of tool life comparing to later stages.

The extent of delamination is related to thrust force in drilling of laminated composites. Therefore thrust force is a key index to assess machinability of composites [69]. A direct correlation has been observed between thrust force and delamination, therefore solutions which can decrease thrust force have been addressed for reduced delamination damage in drilling of composites [65, 69-70]. Among these optimized geometry and process parameters, vibration assisted drilling and high speed drilling can given as effective ways to reduce thrust force noticeably.

In another experimental study, effect of pre-drilled hole was investigated on thrust force in drilling of GFRP [71]. The authors concluded that thrust force was significantly reduced when the pre-drilled hole size was 40% and above of the final hole size.

2.3.2 Hole Quality

Tight dimensional and geometric tolerances have been required in composite structural parts nevertheless it is not easy to achieve these tolerance due to the nature of composite materials.

Delamination is an inter-laminar type of damage and can be induced in drilling operation. Delamination has been recognized as a major damage in composite structures since it can reduce load carrying capacity, bearing strength, structural integrity and potential damage of long term performance of the composite parts with reduced fatigue life [7, 53-54, 58, 72-76]. It has been reported that delamination is responsible for approximately 60% of all rejections of composite components in the aircraft industry [58, 70]

Experimental observations have indicated that delamination can occur both at the entrance side and at the exit side of the hole in drilling of composites [52, 58, 61, 70, 73-74, 77-86]. If the induced thrust force is greater than the

bonding strength between the adjacent laminas, the delamination can take place. In practice, it was observed that the exit delamination is more severe than the entrance delamination [28, 58, 66, 69].

The effects of machining process parameters on induced delamination have been investigated by a number of researchers. Most of the investigators stated that feed rate is the dominant factor on delamination in drilling of composites [13, 58, 69, 72, 77, 87-95]. It was observed that drilling induced delamination increases with the increased feed rate which attributes to the increase in thrust force. Different correlations have been observed between the cutting speed and delamination. Delamination has increased with the cutting speed in drilling of composite [13, 77, 88, 90, 93], however a contrary tendency has been also indicated by some investigators [58, 69, 72, 89, 92, 95].

The tool geometry is another important aspect of drilling of composite. The effect of point angle on delamination has been studied. Gaitonde et al. [72, 92] reported that drilling induced delamination increased with increased point angle of carbide twist drill bit in drilling of CFRP laminated workpieces whereas Kilickap [93] stated that delamination decreased with the increased point angle of HSS twist drill bit in drilling of GFRP workpieces. It was reported that damage is associated to the angle between the fibres orientation and cutting edges [52, 96]. Aoyama et. al [96] concluded that the damage is larger when the angle between the cutting edge and fibre orientation is 45°.

The extent of drilling induced delamination is related to thrust force, therefore the relation between thrust force and delamination is subject to a number of investigations.

A positive linear correlation between drilling induced delamination and thrust force was observed in drilling of composite with various drills [65, 69, 83, 97]. This finding has confirmed that delamination is closely related with thrust force and delamination can be avoided by controlling thrust force.

Critical thrust force is expressed as the thrust force which is the limit for the initiation of a delamination in drilling of composites. Delamination takes place beyond this thrust force [98]. The first analytical model to calculate critical thrust force has been proposed by Hocheng and Dharan [74]. Linear elastic

fracture mechanics was employed where the critical thrust force was modelled as a single concentrated load. Later Hocheng and Tsao have developed a series of analytical models to determine critical thrust force in drilling of composite with various drill geometry, including twist, slot, brad point, step and core drill bits [82-83, 98-101]. However, relatively simplified and idealized thrust forces have been employed in these models.

As it has stated drilling induced delamination is the major concern in drilling of composite materials [80, 102]. Hence, some research has been conducted to avoid or minimize delamination in drilling of composite materials.

It has been understood that it is difficult to obtain delamination free drilling with the use of conventional twist drills [70, 73]. For this reason, various drill bit geometries have been developed and investigations were carried, including brad spur [103], straight flute [63, 68, 104-105], step [28, 61, 82, 91, 99], core [73, 82-83, 101], step-core drill bits [106]. It was clearly observed that delamination was decreased significantly comparing to twist drill by reducing thrust force and increasing critical thrust force. The productivity has been also developed by allowing drill bits to cut at higher feed rates without delamination.

Piquet et al. [104] investigated drilling of CFRP by conventional two-flute twist drill and three-flute twist drill. Authors concluded that hole quality was significantly developed with the use of three-flutes twist drill due to the smaller contact length between the drill and the hole. However, in another study three flute twist drill with high point angle has failure to improve delamination in drilling of GFRP [103].

The influence of the roundness of the drill on delamination was studied by Tsao and Hocheng [107]. It was found that higher roundness resulted in increased thrust force, thus more severe delamination. The effect of the chisel edge and eccentricity on delamination was also studied by Tsao and Hocheng [108]. Authors concluded that thrust force can be significantly reduced by the minimisation of the chisel edge, as a result delamination can be avoided. Moreover, Tsao and Hocheng [97] investigated the effect of drill diameter on

delamination in drilling of CFRP with twist, candle stick and saw drills. Drill diameter was found a dominant factor on delamination whereas candle stick and saw drills were found to be more effective comparing to twist drill since less amount of delamination was generated by them.

Drilling induced delamination can also be reduced by a support plate underneath the composite workpiece. Some investigations have been performed in drilling of composite with different drill bit geometries and reduced delamination has been observed in the studies [80, 109]. The support plate improves the critical thrust force, thus significant reduction in delamination can occur. This method is commonly utilized in the manufacturing industry.

Another approach to reduce delamination is the use of pilot holes. Some analytical and experimental investigations have been carried out on drilling of composites with pilot holes with various drill bits [107, 110-111]. Authors concluded that significant reduction in delamination can be obtained with the application of this technique due to reduction in thrust force by the elimination of the effect of chisel edge of drill bit.

2.3.3 Tool Damage

Tool damage can be seen as tool wear, plastic deformation and built up edge in machining operations. Once the initial geometry of cutting tool is changed, cutting is performed ineffectively and the required tolerances and quality would be difficult to obtain in the workpiece [112].

Tool wear is a complex phenomenon and is generally expressed as material removal from the cutting edge or surfaces of the tool. Tool wear occurs due to several mechanisms which include abrasion, diffusion, erosion, corrosion, and fracture [113]. Under a set of cutting conditions, some of these wear mechanisms and their interactions may occur in machining. Tool wear causes increases in cutting forces and temperatures, reductions in the strength and integrity of the cutting tool, deterioration of machined surfaces, thus loss in dimensional accuracy, productivity and costs. Hence, to achieve the required quality of holes and to extend tool life, it is necessary to understand tool wear

and related mechanisms. For this purpose, a number of research studies have been carried out in drilling of composite materials.

Tool wear occurs due to various mechanisms and it depends on various factors such as workpiece and tool materials, machining parameters and environment conditions in drilling of composite materials. Abrasion and chipping are commonly attributed to the tool wear mechanisms in drilling of composite materials however adhesion can be also seen on tool edges.

A number of research works have identified abrasive wear as dominant tool wear mechanisms in drilling of composite materials owing to the highly abrasive nature of the reinforcement, particularly carbon and glass fibres [56, 64, 67, 114]. The abrasive wear mechanism is characterized by scratches and grooves on tool surfaces under high cutting pressures due to the existence of hard fibres in the composite workpieces. Anisotropic abrasive reinforcements cause excessive tool wear and shorten tool life substantially.

Chipping has been observed by a number of investigators [28, 64, 115]. It was reported that, chipping has appeared due to high contact cutting stress at the beginning of the cutting as drill edges were sharp. In addition to that, adhesion has been reported on the flank face due to high cutting temperatures [64, 67]. However, both chipping and adhesion were not found as the dominant wear mechanism in drilling of composite.

A range of materials is used in the manufacturing of cutting tools. These materials can be classified into three main groups; high-speed steels (HSS), cemented carbides, and super hard materials. Each group has its unique characteristic such as mechanical and thermal properties, and tribological behaviour [116].

High-speed steels are one of the oldest tool materials which have high toughness and moderate strength with low to moderate hardness. They can be easily shaped and imparted their hardness by heat treatment. Due to low cost, they have been used extensively, however they are not very suitable for machining of composites due to their low to moderate hardness and low wear resistance [116].

The cemented carbide group is mostly made from tungsten carbide (WC) and some other carbides including TiC, TaC. Cemented carbide cutting tools are produced by first cold pressing of powder mixtures and then sintering around 1400 °C. They provide high hardness, high toughness, moderate to high wear resistance, and are able to retain their properties at relatively higher temperatures than high steel alloys since their hardness are imparted by the hard phase not heat treatment. Cemented carbides are the widest range of tool materials since they are medium cost tool materials, able to machine most of the engineering materials and their tailored properties can also be improved by various coatings [116].

Super hard materials includes ceramics, poly crystal diamonds (PCD), cubic boron nitride (CBN) and single crystal diamond. They are developed for extra long tool life and high productivity, but required special attention and tool machines for the possible applications, therefore they are high cost. Except the single crystal diamond, they are produced by sintering method at very high temperatures and pressures. They generally provide very high strength and wear resistance, but not high toughness due to very brittle structure [116].

Since tool materials play important roles in many aspects, such as wear and tool life, drill bits made from different materials as explained above, such as high speed steel (HSS) [20-21, 79, 82-83, 90, 97, 103], uncoated cemented carbides [20-21, 28, 56, 63-65, 75, 90, 103, 114], coated cemented carbides [28, 63, 114], and polycrystalline diamond (PCD) [44, 47-48, 55, 57-58] have been used to understand the drilling processes of composite laminates. Although different tool wear mechanisms exist in drilling of composite materials, the major tool wear mode was found as flank wear in many studies [20-21, 28, 56, 64-65, 67, 114]. Studies have shown that abrasive based flank wear was found on HSS [20, 103], uncoated carbide [20-21, 28, 63-65, 114] and various coated carbide drills [28, 63, 114] in drilling of composite materials. Coated carbide and PCD tools suffer from wear less comparing to HSS tool and present lower delamination damage in machining of composite materials. Moreover the use of PCD and coated carbide tools provide longer tool life in drilling of composites that the one with HSS. Nevertheless PCD tools are extremely expensive.

Tool wear is sensitive to cutting parameters, thus the relation between cutting parameters and tool wear is a subject of matter in drilling of composites. In generally it was observed that tool wear increased with the increasing cutting speed and feed rate [115].

Tool wear can also result in serious workpiece damages such as delamination and surface roughness [64, 66, 71, 79]. It was stated that an increase in tool wear provokes an elevation in thrust force in drilling of composites. This can deteriorate the quality of holes in the workpiece [71, 115].

2.3.4 Numerical Study

Material removal is a subject of numerical studies in the literature however the majority of them are concerned with metal machining. Nevertheless, machining of composites is rather different from metals.

Mahdi and Zhang [117] studied orthogonal cutting of laminated composites. The finite element analysis was 2-D and utilized the Tsai-Hill criteria for chip generation. Cutting forces was predicted. In another study [118], the authors proposed an adaptive mesh algorithm. Arola et al. [119-120] also developed a finite element model to investigate the chip formation during orthogonal cutting of a laminated composite material with unidirectional oriented fibres. Different cutting geometries were utilized as rigid and deformable body in the analysis. The authors concluded that the model was able to predict cutting forces in orthogonal cutting of composite. The influences of fibre orientation and tool geometry on the fracture stress were also discussed. Later Zitoune et. al. [121] performed drilling of composite material by using a simplified framework with orthogonal cutting. The authors showed the influence of fibre orientation and cutting speed on drilling. In another study, Singh et. al. [60] developed a finite element model in drilling of unidirectional GFRP. 3-D twist drill geometries were used to understand the influences of geometry on force, torque and delamination. The maximum stress and the maximum strain and Tsai-Wu failure criteria were utilized to represent the material failure [60]. The authors concluded that smaller point angle should be used in drilling of GFRP.

These approaches were due to the complexity of machining process, stress and delamination analysis of laminated composites. In these studies FE stress and failure analyses have been conducted using maximum stress and Tsai-Hill criteria owing to the limited capabilities of computer processors and FE tools.

Latest advances in computational processors and improved FE formulations have allowed the development of complicated and more realistic 3D models to be solved with improved computational efficiency. In recent years, numerical predictions of delamination and critical thrust force have been performed in drilling of laminated composites [122-124]. The onset of delamination is modeled by virtual crack extension (VCE) method [124] and cohesive zone elements (CZE) [122-123]. The latter approach of CZE overcomes some of the difficulties of the former methods of VCE. For example a pre-defined crack front is not required in CZE. These elements use a failure criterion that combines aspects of strength based analysis to predict the onset of the softening process, and a fracture mechanics based approach to predict the growth of delamination which is governed by the inter-laminar through-thickness stress components. However these studies suffer from some significant drawbacks such as lack of a progressive damage model for intra-laminar and inter-laminar properties. Moreover, the complex geometry of drill bit and machining process parameters such as feed rate and cutting speed have not been taken into account.

2.4 Drilling of Titanium

Titanium and its alloys are attractive for many applications due to their superior properties. However, Ti has been classified as difficult-to-machine material. There are several reasons of this depending on the application. Among all machining methods, drilling is significantly important for titanium since it is generally the final step of the machining. It accounts approximately 40-60 % of all material removal processes and is essential for many applications, thus has considerable economical importance [125-126].

Several researches have been carried out to understand machining or titanium and its alloys better. This section will review on mechanical drilling

processes for Ti. It covers several essential aspects, such as cutting forces, cutting temperatures, tool damage, hole quality and numerical approaches.

2.4.1 Cutting Forces

Cutting force is one of the indicators of machinability of a workpiece [127-128]. In practice, a smaller cutting force is desired however it may not be easy to achieve since it can be affected several factors. An increase in the cutting force can provoke wear and vibration, consequently poor quality of machined surfaces and shorten tool life. High torque often indicates large friction between the cutting tool and workpiece and can cause high cutting temperatures. The relations between machining parameters, cutting tool geometry, wear, and thrust force and torque in drilling of titanium have been studied by a number of researchers.

Process parameters have influence on cutting forces. Feed rate has been observed as the dominant process parameters on thrust force and torque in drilling of Ti alloy [20, 127, 129-130]. It was reported that thrust force and torque increased with the increasing feed rate. In contrary, it was stated that an increase in cutting speed reduce the thrust force and torque in drilling Ti alloys [127, 131-132]; however in another study an increase was reported in torque [129]. The cutting power and cutting forces in drilling of titanium have been found similar to that in drilling steels [2, 133], however higher stresses on cutting tool have been reported in drilling of Ti-6Al-4V comparing to that drilling steel [134]. This was attributed to high strength and low elasticity modulus at elevated temperatures which cause small contact area between chip and cutting tool.

Geometry of drill bit has significant effects on cutting forces in drilling of titanium, thus it has been subject of a limited number of research works. Low negative rake angle and large helix angle has been addressed to reduce thrust force and torque [131, 135]. Special geometries such as helical drill and split point drill were reported to lower the thrust force in drilling of titanium [17, 131]. Thinner web was stated beneficial to reduce thrust force [131]

The effect of tool material on thrust force and torque has been investigated. It was reported that carbide tools outperformed HSS and HSS-Co tools. Lower thrust force and torque values were observed with carbide tools in drilling of titanium and titanium/graphite stack [131, 136].

The effect of coolant on thrust force and torque has been investigated in drilling of titanium by Li et al. [131]. It was observed that internal coolant caused an increase in thrust force and it was attributed to hydrodynamic force whereas external coolant did not affect remarkably.

2.4.2 Cutting Temperature

Typically, 90 % of the work of plastic deformation and friction are converted into heat in drilling of a metal based material and consequently high cutting temperatures are generated in drilling region and surrounding area such as tool body [2, 131, 137-138]. The generated heat is removed from the by tool, workpiece, chip and coolant if it used in drilling, thus the partition of heat depends on the thermal properties of both materials. Since titanium has a low thermal conductivity coefficient, a large fraction of heat is forced to be absorbed by cutting tool [131, 134]. The thermal conductivity of titanium is approximately 15% of steel, thus the heat fraction of tool during drilling of titanium has been reported higher than drilling steel [133, 139].

Cutting temperature distribution has been investigated and it was observed that temperature gradients were much steeper whereas heat affected zone was much smaller and closer to cutting edge in titanium comparing to steel. This was attributed to smaller contact due to thinner chip which causes to high cutting temperatures as high as 1100 °C. [140-143]. The high cutting temperatures around the cutting edge of the tool have been stated as the principal reason of the rapid tool wear in drilling titanium [2]. Rahim and Sharif [132] reported that the average cutting temperature increased with the increasing cutting speed whereas the temperature oscillation has decreased.

2.4.3 Hole Quality

Hole quality can be evaluated in terms of surface roughness, and burr in drilling of titanium alloys (Kim et al., 2001). Generally high quality of holes are required, thus hole quality is a subject matter for investigators in drilling of titanium alloys.

Surface of titanium alloys can be easily damaged in machining in forms of microcracks and plastic deformation [133, 139, 142, 144]. High surface roughness could cause to catastrophic fatigue and excessive wear. It was observed that cutting speed has a noticeable influence on surface roughness in drilling of titanium [21]. It was reported that surface roughness decreased with increasing cutting speed with carbide drill, however a contrary tendency was observed in drilling of titanium with HSS-Co drills [132, 136, 145]. Generally it was observed that lower surface roughness were achieved with carbide drills comparing to HSS drills [21, 136], and similarly coated carbide drills outperformed uncoated carbide drills in drilling of titanium. This was attributed to wear mechanisms and tool wear rate [145].

Burr is a common defect in machining of titanium alloys due to plasticity and it can occur at both entrance and exit sides of the holes. Generally the exit burr was observed larger than the entrance burr. It can reduce the fatigue life of the structure and 30% of some components is estimated due to deburring operations [17].

The process parameters has a noticeably effect on burr size. It was found that burr height is closely related to thrust force in drilling and larger exit burrs are induced in drilling with lower feed rates whereas burr height increases with cutting speed [136].

Dornfeld et. al [17] have also investigated the effect of tool geometry on burr and concluded that burr height can be minimized by the use of drills with large helix angle and large point angle. Helical point drills were performed better comparing to split point drills by means of burr sizes. Kim et. al. [136] observed that carbide drills produced smaller burrs at the exit than HSS-Co

drills did due to reduced thrust force and wear. Dornfeld et. al [17] stated that cutting fluids minimize the drilling induced burr in workpieces.

2.4.4 Tool Damage

Severe tool wear is the main reason of high machining cost of titanium. Thus tool life and tool wear have been subject of matter by many researcher in drilling of titanium. Wear mechanisms in machining of titanium depends on several aspects such as material process parameters, material combination, tool geometry and coolant. Tool wear occurs due to several mechanisms which include abrasion, diffusion and fracture in drilling of titanium. Some of these wear mechanisms and their interactions can occur during drilling [2, 132, 145].

Tool wear develops fast due to excessive cutting temperatures and strong adhesion between the tool and workpiece in the machining of Ti [142].High cutting stresses on the cutting edges of the tool accelerates tool wear and may result in plastic deformation [2, 17, 19, 134, 140, 145]. In addition to this built-up-edge (BUE) can occur on the cutting tool under high cutting stresses and temperatures [146]. The local welding between cutting tool and workpiece or chip often leads to chipping and sudden fracture of the cutting tool.

Influences of process parameters on wear have been also studied. It was found that tool wear is predominantly affected by feed rate [2, 19, 131, 147]. It was reported that tool wear increased significantly with the increasing feed rate and reduced tool life in drilling of titanium [131]. Cutting speed was found to have significant influence on tool wear [2, 19]. It was reported that at high cutting speed cutting tools suffered from excessive tool wear and the life of cutting tool reduced drastically [2, 132, 145]. Similar to feed rate, lower cutting speed was suggested in drilling of titanium, but this will reduce the productivity significantly [19].

Effect of tool geometry has been investigated by a limited number of investigators in drilling of titanium. Larger helix angle has been reported to increase tool life by improving chip removal [135, 146]. Aust and Niemann [147] studied drilling of γ titanium alloys and concluded that larger drill diameter can provoke a reduction in tool life. High clearance angle and high negative

rake angle have been suggested to reduce tool wear in drilling of titanium alloys [148-149].

Over the last few decades, there have been great developments in cutting tool materials, including coated carbides, ceramics, cubic boron nitride (CBN), polycrystalline diamond (PCD) and various coatings. Most of these materials have been found to be useful in various machining applications however not completely successful to improve machining of titanium alloys due to several reasons.

Cutting tool materials have to withstand with high strength, high cutting temperatures and high diffusion in drilling of titanium alloy therefore tool material requires high strength, hardness and toughness even at elevated temperatures, high thermal conduction coefficient and high chemical inertness.

Different tool materials show different responses and wear mechanisms during machining of titanium alloys. It was reported that HSS tools suffer from various wear types. Due to moderate cutting temperatures above 500-600 °C in machining of titanium, they lose their hardness [134]. This can also cause to severe plastic deformation which can accelerate the rate of wear. The high cutting temperatures can also lead to built-up-edge [3, 140] . High alloy HSS, such as M33, M40 and M42 might be useful in some machining applications of titanium alloys by special care [133].

Many investigators have reported the advantage and performance of carbide tools over HSS tools due to higher hardness and wear resistance in machining of titanium alloys [2, 140, 148, 150]. K grade carbide tools outperformed HSS tools in wear rate due to toughness and hardness, however P grade carbides was not suggested due to similar wear rate to HSS and their thermal properties [134, 140, 151]. Various coated P grade carbides did not perform well in machining of Ti alloys [151-152]. It was reported that uncoated and coated P grade carbide tools were suffered from larger plastic deformation, crater wear and diffusion than K grade carbides in machining of Ti.

The superhard cutting tool materials such as cubic boron nitride (CBN), ceramics and polycrystalline diamond (PCD) have shown some good performance, such as wear rate, in machining of titanium [2, 19, 140]. However,

their relatively low fracture toughness, poor thermal conductivity and high costs are limiting their applications [153]. The coated tools performed well and suffered less damage and reduced wear rate [145].

The use of cutting fluids in machining of titanium alloy is essential since the coefficient of thermal conductivity of titanium is very low. It was reported that tool wear can be reduced up to 10 times by application of cutting fluids via drill coolant holes [131]. It was also stated that cutting fluids which contain phosphates serves better in machining of titanium [2-3]

2.4.5 Numerical Study

Very few investigators have studied machining of Ti-6Al-4V numerically. Li and Shih [154] conducted finite element analysis of drilling of titanium alloy. They investigated cutting temperature and stresses on drill bit in drilling of Ti-6Al-4V. A thermo-mechanical FE model has been utilized to predict temperature and stress. The study enabled to design 3-D drilling and demonstrated of effectiveness of FE analysis to design cutting tool.

Umbrello [155] has investigated finite element analysis of conventional and high speed machining of Ti-6Al-4V. He focused on the effects of constitutive law parameters on the predicted cutting force and chip morphology. He implemented the Johnson Cook material model for the 2-D orthogonal machining of Ti alloy with rigid tool. Results indicated a reasonable prediction of cutting force and chip morphology for both conventional and high speed machining of Ti-6Al4V.

Calamaz et al [156] has performed a finite element study to investigate chip formation and shear localisation in machining of titanium. The numerical analysis was based on orthogonal cutting in 2D to simulate segmented chips with regard to the process parameters. Due to the use of cutting speeds beyond 60-65 m/min, segmented chip is formed and adiabatic shear bands should be taken into account in machining of Ti-6Al-4V. Thus authors proposed modified Johnson-Cook constitutive material law to introduce strain softening during machining of titanium alloy. With the use of a rigid cutting tool, chip morphology, cutting stresses and cutting temperatures was predicted in

orthogonal cutting of Ti6Al4V. These contributions reveal that material flow stress and finite element formulation greatly affects not only chip formation mechanism but also stresses, forces and temperatures predicted in high speed machining of Ti-6Al-4V.

Sima and Ozel [157] have also studied serrated chip formation in machining of Ti-6Al-4V. Chip formation process with adiabatic shear has been investigated via FEA with the proposed material model. Sima and Ozel have developed a tanh model very similar to that of Calamaz et al. The only difference is the S exponent of the tanh function whose value is near 1. This setting does not fundamentally change the shape of the stress-strain curve. A higher value of the parameter S leads to a faster entrance to the softening regime of the workpiece material with respect to increasing strain and decreases the slope of the softening part of the flow stress curves without changing the value of the minimum flow stress. A lower value of the parameter S causes minimum flow stress to take place at a higher strain. 2-D finite element simulations of orthogonal cutting were performed with the use of deformable tools which are uncoated carbide and TiAlN coated carbide tools. The finding of the study was similar to Calamaz et. al. work [156].

2.5 Drilling of Hybrid Structures

CFRP metals are used increasingly in form of stack to optimize the weight/strength ratio in various applications, such as wing structures and fuselages [23, 26]. Assembly of these materials generally requires high number of rivets or bolts [5]. Drilling of composites and titanium alloys have been explained in the previous subsections. Nevertheless, drilling CFRP/metal stacks has been studied only by very few researchers. Not surprisingly different problems may arise due to combination of very different attributes of these materials during drilling of multi-layer materials. The previous work on drilling of composite/metal stack is summarized below.

Ramulu et. al. [20] carried out an experimental study to understand effect of tool material in drilling of graphite-bismaleimide/titanium (Gr-Bi/Ti) stacks. Authors observed that dissimilar material properties had significant influences

on tool life and workpiece defects. Due to high cutting temperatures matrix degradation in CFRP and burr formation in Ti, surface roughness of the workpieces and tool wear increased in all HSS, HSS-Co and carbide tools, thus only very few holes could be drilled. It was concluded that carbide tools outperformed HSS and HSS-Co tools.

Brinkesmeier and Janssen [158] has investigated drilling of CFRP/Al and Al/CFRP/Ti stacks. The authors aimed to optimize the influence of tool geometry and process parameters with regard to quality of holes and tool wear by using conventional and optimized tool design with the application of coolant. The authors concluded that optimized step drill, which has about 0.96 step ratio, improved the quality of holes whereas coating only affected tool wear.

Kim and Ramulu [21] studied the drilling process of graphite-bismaleimide/titanium alloy (Gr-Bi/Ti) stack. They focused on assessment of hole quality and optimisation of process parameters. They stated that quality of hole in drilling of composite is very dependent on properties of the composite. They suggested a combination of low feed rate and low cutting speed as optimum process parameters with C2 grade carbide drills whereas relatively higher feed rate and cutting speed with HSS-Co split point drills.

Zitoune et al. [159] has investigated drilling of CFRP/Al stack. They carried out an experimental study to optimize process parameters. They concluded that effect of drill diameter and feed rate are dominant on chip breakability whereas effect of spindle speed can be ignored. A similar relation has been observed between surface roughness and process parameters in CFRP whereas more smooth surfaces were obtained in Al with the use of K20 carbide tool. They concluded that thrust force was more sensitive to wear in drilling of CFRP part than Al.

Shyha et. al. [160] investigated the quality of holes in the drilling of Ti/CFRP/Al stack with the use of uncoated carbide, CVD diamond coated carbide and AlTiN-Si3N4 composite coated carbide. They observed that delamination was reduced significantly in drilling stack comparing to drilling CFRP alone. The burr height was found noticeably higher at the exit of Al

comparing to Ti. The authors suggested the use of internal cooling through drill holes comparing to spray mist cooling due to improvement in the quality of holes. They also observed that hole edges of CFRP were damaged due to burrs and chips.

Park et. al. [161] carried out a study to understand wear mechanism in drilling of CFRP/titanium stack with carbide and polycrystalline diamond (PCD) tools. The authors observed that abrasion and adhesion were found to be the dominant tool wear mechanisms in drilling of CFRP/Ti stack due to abrasive carbon fibres and chemically reactive Ti. Adhesion of titanium occurred on carbide drills severely whereas PCD shows significantly higher wear resistance against adhesion however PCD drills was suffered from chipping. The increase in the cutting forces was observed much steeper in the experiments with WC tools than that with PCD drills. The wear was observed to be more sensitive to spindle speed in WC drills. In overall the authors concluded that PCD drills outperformed WC drills in stack drilling in the given tests conditions.

Chapter 3

Experimental Methodology

This chapter discusses experimental research in drilling of Ti-6Al-4V, carbon fibre reinforced composite and stack of these two materials. The entire experimental study includes on-line and off-line measurements and investigations to assess performance of drilling.

First, drilling of Ti-6Al-4V and CFRP were carried out separately to study drilling of each material. Since characteristics of these materials are considerably different from each other, investigations were performed to study machinability of them separately. The force and torque output were measured on-line throughout the drilling experiments. Tool wear was observed and examined during drilling. Burr formation of Ti-6Al-4V and delamination of CFRP were investigated. Surface quality of drilled holes was analysed after drilling tests. The effects of process parameters on these outputs were studied.

Second, some drilling experiments were performed in stack of CFRP and Ti-6Al-4V. All the measurements and observations which were carried out in drilling of these materials were also performed for drilling of stack to understand the machinability of stacked materials.

The drilling experiments were conducted at Advanced Manufacturing Research Centre of University of Sheffield, located in Rotherham, UK. The details of the experimental work including materials, techniques and parameters are explained in detail in the following sections.

3.1 Materials

The CFRP work pieces were comprised of unidirectional carbon fibre as the reinforcements and epoxy as the matrix material. The unidirectional prepregs, Hexcel HEXPLY UD T700 268 M21 34% T700-M21, were fabricated

out of T700 carbon fibres. The prepregs were cured and laminated work pieces were supplied by Airbus. The nominal fibre volume fraction of the prepregs was 59%. The laminates were designed to have quasi-isotropic properties including 80 plies. The lay-up sequence was [(90°/-45°/0°/45°)]5s. The final cured thickness of the laminated work pieces were 20.8 mm. The physical and mechanical properties of the unidirectional prepregs are illustrated in Table 3-1.

Table 3-1: The Material Properties of CFRP [162-163]

ρ (kg/m^3)	E_L (GPa)	E_T (GPa)	υ_{LT}	G_{LT} (GPa)	$\sigma^{f,t}{}_L$ (Mpa)	$\sigma^{f,c}{}_L$ (Mpa)	$\sigma^{f,t}{}_T$ (Mpa)	$\sigma^{f,c}{}_T$ (Mpa)
1580	112	8.2	0.3	4.5	1900	1000	84	250

Ti-6Al-4V is most widely used Titanium alloy in aircraft industry because of its high specific strength. The machinability of the material is poor because of high hardness and strength. The final thickness of the Ti-6Al-4V work pieces were 20 mm. The mechanical, physical and thermal properties of workpiece materials are given in Table 3-2 whereas the chemical composition of the material is shown in Table 3-3.

Table 3-2: The Material Properties of Ti-6Al-4V [16]

ρ (kg/m^3)	E (Gpa)	υ	G (Gpa)	σ_u (Mpa)	σ_y (Mpa)	C_p (J/kg.°K)	K (W/m.°K)
4430	105-116	0.26-0.36	41-45	900-993	830-924	580 (at 20°C)	6.6 (at 20°C)

Table 3-3: The Chemical Composition of Ti-6Al-4V [16]

Al	V	N	C	H	Fe	O
6.0	4.0	0.05	0.1	0.01	0.3	0.2

The selection of drill bit was not easy. In order to withstand the high thrust force a high point angle drill bit was chosen. Commercially available appropriate coating was opted to withstand the high abrasive wear of fibres. The drill bits used in drilling tests of CFRP and Ti-6Al-4V, are coated solid carbide twist drill made by Sandvik Coromant. The drill is CoroDrill Delta-C R846 product which is 3 μm multilayer TiAlN/TiN PVD coated solid tungsten carbide drill. It is a 2-flute through-coolant right hand drill with 140° point angle,

30° helix angle and 8 mm diameter. The hardness of TiAlN is between 2500-4000 HV[164-166] whereas TiN 2000-2250 HV[164-165]. Multilayer coating exhibit higher hardness and toughness due to the interfaces between coating layers. The carbide grade is Sandvik grade GC1220 or ISO S30. The drill particularly designed for application of producing holes in aerospace materials and is shown in Figure 3-1.

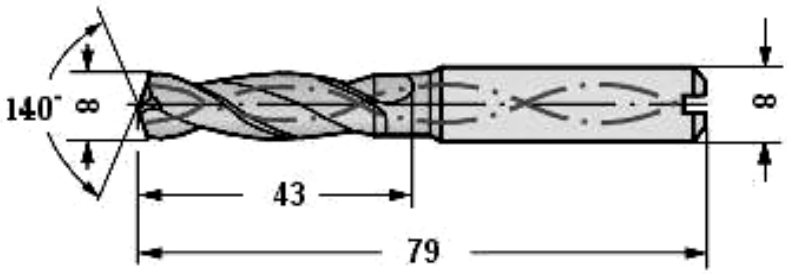

Figure 3-1: The twist drill geometry

3.2 Drilling Tests

All drilling experiments were carried out on a vertical CNC machining centre Mori Seiki SV-500 with a maximum spindle speed 10,000 rpm. Figure 3-2 shows the Mori Seiki vertical machining center used in the experimental work.

Figure 3-2: The machining centre

All drilling experiments were carried out with high pressure cooling through tool coolant holes of drills. 5 percent emulsion of Hocut 795B cutting fluid was applied in wet cutting experiments at a constant 38 bar coolant pressure (equal flow rate of ~2.4 l/min). Experiments were repeated 5 times. The

diameter is chosen 8 mm as it is one of the most common required hole size in aircraft industry. Since the mechanical and physical properties of CFRP and Ti-6Al-4V are quite distinct, different cutting parameters were selected for drilling of these different materials. In the first scenario (Scenario-A), the effects of drilling parameters were investigated in drilling of CFRP and Ti-6Al-4V. Table 3-4 shows the process parameters used in the experiments for each material in Scenario-A. These machining parameters were determined according to the industrial experiences and available ranges for each material.

Table 3-4: Cutting parameters (Scenario-A)

Material	Spindle Speed (rpm)	Feed Rate (mm/min)
CFRP	3000, 4500, 6000, 9000	355, 457, 585, 684
Ti-6Al-4V	1000, 1400, 1800	95, 119, 142, 171
CFRP/Ti-6Al-4V	4500,6000 (CFRP) 1400,1800 (Ti-6Al-4V)	355,457 (CFRP) 95,119 (Ti-6Al-4V)

The second scenario (Scenario-B) was performed for the effects of tool wear on drilling of CFRP and Ti-6Al-4V. Table 3-5 shows the process parameters used in the experiments for each material in Scenario-B.

Table 3-5: Cutting parameters (Scenario-B)

Material	Spindle Speed (rpm)	Feed Rate (mm/min)
CFRP	4500	457
Ti-6Al-4V	1400	119
CFRP/Ti-6Al-4V	4500 (CFRP) 1400 (Ti-6Al-4V)	457 (CFRP) 119 (Ti-6Al-4V)

Due to high cutting forces, drill can be broken very easily in drilling of Ti-6Al-4V work pieces. Therefore small drilling cycles (2 mm depth per cycle), which is called peck drilling, has been used in drilling of titanium in both scenarios.

3.3 Force & Torque Measurement

The thrust force and torque signals during the drilling experiments were measured using a multi-component dynamometer Kistler model 9255B. The dynamometer mounted on the machine tool is shown in Figure 3-3.

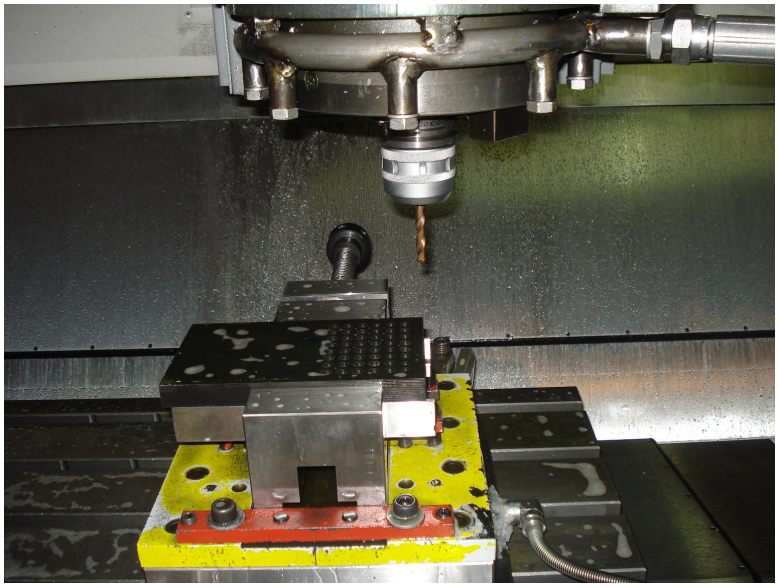

Figure 3-3: The Experimental Set-up

The dynamometer has the capability to measure forces in X, Y and Z directions and the calculate torque component in Z direction. Specifications of the dynamometer are given in Table 3-6.

The data acquisition system used for the drilling experiments is comprised of a multi-channel charge amplifier, Kistler model 5017, data acquisition card fitted inside a notebook PC, and a software application, Dynoware, developed by Kistler. Dynamometer was charged and the signals were collected by the multi-channel amplifier. The amplifier converted the induced signals, which were proportional to the applied force, to voltage. These voltage signals were gathered through the data acquisition system. The resulting signals were converted to the force by the calibrated data in the software. The data acquisition system is shown in Figure 3-4.

Table 3-6: Specifications of Dynamometer

Specifications			Type 9255B
Calibration			calibrated
Measuring Range	Fx, Fy Fz	kN kN	±20 -10...40
Sensitivity	Fx, Fy Fz	pC/N pC/N	≈-8 ≈-3.7
Natural Frequency	fnx, fny, fnz	kHz	≈3
Operating temperature range		°C	0...70
Length		mm	260
Width		mm	260
Height		mm	95
Connection			Fischer 9 pol. neg.
Sealing			welded/epoxy (IP67) With connecting cable Types 1687B5, 1689B5
Mass		kg	52

Before the experiments, the dynamometer was sealed perfectly due to the use of coolant and calibrated. Measurements were obtained with a frequency of 1000 throughout drilling of holes. Force and torque were measured in each hole in drilling of CFRP, Ti-6Al-4V and CFRP/Ti-6Al-4V stack. The force and torque characteristics were investigated. The effects of process parameters on the thrust force and torque in drilling of CFRP and Ti-6Al-4V and CFRP/Ti-6Al-4V stacks are reported in Chapter 6, 7 and 8, respectively. The effects of wear on thrust force and torque also reported in the results.

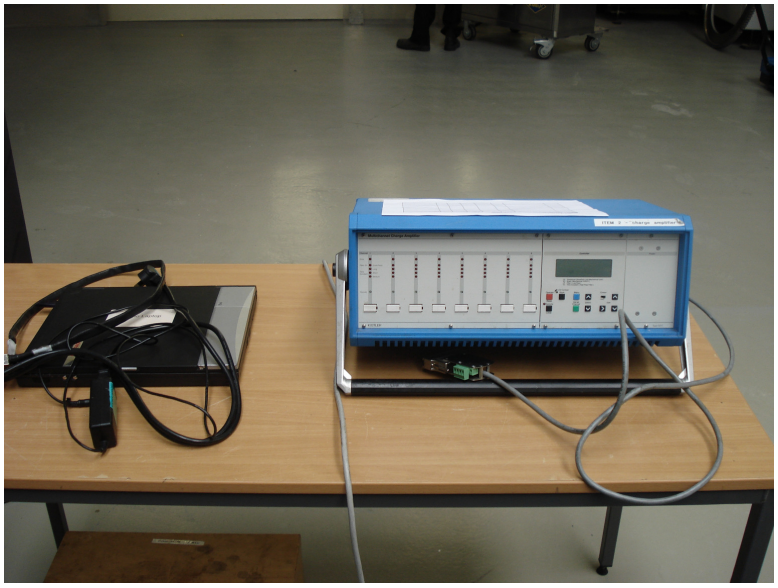

Figure 3-4: The data acquisition system

3.4 Delamination Measurement & Analysis

Figure 3-5 shows typical delamination damage of a hole after drilling composite material. The delamination factor has been recognized and widely used to determine the level of damage on the composite structures. The delamination factor is frequently calculated as the ratio of the maximum diameter of the delamination zone to the nominal hole diameter as given in Eq. 3.1. Delamination factor can also be calculated from the ratio of the delaminated area to the nominal hole area in Eq. 3.2. The former factor can be called as conventional delamination factor (F_D) whereas the latter is called alternative delamination factor (F_A). Both factors are calculated through analysis and reported in the results.

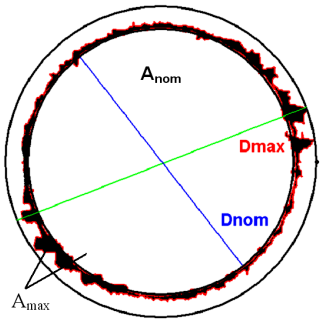

Figure 3-5: Illustration of Delamination Damage around a Hole

$$F_D = \frac{D_{\max}}{D_{nom}} \qquad \textbf{Eq. (3.1)}$$

$$F_A = \frac{A_{\max}}{A_{nom}} \qquad \textbf{Eq. (3.2)}$$

The conventional delamination factor can be used where the damage is in regular form, such as glass fibre reinforced plastics. The alternative delamination factor have been used in a limited number of studies [167-168] due to complexity of the calculation of the area of an arbitrary damaged region at the hole vicinity. However it is required to be used where the damage is in irregular form and generally occurs in arbitrary shape, such as CFRP.

Several techniques can be employed in the observation and evaluation of the damage around the holes after drilling of composites. Optical microscopy, computerized tomography and CT-Scan, shadow moiré laser imaging,

microwave nearfield non-destructive testing, thermal imaging and digital photography are some of these methods. In this study, optical microscopy and digital image analysis were used in the characterisation and analysis of the delamination at the hole vicinity of the CFRP work pieces. The delamination was observed under a tool microscope system which consists of Sanyo high resolution colour CCD camera, model VCC 2972, and Metric PE data image software as shown in Figure 3-6. The hole vicinity were cleaned with acetone carefully and dried completely to provide correct detection of the damaged areas and to avoid visual errors. The CCD camera processes the resulting data into an image, and the image is captured into the image software for the visual inspection. The generated images were used in the developed algorithm for the analysis of delamination factors. The digital image analysis algorithm was developed in Matlab software and explained below.

Figure 3-6: The tool microscope system

Figure 3-7 illustrates the flow diagram of the digital image analysis procedure. The algorithm has been developed in Matlab software. The image from optical microscope input to the software. In order to obtain an image with acceptable quality, a series of parameters must be appropriately selected. First thresholding was applied to the image then the noise was suppressed in order to make a clear image by filtering very small unconnected zones from the image. After the application of region property module, the image was divided into enclosed areas to enable obtaining quantitative data on the image,

including the area of enclosed zones, perimeter of the areas based on the detected edges, equivalent diameter, centre and eccentricity. Finally, the maximum diameter and damaged area were obtained and delamination factors were calculated using Eq. (1) and (2).

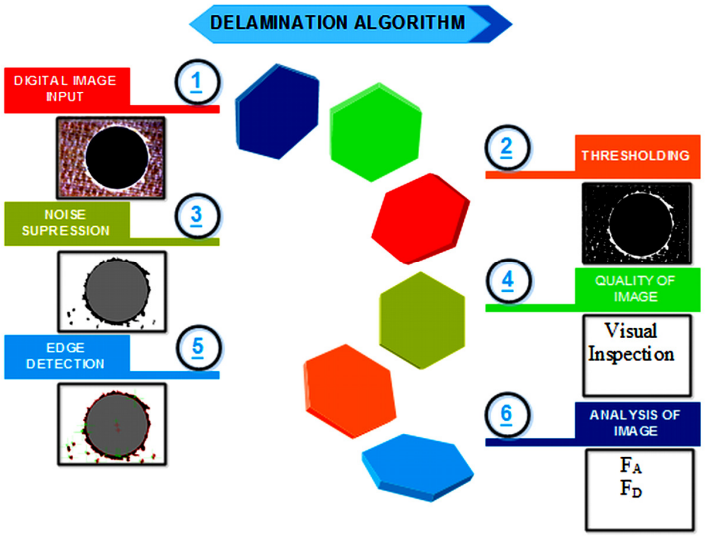

Figure 3-7: The Flow Diagram of the Digital Image Analysis

The influences of process parameters on delamination at both entry and exit sides are discussed for both CFRP workpieces, drilled alone and in stack with Ti-6Al-4V in Chapter 6 and 8, respectively. The effect of wear on delamination is also reported.

3.5 Burr Measurements

There are different methods to measure burr geometry characteristics such as burr height and thickness. These several techniques can be listed as contact methods such as measuring with the use of micrometers and profilometers, and non-contact methods such as optical microscope, light shadow, laser measurement, interferometry and conoscopic holography.

The burr formation formed at the hole entry and hole exit in Ti-6Al-4V workpieces were observed and sizes of burr geometry were measured for every hole after drilling Ti-6Al-4V alone and in stack form with CFRP. The burr height was measured with one of the contact techniques. The burr height at the entry and the exit side of the drilled holes was measured with the use of a

surface profilometer, Mitutoyo model SV-602. First, the workpieces' surfaces were cleaned with acetone carefully, without making any damage to the burr formation. Next, the top and bottom surfaces of the workpieces were taken as reference. Later, the surface profiles of the workpieces, including the burrs, were measured and the corresponding vertical displacement of the stylus was recorded. The burr heights were calculated from the vertical difference between the highest point at burrs and reference surfaces of the workpieces. This procedure was used to measure the burr heights at the entry and exit sides of the drilled holes of Ti-6Al-4V workpieces in drilling of Ti-6Al-4V alone and in stacked with CFRP. In order to reduce variability, the measurements of the burr heights were carried out in every 90 degree around the drilled hole at both sides. The measurements were repeated 5 times to provide accuracy and reliability of the results and the averages are reported in Chapter 7.

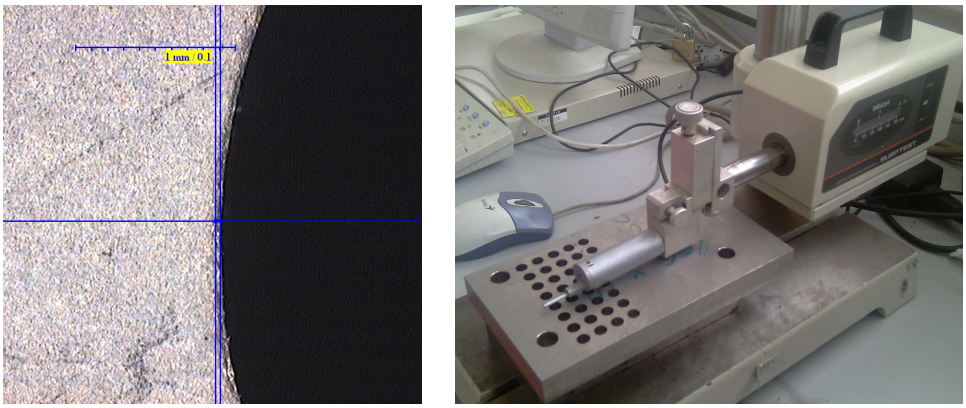

(a) (b)

Figure 3-8: Measurement of Burr Formation (a) Burr Width (b) Burr Height

The burr width was measured with one of the optical techniques. The burr form was observed and burr width at the entry and the exit side of the drilled holes was measured with the use of a tool microscope system including Sanyo high resolution colour CCD camera model VCC 2972 and Metric PE data image software. First, the workpieces' surfaces were cleaned carefully by acetone to avoid errors due to chips and cutting fluid. Next, the images of the drilled holes were taken from the normal direction at entry and exit of the drilled holes. Further, the burr widths were measured from the radial difference between the inner surface of the drilled hole and the outer surface of the damaged region, in other words the widths of the burr skin, as shown in Figure 3-8 (a). The

procedure was performed at each 90 degree around the drilled hole at both sides. As it was mentioned above for the burr height, the burr width measurements were replicated 5 times for the accuracy and reliability of the results and the averages are reported in Chapter 7 and 8.

3.6 Surface Roughness Measurements

The surface irregularities of the drilled holes were investigated to understand machinability of CFRP, Ti-6Al-4V and stack of these materials. A Mitutoyo Surftest SV-602 Surface Roughness Test measuring instrument shown in Figure 3-9 was used to measure the surface roughness of drilled holes.

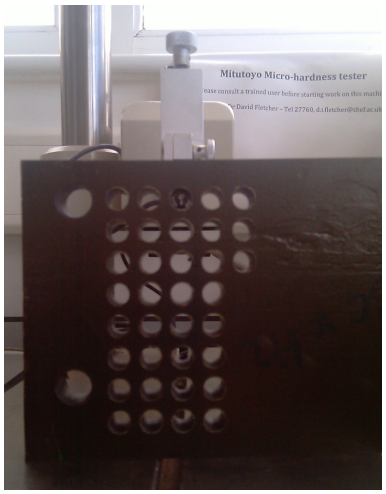

Figure 3-9: Surface Roughness Measurement of Drilled Holes

The profilometer is a stylus type surface roughness measuring instrument developed to detect quality of the surfaces. It is equipped with a diamond stylus having a tip radius 2 μm. The stylus of the SV-602 traces the minute irregularities of samples' surfaces. Surface roughness is determined from the vertical displacement of the stylus during traversing over the surface. The irregularities can be analyzed with different methods such as arithmetic average of absolute values, Ra, and root mean squared, Rq. In this study Ra was considered as it is the most common method of the analysis of surface roughness.

The cut-off length, traverse length and traverse speed used in the surface roughness measurements were 2 mm, 16 mm and 0.5 mm/sec, respectively. The

surfaces of the drilled holes were cleaned carefully by acetone to avoid errors due to chip, dust and cutting fluid. The measured surface data was analyzed for evaluation of the roughness parameters by Mitutoyo Surfpak software and recorded to the PC. The procedure was performed at each 90 degree in the drilled hole. The surface roughness measurements were replicated 5 times for the accuracy and reliability of the results and the averages are reported in the Chapter 6, 7 and 8. The effects of process parameters on the surface roughness in drilling of CFRP and Ti-6Al-4V, and the influences of wear on the surface roughness in drilling of CFRP, Ti-6Al-4V and stacks of these materials are discussed in Chapter 6, 7 and 8, respectively.

3.7 Tool Wear Measurements & Analysis

The type of the wear depends on the material couple, machining process parameters and environmental factors such as temperature and the use of coolant. A major or combinations of different wear mechanisms can be seen therefore different criteria are used to decide tool life. Progressive wear can be seen on flank and rake surfaces of the drill bits. Tool life criteria, recommended by the International Standard Organisation, are widely accepted in industry. These criteria are entirely concerned with the profile of the wear area growth for flank and crater wear as shown in Figure 3-10. The tool wear criteria are given in Table 3-7 for 8 mm diameter drill for flank wear and crater wear according to experience of the industry. If wear profiles on the flank and rake surfaces are uniform as shown in Figure 3-10 for the 2nd regions of both wear profile, the drill can be used until the wear land reaches any of the ultimate average value of the specific wear profile criterion, as given in Table 3-7. Otherwise, in the case of irregular wear land is observed as shown for 3rd regions for both wear profile in Figure 3-10, tool life criteria can be taken as the ultimate maximum value of the wear profiles, as given in Table 3-7.

Table 3-7: Wear Criterion of Drill

Wear Type	**V_B**			**K_B**		
Region	**1**	**2**	**3**	**1**	**2**	**3**
Ultimate wear (mm)	0.2	0.25	0.3	0.25	0.25	0.25

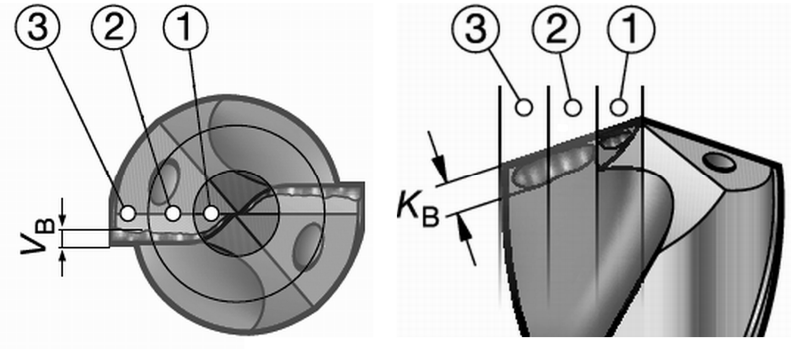

Figure 3-10: Wear on Drill

The wear formation of the both cutting edges was observed and measured during drilling of Ti-6Al-4V, CFRP and CFRP/Ti-6Al-4V stack. For the measurements and investigations a tool microscope system including Sanyo high resolution colour CCD camera and Metric PE data image software were used. This CCD camera processes the resulting data into an image, and the image thus obtained is captured into the image software for the visual inspection. Measurements were carried out at the end of each three holes and the drilling experiments were performed until any of the tool criteria was reached. Progressive wear was observed at both flank and rake surfaces of the two cutting edges of the drills. In addition, any other irregularities such as chipping or sudden failures were also investigated. In the measurements, the drills were kept mounted on the tool holder. The drill bits were cleaned with acetone carefully and dried completely to facilitate correct detection of the worn areas and to avoid visual errors. For the accuracy and reliability of the results, each measurement was repeated 5 times at both flank and rake surfaces and the average values are reported in Chapter 6, 7 and 8. The wear mechanisms in drilling of both workpieces are discussed. In addition to that effects of wear on drilling outputs such as thrust force, torque, delamination, burr and surface roughness are also investigated separately in the result sections.

3.8 Summary

The experimental methodology used in this study was presented in this chapter. The drilling characteristic of Ti-6Al-4V and Hexcel M21 T700 CFRP are investigated separately and in stack form of them by the use of coated carbide twist drill.

In-situ measurements were performed for thrust force and torque in drilling both workpiece materials at different process parameters. The effects of drilling parameters and the effects of wear on thrust force and torque are broadly discussed in Chapter 6, 7 and 8 for each drilling scenario.

Indirect measurements were performed after drilling for both materials. For the surface quality of the CFRP workpieces, delamination and surface roughness were investigated whereas burr formation and surface roughness were investigated for Ti-6Al-4V in both scenarios, separate and together in stack form. The contact and non-contact methods were explained. The effects of process parameters and tool wear on delamination, burr formation and surface roughness are discussed in detail in Chapter 6, 7 and 8.

Tool wear mechanism was observed and the amount of wear was measured through the drilling of both materials at the end of each three holes by optical methods. The detailed discussion is made in Chapter 6, 7 and 8.

Chapter 4
Numerical Methodology

In this chapter the components of the numerical models, the stress analysis, the failure analysis and the material degradation analysis are explained in a framework of progressive failure analysis for Ti-6Al-4V and CFRP. CFRP workpiece is modelled in meso-level via discrete modelling of unidirectional fibre reinforced plies and the interfaces between these plies where delamination occurs. Therefore, the numerical models for CFRP are utilized for intra-laminar level and inter-laminar level separately.

First, progressive damage model is explained for Ti-6Al-4V. A three-dimensional finite element algorithm is developed to analyze the three-dimensional state of stress in drilling as a sophisticated problem. A detailed explanation of the theoretical basis of the finite element formulation is presented which includes three stages of progressive damage modelling; stress analysis, failure analysis and finally material degradation rules. Initially the stress analysis is explained under multi-axial state of stress. The existence of material nonlinearity and its dependency to various factors are accounted in the numerical analysis of Ti-6Al-4V. Later, failure analysis is discussed. Similar to the stress analysis the effect of material nonlinearity is considered in failure criterion of Ti-6Al-4V. Finally, material property degradation is discussed as evolution of damage in Ti-6Al-4V. To simulate material degradation, gradual stiffness and strength degradation are utilized in multi axial state in Ti-6Al-4V.

Second, progressive damage model of CFRP is explained on a macroscopic level. Unidirectional fibre reinforced plies are modelled individually by taking into account of their fibre orientations. Intra-laminar behaviours of these plies are adopted for solid like and fully solid structural frameworks under multi-axial state of stress. The stress analysis of CFRP workpiece is performed ply by ply for both frameworks. Afterwards, stress-based failure criteria are employed ply by ply to detect failure modes of intra-laminar composite structure, such as

fibre tension, fibre compression, matrix tension and matrix compression under multi-axial state of stress. At last, degradation rules are utilized to each failure modes in ply based analysis of intra-laminar behaviour of CFRP.

Third, progressive damage model of delamination of CFRP is explained in meso level. Discrete cohesive zones have been modelled between UD CFRP plies to represent delamination. The inter-laminar behaviour is discretised using two approaches; finite thickness cohesive elements and zero thickness cohesive surfaces. A stress analysis is utilized for both cohesive approaches under multi-axial state of stress. Following that, a stress based failure criterion is employed and followed with gradual stiffness and strength degradation rules. The applications of these techniques are discussed.

4.1 Progressive Damage Modeling of Ti-6Al-4V

As shown in Figure 4-1, the physical and material properties, boundary and contact conditions of the problem and geometrical details are provided to the finite element model at the beginning of the analysis. Appropriate type of analysis is chosen and the simulation is started.

First, stress analysis is applied at the end of each increment. All components of stress, related deformations and strains are calculated. Next, failure analysis is performed according to the given failure criterion and the failure initiation is checked. If failure criterion is not met, the analysis can start to next increment without any material property degradation as at the beginning of the analysis. As the failure criterion is reached in a certain element, damage is initiated at that specific element. Subsequently, material degradation analysis is performed to change material properties, hence stiffness matrix and material behaviour of certain damaged element according to specified degradation rules. If the catastrophic level of failure is not met, the analysis continues for the elements where damage has initiated; else stresses of those elements are equal to zero due to complete failure and elements are removed from the analysis.

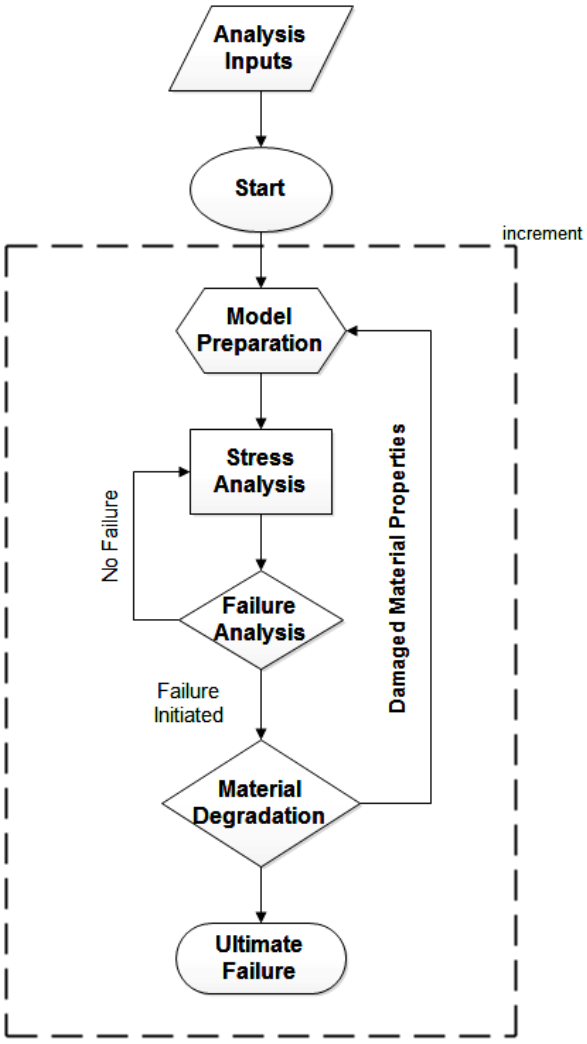

Figure 4-1: Flowchart of progressive damage model for Ti-6Al-4V

In the following subsections, the parts of the progressive damage model for Ti-6Al-4V are explained in detail.

4.1.1 Stress Analysis (Constitutive Model)

The modeling and simulation of metal cutting have become very important in order to decrease the cost of experimental investigations. Finite element methods (FEM) are employed to predict various machining outputs such as cutting forces, temperatures and stresses. Accurate and reliable constitutive models are required to represent the material behavior of workpiece undergoing deformations. The success of a particular constitutive model depends on how effectively it represents physics of metal cutting as well

as its ability to capture all relevant deformation parameters in a constitutive equation.

The flow stress in machining is mostly influenced by various process and environmental factors therefore it must be entirely captured by an empirical constitutive model. Several researchers have proposed different constitutive models to express the flow stress in metal cutting. Oxley [169] proposed a flow stress which is expressed by work-hardening behaviour. The model has been used in the modelling of orthogonal cutting of low and medium carbon steels. In another study, Maekawa [170] developed a constitutive model by taking into account of the effects of strain rate and temperature. However, the model is difficult to implement in finite element analysis without modifications. Johnson-Cook [171] model is widely used for high-strain rate applications in which models describe the flow stress of a material as functions of strain, strain rate and temperature effects. It is also a numerically robust constitutive material model which is highly utilized in finite element modelling. Zerilli-Armstrong [172] constitutive model is also used to describe the flow stress. The material model is based on simplified dislocation mechanics theory and taking into account of the crystal structure of materials. The model makes a distinction between body cubic centred (BCC), face cubic centred (FCC) and hexagonal closest packing (HCP) lattice structure of the material. Calamaz et. al. [156] and Sima and Ozel [157] modified the Johnson-Cook constitutive model for high cutting speed machining. These models take into account of the phenomenon of strain softening due to adiabatic shear bands. They are useful to model serrated chips at high cutting conditions.

Being a numerically robust constitutive material model and highly utilized in finite element modeling, the Johnson-Cook model is used in this study. In addition to that, cutting speed between 25 and 45 m/min were used in the experimental drilling tests and continuous chip formation was observed. Typically beyond 60 m/min, serrated chips are formed and the adiabatic shear bands should be taken into account in machining of titanium alloys. Since the range of cutting speed is below this limit in this study, Johnson Cook material model is more suitable in definition of the material behaviour.

Typical stress-strain behaviour of a ductile material undergoing damage is shown in Figure 4-2. In an elastoplastic metallic material with hardening, damage can be observed in two forms: softening in the yield stress and degradation of the elasticity. The solid curve (B-C-D) in Figure 4-2 represents the damaged stress-strain response, while the dashed curve (B-C^{l}) is the response in the absence of damage.

In the Johnson-Cook constitutive model, the flow stress is defined as a function of strain, strain rate and temperature as described in Eq. (2-5) in order to reflect the strain-rate hardening and thermal softening [171].

$$\bar{\sigma} = \left[A + B(\bar{\varepsilon})^{n} \right] \left[1 + C \ln \left(\frac{\dot{\bar{\varepsilon}}}{\dot{\bar{\varepsilon}}_0} \right) \right] \left[1 - \left(\frac{T - T_0}{T_m - T_0} \right)^{m} \right] \qquad \textbf{Eq. (4.1)}$$

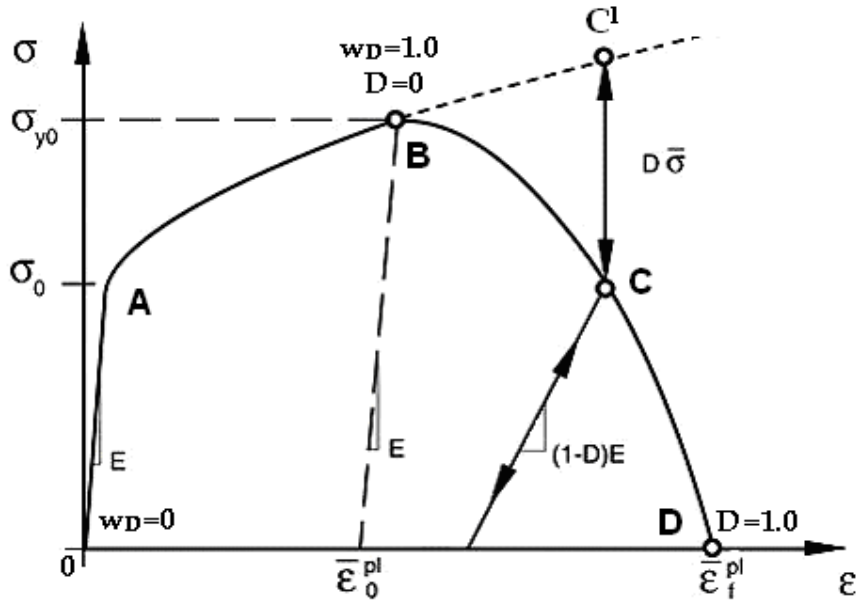

Figure 4-2: Stress-Strain Diagram of a Ductile Material

In Eq. (2-5) the parameter *A* is the initial yield strength of the material at room temperature and B is the hardening coefficients. The equivalent plastic strain rate, $\dot{\bar{\varepsilon}}$, is normalized with the reference strain rate, $\dot{\bar{\varepsilon}}_0$. T is the current temperature of the material, T_0 is room temperature, and T_m is the melting temperature of the material. The parameter n, m and C take into account the strain hardening effect, the thermal softening effect and strain rate sensitivity,

respectively. These constants can be evaluated from Split-Hopkinson dynamic bar tests.

4.1.2 Failure Analysis (Damage Initiation)

Machining is a metal removing process in which the desired shape is produced by removing the unwanted material from the workpiece. In a traditional machining process, such as drilling and turning, a cutting tool removes the material in the form of chip. A separation criteria or a damage law is needed to model fracture of material. Since the visual segmentation of chip formation requires very high density of mesh, it is not feasible by means of computational time in a 3-D drilling operation. Thus modelling of chip formation is only considered as removing the fractured elements from the workpiece by proper failure laws.

Constitutive material model for titanium alloy is dependent on strain rate and temperature as explained above. In the modelling of failure, a model which is dependent on strain rate and temperature is required. In order to model such behaviour, Johnson-Cook failure model is used in the study to utilize with the Johnson-Cook constitutive material model. The damage initiation is derived from Eq. (4.2). When the damage initiation criterion, w_D, reaches to 1.0 at point B in Figure 4-2, the damage has initiated and the fracture occurs.

$$w_D = \int \frac{d\bar{\varepsilon}^{pl}}{\bar{\varepsilon}_f^{pl}} \qquad \textbf{Eq. (4.2)}$$

In the equation above the equivalent plastic strain at failure, $\bar{\varepsilon}_f^{pl}$, is calculated from Eq. (2-28).

$$\bar{\varepsilon}_f^{pl} = \left[d_1 + d_{2\exp}\left(d_3 \frac{p}{q} \right) \right] \left[1 + d_4 \ln\left(\frac{\dot{\bar{\varepsilon}}^{pl}}{\dot{\varepsilon}_0} \right) \right] \left(1 + d_5 \frac{T - T_{rf}}{T_m - T_{rf}} \right) \qquad \textbf{Eq. (4.3)}$$

4.1.3 Material Property Degradation (Damage Evolution)

Material property degradation is utilized to model material behaviour after failure initiation. As shown in Figure 4-2, the solid curve (B-C-D) represents the damaged stress-strain response in a typical ductile material. The degradation rule accounts for the damage evolution by stiffness and stress degradation.

The overall damage variable, D, is equal to zero prior to damage. As fracture initiated at B as shown in Figure 4-2, overall damage variable is activated to form the stiffness of and strength of the damaged elements. When the overall damage variable reaches 1.0, the failure reaches the ultimate point and the elements are assumed fully damaged at point D in Figure 4-2. Beyond the onset of damage initiation point, B, the effective stress of an element is computed as below:

$$\bar{\sigma} = (1 - D)\sigma \qquad \textbf{Eq. (4.4)}$$

The evolution of the damage can be specified by either the energy criteria or plastic displacement criteria. In this study the plastic displacement criteria is used in the damage evolution.

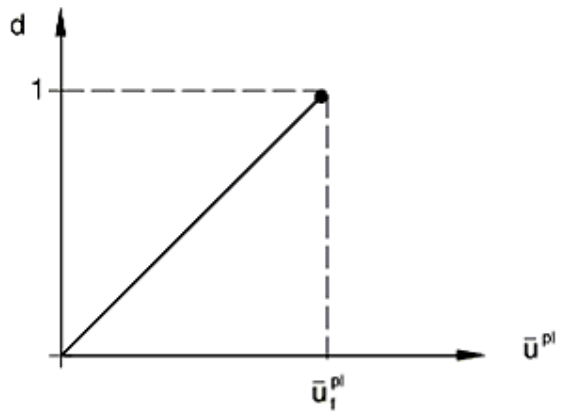

Figure 4-3: Damage Evolution by Displacement

The progressive damage evolution is assumed linear with the plastic displacement as shown in Figure 4-3. The evolution of the damage is specified with the displacement criteria and the damage evolution operator, D, can be computed from the following equation.

$$D = \frac{L_c \bar{\varepsilon}^{pl}}{\bar{u}_f^{pl}} = \frac{\bar{u}^{pl}}{\bar{u}_f^{pl}} \qquad \textbf{Eq. (4.5)}$$

The equivalent plastic displacement at failure, $\bar{u}_f^{pl}$, depends on the characteristic length, Lc, of the element. The use of stress-strain relation based damage model introduces a strong mesh dependency. It requires relatively refined mesh so that the energy dissipation decreases.

4.2 Progressive Damage Modeling of CFRP (Intra-Laminar Behaviour)

In order to model intra-laminar behaviour of CFRP workpiece, a meso-level discrete model is used in the study. Each unidirectional fibre reinforced ply is modelled individually and combined with cohesive interfaces to form CFRP workpiece. This meso-level model enables to analyse intra-laminar and inter-laminar levels behaviours separately. The overall laminated CFRP structure is shown in Figure 4-4.

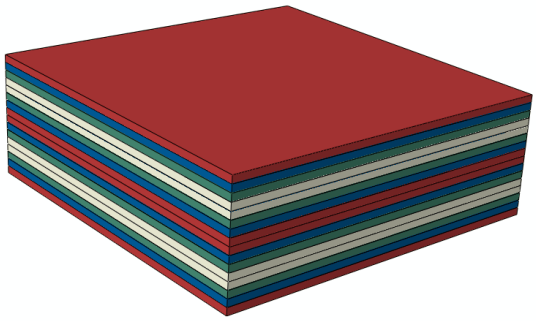

Figure 4-4: Meso Level Composite Lamina Model

In Figure 4-4, each different coloured structure symbolises a unidirectional fibre reinforced epoxy. The interfaces between each of them are the cohesive zone where the delamination is expected. A unidirectional ply is shown in Figure 4-5. The x, y and z axes are the longitudinal, transverse and normal directions, respectively.

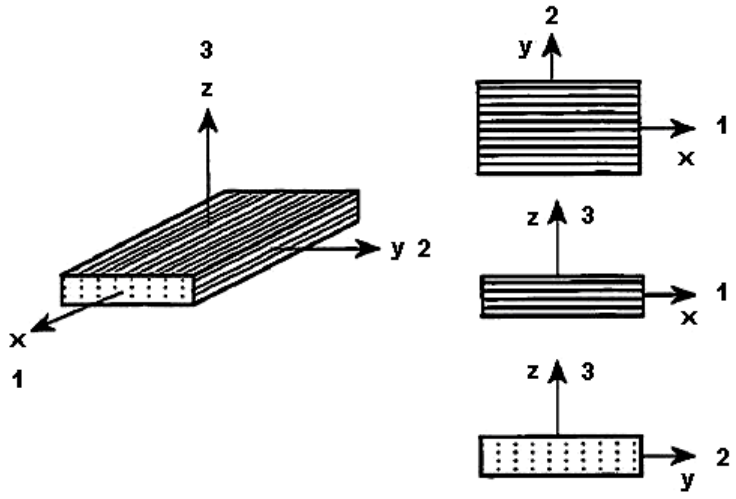

Figure 4-5: Unidirectional Composite Ply

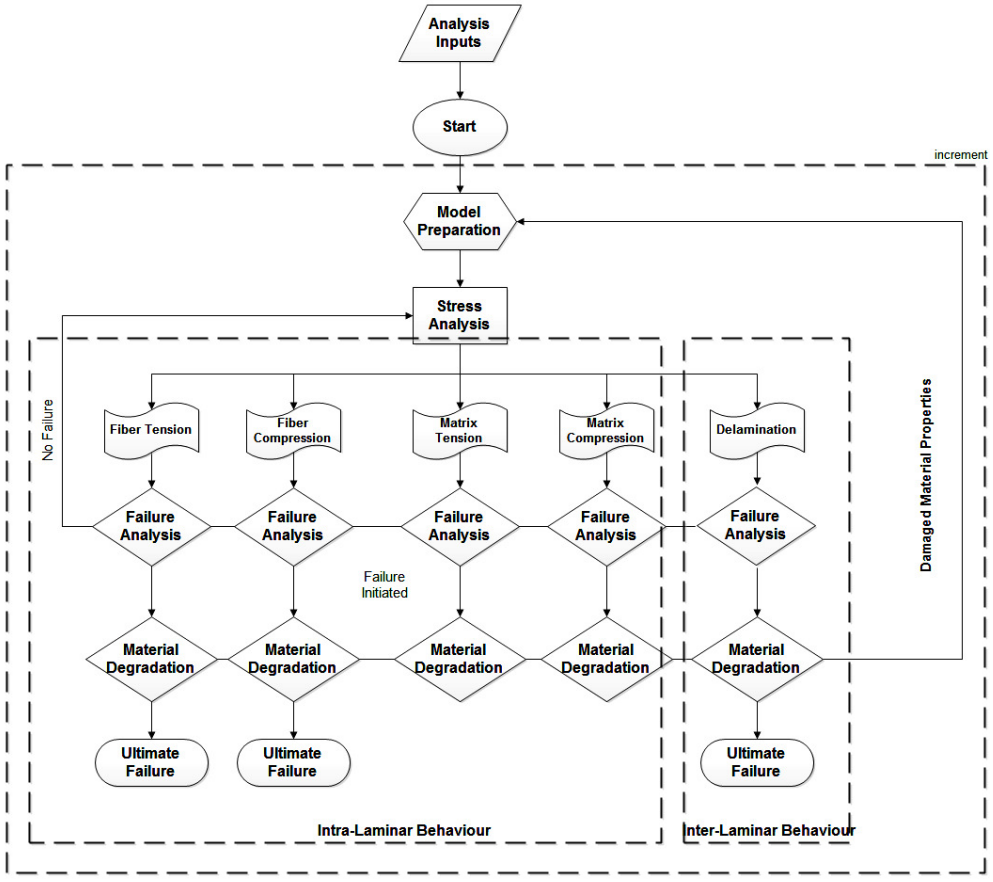

Figure 4-6: Flowchart of progressive damage model of unidirectional ply

Figure 4-6 shows the progressive damage model for a unidirectional fibre reinforced composite. The material data, boundary and contact conditions of the problem are employed to the input file at the beginning of the analysis. As

the boundary conditions are applied in the increment, deformation is induced and the stress analysis is utilized. In addition to that failure analysis is performed for both levels; intra-laminar and inter-laminar material behaviours separately by taking into account of the different failure modes. When any failure criterion is reached in certain elements, material degradation analysis is employed for the specific element. The material stiffness and state of stress are updated. In the case of catastrophic level of failure, ultimately failed elements are removed from the analysis.

4.2.1 Stress Analysis (Constitutive Model)

4.2.1.1 Solid-Like (Continuum Shell) Framework

Each individual unidirectional CFRP ply is modelled as a linear elastic material with orthotropic behaviour prior to failure in any mode. Then fibre orientations are specified for each ply individually. The stress-strain relations can be expressed by Eq. (4.6).

$$[\sigma] = [C_m][\varepsilon] \qquad \textbf{Eq. (4.6)}$$

$$\begin{bmatrix} \sigma_{11} \\ \sigma_{22} \\ \tau_{12} \end{bmatrix} = \begin{bmatrix} \frac{E_1}{1-\upsilon_{12}\upsilon_{21}} & \frac{\upsilon_{21}E_1}{1-\upsilon_{12}\upsilon_{21}} & 0 \\ \frac{\upsilon_{12}E_2}{1-\upsilon_{12}\upsilon_{21}} & \frac{E_2}{1-\upsilon_{12}\upsilon_{21}} & 0 \\ 0 & 0 & G_{12} \end{bmatrix} \begin{bmatrix} \varepsilon_{11} \\ \varepsilon_{22} \\ \gamma_{12} \end{bmatrix} \qquad \textbf{Eq. (4.7)}$$

where 11 and 22 denote local longitudinal and transverse directions respectively.

The finite elements in this framework are based on first-order transverse shear flexible theory in which the transverse shear strain is assumed to be constant through the thickness of the shell. Therefore they require out-of-plane shear stiffness correction factors. For a homogeneous material with a linear, orthotropic elasticity the transverse shear stiffness are expressed as below.

$$K_{11} = \frac{5}{6} G_{13} T_0$$
$$K_{22} = \frac{5}{6} G_{23} T_0 \qquad \textbf{Eq. (4.8)}$$

Where T_0 is the thickness of a unidirectional ply.

4.2.1.2 Solid (Three dimensional) Framework

Orthotropic material properties are assigned to each unidirectional composite lamina according to the fibre orientation by using a pre-defined local coordinate system. Linear elastic material behaviour is assumed prior to any damage and the stress-strain relation can be formulised as below.

$$\begin{bmatrix} \sigma_{11} \\ \sigma_{22} \\ \sigma_{33} \\ \sigma_{12} \\ \sigma_{31} \\ \sigma_{23} \end{bmatrix} = \begin{bmatrix} \frac{1-\nu_{23}\upsilon_{32}}{E_2E_3\Delta} & \frac{\nu_{21}+\nu_{31}\upsilon_{23}}{E_2E_3\Delta} & \frac{\nu_{31}+\nu_{23}\upsilon_{32}}{E_2E_3\Delta} & 0 & 0 & 0 \\ \frac{\nu_{12}+\nu_{13}\upsilon_{32}}{E_3E_1\Delta} & \frac{1-\nu_{31}\upsilon_{13}}{E_3E_1\Delta} & \frac{\nu_{32}+\nu_{31}\upsilon_{21}}{E_3E_1\Delta} & 0 & 0 & 0 \\ \frac{\nu_{13}+\nu_{12}\upsilon_{23}}{E_1E_2\Delta} & \frac{\nu_{23}+\nu_{13}\upsilon_{21}}{E_1E_2\Delta} & \frac{1-\nu_{12}\upsilon_{21}}{E_1E_2\Delta} & 0 & 0 & 0 \\ 0 & 0 & 0 & 2G_{12} & 0 & 0 \\ 0 & 0 & 0 & 0 & 2G_{31} & 0 \\ 0 & 0 & 0 & 0 & 0 & 2G_{23} \end{bmatrix} \begin{bmatrix} \varepsilon_{11} \\ \varepsilon_{22} \\ \varepsilon_{33} \\ \varepsilon_{12} \\ \varepsilon_{31} \\ \varepsilon_{23} \end{bmatrix} \qquad \textbf{Eq. (4.9)}$$

Where

$$\Delta = \frac{1-\nu_{12}\nu_{21}-\nu_{23}\nu_{32}-\nu_{31}\nu_{13}-2\nu_{12}\nu_{23}\nu_{31}}{E_1E_2E_3} \qquad \textbf{Eq. (4.10)}$$

4.2.2 Failure Analysis of Composite Plies (Damage Initiation)

There are many proposed failure theories to predict the onset of failures and their progression in composites. Most of the failure criteria are based on the stress state of a laminate rather than individual plies. Those failure criteria are intended to predict the macroscopic failures, therefore microscopic damages such as debonding of a fibre from the matrix cannot be determined. Failure criteria of composite materials can be divided into two main groups; independent failure criteria and polynomial failure criteria.

The maximum stress criteria and the maximum strain criteria are the examples of the independent failure criteria. In these criteria, there is not any dependence between the stress and strain components. This means any component in the longitudinal direction does not affect the component in the transverse direction or stacking direction. Polynomial maximum stress criterion, Polynomial maximum strain criterion, Tsai [173], Hill [174], Tsai-Azzi [175], Hoffman [176], Tsai-Wu [177], Hashin [178-179] criteria and World-Wide Failure-Exercise (WWFE) [180] are the examples of the polynomial failure criteria. In all these criteria, there is dependence between the components in each direction. However, in all above Hashin criteria and WWFE can predict the initial failure regarding to the mode of failure namely fibre and matrix. In other words, only Hashin criteria and WWFE can distinguish failure modes among the failure criteria above. Since only Hashin criteria is available in Abaqus software, Hashin criteria was chosen for damage criteria in CFRP.

Due to the fact that fibre composites consist of mechanically dissimilar phases such as stiff elastic brittle fibres and soft matrix, the failure occurs significantly different for each constituent. Fibres may rupture in tension or buckle in compression and the matrix may fail due to the transferred load from the fibres. Moreover, failure mechanisms are different in tension and compression in each direction. Since Hashin criteria are capable of distinction of different modes of failure and are compatible with finite elements analysis, they are utilized under multi-axial state of loading in analysis of drilling of CFRP.

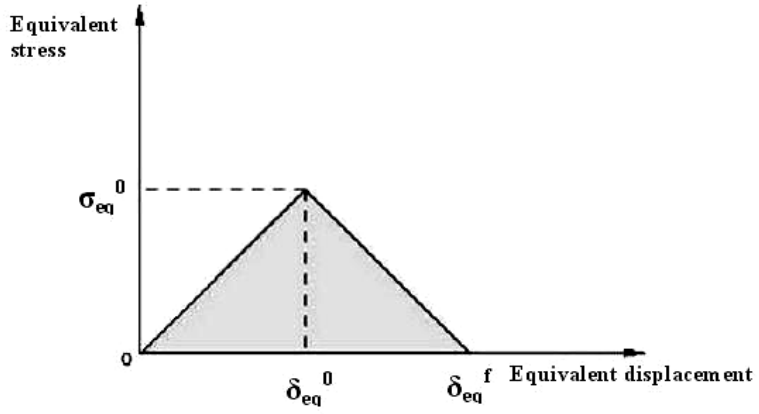

Figure 4-7: Equivalent Stress-Displacement Diagram of a Unidirectional Ply

Typical stress-displacement behaviour of such material is shown in Figure 4-7. The positive slope of the stress-displacement graph presents the material behaviour prior to damage initiation; the negative slope of the graph displays the damage evolution after damage initiation in any mode. Typically, in brittle materials, the degradation occurs very suddenly after the damage initiation point.

4.2.2.1 Solid-Like (Continuum Shell) Framework

The damage initiation criteria for unidirectional fibre reinforced plastic composites are based on Hashin theory [178-179]. The initiation behaviour is also assumed to be orthotropic in each mode and the initiation criteria consider four different damage initiation mechanisms namely fibre tension, fibre compression, matrix tension, and matrix compression.

Fibre Tension

Fibre tension failure mode $(\sigma_{11} > 0)$ of a unidirectional ply under a multi-axial state of stress is expressed with the following criterion:

$$F_{fb}^{T} = \left(\frac{\sigma_{11}}{\sigma_{11}^{f,T}}\right)^2 + \alpha\left(\frac{\tau_{12}}{\tau_{12}^{f}}\right)^2 \qquad \textbf{Eq. (4.11)}$$

where $\sigma_{11}^{f,T}$, σ_{11}, τ_{12}^{f}, τ_{12}, α are the longitudinal tensile strength, longitudinal normal stress, the in-plane shear strength in x-y plane, in-plane shear stress in x-y plane and the coefficient of shear interaction of a unidirectional ply, respectively. F, T, fb and f denote failure index, tension, fibre and failure, respectively. It must be mentioned that fibre tension failure is a catastrophic failure type which means that the ply cannot carry any type of combination of load and stress thereafter. Thus material properties are degraded completely and the ply fail catastrophically. When fibre tension failure index reaches 1.0, the failure is initiated in this mode. As failure is completed in element in this mode, the stress of the related element set to zero and element is deactivated in the analysis.

Fibre Compression

Fibre compression failure mode $(\sigma_{11} \leq 0)$ of a unidirectional ply under a multi-axial state of stress is given with the following criterion:

$$F_{fb}^{C} = \left(\frac{\sigma_{11}}{\sigma_{11}^{f,C}} \right)^2 \qquad \textbf{Eq. (4.12)}$$

where $\sigma_{11}^{f,C}$ and σ_{11} are the longitudinal compressive strength and longitudinal normal stress of a unidirectional ply, respectively. F, C, fb and f denote failure index, compression, fibre and failure, respectively. As noticed from Eq. (4.12) this mode of failure does not consider interaction of shear stress term since the effect of shear stress on the compressive behaviour of a unidirectional ply is not well understood. It must be added that the fibre compression failure is also a catastrophic failure mode. The failed ply under this failure mode cannot of carry any stress thereafter. When fibre compression failure index reaches 1.0, failure is initiated in this mode.

Matrix Tension

Matrix tension failure mode $(\sigma_{22} > 0)$ of a unidirectional ply under a multi-axial state of stress is derived with the following criterion:

$$F_{m}^{T} = \left(\frac{\sigma_{22}}{\sigma_{22}^{f,T}} \right)^2 + \left(\frac{\tau_{12}}{\tau_{12}^{f}} \right)^2 \qquad \textbf{Eq. (4.13)}$$

where $\sigma_{22}^{f,T}$, σ_{22}, τ_{12}^{f} and τ_{12} are the transverse tensile strength, transverse normal stress, the in-plane shear strength in x-y plane and in-plane shear stress in x-y plane of a unidirectional ply, respectively. F, T, m and f denote failure index, tension, matrix and failure, respectively. When matrix tension failure index reaches 1.0, the failure is initiated in this mode.

Matrix Compression

Matrix compression failure mode $(\sigma_{22} \leq 0)$ of a unidirectional ply under a multi-axial state of stress is expressed as below:

$$F_{m}^{C} = \left(\frac{\sigma_{22}}{2\tau_{12}^{f}} \right)^2 + \left[\left(\frac{\sigma_{22}^{f,C}}{2\tau_{12}^{f}} \right)^2 - 1 \right] \frac{\sigma_{22}}{\sigma_{22}^{f,C}} + \left(\frac{\tau_{12}}{\tau_{12}^{f}} \right)^2 \qquad \textbf{Eq. (4.14)}$$

where $\sigma_{22}^{f,C}$, σ_{22}, τ_{12}^{f} and τ_{12} are the transverse compressive strength, transverse normal stress, the in-plane shear strength in x-y plane and in-plane shear stress in x-y plane of a unidirectional ply, respectively. F, C, m and f denote failure index, compression, matrix and failure, respectively. When matrix compression failure index reaches 1.0, the failure is initiated in this mode.

4.2.2.2 Solid (Three dimensional) Framework

The intra laminar damage initiation criteria for unidirectional fibre reinforced plastic composites in 3-D case are based on Hashin theory [179]. The initiation behaviours are assumed to be orthotropic. The initiation criteria consider four different damage initiation mechanisms namely fibre tension, fibre compression, matrix tension, and matrix compression by taking into accounts of the out-plane effects.

Fibre Tension

Fibre tension failure mode $(\sigma_{11} > 0)$ of a unidirectional ply under a multi-axial state of stress is expressed with the following criterion:

$$F_{fb}^{T} = \left(\frac{\sigma_{11}}{\sigma_{11}^{f,T}}\right)^2 + \alpha\left(\frac{\tau_{12}}{\tau_{12}^{f}}\right)^2 + \beta\left(\frac{\tau_{13}}{\tau_{13}^{f}}\right)^2 \qquad \textbf{Eq. (4.15)}$$

where $\sigma_{11}^{f,T}$, σ_{11}, τ_{12}^{f}, τ_{12}, τ_{13}^{f}, τ_{13}, α and β are the longitudinal tensile strength, longitudinal normal stress, the in-plane shear strength in x-y plane, in-plane shear stress in x-y plane, the out-of-plane shear strength in x-z plane, out-of-plane shear stress in x-z plane, the coefficient of x-y shear interaction and the coefficient of x-z shear interaction of a unidirectional ply, respectively. F, T, fb and f denote failure index, tension, fibre and failure, respectively. As it is expressed in Eq. (4.15) out-of-plane effects are included as well. It must be mentioned that fibre tension failure is a catastrophic failure type which means that the ply cannot carry any type of combination of load and stress thereafter. Thus material properties are degraded completely and the ply fail catastrophically. Finite elements are deactivated as they fail in this mode. When fibre tension failure index reaches 1.0, the failure is initiated in this mode.

Fibre Compression

Fibre compression failure mode ($\sigma_{11} \leq 0$) of a unidirectional ply under a multi-axial state of stress is given with the following criterion:

$$F_{fb}^{C} = \left(\frac{\sigma_{11}}{\sigma_{11}^{f,C}} \right)^2 \qquad \textbf{Eq. (4.16)}$$

where $\sigma_{11}^{f,T}$ and σ_{11} are the longitudinal compressive strength and longitudinal normal stress of a unidirectional ply, respectively. F, C, fb and f denote failure index, compression, fibre and failure, respectively. As it can be noticed from the Eq. (6) this mode of failure does not consider interactions of shear stresses since the effects of in-plane and out-plane shear stresses on the compressive behaviour of a unidirectional ply are not well understood. It must be added that the fibre compression failure is also a catastrophic failure mode. The failed ply under this failure mode cannot of carry any stress thereafter. When fibre compression failure index reaches 1.0, the failure is initiated in this mode.

Matrix Tension

Matrix tension failure mode $(\sigma_{22} + \sigma_{33}) > 0$ of a unidirectional ply under a multi-axial state of stress is derived with the following criterion:

$$F_{m}^{T} = \left(\frac{1}{\sigma_{22}^{f,T}} \right)^2 (\sigma_{22} + \sigma_{33})^2 + \left(\frac{1}{\tau_{23}^{f}} \right)^2 (\tau_{23}^2 - \sigma_{22}\sigma_{33}) + \left(\frac{1}{\tau_{12}^{f}} \right)^2 (\tau_{12}^2 + \tau_{13}^2) \qquad \textbf{Eq. (4.17)}$$

where $\sigma_{22}^{f,T}$, σ_{22}, σ_{33}, τ_{12}^{f}, τ_{12}, τ_{23}^{f} and τ_{13} are the transverse tensile strength, transverse normal stress in y direction, transverse normal stress in z direction, the in-plane shear strength in x-y plane, in-plane shear stress in x-y plane, the out-of-plane shear strength in y-z plane and out-of-plane shear stress in x-z plane of a unidirectional ply, respectively. F, T, m and f denote failure index, tension, matrix and failure, respectively. When matrix tension failure index reaches 1.0, the failure is initiated in this mode.

Matrix Compression

Matrix compression failure mode $(\sigma_{22} + \sigma_{33}) \leq 0$ of a unidirectional ply under a multi-axial state of stress is expressed in Eq. (4.18).

$$F_m^C = \left(\frac{1}{\sigma_{22}^{f,C}}\right)\left[\left(\frac{\sigma_{22}^2}{2\tau_{23}}\right)^2 - 1\right]\left(|\sigma_{22}+\sigma_{33}|\right) + \left(\frac{1}{2\tau_{23}^f}\right)^2(\sigma_{22}+\sigma_{33})^2 + \left(\frac{1}{\tau_{23}^f}\right)^2\left(\tau_{23}^2 - \sigma_{22}\sigma_{33}\right) + \left(\frac{1}{\tau_{12}^f}\right)^2\left(\tau_{12}^2+\tau_{13}^2\right) \quad \textbf{Eq. (4.18)}$$

where $\sigma_{22}^{f,C}$, σ_{22}, σ_{33}, τ_{12}^f, τ_{12}, τ_{23}^f and τ_{13} are the transverse tensile strength, transverse normal stress in y direction, transverse normal stress in z direction, the in-plane shear strength in x-y plane, in-plane shear stress in x-y plane, the out-of-plane shear strength in y-z plane and out-of-plane shear stress in x-z plane of a unidirectional ply, respectively. F, C, m and f denote failure index, compression, matrix and failure, respectively. When matrix compression failure index reaches 1.0, the failure is initiated in this mode.

4.2.3 Material Property Degradation (Damage Evolution)

In this section, material property degradation rules are established for each failure mode of a unidirectional ply under a multi-axial state stress to model intra-laminar behaviour of unidirectional ply. After failure occurrence in any mode of a unidirectional ply, the failed region of the ply is replaced by degraded material properties according to the rules of the failure mode. When a catastrophic failure occurs, the whole material is damaged completely and cannot sustain any more stress and load. The mathematical approaches are adopted for solid like and fully solid frameworks of a unidirectional ply in each failure mode.

4.2.3.1 Solid-Like (Continuum Shell) Framework

As explained in the previous subsections, when the Hashin failure criteria have been fulfilled in any mode, damage has initiated and evolution has started in that specific mode. The damage operator becomes significant in the criteria for damage initiation of other modes. The effective stress can be computed by Eq. (4.19).

$$\bar{\sigma} = C_d \varepsilon \quad \textbf{Eq. (4.19)}$$

$$\begin{bmatrix}\sigma_{11}\\ \sigma_{22}\\ \sigma_{12}\end{bmatrix}=\begin{bmatrix}\frac{(1-d_{fb})E_1}{\Delta} & \frac{(1-d_{fb})(1-d_m)\upsilon_{21}E_1}{\Delta} & 0\\ \frac{(1-d_{fb})(1-d_m)\upsilon_{12}E_2}{\Delta} & \frac{(1-d_m)E_2}{\Delta} & 0\\ 0 & 0 & (1-d_s)G_{12}\end{bmatrix}\begin{bmatrix}\varepsilon_{11}\\ \varepsilon_{22}\\ \varepsilon_{12}\end{bmatrix} \quad \textbf{Eq. (4.20)}$$

$$\Delta = 1-(1-d_{fb})(1-d_m)\upsilon_{12}\upsilon_{21} \quad \textbf{Eq. (4.21)}$$

Where $\bar{\sigma}$ C_d, d_{fb}, d_m and d_s are the effective stress, stiffness matrix after failure initiation in any mode of unidirectional ply, fibre damage variable, matrix damage variable and shear damage variable.

Fibre tension failure mode and fibre compression failure mode of a unidirectional ply as given by Eq. (4.11) and Eq. (4.12) are a catastrophic mode of failure and when it occurs, the failed material cannot carry any type or combination of load. Since these failure modes are catastrophic, the other failure modes do not need to be verified. Sudden degradation rules are utilized in material property degradation of a unidirectional ply under multi-axial state of stress. Thus, all material properties of the failed ply are reduced to zero. The fibre modes are the dominant failure modes in the composite structure, so the failed regions are deactivated in the finite element analysis and removed from the area in order to model chip removal.

As expressed by Eq. (4.13) and Eq. (4.14), matrix tension failure mode and matrix compression failure mode of a unidirectional ply affect the behaviour of the unidirectional ply in matrix direction and its interactions. They are not catastrophic failure modes, so only material properties in transverse directions and their interactions are degraded, other material properties are left unchanged. The other modes of failure must be verified.

The damage variables of stiffness matrix for a particular mode can be defined as defined in Eq. (4.22)

$$d_{fb}=\begin{cases}0 & if\ \bar{\sigma}_{11}\rangle 0\ \ and\ \ F_{fb}^{T}\langle 1,\\ 1 & if\ \bar{\sigma}_{11}\rangle 0\ \ and\ \ F_{fb}^{T}\geq 1,\\ 0 & if\ \bar{\sigma}_{11}\leq 0\ \ and\ \ F_{fb}^{C}\langle 1,\\ 1 & if\ \bar{\sigma}_{11}\leq 0\ \ and\ \ F_{fb}^{C}\geq 1,\end{cases}$$

$$d_{m}=\begin{cases}0 & if\ \bar{\sigma}_{22}\rangle 0\ \ and\ \ F_{m}^{T}\langle 1,\\ 1 & if\ \bar{\sigma}_{22}\rangle 0\ \ and\ \ F_{m}^{T}\geq 1,\\ 0 & if\ \bar{\sigma}_{22}\leq 0\ \ and\ \ F_{m}^{C}\langle 1,\\ 1 & if\ \bar{\sigma}_{22}\leq 0\ \ and\ \ F_{m}^{C}\geq 1,\end{cases} \qquad \textbf{Eq. (4.22)}$$

$$d_{s}=1-(1-d_{fb})(1-d_{m})$$

where F, fb, m, s, C and T denote failure index, fibre, matrix, shear, compression and tension respectively.

4.2.3.2 Solid (Three dimensional) Framework

As explained in the previous subsections, when the Hashin failure criteria have been fulfilled in any mode, damage has initiated and evolution has started in that specific mode. In 3-D solid framework, the effects of out-of-plane are also included. The effective stress can be computed by the modified stiffness matrix as expressed in Eq. (4.23).

$$\bar{\sigma}=C_{d}\varepsilon \qquad \textbf{Eq. (4.23)}$$

$$\begin{bmatrix}\bar{\sigma}_{11}\\ \bar{\sigma}_{22}\\ \bar{\sigma}_{33}\\ \bar{\sigma}_{12}\\ \bar{\sigma}_{31}\\ \bar{\sigma}_{23}\end{bmatrix}=\begin{bmatrix}\frac{1-\nu_{23}\upsilon_{32}}{E_2^{*}E_3^{*}\Delta^{*}} & \frac{\nu_{21}+\nu_{31}\upsilon_{23}}{E_2^{*}E_3^{*}\Delta^{*}} & \frac{\nu_{31}+\nu_{23}\upsilon_{32}}{E_2^{*}E_3^{*}\Delta^{*}} & 0 & 0 & 0\\ \frac{\nu_{12}+\nu_{13}\upsilon_{32}}{E_3^{*}E_1^{*}\Delta^{*}} & \frac{1-\nu_{31}\upsilon_{13}}{E_3^{*}E_1^{*}\Delta^{*}} & \frac{\nu_{32}+\nu_{31}\upsilon_{12}}{E_3^{*}E_1^{*}\Delta^{*}} & 0 & 0 & 0\\ \frac{\nu_{13}+\nu_{12}\upsilon_{23}}{E_1^{*}E_2^{*}\Delta^{*}} & \frac{\nu_{23}+\nu_{13}\upsilon_{21}}{E_1^{*}E_2^{*}\Delta^{*}} & \frac{1-\nu_{12}\upsilon_{21}}{E_1^{*}E_2^{*}\Delta^{*}} & 0 & 0 & 0\\ 0 & 0 & 0 & 2G_{12}^{*} & 0 & 0\\ 0 & 0 & 0 & 0 & 2G_{31}^{*} & 0\\ 0 & 0 & 0 & 0 & 0 & 2G_{23}^{*}\end{bmatrix}\begin{bmatrix}\varepsilon_{11}\\ \varepsilon_{22}\\ \varepsilon_{33}\\ \varepsilon_{12}\\ \varepsilon_{31}\\ \varepsilon_{23}\end{bmatrix} \qquad \textbf{Eq.(4.24)}$$

Where;

$$\Delta^* = \frac{1-\nu_{12}\nu_{21}-\nu_{23}\nu_{32}-\nu_{31}\nu_{13}-2\nu_{12}\nu_{23}\nu_{31}}{E_1^* E_2^* E_3^*}$$

$$\begin{aligned} E_1^* &= E_1(1-d_{fb}) \\ E_2^* &= E_2(1-d_{fb})(1-d_m) \\ E_3^* &= E_3(1-d_{fb})(1-d_m) \\ G_{12}^* &= G_{12}(1-d_s) \\ G_{31}^* &= G_{31}(1-d_s) \\ G_{23}^* &= G_{23}(1-d_s) \end{aligned} \qquad \textbf{Eq. (4.25)}$$

As given by Eq. (4.15) and Eq. (4.16), fibre tension failure mode and fibre compression failure mode of a unidirectional ply are a catastrophic mode of failure in unidirectional fibre oriented composite ply. When it occurs, the material cannot carry any type or combination of load in any direction or mode. Since these failure modes are catastrophic, matrix tension and matrix compression modes do not need to be verified. Sudden degradation rules are utilized in material property of a unidirectional ply under multi-axial state of stress. Thus, all material properties of the failed ply are reduced to zero in any fibre failure mode. The fibre modes are the dominant failure modes in the composite structure, so the failed regions are deactivated in the finite element analysis and removed from the area in order to model chip removal.

Matrix modes are the combinations of both transverse directions. Matrix tension failure mode (given by Eq. 4.17) and matrix compression failure mode (given by Eq. 4.18) of a unidirectional ply control the behaviour of the unidirectional ply in both transverse directions and their interactions with the fibre direction behaviour. Matrix failure modes are not catastrophic failure modes, so only material properties in transverse directions and their interactions are degraded whereas material properties in fibre directions are left unchanged. The other modes of failure must be verified for the state of catastrophic failure.

The damage variables of stiffness matrix for particular modes can be expressed by Eq. 4.26.

$$d_f = \begin{cases} 0 & if\ \bar{\sigma}_{11} \rangle 0\ \ and\ \ F_{fb}^{T} \langle 1, \\ 1 & if\ \bar{\sigma}_{11} \rangle 0\ \ and\ \ F_{fb}^{T} \geq 1, \\ 0 & if\ \bar{\sigma}_{11} \leq 0\ \ and\ \ F_{fb}^{C} \langle 1, \\ 1 & if\ \bar{\sigma}_{11} \leq 0\ \ and\ \ F_{fb}^{C} \geq 1, \end{cases}$$

$$d_m = \begin{cases} 0 & if\ (\bar{\sigma}_{22} + \bar{\sigma}_{33}) \rangle 0\ \ and\ \ F_{m}^{T} \langle 1, \\ 1 & if\ (\bar{\sigma}_{22} + \bar{\sigma}_{33}) \rangle 0\ \ and\ \ F_{m}^{T} \geq 1, \\ 0 & if\ (\bar{\sigma}_{22} + \bar{\sigma}_{33}) \leq 0\ \ and\ \ F_{m}^{C} \langle 1, \\ 1 & if\ (\bar{\sigma}_{22} + \bar{\sigma}_{33}) \leq 0\ \ and\ \ F_{m}^{C} \geq 1, \end{cases} \qquad \textbf{Eq. (4.26)}$$

$$d_s = 1 - (1 - d_f)(1 - d_m)$$

4.3 Progressive Damage Modeling of Interfaces (Inter-Laminar Behaviour)

Inter-laminar damage, delamination, is one of the predominant defects in a composite structure. Lack of reinforcement in thickness direction and weak inter-laminar shear strengths are the main reasons of delamination. Delamination can cause a significant reduction, particularly in the compressive load capacity of the structure. The fracture process of composite laminates requires both inter-laminar and intra-laminar damage mechanisms. Therefore, UD laminated composite work piece is composed of stacked plies with specified fibre orientations and interfaces between these plies.

Techniques such as the Virtual Crack Closure Technique (VCCT) [181-182], the J- integral method [183], the virtual crack extension [184] and stiffness derivative [185] based on Linear Elastic Fracture Mechanics (LEFM) have often been used to predict delamination growth owing to be effective. However, these techniques cannot be applied without an initial crack to predict delamination growth [186-187].

Cohesive zone formulations are utilized to predict onset of delamination and growth of delamination. There are two main strategies in the literature to implement cohesive zone formulations: discrete finite thickness cohesive zone (inter-laminar cohesive elements) and discrete zero thickness cohesive zone (inter-laminar cohesive surfaces). In finite thickness cohesive zone, inter-

laminar cohesive elements between plies are used and cracks develop on these cohesive elements. This approach is widely used in analysis of delamination [122-124, 188-202]. In zero thickness cohesive zone (inter-laminar cohesive surfaces), the discontinuity, in other words delamination, is advanced on the zero thickness cohesive surfaces which are located at the interfaces of the plies [203-209]. The advantage of the latter method is mesh independency. Both technique are used in this study and explained in the following subsections.

4.3.1 Stress Analysis (Constitutive Model)

Cohesive zone formulations are utilized to predict onset of delamination and growth of delamination. The traction-separation cohesive behaviour is shown in Figure 4-8.

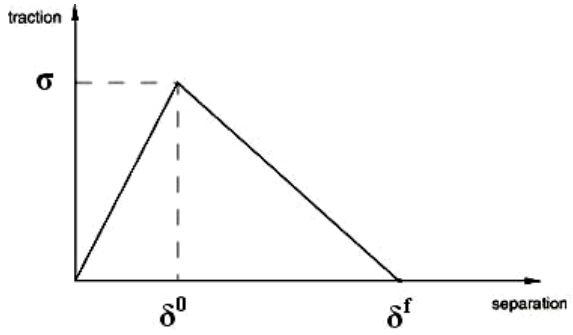

Figure 4-8: Traction-Separation Response in Cohesive Zone

4.3.1.1 Finite Thickness Cohesive Zone (Cohesive Elements)

Framework

In this method, finite thickness cohesive elements have been used to model material discontinuities. Delamination is modelled by the use of cohesive elements between adjacent unidirectional plies where delamination is expected. The traction-separation cohesive material model assumes a linear elastic behaviour for the interface as shown in Figure 4-8. The stress-strain behaviour of the cohesive zone is defined as below.

$$[\sigma] = [K][\varepsilon] \qquad \textbf{Eq. (4.27)}$$

$$\begin{bmatrix}\sigma_n\\ \sigma_s\\ \sigma_t\end{bmatrix}=\begin{bmatrix}K_{nn} & 0 & 0\\ 0 & K_{ss} & 0\\ 0 & 0 & K_{tt}\end{bmatrix}\begin{bmatrix}\varepsilon_n\\ \varepsilon_s\\ \varepsilon_t\end{bmatrix} \quad \textbf{Eq. (4.28)}$$

Where

$$\varepsilon_i=\frac{\delta_i}{T_0} \qquad i=n,s,t \quad \textbf{Eq. (4.29)}$$

$$K_{nn}=\frac{E_3}{T_0}, \qquad K_{ss}=\frac{G_{13}}{T_0}, \qquad K_{tt}=\frac{G_{23}}{T_0} \quad \textbf{Eq. (4.30)}$$

Where σ, K and δ are traction stress, traction separation stiffness modulus and separation for normal and shear directions, respectively. n, s, t denote normal, shear on x-z and shear on y-z planes.

4.3.1.2 Zero-Thickness Cohesive Zone (Cohesive Surface)

Framework

Zero thickness surface-based cohesive behaviour approach is similar to the cohesive element approach proposed by Alfano and Crisfield [197, 210]. The bi-linear traction–separation law ensures a linear elastic response up to delamination initiation and expressed as below.

$$[\sigma]=[K][\delta] \quad \textbf{Eq. (4.31)}$$

$$\begin{bmatrix}\sigma_n\\ \sigma_s\\ \sigma_t\end{bmatrix}=\begin{bmatrix}K_{nn} & 0 & 0\\ 0 & K_{ss} & 0\\ 0 & 0 & K_{tt}\end{bmatrix}\begin{bmatrix}\delta_n\\ \delta_s\\ \delta_t\end{bmatrix} \quad \textbf{Eq. (4.32)}$$

Where σ, K and δ are traction stress, traction separation stiffness modulus and separation for normal and shear directions, respectively. n, s, t denote normal, shear on x-z and shear on y-z planes.

4.3.2 Failure Analysis (Damage Initiation)

Delamination damage is initiated when the specified failure criterion is met. Conventional stress-based failure criteria are utilized to predict failure initiation. These can be maximum traction criterion and quadratic traction criterion [211] as given in Eq (4.33) and Eq. (4.34), respectively. The latter is employed for the both cohesive zone technique to obtain more accurate result, however it must be noted that this could affect the solution time.

$$\max\left\{\frac{\langle\sigma_n\rangle}{\sigma_n^0},\frac{\sigma_s}{\sigma_s^0},\frac{\sigma_t}{\sigma_t^0}\right\}=1 \qquad \textbf{Eq. (4.33)}$$

$$\left\{\frac{|\sigma_n|}{\sigma_n^0}\right\}^2+\left\{\frac{\sigma_s}{\sigma_s^0}\right\}^2+\left\{\frac{\sigma_t}{\sigma_t^0}\right\}^2=1 \qquad \textbf{Eq. (4.34)}$$

4.3.3 Material Property Degradation (Damage Evolution)

In this section, material property degradation rule is established for cohesive zone of a unidirectional ply under a multi-axial state stress to model growth of damage in inter-laminar behaviour of a unidirectional ply. After failure is initiated, the failed region of the cohesive zone is replaced by degraded material properties. The mathematical approaches are valid for both finite thickness cohesive zone and zero thickness cohesive zone frameworks of a unidirectional ply.

As explained in the previous subsection, when the failure initiation criterion has been fulfilled, damage has initiated and evolution has started in cohesive zone. The damage operator D represents the overall damage in the material and the effective stress components of the cohesive model are calculated according to Eq. (4.35).

$$\begin{aligned}\overline{\sigma_n}&=\begin{cases}(1-D)\sigma_n, & \sigma_n\geq 0\\ \sigma_n & otherwise\end{cases}\\ \overline{\sigma_s}&=(1-D)\sigma_s,\\ \overline{\sigma_t}&=(1-D)\sigma_t,\end{aligned} \qquad \textbf{Eq. (4.35)}$$

The catastrophic failure criterion for damage propagation is expressed with power law criterion as given in Eq. (4.36).

$$\left\{\frac{G_n}{G_n^C}\right\}^{\alpha} + \left\{\frac{G_s}{G_s^C}\right\}^{\beta} + \left\{\frac{G_t}{G_t^C}\right\}^{\gamma} = 1 \qquad \textbf{Eq. (4.36)}$$

where G_n , G_s and G_t are the individual components of energy release rate in normal and shear directions, respectively. α, β and γ are material constants.

The behaviour of material degradation is assumed to be linear with the effective traction-separation behaviour and the damage operator is defined by Eq. (4.37).

$$D = \frac{\delta_m^f(\delta_m^{\max} - \delta_m^0)}{\delta_m^{\max}(\delta_m^f - \delta_m^0)} \qquad \textbf{Eq. (4.37)}$$

Where

$$\delta_m = \sqrt{\langle \delta_n \rangle^2 + \delta_s^2 + \delta_t^2} \qquad \textbf{Eq. (4.38)}$$

$$\delta_m^f = 2G^C / \sigma^0$$

$$G^C = G_n + G_s + G_t \qquad \textbf{Eq. (4.39)}$$

4.4 Requirements

In order to apply progressive damage modeling for the material behaviour of Ti-6Al-4V and CFRP in drilling process a complete set of material properties of both materials is prerequisite. Moreover each individual unidirectional ply must be defined with local fibre and matrix directions. The components of progressive damage modeling must be fully provided. In addition to that boundary and loading conditions must be fully characterized with the contact details. The proper set of computer resources and the connections between these resources, such as settings between programming tools and FE tools, are essentials. In the next chapter the finite element modeling with Abaqus software is explained, the selections are discussed and all these material parameters and related data for drilling of CFRP and Ti-6Al-4V are provided.

4.5 Summary

Three-dimensional finite element algorithms are developed for drilling of Ti-6Al-4V and CFRP in this chapter. First, progressive damage modeling of Ti-6Al-4V is introduced. The constitutive material models are summarized and the reason of specified model is explained. The plasticity is considered and the stress analysis is explained. The effects of strain rate and temperature on the state of stress and failure analysis are stated. The gradual material degradation is also established for Ti-6Al-4V. Later, progressive damage modeling of unidirectional CFRP is presented in meso level to detect intra and inter-laminar material response under multi-axial state of stress. The intra-laminar behaviour is acquainted ply by ply under multi-axial state of stress. The failure modes and related degradation rules of a unidirectional ply are explained in detail for solid-like and fully solid frameworks. Finally inter-laminar discontinuity, delamination, is described by the application of discrete cohesive zone. The components of progressive damage model are discussed for two different techniques; finite thickness and zero thickness cohesive zone frameworks. The traction-separation behaviours of cohesive structures are formulated at prior to damage. The failure initiation is defined and the material degradation with gradual stiffness and gradual strength degradations are established for interfaces of a unidirectional ply.

Chapter 5

Finite Element Modeling

The progressive damage analysis of CFRP and titanium alloy under multi-axis state of stress has been considered in detail in Chapter 4. In this chapter, finite element modelling of drilling process of fibre reinforced composite, Ti-6Al-4V and their stack are explained. The entire finite element analysis of drilling of CFRP and Ti-6Al-4V has performed to investigate of the effects of process parameters and cutting tool geometry on drilling.

The problem is described in Section 5.1, and the type of analysis and solution is considered in Section 5.2. The materials and related input data are given in Section 5.3. The geometry of workpieces and cutting tools, and mesh attributes are introduced in details in Section 5.4 and 5.5, respectively. The boundary conditions and related process parameters are described in Section 5.6 whereas the related contact between the workpieces and drill is explained in Section 5.7. Finally, Section 5.8 presents the extra finite element simulations to validate delamination model by Asymmetric Double Cantilever Beam (ADCB) tests.

5.1 Problem Description

Machining of materials is considerably complex and affected by several parameters. Drilling operation is dependant on the tribological interaction between the work piece material and tool material; cutting parameters such as cutting speed and feed rate; operation environment e.g., ph, temperature and existence of cutting fluid; and geometry of cutting tool. A complete experimental study is generally uneconomic by means of time and cost. Thus, finite element method (FEM) is required to simulate the drilling of materials with an advantage of parametric modelling.

A realistic finite element analysis should cover the above situations as much as possible. In this study, 3-D finite element models were developed using the commercial Computer Aided Engineering package Abaqus and Computer Aided Drawing package Solidworks. The aims of the finite element models were to model the drilling process, to simulate progressive damage initiation and evolution in the work piece material and to predict induced cutting force, torque and workpiece defects such as delamination and burr. The developed 3-D models should enable the investigation of the effects of process parameters on drilling process, thus the movement of the drill bit was modelled as in the real life via rotational and translational velocities. Moreover, the analysis should inspect the influences of tool geometry on drilling process. This requires the use of complex 3-D drill bits which increases the complexity of the problem however it was covered in the study. The limitations of the FE models were heat generation and chip formation. Since there was sufficient coolant used in the drilling experiments, heat generation was not taken into account. The modelling of chip formation was not considered due to requirement of very high density of mesh and adaptive remeshing. These techniques can avoid possible distortion problems in chip formation however it would increase the required computational time and resources exponentially. Details of the FE models are introduced in the following sections.

5.2 Analysis Type

Since cutting tool penetrates into material to remove unwanted material from the workpiece, the load does not remain static. The relative motion between cutting tool and workpiece, unstatic type of load, dynamic material behaviour under multi axis state of load and high strain rate deformation make drilling process a dynamic procedure. Thus a dynamic explicit finite element analysis approach has been proposed in this study.

Stability of the solution in finite element analysis is the only concern in an explicit integration, which requires very small time increments. The minimum time increment is the smallest transit time of a dilatational wave across of the smallest element size in the mesh. Therefore, it is dependent on the density and

the element size in the model. Typical minimum time increments were around 10^{-8} – 10^{-10} time unit in the proposed finite element models of drilling of CFRP and Ti-6Al-4V. In order to investigate the effects of process parameters, real time requirements have been used in the analysis, therefore FE models required relatively large computational times depending on the machining parameters. As time increment has been expressed to depend on the mesh, the element size should be defined by taking into account of the accuracy of the finite element analysis results and efficiency of the finite element approach. The optimisation of the element size in the finite element modelling has been investigated and will be discussed in the geometry subsection.

5.3 Materials

5.3.1 CFRP Workpiece

In the finite element analysis of drilling, a commercial carbon fibre reinforced composite material and commercial titanium alloy were used as work pieces. As it was explained in previous chapter, linear elastic material model with orthotropic behaviour was utilized for Hexcel T700GC M21 carbon fibre reinforced epoxy workpiece. The built-in Hashin Failure criteria were employed for solid-like (continuum shell) framework whereas a user subroutine was developed for the progressive failure of CFRP workpiece for solid framework. The required input data for the finite element analysis; material properties and damage properties of CFRP, are given in Table 5-1.

Table 5-1:The Material Properties of CFRP Workpiece [121, 162-163]

Constitutive Material Properties								
E_1 (GPa)	**E_2 (GPa)**	**E_3 (GPa)**	**G_{12} (GPa)**	**G_{13} (GPa)**	**G_{23} (GPa)**	**υ_{12}**	**υ_{13}**	**υ_{23}**
112	8.2	8.2	4.5	4.5	3	0.3	0.3	0.4
Damage Model Parameters								
$\sigma_{11}^{f,t}$ (MPa)	**$\sigma_{11}^{f,c}$ (MPa)**	**$\sigma_{22}^{f,t}$ (MPa)**	**$\sigma_{22}^{f,c}$ (MPa)**	**$\sigma_{33}^{f,t}$ (MPa)**	**$\sigma_{33}^{f,c}$ (MPa)**	**τ_{12}^{f} (MPa)**	**τ_{13}^{f} (MPa)**	**τ_{23}^{f} (MPa)**
1900	1000	84	250	84	250	60	110	110

Cohesive zone approach has been used to model delaminaton. As explained in the previous chapter, bi-linear traction-separation model has been utilized for the behaviour of the interfaces. The built-in cohesive elements and related failure model have been employed for finite-thickness cohesive zone framework. Any extra element was required for zero-thickness cohesive zone, thus the interfaces were defined as contacts between the unidirectional fibre reinforced plies and the failure model was utilized as contact property. The mechanical properties and the damage model parameters of cohesive interfaces are given in Table 5-2. The critical energy release rate values in mode I and mode II for interfaces of CFRP were obtained from the fracture mechanics tests by Zitoune and Collombet [124]. The tests were performed according to the standard (NF ISO 15024). The fracture energy release rate were determined by using double cantilever beam (DCB)-type geometries and end notched flexure (ENF) [124]. The coefficients of energy release rate in energy criteria; α,β and γ, were based on their numerical study [124]. Damage model parameters were obtained from the numerical study of Bertolini et. al. [212]. In order to avoid convergence problems, a value of 10^6 N/mm^3 was employed for cohesive stiffness which was recommended by Camanho et. al. [199].

Table 5-2: The Material Properties of Interfaces of CFRP Workpieces [124, 199, 212]

Constitutive Material Parameters								
K_n **(N/mm³)**	K_s **(N/mm³)**	K_t **(N/mm³)**						
10^6	10^6	10^6						
Damage Model Parameters								
σ_n^0 **(MPa)**	σ_s^0 **(MPa)**	σ_t^0 **(MPa)**	G_n^C **(N/mm)**	G_s^C **(N/mm)**	G_t^C **(N/mm)**	α	β	γ
60	110	110	0.33	1.209	1.209	1.6	1.6	1.6

5.3.2 Ti-6Al-4V Workpiece

The Johnson-Cook material model and failure model has been employed for the progressive failure behaviour of Ti-6Al-4V in drilling process. The built-in Johnson-Cook material and failure models have been utilized for titanium

workpiece. The required properties; physical and mechanical properties, Johnson-Cook material model parameters and Johnson-Cook failure model parameters, are given in Table 5-3. The Johnson-Cook material model parameters were determined using Hopkinson bar tests at a high-strain rate and a low-strain rate by Donald R. Lesuer [16, 213].

Table 5-3: The Material Properties of Ti-6Al-4V Workpiece [16, 213]

The Physical and Mechanical Properties of Ti-6Al-4V							
P (kg/m^3)	E (GPa)	ϒ					
4428	105	0.23					
The Johnson-Cook Constitutive Material Model Parameters of Ti-6Al-4V							
A (MPa)	B (MPa)	C	n	m	$\frac{\bullet}{\varepsilon 0}$ (s-1)	T_0 (°C)	Tm (°C)
862	331	0.012	0.8	0.34	1	20	1605
The Johnson-Cook Damage Model Parameters of Ti-6Al-4V							
d_1	D_2	d_3	d_4	d_5			
-0.09	0.25	-0.5	0.014	3.87			

5.3.3 Cutting Tool

The cutting tools were modelled as rigid tools. Since there was no stress and strain computation on the drill bits, no material input was required for the progressive analysis. However, in order to add the mass and inertia effects of 3-D complex drill geometries, the CAD based tools were used to calculate volume, mass and inertia from the geometry. At this stage, tungsten carbide was used as tool material. The properties of the drill are given in Table 5-4.

Table 5-4: The Material Properties of Cutting Tool [116]

d (kg/m^3)	E (GPa)	ν
14500	580	0.22

5.4 Geometry

5.4.1 CFRP Workpiece

In order to model mechanical behaviour of CFRP workpiece, a meso-level discrete model was used in the study. Each unidirectional fibre reinforced ply was modelled individually and combined with cohesive interfaces to form CFRP workpiece. The meso-level model enabled to analyse intra-laminar and inter-laminar levels behaviours of unidirectional fibre reinforced composite workpiece separately. Inter-laminar delamination is one of the most common types of damage in laminated fibre reinforced composites due to their weak inter laminar strengths. The overall laminated CFRP structure is symbolised in Figure 5-1.

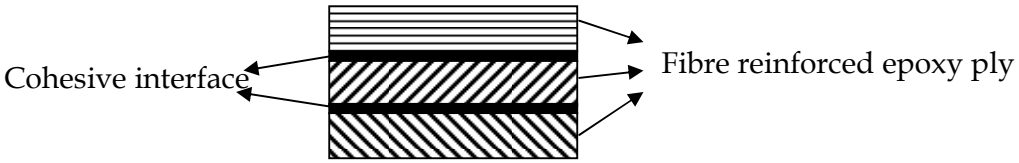

Figure 5-1: The Structure of the Composite Model

Unidirectional carbon fibre reinforced laminated composite work piece consisted 16 plies with a stacking sequence of $[90/-45/0/45]_{2s}$. The ply thickness was modelled to be equal to 0.26 mm, which was the nominal thickness of the pre-impregnated material given in the manufacturer's datasheet [162]. As it has been explained in the previous section, the inter-laminar behaviour of the unidirectional fibre reinforced composite workpiece was modelled by using two different approaches; zero-thickness cohesive zone and finite-thickness cohesive zone. The both approaches can model the inter-laminar behaviour of CFRP, however there was small difference in the geometry of these two models. The cohesive element thickness was suggested to have one fiftieth of ply thickness in the literature [201], so the thickness of the finite-thickness cohesive zone was equal to 0.005 mm. It must be noted that finite-thickness cohesive zone framework has brought extra elements into the model. The zero-thickness cohesive zone framework did not add any extra thickness to the geometry

therefore the overall dimensions the CFRP workpieces are 40 mm x 40 mm with a total thickness of 4.16 and 4.235 mm in the zero-thickness and finite-thickness cohesive frameworks, respectively. The geometry of CFRP workpiece is shown in Figure 5-2.

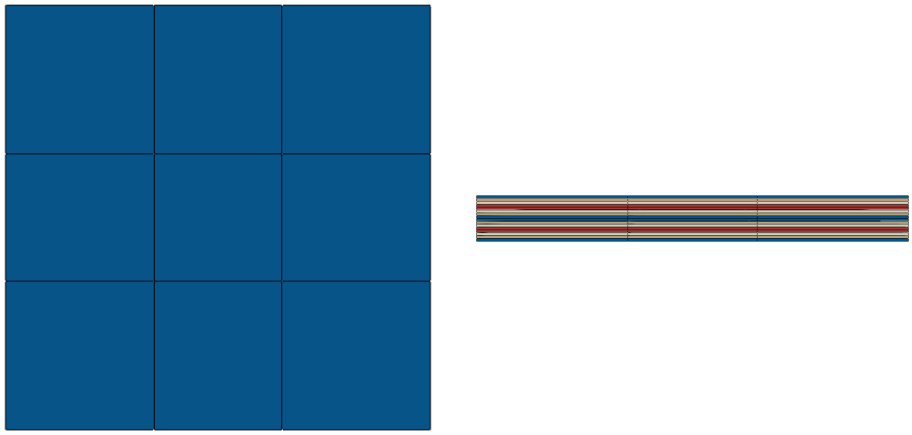

(a) (b)

Figure 5-2: CFRP Workpiece (a) Top View (b) Side View

5.4.2 Ti-6Al-4V Workpiece

The modelling of titanium alloy workpiece was straightforward. The workpiece was designed as a solid plate with 40 mm X 40 mm dimensions with a thickness of 5 mm.

5.4.3 Cutting Tool

In order to predict the drilling process of CFRP, Ti-6Al-4V and stack of CFRP/Ti-6Al-4V, real 3-dimensional cutting tool geometry was included in the finite element analysis. For this purpose, complex 3-D drill geometries were modelled using Solidworks CAD software and imported into the FE simulation. For validation purposes, the drill geometry used in the experiments was generated. The 8 mm diameter twist drill with 140° point angle and 30° helix angle geometry was used in drilling of CFRP, Ti-6Al-4V and stack of them. First, the drill was assumed fully elastic deformable material to calculate the mass and inertia in the FE model. Then it was modelled as a rigid body. Mass and inertia were added to the rigid tool to simulate the equivalent kinematics of

the process. The use of rigid tool in the FE simulation would decrease computational time and maintain the efficiency of the FE analysis.

The drilling process of CFRP and Ti-6Al-4V, can be optimised by the use of a step geometry drill. In order to investigate the effects of drill geometry, step drill geometries were generated in Solidworks CAD environment and imported into the FE models. The step drills were used as rigid drill in the FE models. The details of drill geometries used in the FE analysis are given in Table 5-5 and Figure 5-3.

Table 5-5: The Geometry of Drills

	Twist Drill	Step Drills				
	A	**B**	**C**	**D**	**E**	**F**
Drill Diameter (mm) [D]	8	8	8	8	8	8
Step Diameter (mm) [Ds]	-	4.5	5	5.5	6	6.5
Step Ratio	-	0.5625	0.625	0.6875	0.75	0.8125
Point Angle (°) [P]	140	140	140	140	140	140
Helix Angle (°)	30	30	30	30	30	30
Cutting Length (mm) [Lc]	43	43	43	43	43	43
Step Length (mm) [Ls]	-	20	20	20	20	20
Total Length (mm) [L]	79	79	79	79	79	79

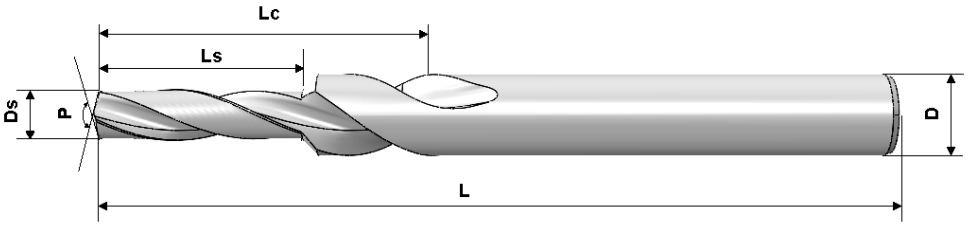

Figure 5-3: Step Drill Geometry

5.5 Element and Mesh

The behaviour of fibre reinforced composite workpiece was modelled in different approaches as explained in the previous chapter. These different

scenarios required different mesh element type. In the progressive analysis of intra-laminar behaviour, solid and solid-like frameworks have been employed. In solid frameworks, 8-node hexahedron fully solid elements (C3D8R) were utilized whereas in solid-like framework 8-node hexahedron continuum shell elements (SC8R) were used to model unidirectional fibre reinforced epoxy plies. In the progressive analysis of inter-laminar behaviour, finite thickness and zero thickness cohesive zones were used between each unidirectional fibre reinforced ply, where delamination was expected to occur. The interfaces were modelled with 8-node cohesive elements (COH3D8) in finite-thickness cohesive framework whereas zero-thickness cohesive scenario did not require any extra element between the adjacent unidirectional fibre reinforced plies. Titanium alloy workpiece was modelled with 8-node hexahedron solid elements (C3D8R).

The drill bits were assumed as rigid body to reduce the computational time, therefore 3-node triangular facet rigid body elements (R3D3) were used on the surfaces of drills. It should be noted that there was no stress calculation on the drill. This was mainly to keep the computational time and resources required minimal. The fine mesh on the drill reassured that high resolution contact surface elements were produced to model 3-D tool surface accurately. Since there was no stress analysis on the rigid tool, the computational time would not be affected by the refined mesh on the drill.

In all simulations, reduced integrated elements have been used in order to reduce computation time. Reduced integration means that less Gauss points are used in the finite element solution. The reduced integration provided the most efficient computational time for the finite element analysis of drilling process. The elements with reduced integration had a good accuracy, they are not sensitive against mesh distortions, and they can avoid shear and volume locking. However, reduced integration can make the elements too soft and cause hourglass and unstable analysis. Thus reduced integrated elements have to be stabilized by using hourglass control modes which is a technique of introduction of an artificial stiffness to the elements. Severe mesh distortion is one of the most common problems in the machining simulations. Hourglass control can also minimize these problems without introducing excessive

constraints. The optimum built-in hourglass control was found stiffness hourglass control and reduced-stiffness hourglass control for CFRP and Ti-6Al-4V, respectively.

Finite element analysis is highly dependent on the size of elements and significant differences can be observed in the response of material behaviour. In order to find an optimum element size, several simulations have been carried out and the results of the simulations will be given in Appendix C. In order to investigate the effect of mesh size on the outputs, 2 mm, 1mm, 0.5 mm and 0.26 mm element sizes used in the finite element analysis of drilling process. Due to the large stress gradients and potential damage at the boundary of the hole, the mesh was refined only in the hole vicinity with an aspect ratio of 1.0 in the latest model. The density of mesh was reduced outside of the hole vicinity in the workpieces to reduce solution time as the outside region was less critical in the analysis. A maximum aspect ratio of 4.0 was used away from the hole region. The meshes of the workpieces are shown in Figure 5-4.

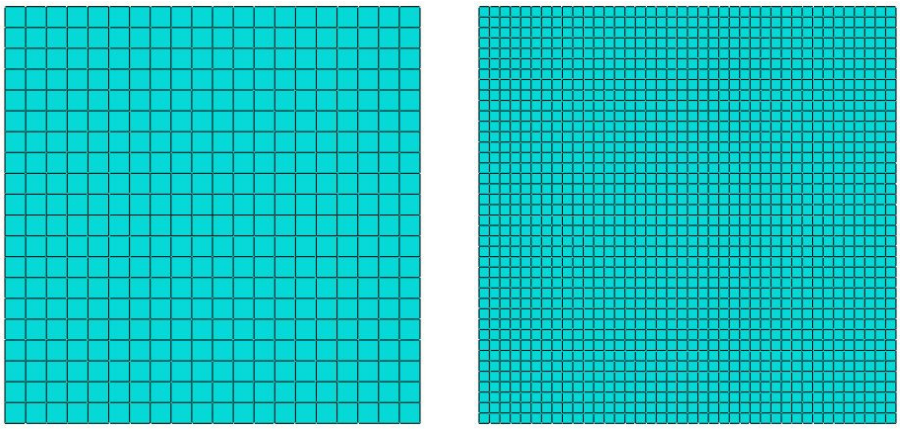

(a) **(b)**

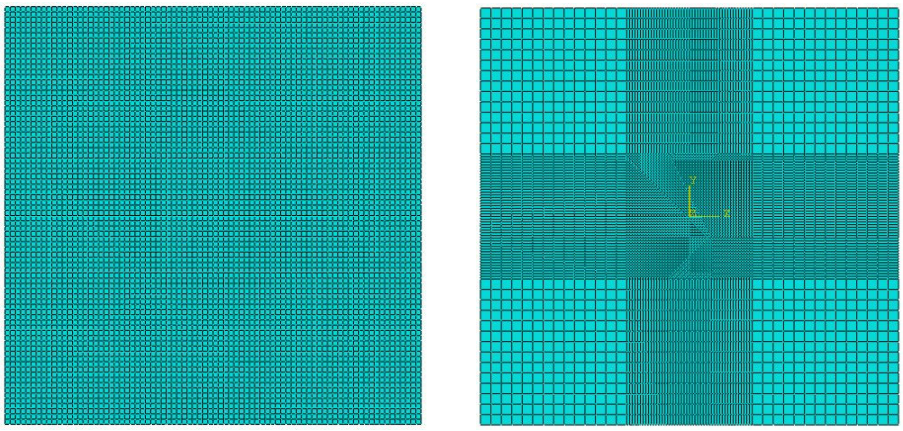

(c) (d)

Figure 5-4: Mesh Size of Workpieces (a) 2 mm (b) 1 mm (c) 0.5 mm (d) Graded (0.26 mm & 1 mm)

Considering the very complicated geometry and the need for extremely high computing resources a balance between the high accuracy results and reasonable element size should be made. The graded mesh was found as the optimum mesh. The elements size was set to 0.26 mm in thickness direction. The mesh size of the work piece was refined in the drilling area in order to model accurately the drilling induced stresses, forces and the progressive damage of the work piece. The elements in the machining region were removed when the failure criteria has met during the simulation. The element size was 0.2 mm and 0.5 mm on the tip of cutting tool and tool body, respectively.

The total numbers of elements in the CFRP work pieces were approximately 90,000 and 175,000 for the zero-thickness cohesive zone framework and finite-thickness cohesive zone framework, respectively. In titanium alloy workpiece, the number of elements was approximately 115,000. The final mesh of 3-D finite element model of drilling of CFRP/Ti-6Al-4V stack with twist drill is shown in Figure 5-5.

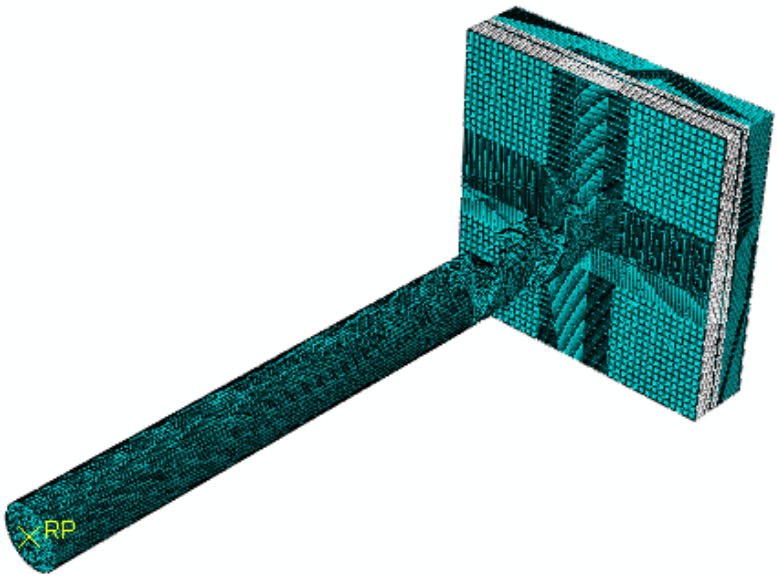

Figure 5-5: The Meshed FE Model of drilling of CFRP/Ti-6Al-4V stack

5.6 Boundary Conditions and Loading

The 3-D finite element analysis of drilling process is the application of cutting forces by drill tip and cutting edges of a 3-D drill geometry on to the region which is going to be removed from the workpiece. Since the cutting forces are unknown, the FE simulation was performed by the utilisation of displacement and rotation of the cutting tool by the specified cutting parameters. The boundary and loading conditions of FE models are shown in Figure 5-6. All degrees of freedom of workpieces were constrained at the fixed end to simulate the fully clamped end. Similarly, the movement and rotation drill was constrained in x and y directions (ux=uy=urx=ury=0) to hold the drilling process in the right axis. Rotational and translational velocities were applied to the drill body as spindle speed and feed rate, respectively. The heat generation was ignored to minimize computational time since high amount of coolant has been used in the experiments to keep the temperature close to the room temperature. The environment temperature was set to 20 °C in finite element analysis of drilling of CFRP and Ti-6Al-4V.

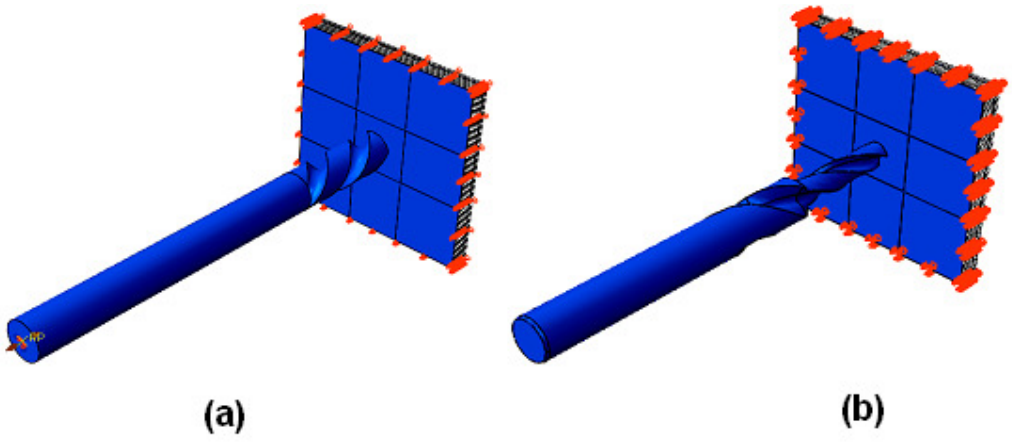

Figure 5-6: FE model of drilling (a) Twist Drill (b) Step Drill

In order to investigate the effect of cutting parameters on drilling, finite element analyses of 3-D drilling of CFRP and Ti-6Al-4V have been performed at different machining conditions which were same with the experimental drilling tests. The spindle speed was incorporated by the use of rotational speed in terms of angle per second, whereas the feed rate was given by the vertical velocity of the tool per second. The cutting parameters used in the simulations are given in Table 5-6.

Table 5-6: Cutting parameters used in FE Analysis of Drilling

Material	Spindle Speed (rpm)	Feed Rate (mm/min)
CFRP	3000, 4500, 6000, 9000	355, 457, 585, 684
Ti-6Al-4V	1000, 1400, 1800	95, 119, 142, 171
CFRP/Ti-6Al-4V	4500, 6000 (CFRP) 1400, 1800 (Ti-6Al-4V)	355, 457 (CFRP) 95, 119 (Ti-6Al-4V)

The peck drilling was not taken into account in the FE analysis since there was no chip formation considered in the simulation.

5.7 Contact Modelling

The contact model controls the interaction between the surfaces of the tool and work piece material such as friction. The friction between the tool and work piece is influenced by number of factors such as cutting speed, feed rate,

geometry and the surface properties. Estimation of friction in machining process is very complicated and is considered as one of the challenges by researchers. It is widely accepted that the friction at the tool-work piece interface can be represented by a relationship between the normal and frictional stress over the cutting edges of the tool. In drilling, friction can occur in three ways: the friction at the chisel edge-work piece interface, the friction at cutting edge-work piece interface, and the friction at the drill rake face-chip interface. In this study, chip generation was not modeled due to adding complexity to the requirement of huge computational resources. Therefore the friction between chip and drill was ignored. Based on Coulomb friction model, which is given in Eq (5.1), it was assumed that the frictional stress on the drill was proportional to the normal stress with a constant friction coefficient.

$$\tau_n = \mu\sigma_n \qquad \textbf{Eq. (5.1)}$$

The interaction between the work piece and the tool was utilized by Lagrangian contact mechanics with hard contact algorithm such as the pressure-overclosure algorithm and surface-surface kinematic contact enforcement which are already available in ABAQUS/Explicit. The surface of the tool was set as the master object and the surface of the workpiece was set as the slave object. This means that the workpiece will deform according to the motion of the tool. Moreover the elements in the workpiece could not penetrate into the tool. Gardner and Dornfeld [214] have recommended a friction coefficient between 0.5-0.6 for machining process. Since high amount of coolant was used in drilling experiments, the lower side of the recommended friction coefficient range was considered and the friction coefficient was assumed 0.5 between drill and Ti-6Al-4V workpiece. The coefficient of friction was set equal to 0.15 between drill and CFRP workpiece which was obtained from pin on disk tests. Perfect bonding was assumed between the lamina at the beginning of the process and the friction coefficient was assumed to be zero between the plies after the separation. However, these assumptions would have some effects on the FE predictions.

5.8 Validation of Delamination

An important computational step is the verification of the proposed numerical model for mixed-mode delamination propagation for non-unidirectional laminates. For this purpose, a FE model has been developed to analyze the asymmetric double cantilever beam (ADCB) test and compared with the previous study [202]. The crack interface was chosen to be 0/45 and the effort was particularly focused on delamination in mode I owing to the significance of thrust force in drilling of CFRP.

The 3-D composite laminate was modelled in order to investigate the delamination prediction capability of the current FE model. The stacking sequence of the test specimen was 0/45/-45/-45/45/0 // 45/0/-45/0/-45/-45/45/45/0/45/0/-45, where ''//'' indicates the delamination surface as in the previous study [202]. The material behaviour and material properties were the same as in the drilling model explained above. The ADCB FE model and the test data of the specimen are given in Figure 5-7 and Table 5-7, respectively. The specimen was fixed at one end and loaded at the other end with an increasing traction force. The resulting force and displacement are given in the following chapter.

Table 5-7: Specimen and test data of ADCB test

L (mm)	B (mm)	t (mm)	a_0 (mm)
170	20	4.68	85

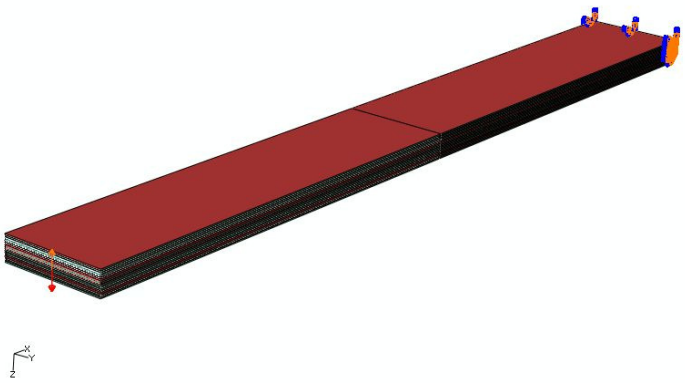

Figure 5-7: FE model and Boundary Conditions of ADCB test specimen

5.9 Summary

The finite element models of drilling of CFRP, Ti-6Al-4V and CFRP/Ti-6Al-4V stack have been introduced in detail in Chapter 5. Three-dimensional models have been developed. The materials have been defined for finite element analysis and all the related data have been provided. The user material subroutine has been developed in Fortran programming language and adopted in Abaqus for drilling of CFRP. The geometries of CFRP and Ti-6Al-4V workpieces were explained based on different frameworks and the drill bit geometries have been introduced in the geometry section. The step drill geometries were generated for CAD based optimisation of drilling of workpieces. The mesh and element attributes have been discussed to optimize the finite element procedure of drilling process. For this purpose the influences of element size and hourglass control on FE results have been investigated. The interaction between the cutting tool and workpieces were elaborated in loading and contact sections. The boundary conditions of the drilling process have been expressed. In addition, finite element analysis of asymmetric double cantilever beam (ADCB) test has been performed to validate delamination model in a simple case. The results are discussed in detail in Chapter 6, 7 and 8 for CFRP, Ti-6Al-4V and CFRP/Ti-6Al-4V stack, respectively.

Chapter 6

Results and Discussions of Drilling of CFRP

Machinability of materials is important to achieve structures with high integrity and lows cost of manufacturing. To understand and provide high machinability of CFRP, the effects of process parameters and tool geometry have been investigated in various aspects of drilling including thrust force, torque, delamination, surface roughness, wear and workpiece stress through experiments and finite element analysis.

6.1 Validation

6.1.1 Force and Torque

Figure 6-1 (a) and Figure 6-1 (b) show the experimental and simulated thrust force and torque in drilling of CFRP without a support plate at 457 mm/min feed rate and 4500 rpm spindle speed (113 m/min cutting speed), respectively. It was observed that the thrust force in the experimental trial was 230 N. whereas the FE model with fully solid elements estimated 227 N. The experimentally measured torque was 0.290 N.m compared to the torque value predicted as 0.297 N.m by the FE simulation. This shows that the FE model estimated the thrust force and torque accurately with 1.30% and 2.41% deviation from the test results, respectively. The estimations of the FE model with solid-like elements and finite-thickness cohesive elements were slightly more diverged, with 2.17% and 4.83% for thrust force and torque, respectively. Only the closest results which were obtained by the application of solid elements were plotted clearly. Since CFRP is a elastic and brittle material, FE model predicted the material behaviour very well. The minor diversion in

thrust force could be due to the material data tested in lower speeds. These close results gave the confidence about the capability of the FE model in its prediction of the thrust forces and torque values for the future works.

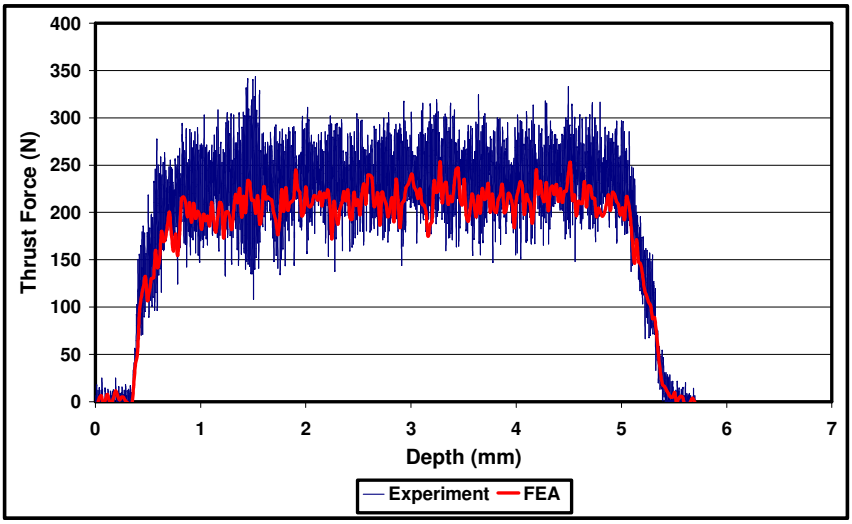

(a)

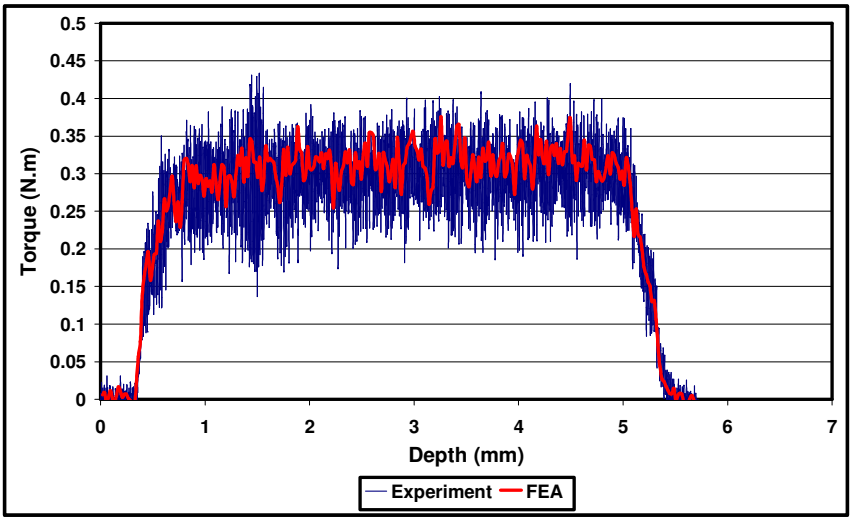

(b)

Figure 6-1: Drilling of CFRP (a) Thrust Force (b) Torque (S=4500 rpm, f=457 mm/min)

6.1.2 Verification of Delamination Prediction

Figure 6-2 shows the stress distribution and the delamination after the ADCB test. As shown in Figure 6-2, both arms have identical displacement at the end of the simulation. The simulations were performed until the displacement is 13.6 mm for the given 85 mm crack length.

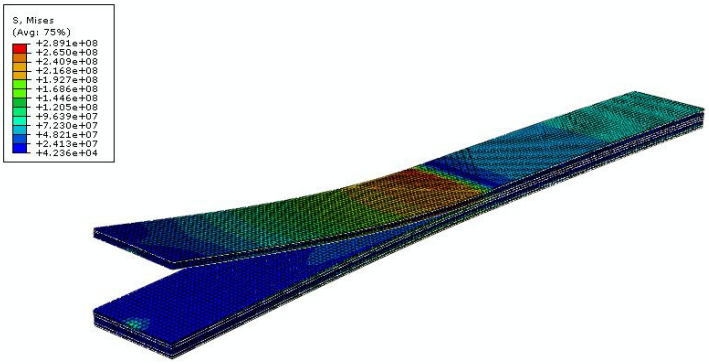

Figure 6-2: Stress distribution and delamination of CFRP specimen in ADCB test

As plotted in Figure 6-3, the result of FE model was in good agreement with the experimental result. The average critical force was slightly underestimated as 33.6 N for 0.26 mm in-plane element sized tests specimens. This means dispersions was only 1.67% compared to the experimental test results. The good correlation of the outputs confirmed that the delamination onset and growth of CFRP laminates can be predicted reasonably during drilling and this gives confidence about the assumptions made in this present study.

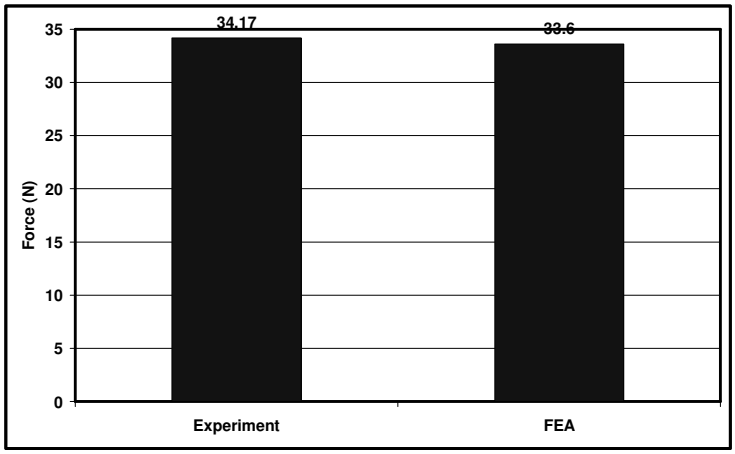

Figure 6-3: Comparison of Critical Force

6.2 Analysis of Thrust Force

Figure 6-4 shows the development of thrust force in drilling of UD-CFRP without back-up plate by 3 μm TiN/TiAlN multilayer coated 8 mm diameter tungsten carbide twist drill with 140° point angle and 30° helix angle at 457

mm/min feed rate and 4500 rpm spindle speed. Drilling of a through hole consists of three stages. In the first phase drill penetrates into work piece. In the second phase, in which the whole cutting edges are in contact with the work piece, a steady state thrust force is obtained. Finally, in the third phase drill point exits or breaks through other side of the work piece. These three stages can be clearly observed in drilling of CFRP in Figure 6-4. In the following paragraphs, the investigations of thrust force are made using the average thrust force which was obtained in the second phase of drilling in experiments and FE analysis.

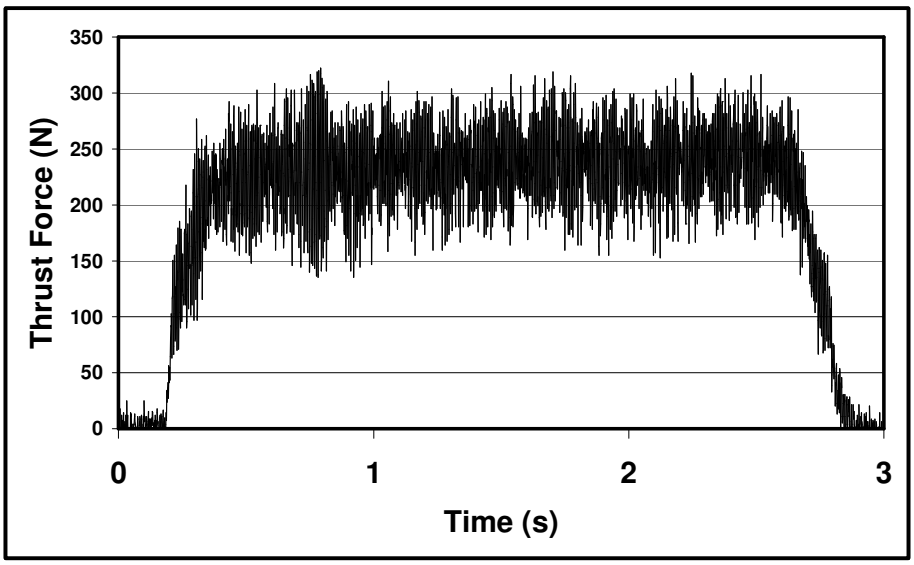

Figure 6-4: Thrust Force through Hole in Drilling of CFRP (S=4500 rpm, f=457 mm/min)

6.2.1 Effects of Process Parameters on Thrust Force

In order to investigate the influences of process parameters on drilling of CFRP, both the experiments and simulations were performed at the combinations of four feed rates and four spindle speeds, a total of 16 sets of cutting condition. All the drilling experiments were conducted with the use of 3 μm TiN/TiAlN multilayer coated 8 mm diameter tungsten carbide twist drill with 140° point angle and 30° helix angle. In order to include the effect of drill geometry and to simulate the drilling process, 3-dimensional complex drill geometry was used in the finite element simulations. The average thrust forces induced in drilling of CFRP at different machining parameters are shown for both experiments and finite element analysis in Figure 6-5 (a) and Figure 6-5 (b),

respectively. It could be observed in Figure 6-5 (a) that drilling induced thrust force was between 193.0 and 295.7 N regarding to the cutting condition in the drilling tests. It could also be seen that thrust force increased with the increasing feed rate and cutting speed. The results point out that feed rate was the predominant factor on thrust force in the tested region. Similar trends between process parameters and thrust force have been reported in literature for fibre composites [57, 59, 215-217]. Although the test region and materials are different in the studies, thrust force has been found more sensitive to feed rate in drilling of CFRP. Zitoune et. al. [159] have reported the decrease of thrust force with increasing cutting speed due to softening of the epoxy matrix. However in this present study, high amount of coolant was used which prevented from temperature rise. The temperatures measured on tip of drill right after the drilling tests were in the range of 30-35°C. Therefore no thermal softening was expected to occur in the epoxy matrix in CFRP. Consequently, higher thrust force was observed whilst drilling at higher spindle speeds.

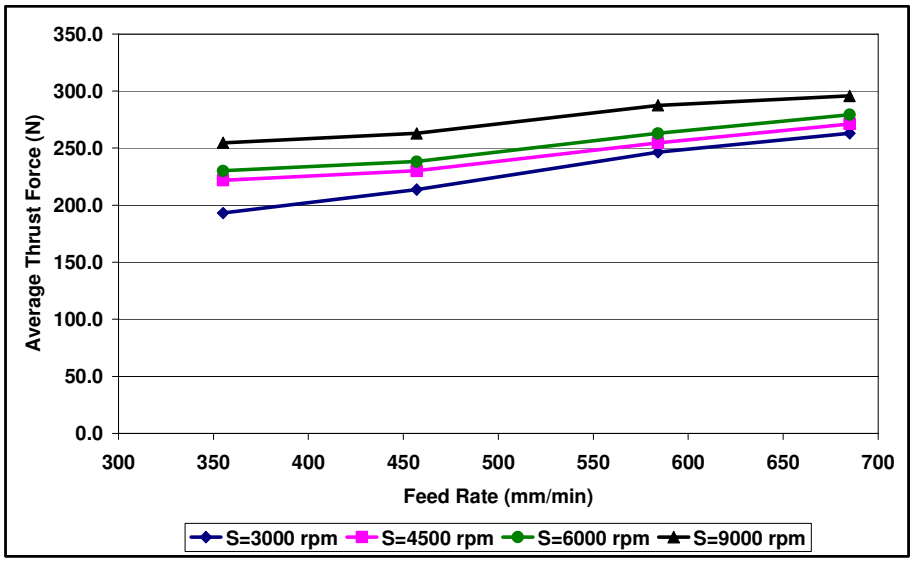

(a)

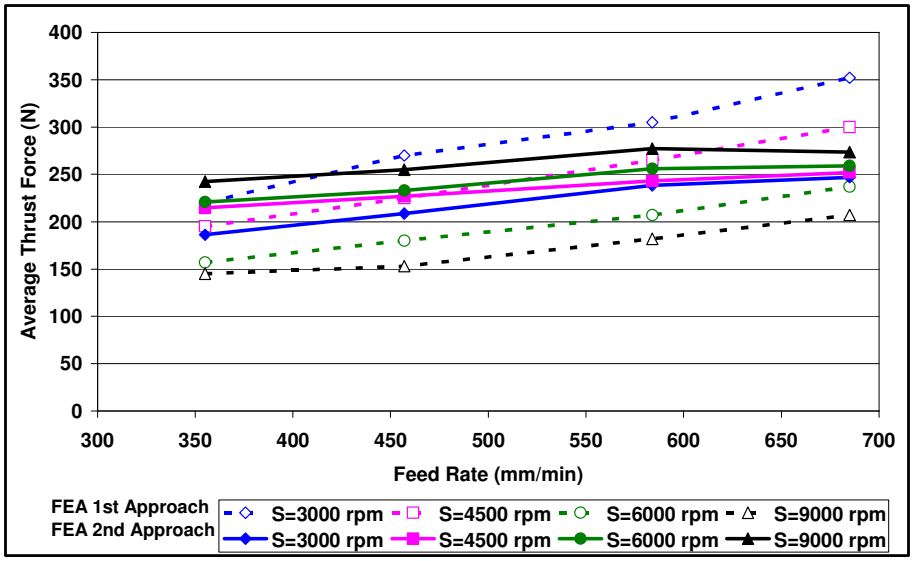

(b)

Figure 6-5: Effects of Cutting Parameters on Thrust Force in Drilling of CFRP (a) Experiments (b) Finite Element Analysis

As it was explained in the methodology section for CFRP, finite element analysis of drilling CFRP was performed by using two approaches. The first approach solid-like (continuum shell) elements and finite-thick cohesive elements were utilized for the intra-laminar and inter-laminar of behaviours of the laminated fibre reinforced composite workpieces, respectively. Whereas the second approach, with the advent of the newer developments in the FEA package, fully solid elements and zero-thickness cohesive surfaces were applied for the intra-laminar and inter-laminar of behaviours of the laminated fibre reinforced composite workpiece, respectively. The main difference between these two models is the implication of the response of the material in the normal direction (out-of-plane) of the workpiece. In addition to that, zero-thickness cohesive surface approach has been found very useful comparing to finite-thickness cohesive elements since it can avoid some of the computational issues and decrease the solution time.

Figure 6-5 (b) shows the effect of cutting parameters on thrust force for the both FE approaches. The first FE model which was employed with solid-like elements for intra-laminar material behaviour predicted thrust force between 145 N and 352 N depending on the cutting parameters. The FE results show that drilling induced thrust force increased with the increased feed rate in all cutting

speeds. The model estimated the trend of thrust force versus feed rate successfully. Moreover it was also estimated that the feed rate was the dominant process parameter on the thrust force. However, thrust force decreased with the increasing cutting speed. This was an opposite trend comparing to the experimental tests, which was not expected. In the case of using coolant would not lead a softening in the epoxy. Moreover, the material response did not have a strain rate and thermal components as in metals thus softening should not be a matter in FE analysis. It was thought that the lack of complete response of the material in the normal direction was likely the reason of this. The lack of 3rd variant of the stress in the intra-laminar behaviour and in damage model would cause to a different response in the material. Thus second FE approach has been developed to overcome this problem. The second FE model which was utilized with fully solid elements for intra-laminar material behaviour estimated thrust force between 186.22 N and 273.53 N regarding to the cutting condition in the drilling tests. The finite element results indicates that the drilling induced thrust force increased with the increased feed rate in all cutting speeds as recorded in the drilling tests. It was clear that feed rate was the dominant machining parameter on thrust force in the simulated region. As it was observed in the cutting experiments, thrust force increased with the increasing cutting speed in the FE analysis with the second model. The inclusions of the 3rd variation completely in the response of the material and in the failure model under the existence of multi-axis state of stress and loading have enabled to obtain a positive correlation between the FE model and experiments.

Table 6-1 shows the experimental and estimated average thrust forces in details for each cutting condition. The experimental results show that the minimum induced thrust force was obtained as 193.0 N in the tests at 3000 rpm spindle speed and 355 mm/min feed rate whereas the maximum induced thrust force was found in test performed at 9000 rpm spindle speed and 685 mm/min feed rate in drilling of CFRP with 8 mm diameter twist drill. 93% higher feed rate resulted between 16.13% and 36.17% greater amount of thrust force depending on the cutting speed; whereas 200% greater cutting speed caused an increase between 12.50% and 31.91% in thrust force according to the feed rate in

drilling of CFRP. However the change in the feed rate was smaller in percentage than the change in the cutting speed in the test region, the thrust force was affected more in the change of the feed rate. This means that thrust force was more susceptible to the change in feed rate.

The overall trends of predicted thrust force with the process parameters have been shown and discussed above. Table 6-1 shows estimated thrust forces for each set of machining parameters in detail for the both FE approaches. According to the first FE approach, the minimum thrust force was predicted to be 145 N at 9000 rpm and 355 mm/min which was the combination of the maximum spindle speed and the minimum feed rate with 8 mm diameter rigid twist drill. The maximum thrust force was estimated 352 N at 3000 rpm spindle speed and 685 mm/min, which was the combination of the minimum cutting speed and the largest feed rate. The results show that 93% higher feed rate caused an increase in thrust force between 42.76% and 60.0% depending on the cutting speed; whereas 200% greater cutting speed led to a decrease between 34.09% and 43.33% in thrust force according to the feed rate in drilling of CFRP. However the percentage change of feed rate was smaller than the change of cutting speed, a higher influence on thrust force has been observed which indicates that feed rate was the dominant process parameters on thrust force. The effect of cutting speed on thrust force was significant and cannot be ignored. Nevertheless, the results based on the 1st FE model has shown that the thrust force has been predicted with deviations between 2% and 43% according to the drilling conditions. The general trend of thrust force versus cutting speed has been predicted in contrary with the experiments due to the lack of the 3rd variant of material responseof the laminated composite, which was the loading or drilling direction.

This problem was overcome with the utilisation of the fully three-dimensional constitutive model and failure model with the related fully solid elements in the laminated fibre reinforced composite material. As can be observed from Table 6-1 for the results of 2nd FE approach, the minimum thrust force was estimated as 186.22 N at 3000 rpm spindle speed and 355 mm/min feed rate which was the combination of the minimum spindle speed and feed rate with the 8 mm diameter rigid drill. The maximum thrust force

was predicted to be 273.53 N at 9000 rpm spindle speed and 685 mm/min feed rate. The FE results indicates that 93% higher feed rate resulted in an increase between 12.80% and 32.57% in thrust force depending on the cutting speed; whereas 200% greater cutting speed caused to an increase between 10.79% and 30.22% in thrust force according to the feed rate in drilling of CFRP. However the change of feed rate was smaller than the change of cutting speed, a slightly higher influence on thrust force has been observed which indicates that thrust force was more susceptible to the change in feed rate in FE analysis. This relation was found similar in experimental results. The FE analysis with fully 3-D elements has ensured a positive correlation between thrust force and process parameters. The deviations of predicted thrust force based on the 2nd FE approach lay between 1.3% and 7.5% underestimation according to the set of process parameters.

Thrust force was estimated to increase with regards to the increase in cutting speed and feed rate. The higher thrust force could cause to higher cutting stresses and consequently accelerated tool wear. High thrust force could lead to increased delamination and other drilling induced defects. Combination of moderately low cutting speed and feed rate could help to maintain high structural integrity and provide longer service life for the tool and workpieces.

It should be mentioned that the trends predicted by the 2nd FE model were in agreement with the experimental values for the thrust force. In general, to obtain very accurate results for thrust force via finite element analysis, extremely fine mesh, accurate contact model and very good damage model are essential. However due to the complexity of the geometry and the process moving to very fine mesh would require huge computing resources. Limitation on the computing resources and extremely long computing times had restricted the FE investigations in terms of the mesh refinement. Within the resources available the accuracy of the predictions of the thrust force for different drilling parameters are acceptable.

Table 6-1: Experimental and Simulation based Thrust Force in Drilling of CFRP

Feed Rate (mm/min)	Spindle Speed (rpm)	Thrust Force (N) Experimental	Thrust Force (N) FEA-1st model	Deviation (%)	Thrust Force (N) FEA-2nd model	Deviation (%)
355	3000	193.04±2.50	220.00	13.97	186.22	-3.53
355	4500	221.79±2.75	195.00	-12.08	214.64	-3.22
355	6000	230.00±3.00	157.00	-31.74	220.83	-3.99
355	9000	254.64±3.22	145.00	-43.06	242.50	-4.77
457	3000	213.57±2.42	270.00	26.42	208.66	-2.30
457	4500	230.00±3.00	225.00	-2.17	227.00	-1.30
457	6000	238.21±3.10	180.00	-24.44	233.02	-2.18
457	9000	262.86±3.44	153.00	-41.79	254.98	-3.00
584	3000	246.43±3.20	305.00	23.77	238.25	-3.32
584	4500	254.64±3.30	265.00	4.07	243.12	-4.53
584	6000	262.86±4.00	207.00	-21.25	256.08	-2.58
584	9000	287.50±3.70	182.00	-36.70	277.11	-3.61
685	3000	262.86±3.75	352.00	33.91	246.88	-6.08
685	4500	271.07±3.80	300.00	10.67	252.01	-7.03
685	6000	279.29±3.95	237.00	-15.14	259.12	-7.22
685	9000	295.71±4.50	207.00	-30.00	273.53	-7.50

Based on these results, it was understood that the second approach in which the FE model was utilized with fully 3-D constitutive model, failure model and related 3-D solid elements and zero-thickness cohesive surfaces simulated the drilling of CFRP successfully. Thus, further investigations based on the finite elements analysis which includes the optimisation of geometry for drilling of CFRP, and drilling of CFRP/Titanium stack have been performed with the use of second finite element approach.

6.2.2 Effect of Tool Geometry on Thrust Force

In order to optimise the drilling of CFRP, different step drill geometries have been modelled in CAD software and have been utilized in the finite element analysis. The estimated thrust force was found to be only 1.30% different than the experiments performed at 4500 rpm spindle speed and 457 mm/min feed rate with 8mm diameter coated carbide drill. This deviation showed that the FE model implemented with 3-D constitutive model, failure model with fully capable 3-D solid elements and zero-thickness cohesive surfaces could estimate thrust force accurately and it gave the confidence about the capability of the FE model. Thus, investigations using step drills were performed based on FE analysis with the second approach.

Figure 6-6 shows the numerical predictions of thrust force in drilling of CFRP without any support plate at 457 mm/min feed rate and 4500 rpm spindle speed (113 m/min cutting speed) for twist drill and various step drills. It must be noted that, due to interest in the estimation of drilling induced delamination in CFRP workpiece, the secondary drilling stage by step drill has been focused in this research. Thus, the thrust forces shown in Figure 6-6 are the average estimated values in the secondary drilling stage. The FE model estimated the thrust force to be 227 N in drilling CFRP by 8 mm diameter twist drill. When step drill was utilized in FE analysis of drilling of CFRP, estimated thrust force was significantly lower than the ordinary twist drill. A comparison of the estimated thrust forces for the twist drill and step drills with various stage ratios is shown in Figure 6-6. Thrust force decreased by approximately 40% when a step drill with an initial 4.5 mm drill diameter; and 70% when a step drill with an initial 6.5 mm drill diameter. As it can be seen the higher stage ratio has provided higher reduction in thrust force. This was due to disappearance of the effects of chisel edge in the second stage cutting of step drill as it was confirmed in drilling with pilot hole in previous research works [106-107, 110]. Moreover, smaller area to be cut by the cutting edges of the step drill required smaller contact between the workpiece and the drill which minimized the need of cutting energy and cutting force.

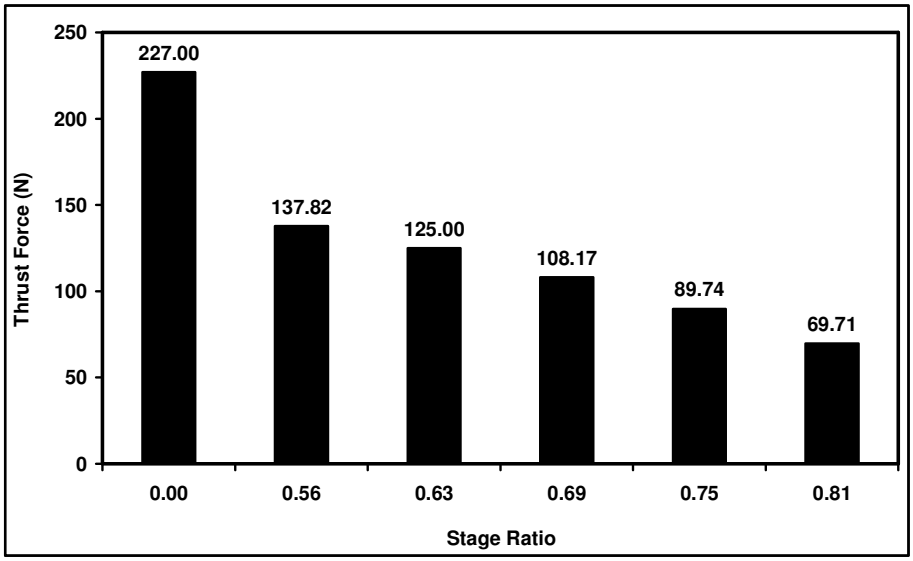

Figure 6-6: Effect of Drill Geometry on Thrust Force

Thrust force was estimated to reduce significantly due to initial step part and disappearance of the chisel edge of the drill. The reduced thrust force would assist to achieve reduced delamination and other drilling induced defects. This could help to maintain high structural integrity and provide longer service life for the workpieces. The use of step drill can also decrease the possible rejections due to tight tolerances, so it could lead low cost of manufacturing. The advantages of the use of step drill will be discussed in torque and delamination parts in the following subsections.

In general, to obtain more accurate results via finite element analysis, deformable cutting tool and extremely fine mesh could be used with regard to the computational facilities. However due to the complexity of the geometry and the process with a deformable cutting tool and very fine mesh would require huge computing resources. A contact model with anisotropy and thermo-mechanical FE analysis would develop the model further.

6.2.3 Effect of Tool Wear on Thrust Force

It is important and worth to determine the number of holes that can be drilled in CFRP workpiece in order to maintain quality and provide economic solution in manufacturing. Progression of the thrust force by the number of

holes can be observed during drilling in addition to the development of the wear regions. Figure 6-7 shows thrust force versus number of holes drilled in CFRP at 457 mm/min feed rate and 4500 rpm spindle speed (113 m/min cutting speed). During drilling experiments of CFRP, thrust forces increased steadily. After drilling 56 holes in CFRP, thrust force rose by 157.5 % from 235 N to 605 N. The final thrust force was remarkable comparing the very initial induced thrust force and clearly presented the importance and influences of wear on thrust force.

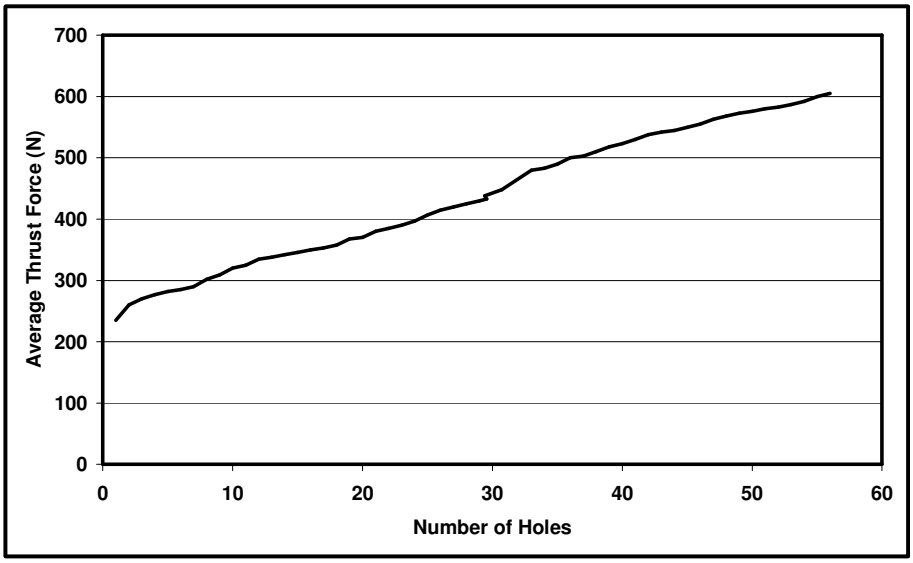

Figure 6-7: Effect of Number of Holes on Thrust Force in Drilling of CFRP (S=4500 rpm, f=457 mm/min)

Since the flank wear has reached the 0.25 mm critical value which has been stated as the tool life criteria based on the industrial experience in the methodology section, the drill was considered to have reached its end of life. Beyond this limit, it is not suggested to continue drilling since thrust force could increase substantially due to the loss of sharpness of cutting edges of the drill. Increased cutting forces could elevate cutting stresses and cutting temperatures due to increased friction between drill and workpiece. This would likely to affect material removal mechanism which can accelerate wear rate. Consequently it could be finalized with uncontrolled tool wear including chipping and sudden tool breakage, unacceptable material defects such as delamination and surface roughness, thus possible rejections and increased manufacturing costs.

6.3 Analysis of Torque

Figure 6-8 shows the progression of induced torque in drilling of UD-CFRP without a support plate with 3 μm TiN/TiAlN multilayer coated 8 mm diameter tungsten carbide twist drill with 140° point angle and 30° helix angle at 457 mm/min feed rate and 4500 rpm spindle speed. The development of torque was similar to the development of thrust force in drilling process. Three stages of drilling are shown clearly in Figure 6-8. In the first phase drill penetrates into work piece. In the second phase, in which the whole cutting edges are in contact with the work piece, a steady state torque is attained. Finally, in the third phase drill point exits or breaks through other side of the work piece. In the following paragraphs, the investigations on torque are made using the average torque which has obtained in the second phase of drilling.

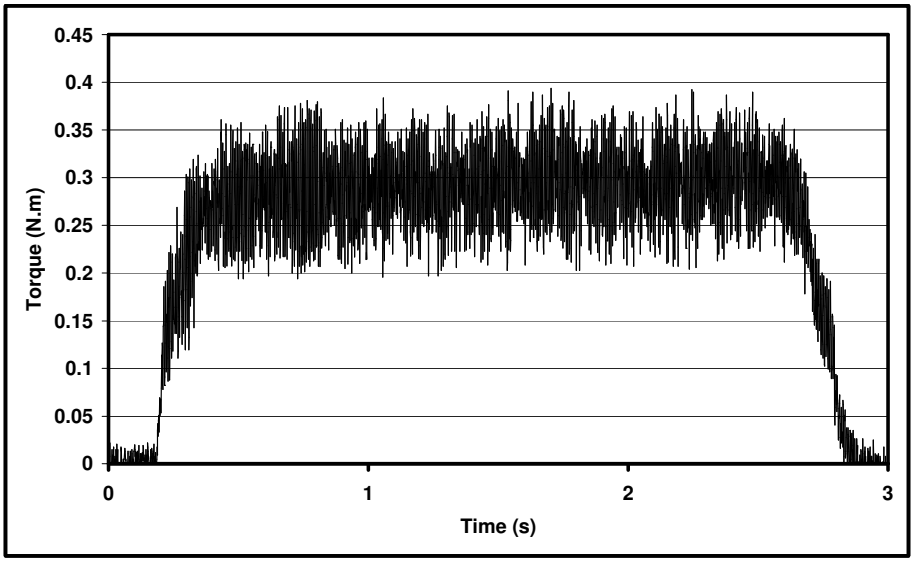

Figure 6-8: Torque through Hole in Drilling of CFRP (S=4500 rpm, f=457 mm/min)

6.3.1 Effects of Process Parameters on Torque

The influences of process parameters on torque have been investigated in drilling of CFRP performed at the combinations of four feed rates and four spindle speeds, a total of 16 set of cutting conditions in both experiments and finite element analysis. All the drilling experiments were conducted with the use of 3 μm TiN/TiAlN multilayer coated 8 mm diameter tungsten carbide twist drill with 140° point angle and 30° helix angle. 3-dimensional complex drill

geometry was employed in the finite element simulations to simulate the drilling process and to investigate the influences of drill geometry. The average torque values induced in drilling of CFRP at different machining parameters are shown for both experiments and finite element analysis in Figure 6-9 (a) and Figure 6-9 (b), respectively. As it is plotted in Figure 6-9 (a), torque altered between 0.237 and 0.373 N.m according to the cutting condition in experimental drilling of CFRP. It could be observed that torque increased with respect to feed rate and cutting speed similar to observations for the thrust force. The results point out that feed rate was the predominant factor on torque in the tested region. Similar trends between process parameters and torque have been reported in literature for fibre composites [57, 59, 215-217]. Despite the fact that different process parameters and materials are reported in the literature, similar reactions have been observed between process parameters and torque. Feed rate was the predominant parameters on torque in drilling of CFRP. Increased feed rate lead to rise in torque, whereas cutting speed did not influence torque as significant as feed rate. Drilling induced torque might have decreased by possible softening of polymer matrix due to cutting temperatures, however in this present study, high amount of coolant was used which prevented from temperature rise. Therefore no thermal softening was expected to occur in the epoxy matrix in CFRP. Consequently, higher torque was observed whilst drilling at higher spindle speeds.

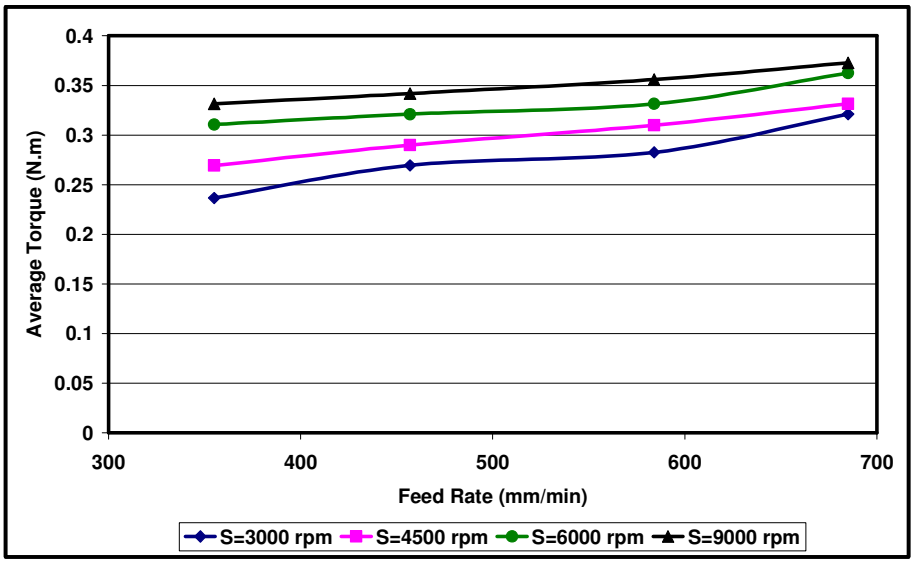

(a)

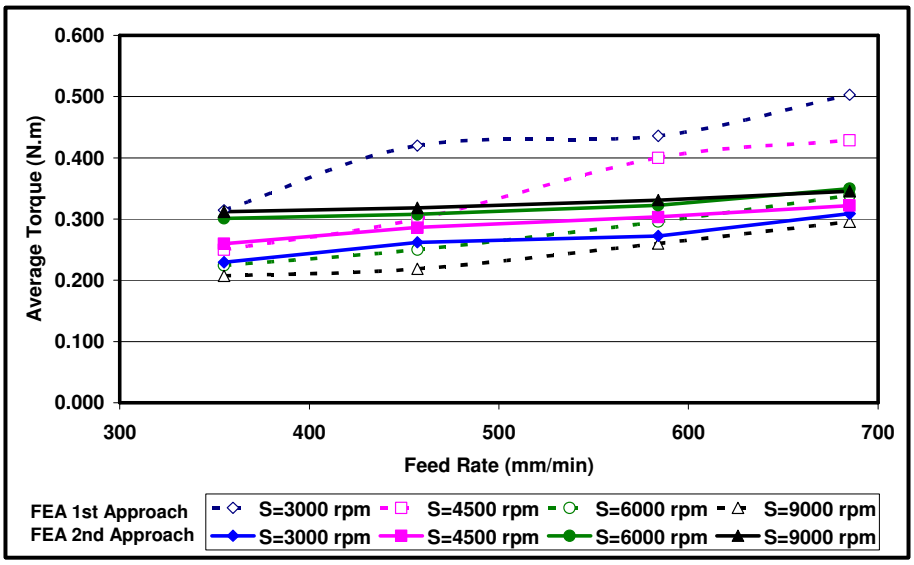

(b)

Figure 6-9: Effects of Cutting Parameters on Torque in Drilling of CFRP (a) Experimental (b) Finite Element Analysis (1st Approach: Shell Elements, 2nd Approach: Solid Elements

Figure 6-9 (b) shows the effect of cutting parameters on torque for the both FE analysis approaches. The first FE model which was employed with solid-like elements for intra-laminar material behaviour predicted torque between 0.207 and 0.503 N.m depending on the cutting parameters. The FE results show that the drilling induced torque increased with the increased feed rate in all cutting speeds. The model estimated the trend of torque versus feed rate successfully. Moreover it was also estimated that the feed rate was the dominant process parameter on torque. However, drilling induced torque decreased with the increasing cutting speed. This was an unexpected and opposite trend comparing to the experimental tests. In the case of using coolant would not lead a softening in the epoxy. Moreover, the material response did not have a strain rate and thermal components as in metals thus softening should not be a matter in FE analysis. It was thought that the lack of complete response of the material in the normal direction was likely the reason of this. The lack of 3rd variant of the stress in the intra-laminar behaviour and in damage model would cause to a different response in the material. Thus second FE approach has been developed to overcome this problem. The second FE model which was utilized with fully solid elements for intra-laminar material behaviour estimated torque

between 0.229 N.m and 0.345 N.m with regard to the cutting condition in the drilling tests. The finite element results indicates that the drilling induced torque increased with the increased feed rate in all cutting speeds as recorded in the drilling tests. It was clear that feed rate was the dominant machining parameter on torque in the simulated region. As it was observed in the cutting experiments, torque increased with the increasing cutting speed in the FE analysis with the second model. The inclusions of the 3rd variation completely in the response of the material and in the failure model under the existence of multi-axis state of stress and loading have enabled to obtain a positive correlation between the FE model and experiments.

Table 6-2 shows the experimental and estimated average drilling induced torque in details for each cutting condition. The experimental results show that the minimum induced torque was obtained as 0.237 N.m in the tests at 3000 rpm spindle speed and 355 mm/min feed rate whereas the maximum induced torque was found to be 0.373 N.m in test performed at 9000 rpm spindle speed and 685 mm/min feed rate in drilling of CFRP with 8 mm diameter twist drill. 93% higher feed rate resulted between 12.50% and 35.70% greater amount of torque depending on the cutting speed; whereas 200% greater cutting speed caused an increase between 16.13% and 40.08% in torque according to the feed rate in drilling of CFRP. However the change in the feed rate was smaller in percentage than the change in the cutting speed in the test region, drilling induced torque was affected more in the change of the feed rate. This means that torque was more susceptible to the change in feed rate.

The overall trends of predicted torque with the process parameters have been shown and discussed above. Table 6-2 shows estimated torque for each set of machining parameters in detail for the both FE approaches. According to the first FE approach, the minimum torque was predicted to be 0.207 N.m at 9000 rpm and 355 mm/min which was the combination of the maximum spindle speed and the minimum feed rate with 8 mm diameter rigid twist drill. The maximum torque was estimated 0.503 N.m at 3000 rpm spindle speed and 685 mm/min, which was the combination of the minimum cutting speed and the largest feed rate. The results show that 93% higher feed rate caused an increase in drilling induced torque between 42.76% and 60.0% depending on the cutting

speed; whereas 200% greater cutting speed led to a decrease between 34.09% and 47.96% in torque according to the feed rate in drilling of CFRP. However the percentage change of feed rate was smaller than the change of cutting speed, a higher influence on torque has been observed which indicates that feed rate was the dominant process parameters on torque. The effect of cutting speed on torque was significant and cannot be ignored. Nevertheless, the results based on the 1st FE model has shown that drilling induced torque has been predicted with deviations between 4.83% and 56.62% according to the drilling conditions. Similar to the findings for thrust force, the general trend between torque and cutting speed has been predicted in contrary with the experiments due to the lack of the 3rd variant of response of the laminated composite, which was the loading or drilling direction.

As it can be observed from Table 6-2 for the results of 2nd FE approach, the minimum torque was estimated as 0.229 N.m at 3000 rpm spindle speed and 355 mm/min feed rate which was the combination of minimum spindle speed and feed rate with the 8 mm diameter rigid drill. The maximum induced torque was predicted to be 0.345 N.m at 9000 rpm spindle speed and 685 mm/min feed rate. The FE results indicate that 93% higher feed rate resulted in an increase between 10.71% and 34.72% in torque depending on the cutting speed; whereas 200% greater cutting speed caused to an increase between 11.78% and 36.03% in torque according to the feed rate in drilling of CFRP. However the change of feed rate was smaller than the change of cutting speed, a slightly higher influence on torque has been observed which indicates that torque was more susceptible to the change in feed rate in FE analysis. This relation was found similar in experimental results. The FE analysis with fully 3-D elements has ensured a positive correlation between torque and process parameters. The deviations of predicted torque based on the 2nd FE approach lay between 2.10% and 7.40%, generally underestimation according to the set of process parameters.

Table 6-2: Experimental and Simulation based Torque in Drilling of CFRP

Feed Rate (mm/min)	Spindle Speed (rpm)	Torque (N.m) Experimental	Torque (N.m) FEA-1st model	Deviation (%)	Torque (N.m) FEA-2nd model	Deviation (%)
355	3000	0.237±0.03	0.314	32.83	0.229	-3.10
355	4500	0.269±0.03	0.250	-7.16	0.260	-3.50
355	6000	0.311±0.04	0.224	-27.82	0.301	-3.10
355	9000	0.331±0.05	0.207	-37.50	0.312	-5.90
457	3000	0.270±0.03	0.420	55.84	0.262	-2.80
457	4500	0.290±0.03	0.304	4.83	0.297	2.41
457	6000	0.321±0.04	0.250	-22.14	0.308	-4.20
457	9000	0.342±0.05	0.219	-36.05	0.318	-6.90
584	3000	0.283±0.03	0.436	54.18	0.272	-3.60
584	4500	0.310±0.04	0.400	29.03	0.303	-2.10
584	6000	0.331±0.05	0.296	-10.78	0.322	-2.70
584	9000	0.356±0.05	0.260	-26.95	0.331	-7.00
685	3000	0.321±0.04	0.503	56.62	0.309	-3.80
685	4500	0.331±0.05	0.429	29.31	0.322	-2.90
685	6000	0.363±0.06	0.339	-6.60	0.350	-3.50
685	9000	0.373±0.06	0.296	-20.69	0.345	-7.40

Torque was estimated to increase with regards to the increase in cutting speed and feed rate. The higher torque would cause to higher friction, thus increased surface roughness and cutting temperatures. These can be minimised by the choice of moderately low feed rate and spindle speed. In addition to minimising the possible rejections, the cost of manufacturing could be reduced.

It should be mentioned that the trend predicted by the 2nd FE model was in agreement with the experimental values for torque. To achieve very accurate

results for prediction of drilling torque using finite element analysis, deformable cutting tool, extremely fine mesh for tool and workpieces, chip formation and very good damage and contact models are necessary. However due to the complexity of the geometry and the process moving to very fine mesh would require huge computing resources. Restrictions on the computing resources have limited us in terms of the mesh refinement and other techniques. Within the resources available the accuracy of the predictions of the torque for different process parameters are acceptable.

6.3.2 Effect of Tool Geometry on Torque

Various step drill geometries have been utilized in the finite element analysis of drilling process of CFRP. The investigations of the effect of the geometry on torque have been performed with FE analysis. The estimated torque was found to be 0.3 N.m which was only 1.30% different than the experiments performed at 4500 rpm spindle speed and 457 mm/min feed rate with 8mm diameter coated carbide drill. This deviation showed that the FE model which was utilized with 3-D constitutive model, failure model with fully capable 3-D solid elements and zero-thickness cohesive surfaces could estimate drilling induced torque accurately and it gave the confidence about the capability of the FE model. Thus, investigations using step drills were performed based on FE analysis with the second approach. All the torque values reported below are the average values from the steady state drilling stage, and the secondary drilling stage for step drills.

Figure 6-10 shows the numerical predictions of torque in drilling of CFRP without any support plate at 457 mm/min feed rate and 4500 rpm spindle speed (113 m/min cutting speed). The FE model estimated torque to be 0.3 N.m in drilling CFRP by 8 mm diameter rigid twist drill. When step drills were utilized in FE analysis of drilling of CFRP without any support plate, torque values were estimated significantly lower than the twist drill. The comparison of the torque values for the twist drill and step drills with various stage ratios is shown in Figure 6-10. The higher stage ratio has provided higher reduction in torque. 0.20 N.m was estimated for the step drill with 0.56 stage ratio or 4.5 mm

step drill diameter whereas the torque was estimated to reduce to 0.08 N.m for 6.5 mm step drill diameter, or 0.81 stage ratio. The smaller area to be cut by the cutting edges of the step drill required smaller contact between the workpiece and the drill. The smaller contact provides smaller friction between the drill surfaces and the workpiece. This minimizes the required torque in addition to thrust force and related cutting energy.

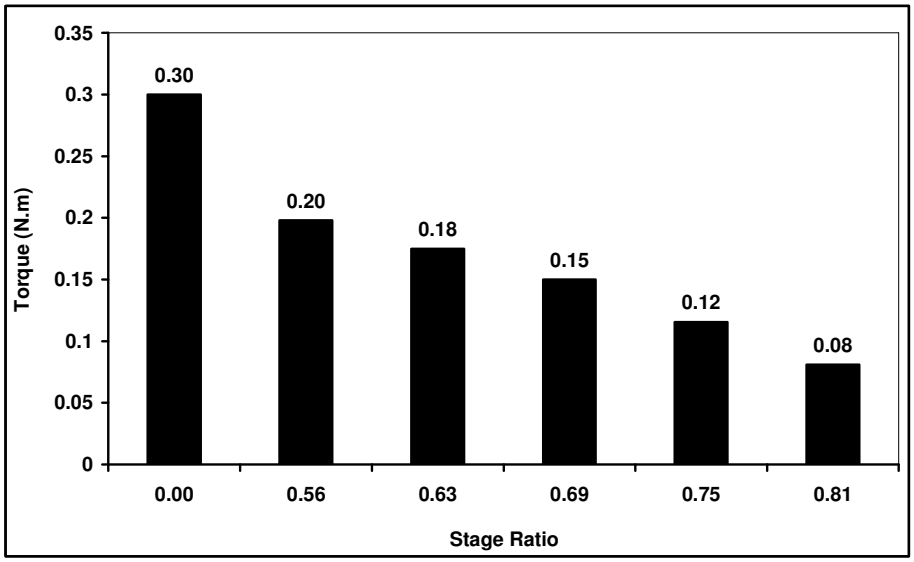

Figure 6-10: Effect of Drill Geometry on Torque

Torque was estimated to reduce significantly due to initial step part of the step drill. The reduced torque would assist to achieve reduced friction, thus reduced surface roughness and cutting temperatures. The thermal defects in the polymer based composites could be minimized with the use of step drill. These could help to maintain high structural integrity and provide longer service life for the workpieces. Possible material rejections could be also decreased, so lower cost of manufacturing could be achieved.

In general, to obtain more accurate results via finite element analysis, deformable cutting tool and extremely fine mesh could be used with regard to the computational facilities. However due to the complexity of the geometry and the process with a deformable cutting tool and very fine mesh would require huge computing resources. A contact model with anisotropy and thermo-mechanical FE analysis would also develop the model further.

6.3.3 Effect of Tool Wear on Torque

The number of holes can be drilled should be determined to provide quality and economic manufacturing process. Figure 6-11 shows the development of induced torque versus number of holes drilled in CFRP without back-up plate at 457 mm/min feed rate and 4500 rpm spindle speed (113 m/min cutting speed). During drilling experiments of CFRP, torque increased steadily. After drilling 56 holes in CFRP, torque rose by 164.5 % from 0.29 N.m to 0.767 N.m. The final torque was remarkable comparing the very initial induced torque. Figure 6-11 clearly presented the importance and influences of wear on torque.

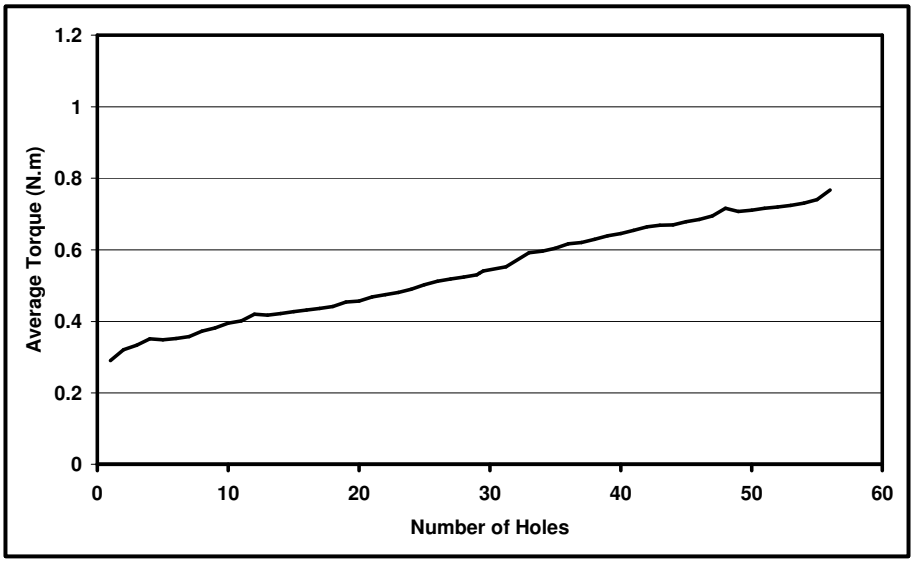

Figure 6-11: Effect of Number of Holes on Torque in Drilling of CFRP (S=4500 rpm, f=457 mm/min)

At the end of 56 holes in CFRP, the flank wear of drill bit has reached the wear criterion which was set to 0.25 mm for 8 mm diameter twist drill according to the industrial experience. The drill was considered to reach its service life, thus cutting action was not suggested beyond this limit since torque might increase remarkably due to the loss of sharpness of cutting edges of the drill. In that case it would be difficult to maintain the quality of the drilled holes due to increase in friction between drill and workpiece and higher mechanical and thermal stresses. This would also cause to possible changes in material

removal mechanisms which could lead to excessive wear rate and material defects.

6.4 Analysis of Delamination

Figure 6-12 shows typical drilling induced delamination and the digital image processing for the assessment of delamination. These delamination figures were used to evaluate the effects of process parameters on delamination after drilling CFRP without back-up plate.

Figure 6-12: Digital Image Processing of Delamination

Figure 6-13 (a) and Figure 6-13 (b) show entrance delamination images for experimentally observed and FE estimation after drilling of CFRP without a support plate at 457 mm/min feed rate and 4500 rpm spindle speed, respectively. The white areas in Figure 6-13 (a) and Figure 6-13 (b) show the complete damaged area after the drilling which is called entrance delamination at the outer surface of the workpiece whereas the red area in Figure 6-13 (b) shows the delamination propagation between two layers what can cause the loss of the strength in the structural component. The damage area was slightly overestimated and the entrance delamination factor has been predicted as 1.3 with the use of 3-D elements. The experimentally obtained entrance delamination factor was 1.2, so the estimation of the FE model could be expressed reasonable. The diversity of estimated entrance delamination factor, F_D, comparing to the experimental obtained result was 8% for the given process parameters. Comparing the FE model with continuum shell elements predicted the delamination factor has been improved from of 1.4 to 1.3. The speed of the drilling process may have an influence on the crack propagation, thus delamination parameters may need to be checked at high speed tests.

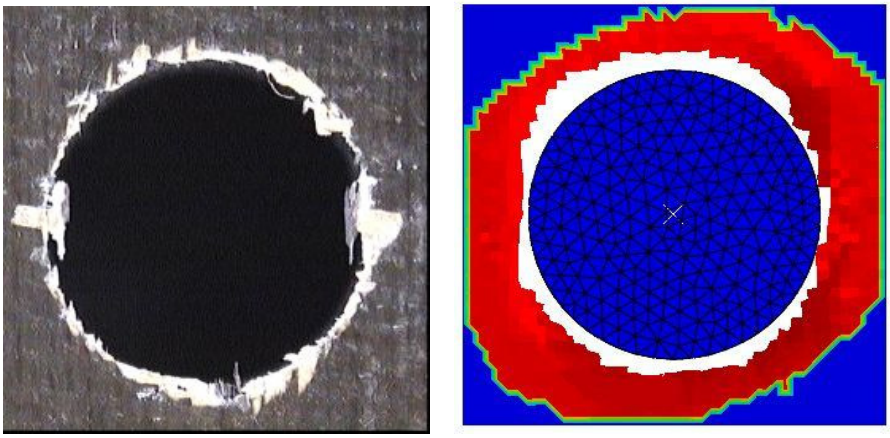

(a) (b)

Figure 6-13: Entrance Delamination (a) Experimental (b) Finite Element Analysis

6.4.1 Effects of Process Parameters on Delamination

Figure 6-14 shows the both delamination factors, conventional delamination factor (F_D) and alternative delamination factor (F_A), obtained under different cutting conditions after experimental drilling of CFRP without support plate at the hole entry. It can be seen that with the use of the alternative delamination factor (F_A), which was related to the damaged area, generally smaller extent of delamination was provided comparing to the conventional delamination factor (F_D) at the hole entrance. The average difference between both conventional factors found to be 2.33%. The conventional delamination factor was dependent on the local maximum damaged point on the vicinity of hole, thus in the image. It can also be noted that delamination increased with the feed rate and decreased with the cutting speed in the test region. When the cutting speed increased 200%, the alternative delamination factor decreased between 8.56% and 14.02% whereas conventional delamination factor reduced between 1.83% and 11.11% with regards to the feed rate in the tests. An increase of the feed rate by 93% caused to an increase in the alternative delamination factor between 4.01% and 9.47% whereas 1.63% and 8.13% increase in the conventional delamination factor depending on the cutting speed.

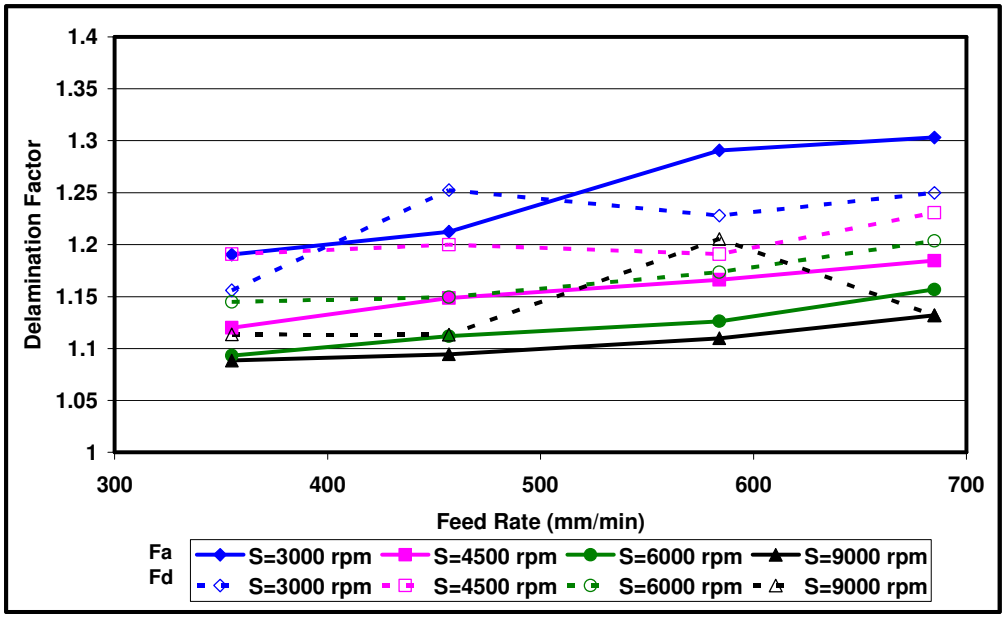

Figure 6-14: Effects of Cutting Parameters on Delamination Factors-Experimentally Obtained (1st Approach: Shell Elements, 2nd Approach: Solid Elements)

Figure 6-15 shows the effects of cutting parameters on conventional delamination factors (F_D) evaluated through the finite element analysis simulation for the both FE approaches. It can be seen that the general trends of the conventional delamination factors in both approaches were similar to the experimental results, delamination increased with the feed rate and decreased with the cutting speed in the range simulated. The finite elements results indicate that the conventional delamination factor was estimated between 1.17 and 1.52 with the first FE approach; 1.15 and 1.38 with the second FE model with regard to process parameters. The average of the conventional delamination factors were 16.58% and 9.15% higher than the experimentally obtained results for the first and second FE approaches, respectively. The FE approach which utilized with fully solid elements for intra-laminar material behaviour and zero-thickness cohesive based surfaces for inter-laminar material behaviour estimated delamination closer to the experimental results. The employment of material model and failure model with the 3rd component of stress in loading direction provided to predict more realistic drilling induced delamination at the entrance of the holes of CFRP.

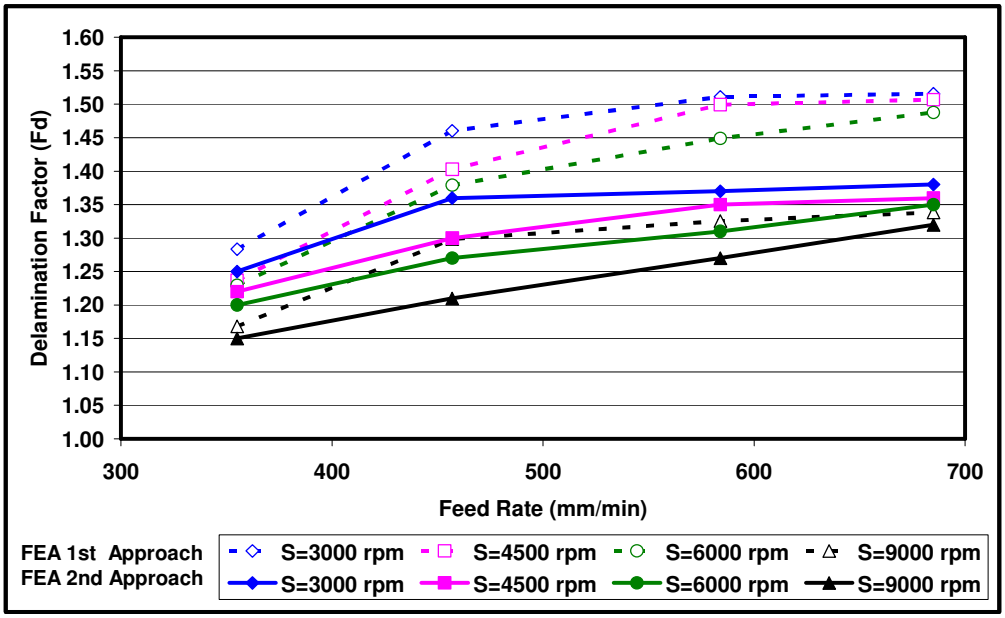

Figure 6-15: The Effect of Cutting Parameters on Drilling Induced Delamination at Entrance- Finite Element Analysis

Table 6-3 shows the experimental and estimated drilling induced conventional delamination factors at the entrance of holes in details for each cutting condition. The experimental results show that the minimum induced conventional delamination factor was obtained as 1.11 in the tests at 9000 rpm spindle speed and 355 mm/min feed rate whereas the maximum induced conventional delamination factor was found to be 1.25 in test performed at 3000 rpm spindle speed and 685 mm/min feed rate in drilling of CFRP with 8 mm diameter twist drill. 93% higher feed rate resulted between 1.63% and 8.13% greater amount of delamination with regard to the cutting speed; whereas 200% greater cutting speed led a decrease between 1.83% and 11.11% in delamination factor according to the feed rate in drilling of CFRP. Both process parameters were found to have influences on delamination factor, however the effect of feed rate on delamination factor was slightly higher than the effect of spindle speed.

The overall trends of simulated drilling induced delamination with the process parameters have been shown and discussed above. Table 6-3 shows estimated the conventional delamination factors at the hole entry for each set of machining parameters in detail for the both FE approaches. According to the

first FE approach, the minimum delamination factor was estimated as 1.17 at 9000 rpm and 355 mm/min which was the combination of the maximum spindle speed and the minimum feed rate with 8 mm diameter rigid twist drill. The maximum conventional delamination factor was calculated 1.52 at 3000 rpm spindle speed and 685 mm/min, which was the combination of the least cutting speed and the largest feed rate. The results show that 93% higher feed rate caused an increase in drilling induced delamination factor between 14.59% and 21.83% depending on the cutting speed; whereas 200% greater cutting speed led to a decrease between 8.99% and 12.27% in delamination factor at the entry according to the feed rate in drilling of CFRP. However the percentage change of feed rate was smaller than the change of cutting speed, a higher influence on delamination factor has been observed which indicates that feed rate was the dominant process parameters on delamination factor in the simulations with the first FE approach. The effect of cutting speed on delamination factor cannot be ignored. Nevertheless, the results based on the 1st FE model has shown that drilling induced delamination has been predicted with deviations between 3.86% and 25.90% according to the drilling conditions.

As it can be observed from Table 6-3 for the results of 2nd FE approach, the minimum delamination factor was calculated 1.15 at 9000 rpm spindle speed and 355 mm/min feed rate which was the combination of the maximum spindle speed and the minimum feed rate with the 8 mm diameter rigid drill. The maximum induced delamination factor was predicted as 1.37 at 9000 rpm spindle speed and 685 mm/min feed rate. The FE results indicate that 93% higher feed rate resulted in an increase between 10.40% and 14.78% in conventional delamination factor depending on the cutting speed; whereas 200% greater cutting speed caused to a decrease between 4.35% and 11.03% in conventional delamination factor according to the feed rate in drilling of CFRP. However the change of feed rate was smaller than the change of cutting speed, higher influence on delamination factor has been observed which indicates that drilling induced delamination was more susceptible to the change in feed rate in FE analysis. The deviations of predicted drilling induced delamination factor based on the second FE approach lay between 2.44% and 16.63%, with overestimation according to the set of process parameters. The difference

between the experiments and simulation results was generally larger at higher feed rates.

Table 6-3: Experimental and Simulation based Delamination in Drilling of CFRP

Feed Rate (mm/min)	Spindle Speed (rpm)	Delamination Factor (F_D) Experimental	Delamination Factor (F_D) FEA-1st model	Deviation (%)	Delamination Factor (F_D) FEA-2nd model	Deviation (%)
355	3000	1.16±0.01	1.28	11.04	1.25	8.13
457	3000	1.25±0.01	1.46	16.62	1.36	8.59
584	3000	1.23±0.02	1.51	23.06	1.37	11.57
685	3000	1.25±0.03	1.51	21.03	1.38	10.40
355	4500	1.19±0.01	1.24	3.86	1.22	2.44
457	4500	1.20±0.02	1.40	16.92	1.30	8.34
584	4500	1.19±0.02	1.50	25.90	1.35	13.36
685	4500	1.23±0.02	1.51	22.43	1.36	10.49
355	6000	1.14±0.01	1.23	7.39	1.20	4.82
457	6000	1.15±0.01	1.38	19.99	1.27	10.49
584	6000	1.17±0.02	1.45	23.47	1.31	11.63
685	6000	1.20±0.02	1.49	23.62	1.35	12.16
355	9000	1.11±0.01	1.17	4.91	1.15	3.27
457	9000	1.11±0.01	1.30	16.65	1.21	8.70
584	9000	1.21±0.02	1.33	9.97	1.27	5.35
685	9000	1.13±0.02	1.33	17.39	1.32	16.63

Delamination was estimated to increase with regards to the increase in feed rate and decrease in the spindle speed. The higher delamination could deteriorate structural integrity and even could be reason for rejection. Combination of moderately low feed rate and higher spindle speed could reduce delamination and provide longer service life for the workpieces.

However it should be noted that the use of high spindle speed would increase the wear rate.

It should be mentioned that the trends predicted by the FE models were in agreement with the experimental values for the delamination. In general, in order to achieve very accurate results for prediction of delamination using simulation, extremely fine mesh and very good damage model are essential. However due to the complexity of the geometry and the process moving to very fine mesh would require huge computing resources. Limitation in the computing resources and computing time had restricted us in terms of the mesh refinement. Within the resources available the accuracy of the predictions of the delamination factors for different process parameters are acceptable.

6.4.2 Effect of Tool Geometry on Delamination

Figure 6-16 shows delamination in the vicinity of holes at both sides, entrance and exit, in FE simulations after drilling of CFRP without back-up plate by step drills at 457 mm/min feed rate and 4500 rpm spindle speed. As shown in Figure 6-16, white areas symbolizes the complete damaged area due to fracture and delamination after drilling CFRP whereas spring colors show the propagation of delamination at the interface of two adjacent plies which can cause to strength degradation of the structure. FE simulations show that the damage area declined with the increase in the stage ratio of step drill. This was mainly due to the fact that the chisel edge effect was avoided in the second stage cutting of step drill. In addition to that less material was cut by the cutting edges of step drill with higher stage ratio. Therefore lower cutting energy and cutting forces were required in high stage ratio step drill. Thrust force and torque estimations shown in Figure 6-6 and Figure 6-10 can be indicators of this.

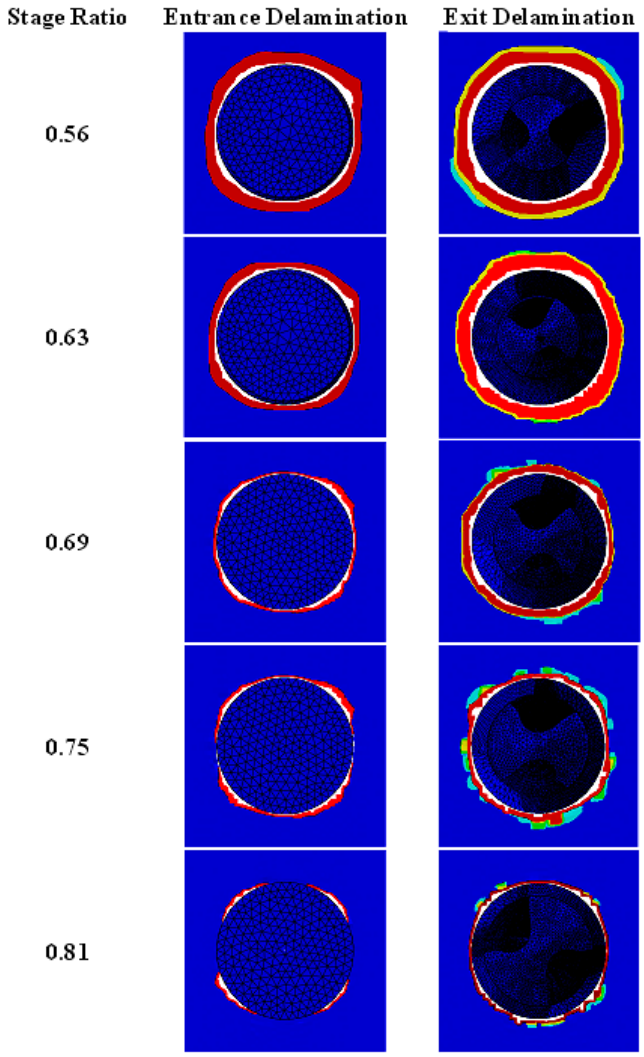

Figure 6-16: Delamination patterns in drilling of CFRP by step drills (S=4500 rpm, f=457 mm/min)

Figure 6-17 shows FE predictions of alternative delamination factors versus stage ratio after drilling of CFRP without back-up plate by step drill at 457 mm/min feed rate and 4500 rpm spindle speed at both sides, entrance and exit. As shown in Figure 6-17, exit delamination factor was estimated greater than the entrance delamination factor since the last plies at exit side were more vulnerable against thrust force. Both entrance delamination factor and exit delamination factor tended to decrease with the increasing stage diameter of the step drill. When the alternative delaminaton factor at the entrance was estimated 1.3 without back-up plate by twist drill, it was predicted 1.07 with step drill with 6.5 mm stage diameter. Similar observations can be made for the

exit delamination. The improvements in delamination factors can show the advantages of step drill in drilling of CFRP. Thrust force, torque and delamination can be declined by the use of step drill with high stage ratio. Work piece defects could be control with the proper selection of step geometry and process parameters. These results have been confirmed by previous research works [100, 110] where the critical thrust force responsible from delamination in drilling of CFRP with pilot hole and step drill was studied. As the ratio of pilot hole or stage ratio of step drill increases, the critical thrust force increases whereas the thrust force decreases which means that the composite structure becomes more resistant against delamination. Prevention of the effects of chisel edge of drill bit in drilling of CFRP minimizes thrust force and delamination.

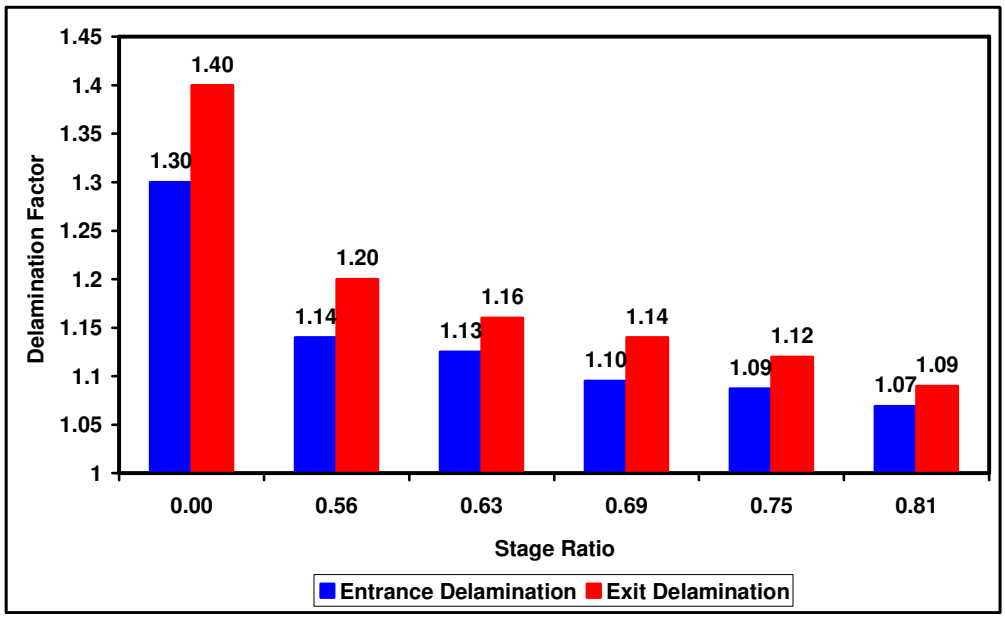

Figure 6-17: Effect of Drill Geometry on Delamination (S=4500 rpm, f=457 m/min)

Delamination was predicted to be substantially lower due to initial step part and disappearance of the chisel edge of the drill. The reduced delamination would mean that higher structural integrity and possibly longer service life. The use of step drill could avoid the possible rejections owing to tight tolerances, so it could boost the improvements in manufacturing costs.

In general, to obtain more accurate results via finite element analysis, deformable cutting tool and extremely fine mesh could be used with regard to

the computational facilities. Nevertheless, the complexity of the geometry and the process with a deformable cutting tool and very fine mesh would require huge computing resources. A contact model with anisotropy and thermo-mechanical FE analysis would develop the model.

6.4.3 Effect of Tool Wear on Delamination

It is important to determine the extent of delamination in the workpiece in order to assess the structural integrity of the machined part. This also provides a limit number of holes that can be drilled in the structures before replacing the tool. Figure 6-18 and Figure 6-19 present the features of the delamination patterns observed at the entry and exit side of the drilled CFRP laminates, respectively. The images were used to measure the extent of the delamination via a developed algorithm based on digital image processing. Figure 6-18 and Figure 6-19 indicate a typical brittle damage due to brittle fibres in the composite structure.

Figure 6-18 (a) and Figure 6-18 (b) show the state of the entry of the hole after drilling of CFRP. Even in the first hole, fibre pull outs and delamination were observed at the entry of the hole as shown in Figure 6-18 (a). After reaching tool wear (V_B=0.25 mm) with drilling 56 holes, significant delaminated area was observed at the hole entry in drilling of CFRP as given in Figure 6-18 (b).

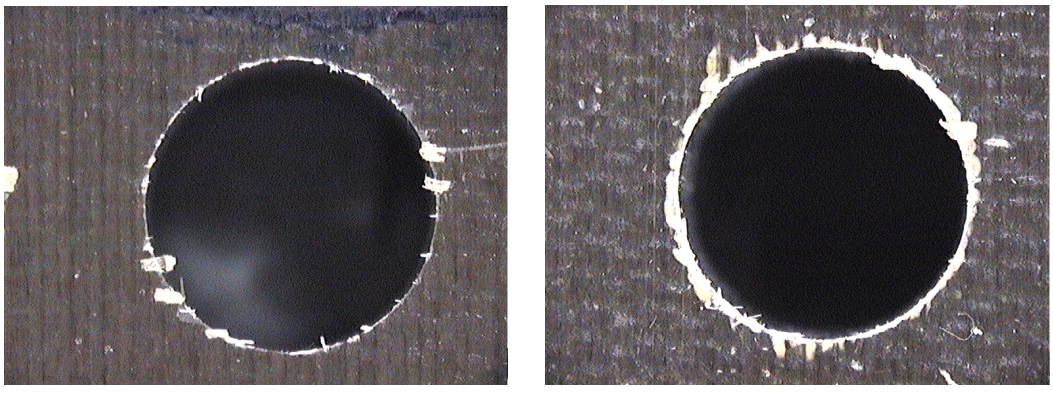

(a) (b)

Figure 6-18: Delamination at Hole Entry (S=4500 rpm, f=457 mm/min) (a) Drilling of CFRP plate-1st Hole (b) Drilling of CFRP -56th Hole

Figure 6-19 (a) and Figure 6-19 (b) show the state of the exit of the hole after drilling of CFRP. As it can be noticed in Figure 6-19 (a), there is a significant indication of fibre pull outs even in the first hole in drilling of CFRP. After 56 holes, excessive delamination with buckled fibres was observed in drilling of CFRP as shown in Figure 6-19 (b). In the test region, the last ply of the CFRP could not withstand thrust force what resulted in very poor exit surface.

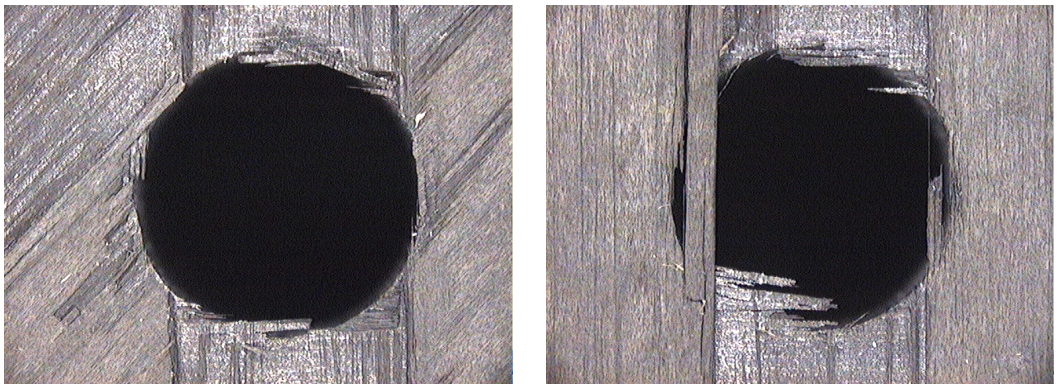

(a) (b)

Figure 6-19: Delamination at Hole Exit (S=4500 rpm, f=457 mm/min) (a) Drilling of CFRP -1st Hole (b) Drilling of CFRP -56th Hole

Since the structural integrity of structures is vital in the aerospace industry, tool life may not be the only criteria to determine a feasible manufacturing operation. In order to preserve the accuracy and quality of drilled hole, a limit number could be decided to replace the tool based on the delamination factor. Figure 6-20 indicates the influence of the number of drilled holes on delamination factors. It shows delamination factors at hole entry versus number of holes drilled in drilling of CFRP without a support plate at constant 457 mm/min feed rate and 4500 rpm spindle speed. As it can be observed from Figure 6-20 both delamination factors rose approximately 10 % after drilling 56 holes in CFRP. It should also be noted that, alternative delamination factor presented lower values comparing to conventional delamination factor. The difference between them remained generally the same as the number of drilled holes increased.

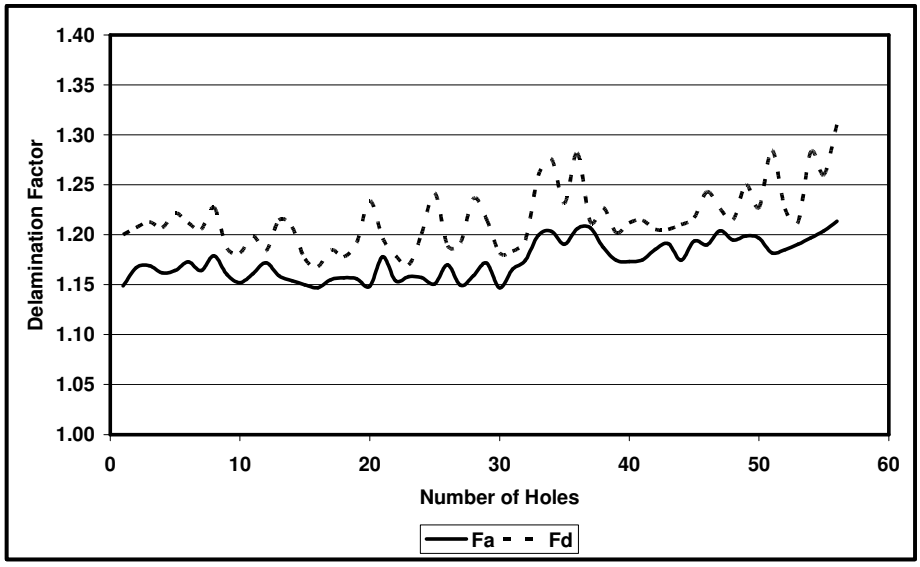

Figure 6-20: Effect of Number of Holes on Delamination Factors (S=4500 rpm, f=457 mm/min-Hole Entry)

6.5 Analysis of Surface Roughness

Influences of process parameters and tool wear on surface roughness have been investigated. In order to investigate the influences of process parameters on drilling of CFRP, experiments were performed at the combinations of four feed rates and four spindle speeds, a total of 16 set of cutting condition. Effect of tool wear on surface roughness was investigated at one set of parameters. All the drilling experiments were conducted with the use of 3 μm TiN/TiAlN multilayer coated 8 mm diameter tungsten carbide twist drill with 140° point angle and 30° helix angle in wet conditions. All experiments were carried out with high pressure cooling through tool coolant holes of drills. 5 percent emulsion of Hocut 795B cutting fluid was applied in wet cutting experiments at a constant 38 bar coolant pressure (equal flow rate of ~2.4 l/min). Each surface roughness measurement was repeated 5 times.

6.5.1 Effects of Process Parameters on Surface Roughness

Figure 6-21 shows influences of cutting parameters on the average surface roughness (Ra) when drilling CFRP at different cutting parameters. The average surface roughness was obtained between 1.78 μm and 6.35 μm in drilling of CFRP workpiece without support plate within the range of cutting parameters

tested. Figure 6-21 shows that the average surface roughness increased with increased feed rate significantly. Feed rate was found the dominant factor on the average surface roughness. Spindle speed had an influence on the average surface roughness. However this effect was not as significant as feed rate. The higher spindle speed led to a decrease in the average surface roughness. The trend of the surface roughness also agreed with the literature [20, 57, 71, 159].

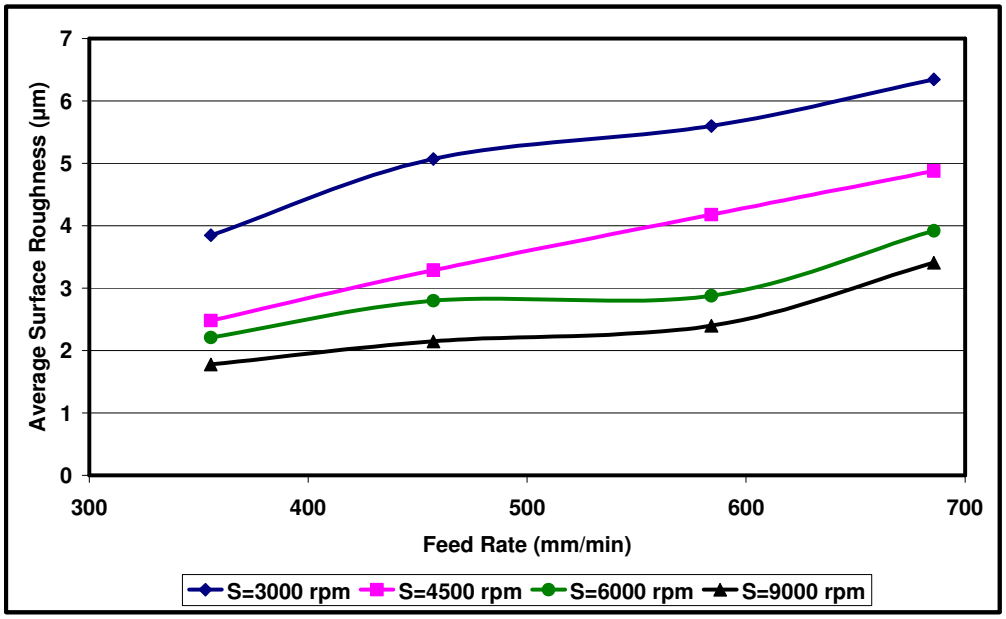

Figure 6-21: Effects of Cutting Parameters on the Average Surface Roughness in Drilling of CFRP

Table 6-4 shows the experimental average surface roughness in details for each cutting condition. The experimental results show that the minimum average surface roughness was obtained as 1.78 µm in the tests at 9000 rpm spindle speed and 355 mm/min feed rate whereas the maximum average surface roughness was found to be 6.35 µm in test performed at 3000 rpm spindle speed and 685 mm/min feed rate in drilling of CFRP with 8 mm diameter twist drill. 93% higher feed rate resulted between 64.87% and 96.69% greater amount of average surface roughness depending on the cutting speed; whereas 200% greater cutting speed caused a decrease between 46.27% and 57.59% in average surface roughness according to the feed rate in drilling of CFRP. However the change in the feed rate was smaller in percentage than the change in the cutting speed in the test region, the average surface roughness

was affected significantly more in the change of the feed rate. This clearly means that the average surface roughness was more susceptible to the change in feed rate.

Table 6-4: Experimentally obtained Average Surface Roughness in Drilling of CFRP

Feed Rate (mm/min)	Spindle Speed (rpm)	Surface Roughness (μm)
355	3000	3.85±0.4
355	4500	2.48±0.3
355	6000	2.21±0.3
355	9000	1.78±0.2
457	3000	5.07±0.4
457	4500	3.29±0.3
457	6000	2.80±0.3
457	9000	2.15±0.2
584	3000	5.60±0.5
584	4500	4.18±0.4
584	6000	2.88±0.3
584	9000	2.40±0.2
685	3000	6.35±0.5
685	4500	4.88±0.4
685	6000	3.92±0.4
685	9000	3.41±0.3

Results show that desired surface roughness in industry which is typically below 3.2 μm R_a can be reached with the selection of medium-high spindle speed and low-medium feed rate in the machining of CFRP using the multilayer TiAlN/Ti coated WC drills. Provided that these suggested process parameters are used, tight tolerances could be achieved and the rejections would be minimized.

6.5.2 Effect of Tool Wear on Surface Roughness

Since the surface roughness is another important aspect and machining criterion, it is worth to determine the number of holes that can be drilled in CFRP workpiece to maintain workpiece quality and low cost manufacturing solution. Progression of the average surface roughness by the number of holes can be observed during drilling in addition to the development of the wear regions. Figure 6-22 shows average surface roughness versus number of holes drilled in CFRP at 457 mm/min feed rate and 4500 rpm spindle speed (113 m/min cutting speed). During drilling experiments of CFRP, average surface roughness increased gradually. Higher oscillation can be observed comparing to drilling of conventional metal due to oriented fibres. After drilling 56 holes in CFRP, average surface roughness increased by 93.94 % from 3.3 μm to 6.4 μm. This was due to the developed tool wear and consequently increased thrust force.

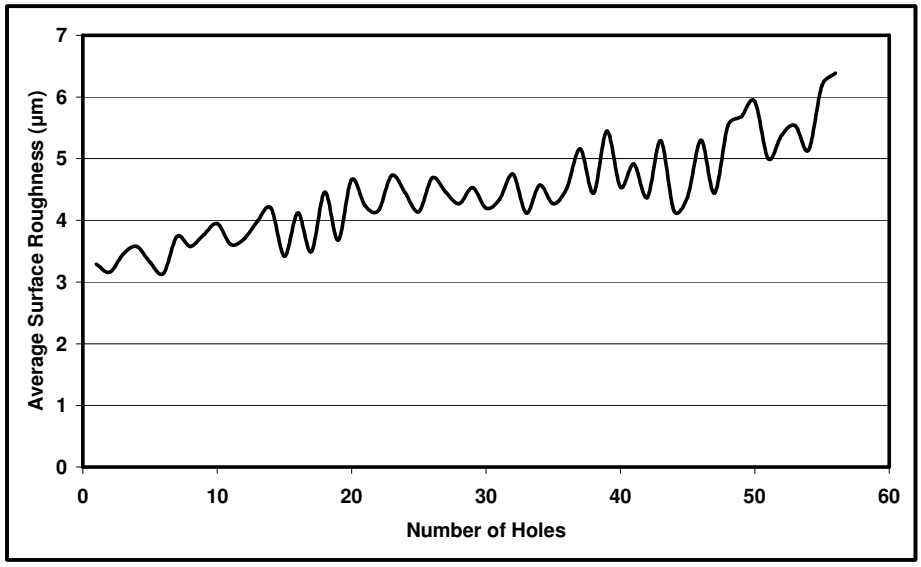

Figure 6-22: Effect of Number of Holes on the Average Surface Roughness in drilling of CFRP (f=457 mm/min S=4500 rpm)

Since the flank wear has reached the 0.25 mm critical value which has been stated as the tool life criteria based on the industrial experience in the methodology section, the drill was considered to have reached its end of life. Beyond this limit, it is not suggested to continue drilling. Average surface

roughness could increase due to increased wear and possible significant increase in thrust force and chatter. Increased surface roughness would elevate contact stresses in the structures due to very local high peaks.

6.6 Analysis of Tool Wear

Severe tool wear in machining of aerospace materials is one the main reasons for machining cost. In order to maintain quality of the machined workpieces, it is important to replace cutting tools as they reach wear criteria as explained in methodology section. Variation of thrust force, torque, delamination and surface roughness versus number of holes drilled can be typical indication of tool wear as discussed in previous subsections.

During drilling of CFRP, thrust force rose steadily from 235 N to just over 605 N after 56 holes. Beyond this number of holes, cutting process would not be stable due to excessive wear of the cutting edges. The gradual loss of sharpness of cutting edges causes a decrease in the capability of tool to cut the material, thus it leads an increase in cutting forces and torques. The increase in tool wear would degenerate the material removal mechanism progressively. Figure 6-23 shows tool wear after drilling 56 holes in CFRP at process parameters of 4500 rpm and 457 mm/min. From the optical observation, it was found that edge wear was the major wear in drilling CFRP. When abrasive fibres are being cut; the broken fibres scratch both flank and crater surfaces of the drills. In addition to that very abrasive fibres are not cut as metals. In metals the main cutting mechanism is plastic deformation as chip flows over the cutting edges. However, there is no plastic deformation in machining of CFRP. Cutting tool induces fracture in the brittle fibres. This generates dusty and abrasive chips which can cause three-body-effect in the cutting mechanism. The dusty chips would result in direct impingement of hard particles on both machined surfaces and tool surfaces. This would consequently cause erosion by abrasion. The flank and crater wear are shown in Figure 6-23 (b) and Figure 6-23 (c).

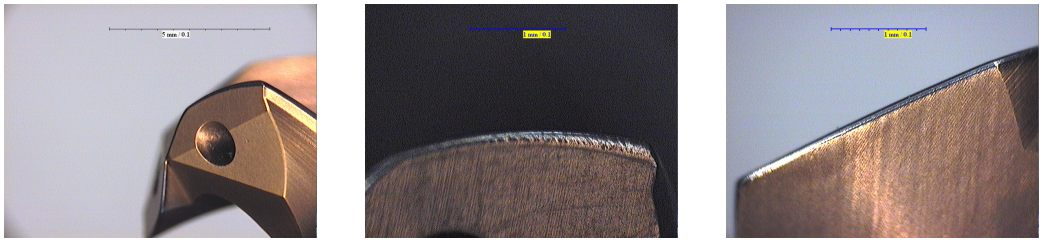

(a) (b) (c)

Figure 6-23: Tool Wear in Drilling of CFRP (S=4500 rpm, f=457 mm/min) (a) Overall (b) Flank Wear (c) Crater Wear

Figure 6-24 shows the effects of the number of holes drilled on tool wear in drilling of CFRP. Both flank wear and crater wear of drill bit versus number of holes drilled are indicated. The drilling parameters for these tests are 457 mm/min of feed rate and 4500 rpm of spindle speed. The flank wear passed beyond the 0.25 mm tool wear criterion after 56 holes whereas crater wear reached to 0.12 mm. The wear on the clearance surface was more significant compared to the wear on the rake surface. This was due to the fact that the drill was mainly in contact with the abrasive fibres on the cutting edges. Due to the lack of chip formation which can seen in drilling metals, the crater wear was less significant in the drilling of CFRP. However it was not negligible. Therefore still flank wear played a role in the wear of cutting edges of the drill. After drilling 56 holes at 4500 rpm spindle speed and 457 mm/min feed rate, 2.5 min tool life was recorded for drilling of CFRP with multilayer TiAlN/TiN coated WC drill.

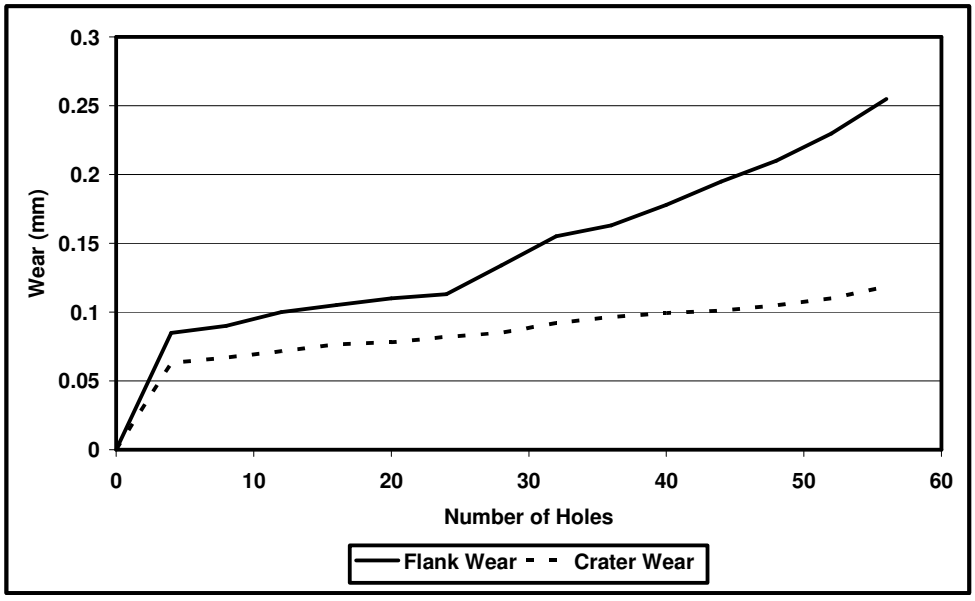

Figure 6-24: Progression of Tool Wear in Drilling of CFRP (S=4500 rpm, f=457 mm/min)

In summary, in drilling of CFRP abrasive wear occurred in both flank and crater surface of the tool due to the brittle fibres. These two wear creates edge wear which grinded the cutting edge gradually. Because of this thrust force, torque, delamination and the average surface roughness increased gradually. There was no sign of plastic deformation and chipping on tool surfaces.

6.7 Analysis of Workpiece Stress Distribution

The progressive damage and the stress distributions of the CFRP work piece during the drilling process are shown in Figure 6-25 (a) and Figure 6-25 (b). 8 mm rigid twist drilled the CFRP workpiece at 4500 rpm spindle speed and 457 mm/min feed rate in the FE analysis. Stress was induced in the work piece as the drill cuts the work piece material surface. As it can be observed from Figure 6-25 (a), the highest stresses induced around the centre of the hole where the drill pushed the material. The induced Mises stress was estimated up to 1.2 GPa whereas after the drilling the residual stress on the workpiece was estimated 60 MPa in some local places as shown in Figure 6-25 (a) and Figure 6-25 (b), respectively.

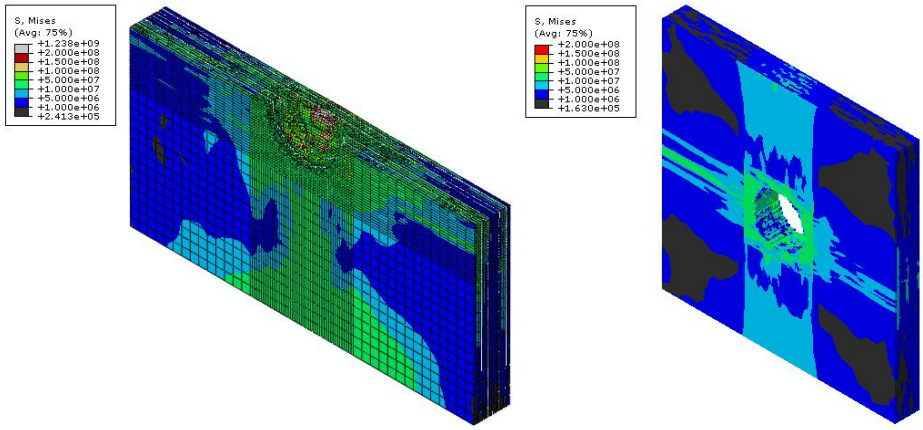

(a) (b)

Figure 6-25: Workpiece Stress Distribution (a) at 0.4 s (b) After drilling (S=4500 rpm, f=457 mm/min)

The dominant mode of failure was predicted matrix failure. Due to the penetration and cutting action of the drill, the matrix failed easily compared to the fibres. Figure 6-26 shows the matrix failure under tension mode after drilling of CFRP. This matrix crack could contribute to delamination initiation and growth which results in fibre buckling.

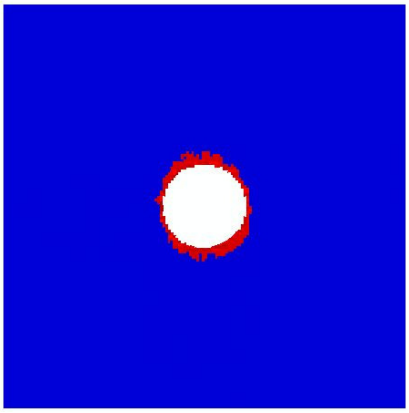

Figure 6-26: Matrix Failure in drilling of CFRP

6.7.1 Effect of Tool Geometry on Workpiece Stress Distribution

The stress distributions of the CFRP work piece after the drilling process are shown in Figure 6-27 (a) and Figure 6-27 (b). As it can be observed in Figure

6-27 (a) and Figure 6-27 (b), the highest stresses were induced around the centre of the hole where the drill cut the material. The Mises stress was estimated lower in drilling of CFRP with 0.63 stage ratio rigid step drill compared to drilling of CFRP with 8 mm rigid twist drill at 4500 rpm spindle speed and 457 mm/min feed rate. This was due to the fact that the step drill performs the secondary stage cutting with a lower contact area compared to the twist drill. The decrease in the contact means less material to be cut. The reduced material would require less energy and force hence less induced stress and damage in the workpiece. The estimated thrust force and torque in the previous sections can be the sign of this reduction.

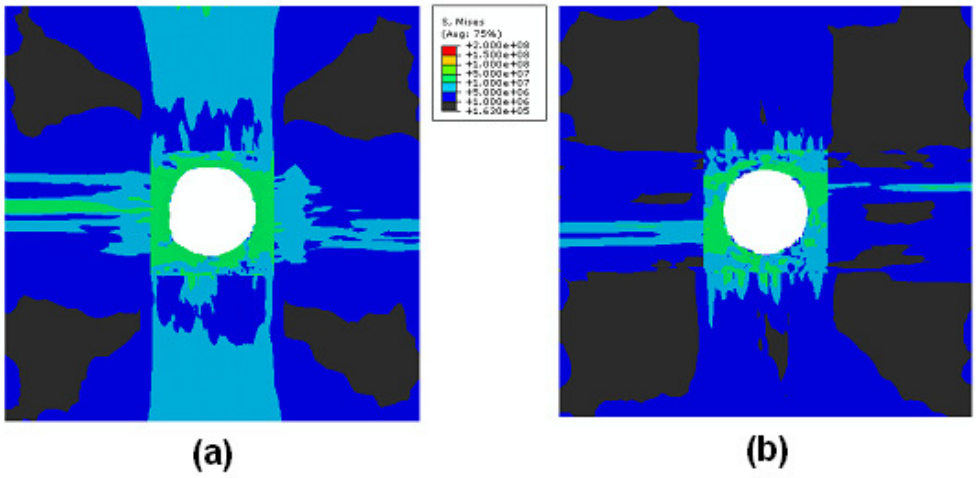

Figure 6-27: Effect of Drill Geometry on Stress (a) Twist Drill (b) Step Drill (S=4500 rpm, f=457 mm/min)

6.8 Summary of Drilling of CFRP

Experimental and finite element simulations were performed for investigations of drilling of CFRP without support plate. The effects of process parameters and complex tool geometry on drilling outputs have been examined in drilling of CFRP. All experiments were carried out with coolant.

Finite element simulations were performed using two approaches. In the first approach solid-like (continuum shell) elements and finite-thickness cohesive elements were utilized for the intra-laminar and inter-laminar behaviour of CFRP with the related in-built material and failure models,

respectively. In the second approach fully solid elements and zero-thickness cohesive surfaces employed for the intra-laminar and inter-laminar of behaviours of the CFRP with the related user defined material model and failure model, respectively. The main difference between these two approaches was the implication of the response of the material in the normal direction (out-of-plane) of the workpiece. The results showed that the second FE approach outperformed the initial approach.

Experimental results showed that an increase in feed rate led to an increase in thrust force, torque, delamination and surface roughness in drilling of CFRP with 8 mm twist drill. The increase in spindle speed caused an increase in thrust force and torque whereas a decrease in delamination and average surface roughness. The development of tool wear led to a significant increase in thrust force, torque, delamination and surface roughness.

Finite element analysis based on the second approach exhibited a good performance. Positive correlations were acquired for thrust force, torque and drilling induced delamination with good accuracy in drilling of CFRP with 8 mm rigid twist drill. The results were also in agreement with the literature. Based on the accuracy and confidence, the effect of drill geometry on drilling of CFRP has been investigated. FE results indicated the advantages of step drill on twist drill from several aspects including thrust force, torque and delamination.

The deviations might be due to the material data. The experimental test are generally carried out at slower speeds comparing to the speed of machining which can affect the material respond, particularly in matrix direction. To provide higher accuracy and improve the reliability, mechanical properties of CFRP should be tested at higher speeds.

Chapter 6

Chapter 7

Results and Discussions of Drilling of Ti-6Al-4V

Machinability of materials is important to achieve structures with high integrity and lows cost of manufacturing. To understand and provide high machinability of Ti-6Al-4V, the effects of process parameters and tool geometry have been investigated in various aspects of drilling including thrust force, torque, burr formation, surface roughness, wear, chip morphology and workpiece stress through experiments and finite element analysis.

7.1 Validation

Figure 7-1 (a) and Figure 7-1 (b) show the experimental and simulated thrust force and torque in drilling of Ti-6Al-4V at 119 mm/min feed rate and 1400 rpm spindle speed, respectively. It was observed that the thrust force in the experimental trial was 750.58 N. whereas the FE model estimated 800.25 N. The experimentally measured torque was 1.00 N.m compared to the torque value predicted as 1.20 N.m by the FE simulation. This shows that the FE model estimated the thrust force and torque with 6.62% and 20.00% deviation from the test results, respectively. Ti-6Al-4V is an elasto-plastic material and the material respond is dependant on the strain rate. Thus, the material respond is very dependant on the material data. Although the material data had been obtained at higher speeds, it is thought that it could be one of the main reasons of the diversity between the results of finite element analysis and experiments. The estimations of the FE model depend on the process parameters and could be acceptable. These results gave the confidence about the capability of the FE model in its prediction of the thrust forces and torque values for the future works.

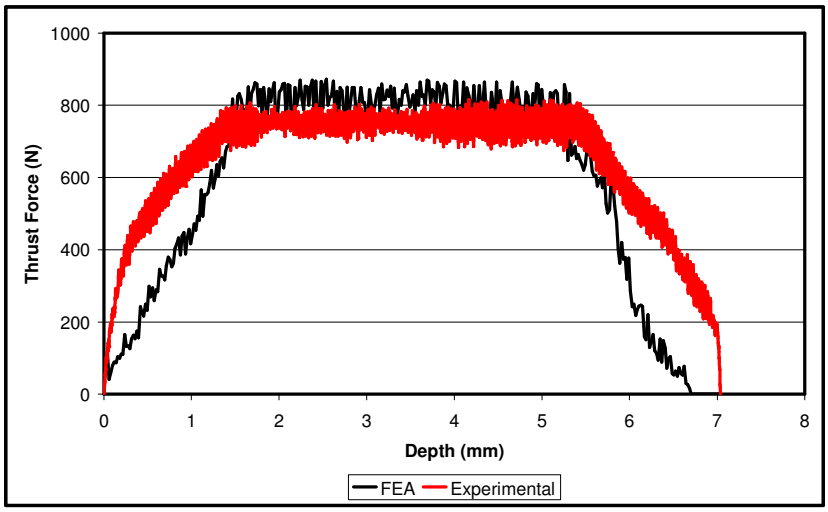

(a)

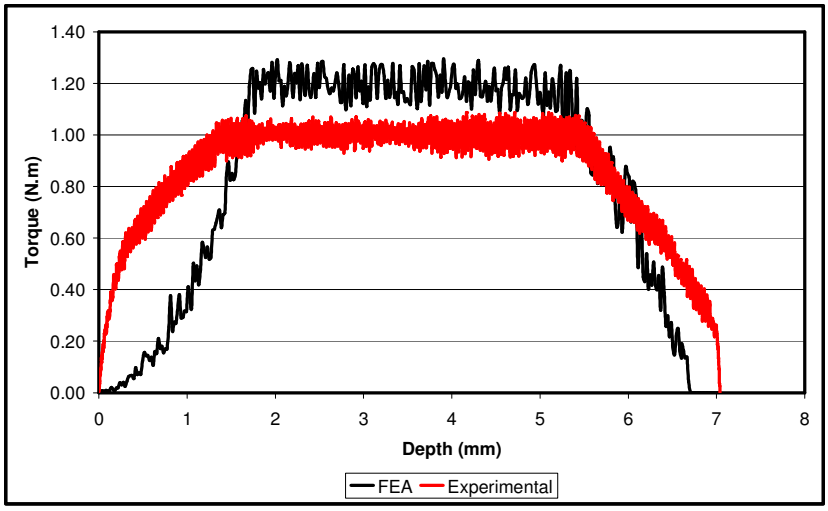

(b)

Figure 7-1: Drilling of Ti-6Al-4V (a) Thrust Force (b) Torque (S=1400 rpm, f=119 mm/min)

7.2 Analysis of Thrust Force

Figure 7-2 shows the development of thrust force in drilling of Ti-6Al-4V workpiece by 3 μm TiN/TiAlN multilayer coated 8 mm diameter tungsten carbide twist drill with 140˚ point angle and 30˚ helix angle at 119 mm/min feed rate and 1400 rpm spindle speed. Typical material drilling of a through hole consists of three stages. In the first phase drill penetrates into work piece. In the second phase, in which the whole cutting edges are in contact with the work

piece, a steady state thrust force is obtained. Finally, in the third phase drill point exits or breaks through other side of the work piece. However, in titanium peck drilling has been applied due to high possibility of tool breakage caused by chip jamming. Thus three cutting stages can be observed interrupted in drilling of Ti-6Al-4V in Figure 7-2. In the following subsections, the investigations of thrust force are made using the average thrust force which has obtained in the second phase of drilling in experiments and FE analysis.

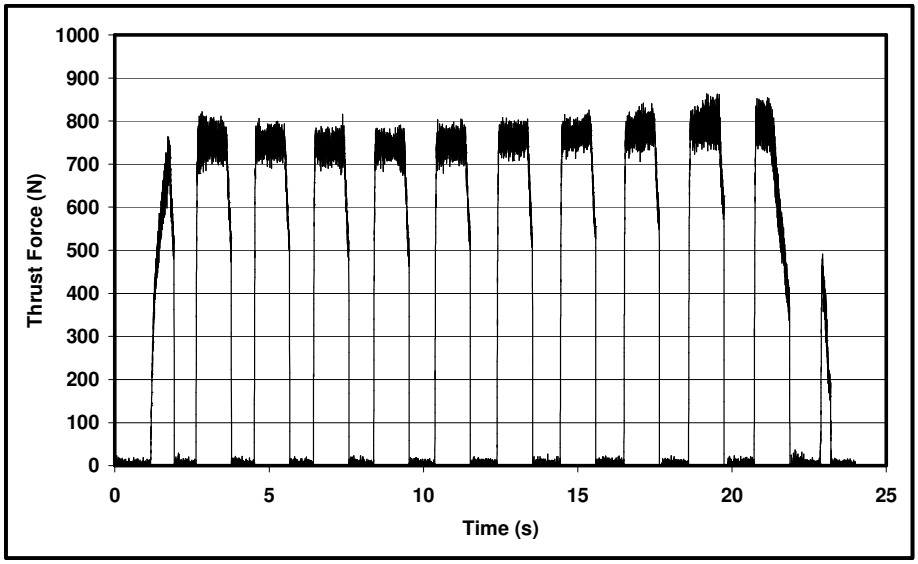

Figure 7-2: Thrust Force through Hole in Experimental Peck Drilling of Ti-6Al-4V (f=119 mm/min S=1400 rpm)

7.2.1 Effects of Process Parameters on Thrust Force

In order to investigate the influences of process parameters on drilling of Ti-6Al-4V, both the experiments and simulations were performed at the combinations of four feed rates and three spindle speeds, a total of 12 set of cutting condition. All the drilling experiments were conducted with the use of 3 μm TiN/TiAlN multilayer coated 8 mm diameter tungsten carbide twist drill with 140° point angle and 30° helix angle. In order to include the effect of drill geometry and to simulate the drilling process, 3-dimensional complex drill geometry was used in the finite element simulations. The average thrust forces obtained in drilling of Ti-6Al-4V at different machining parameters are shown for both experiments and finite element analysis in Figure 7-3. It could be

observed in Figure 7-3 that drilling induced thrust force was between 620.48 and 940.19 N regarding to the cutting condition in the drilling tests. It could also be seen that thrust force increased with the increasing feed rate and decreased with the increasing cutting speed. The results show that feed rate affected thrust force slightly more than spindle speed in the tested region.

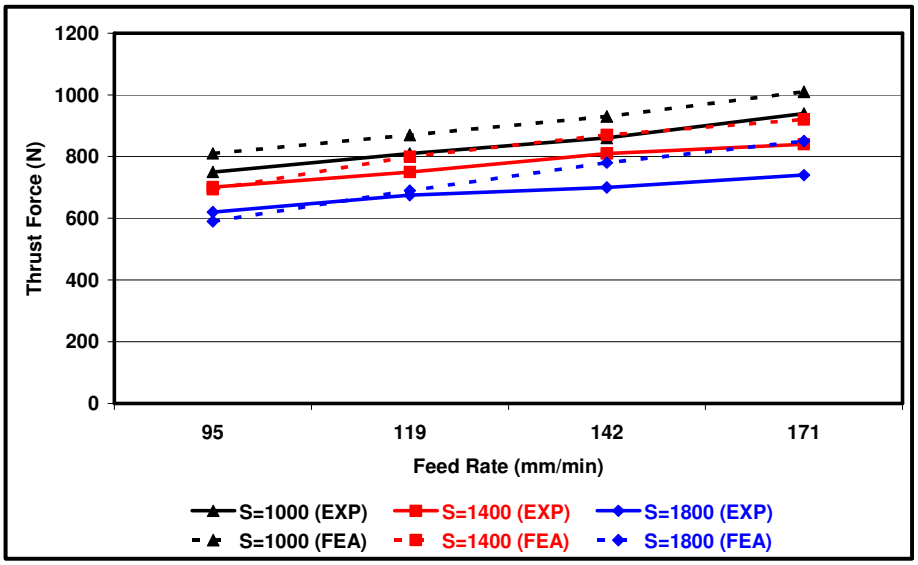

Figure 7-3: Effects of Cutting Parameters on Thrust Force in Drilling of Ti-6Al-4V

Figure 7-3 shows the effect of cutting parameters on thrust force in FE simulations. The FE model predicted thrust force between 590.87 N and 1010.38 N depending on the cutting parameters. The FE results show that drilling induced thrust force increased with the increased feed rate in all cutting speeds. The model estimated the trend of thrust force versus feed rate successfully. Moreover it was also estimated that the feed rate was the dominant process parameter on the thrust force. However, thrust force decreased with the increasing cutting speed as recorded in the drilling tests. A positive correlation has obtained between the FE model and experiments. Similar trends between process parameters and thrust force have been reported for titanium alloys in literature [20, 131-132].

Table 7-1 shows the experimental and estimated the average thrust forces in detail for each cutting condition. The experimental results show that the minimum induced thrust force was obtained as 620.48 N in the tests at 1800

rpm spindle speed and 95 mm/min feed rate whereas the maximum induced thrust force was found in test performed at 1000 rpm spindle speed and 171 mm/min feed rate in drilling of Ti-6Al-4V with 8 mm diameter twist drill. 80% higher feed rate resulted between 19.30% and 25.30% greater amount of thrust force depending on the cutting speed; whereas 80% greater cutting speed caused a decrease between 16.67% and 21.28% in thrust force according to the feed rate in drilling of Ti-6Al-4V. The influence of feed rate on drilling induced thrust force was slightly greater than the effect of spindle speed in the test region.

Table 7-1 shows estimated thrust forces by FE model for each set of machining parameters in detail. FE results show that, the minimum thrust force was predicted to be 590.87 N at 1800 rpm and 95 mm/min which was the combination of the maximum spindle speed and the minimum feed rate with 8 mm diameter rigid twist drill. The maximum thrust force was estimated 1010.38 N at 1000 rpm spindle speed and 171 mm/min, which was the combination of the minimum cutting speed and the largest feed rate. The results indicate that 80% higher feed rate caused an increase in thrust force between 24.73% and 45.89% depending on the cutting speed; whereas 80% greater cutting speed led to a decrease between 15.85% and 27.06% in thrust force according to the feed rate in drilling of Ti-6Al-4V. This shows that the influence of feed rate on thrust force was predominant in drilling of Ti-6Al-4V. However, it was also found that thrust force was more susceptible to the change in process parameters in FE analysis comparing to experiments. The FE results have shown that the thrust force has been predicted with deviations between 0.96% and 14.87% according to the drilling conditions.

Overall, thrust force was estimated to increase with regards to the increase in feed rate and to decrease with regards to the increase in spindle speed. The higher thrust force could cause to higher cutting stresses and consequently accelerated tool wear. High thrust force could lead to increased burr formation and other drilling induced defects. Combination of moderately low feed rate and average cutting speed could help to maintain high structural integrity for workpiece and provide longer service life for the tool.

Table 7-1: Experimental and Simulation based Thrust Force in Drilling of Ti-6Al-4V

Feed Rate (mm/min)	Spindle Speed (rpm)	Thrust Force (N) Experimental	Thrust Force (N) FEA model	Deviation (%)
95	1000	750.12±6.50	810.05	7.99
95	1400	701.19±6.25	694.45	-0.96
95	1800	620.48±5.50	590.87	-4.77
119	1000	810.44±7.25	870.34	7.39
119	1400	750.58±6.40	800.25	6.62
119	1800	675.33±6.60	690.40	2.23
142	1000	860.28±7.00	930.94	8.21
142	1400	810.48±7.20	870.39	7.39
142	1800	700.20±6.70	780.29	11.44
171	1000	940.19±8.10	1010.38	7.47
171	1400	840.44±7.90	920.59	9.54
171	1800	740.12±7.50	850.19	14.87

The trends predicted by the FE model were in agreement with the experimental values for the thrust force. In general, to obtain very accurate results for thrust force via finite element analysis, extremely fine mesh, accurate contact and damage models are essential. However due to the complexity of the geometry and the process moving to very fine mesh would require huge computing resources. Limitation on the computing resources and extremely long computing times had restricted the FE investigations in terms of the mesh refinement. Within the resources available the accuracy of the predictions of the thrust force for different drilling parameters are acceptable.

7.2.2 Effect of Geometry on Thrust Force

In order to optimise the drilling of Ti-6Al-4V, different step drill geometries have been modelled in CAD software and have been utilized in the

finite element analysis. The estimated thrust force was found to be 6.62% different than the experiments performed at 1400 rpm spindle speed and 119 mm/min feed rate with 8mm diameter coated carbide drill. This deviation showed that the FE model could estimate thrust force quire reasonably and it gave the confidence about the capability of the FE model in drilling process. Thus, investigations using step drills were performed based on FE analysis.

Figure 7-4 shows the numerical predictions of thrust force in drilling of Ti-6Al-4V workpiece at 119 mm/min feed rate and 1400 rpm spindle speed (35.18 m/min cutting speed) for twist drill and various step drills. It must be noted that the secondary drilling stage by step drill has been the subject of matter in drilling of Ti-6Al-4V workpiece. Thus, the thrust forces shown in Figure 7-4 are the average estimated values in the secondary drilling stage. The FE model estimated the thrust force to be 800.25 N in drilling Ti-6Al-4V by 8 mm diameter twist drill. When step drills were utilized in FE analysis of drilling of Ti-6Al-4V, estimated thrust forces were significantly lower than that obtained in drilling by twist drill. A comparison of the estimated thrust forces for the twist drill and step drills with various stage ratios is shown in Figure 7-4. Thrust force decreased by approximately 35% when a step drill with an initial 4.5 mm drill diameter; and 67% when a step drill with an initial 6.5 mm drill diameter. As it can be seen the higher stage ratio has provided higher reduction in thrust force. This was due to disappearance of the effects of chisel edge in the second stage cutting of step drill. Moreover, smaller area to be cut by the cutting edges of the step drill required smaller contact between the workpiece and the drill which minimized the need of cutting energy and cutting force.

In general, thrust force was estimated to reduce significantly due to initial step part and disappearance of the chisel edge of the drill. The reduced thrust force would assist to achieve reduced burr formation and other drilling induced defects. This could help to maintain high structural integrity and provide longer service life for the workpieces. The use of step drill could decrease the possible rejections due to tight tolerances, so it could lead low cost of manufacturing. The advantages of using step drill will be discussed for torque and burr formation in the following subsections.

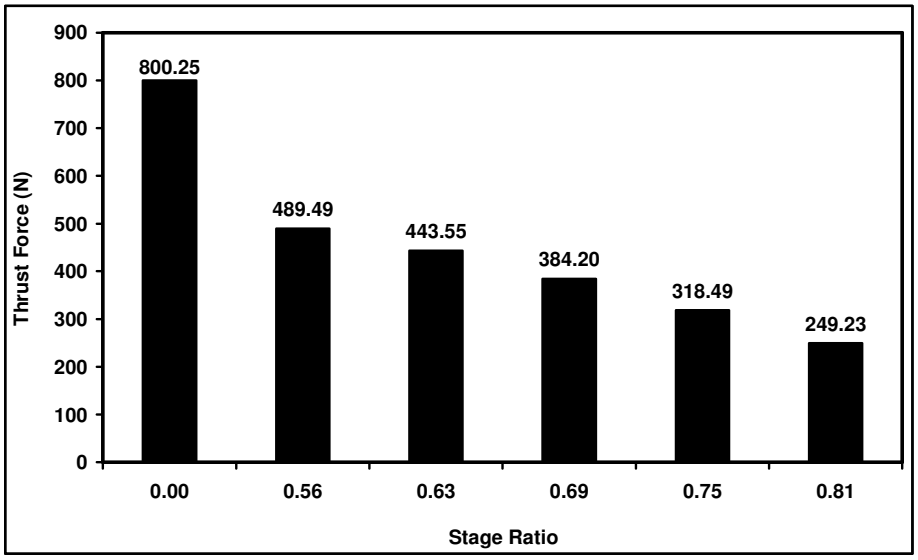

Figure 7-4: Effect of Drill Geometry on Thrust Force in Drilling of Ti-6Al-V (f=119 mm/min S=1400 rpm)

In order to obtain more accurate results via finite element analysis, deformable cutting tool and extremely fine mesh could be used with regard to the computational facilities. However due to the complexity of the geometry and the process with a deformable cutting tool and very fine mesh would require huge computing resources. Inclusion of chip formation, deformable drill and thermo-mechanical FE analysis would develop the model further.

7.2.3 Effect of Hole Number or Tool Wear on Thrust Force

It is important and worthwhile to determine the number of holes that can be drilled in Ti-6Al-4V workpiece in order to maintain quality and provide economic manufacturing. Progression of the thrust force by the number of holes can be observed during drilling in addition to the development of the wear regions. Figure 7-5 shows thrust force versus number of holes drilled in Ti-6Al-4V at 119 mm/min feed rate and 1400 rpm spindle speed. During drilling experiments of Ti-6Al-4V, thrust forces increased steadily. After drilling 32 holes in Ti-6Al-4V, thrust force rose by 15.60% from 750.58 N to 867.22 N.

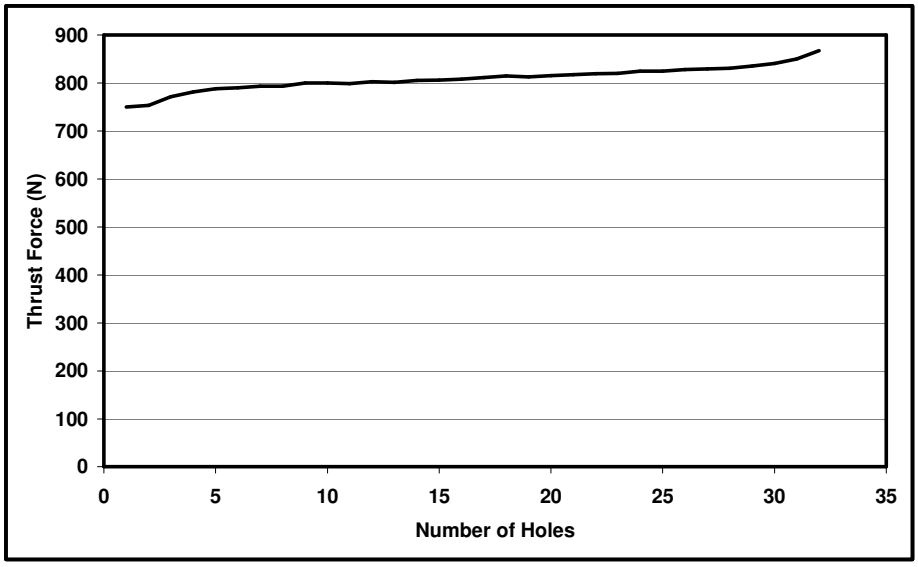

Figure 7-5: Effect of Number of Holes on Thrust Force in Drilling of Ti-6Al-4V (f=119 mm/min S=1400 rpm)

Since the flank wear has reached the 0.25 mm critical value which has been stated as the tool life criteria based on the industrial experience in the methodology section, the drill was considered to have reached its end of life. Beyond this limit, it is not suggested to continue drilling since thrust force could increase substantially due to the loss of sharpness of cutting edges of the drill. This can be observed from final slope of the progression of thrust force. Increased cutting forces could elevate cutting stresses, cutting temperatures due to increased friction between drill and workpiece. This would likely to affect material removal mechanism which can accelerate wear rate. Consequently it could be finalized with uncontrolled tool wear including chipping and sudden tool breakage, unacceptable material defects including excessive burr and surface roughness, thus possible rejections and increased manufacturing costs.

7.3 Analysis of Torque

Figure 7-6 shows the progression of induced torque in drilling of Ti-6Al-4V workpiece with 3 μm TiN/TiAlN multilayer coated 8 mm diameter tungsten carbide twist drill with 140° point angle and 30° helix angle at 119 mm/min feed rate and 1400 rpm spindle speed. The progress of drilling induced torque was similar to the development of thrust force in drilling process. Three stages of

drilling are shown in Figure 7-6 with peck drilling. In the first phase drill penetrates into work piece. In the second phase, in which the whole cutting edges are in contact with the work piece, a steady state torque is attained. Finally, in the third phase drill point exits or breaks through other side of the work piece. In the following paragraphs, the investigations on torque are made using the average torque which has obtained in the second phase of drilling.

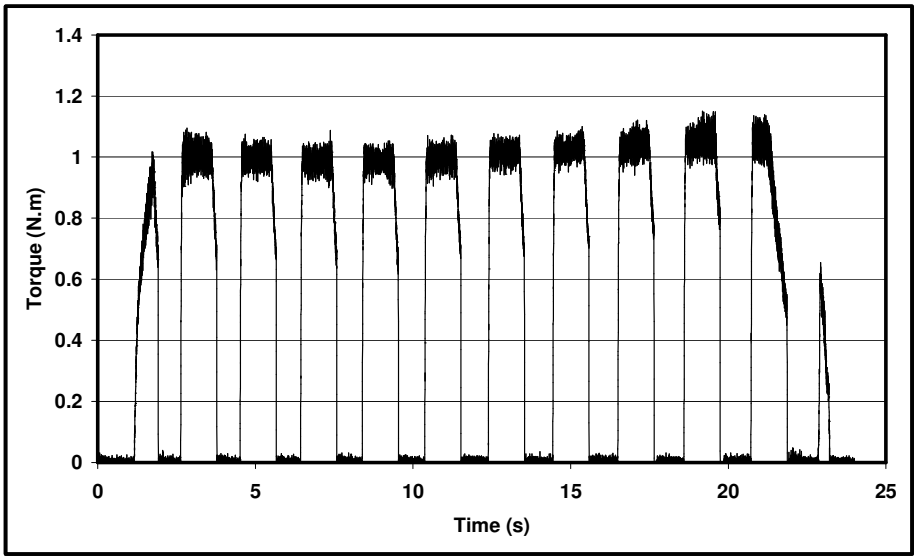

Figure 7-6: Torque through Hole in Experimental Peck Drilling of Ti-6Al-4V (f=119 mm/min S=1400 rpm)

7.3.1 Effects of Process Parameters on Torque

The influences of process parameters on torque have been investigated in drilling of Ti-6Al-4V performed at the combinations of four feed rates and three spindle speeds, a total of 12 set of cutting conditions in both experiments and finite element analysis. All the drilling experiments were conducted with the use of 3 μm TiN/TiAlN multilayer coated 8 mm diameter tungsten carbide twist drill with 140° point angle and 30° helix angle. 3-dimensional complex drill geometry was employed in the finite element simulations to simulate the drilling process and to investigate the influences of drill geometry on torque. The average torque values induced in drilling of Ti-6Al-4V at different machining parameters are shown for both experiments and finite element analysis in Figure 7-7. As it is plotted in Figure 7-7, torque altered between 0.7

N.m and 1.3 N.m with regard to the cutting parameters in experimental drilling of Ti-6Al-4V. It could be observed that torque increased with respect to feed rate and cutting speed similar to observations for the thrust force. The results point out that feed rate was the predominant factor on torque in the tested region. Similar observations have been made with the use of different tool materials such as HSS, WC-Co at different parameters in drilling of titanium alloys in literature [20, 131-132]. Feed rate was the predominant parameters on torque in drilling of Ti-6Al-4V. Increased feed rate led to a rise in torque, whereas increased cutting speed influenced in the other direction; caused to a decrease in torque however the effect of cutting speed in torque was less than that observed for feed rate.

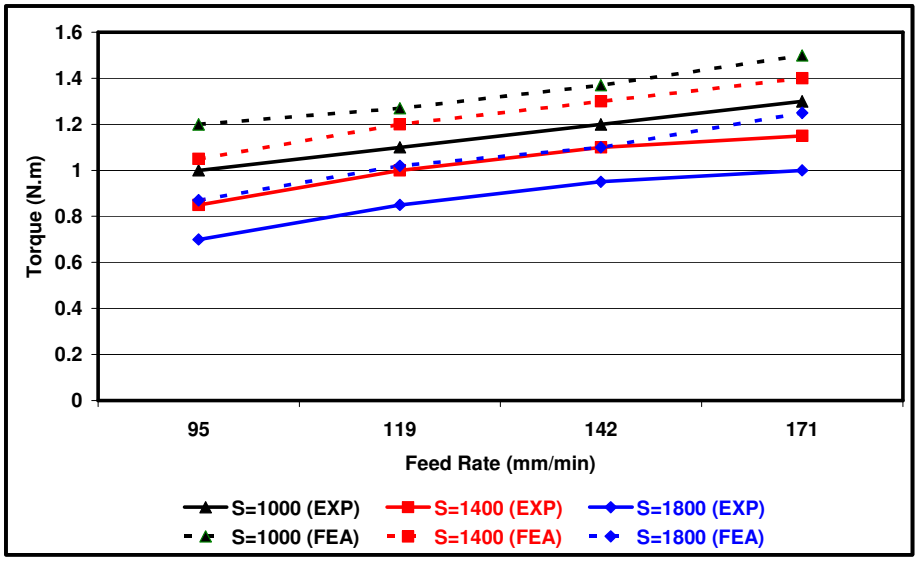

Figure 7-7: Effects of Cutting Parameters on Torque in Drilling of Ti-6Al-4V

Figure 7-7 displays the effect of cutting parameters on torque for FE analysis. The FE model predicted torque between 0.87 N.m and 1.5 N.m in regard to the cutting parameters. The FE results show that the drilling induced torque increased with the increased feed rate in all cutting speeds. The model estimated the trend of torque versus feed rate successfully. Moreover it was also estimated that the feed rate was the dominant process parameter on torque. Drilling induced torque was predicted to decrease with the increasing cutting speed. A positive correlation between FE model and experiments has been obtained under the existence of multi-axis state of stress due to drilling.

Table 7-2 shows the experimental and estimated average drilling induced torque for each cutting parameter in detail. The experimental results show that the minimum induced torque was obtained as 0.7 N.m in drilling tests at 1800 rpm spindle speed and 95 mm/min feed rate whereas the maximum induced torque was found to be 1.3 N.m in test performed at 1000 rpm spindle speed and 171 mm/min feed rate in drilling of Ti-6Al-4V with 8 mm diameter twist drill. 80% higher feed rate has resulted in increases in torque between 30.00% and 42.86% whereas 80% greater cutting speed caused decreases in torque between 20.83% and 30.00% according to the process parameters in drilling of Ti-6Al-4V. As it can be noticed drilling induced torque was more susceptible to the change in feed rate in experiments.

The overall trends of predicted torque with the process parameters have been shown and discussed above. Table 7-2 shows estimated torque values by FE analysis with regard to machining parameters in detail. According to the FE analysis results, the minimum torque was predicted to be 0.87 N.m at 1800 rpm and 95 mm/min which was the combination of the maximum spindle speed and the minimum feed rate with 8 mm diameter rigid twist drill. The maximum torque was estimated 1.5 N.m at 1000 rpm spindle speed and 171 mm/min, which was the combination of the minimum cutting speed and the largest feed rate. The results indicate that 80% higher feed rate caused an increase in drilling induced torque between 25.00% and 43.68% depending on the cutting speed; whereas 80% greater cutting speed led to a decrease between 16.67% and 27.50% in torque according to the feed rate in drilling of Ti-6Al-4V. Results have clearly indicated that feed rate was the dominant process parameters on torque. The effect of cutting speed on torque was significant and cannot be ignored. This relation was found similar in experimental results. The deviations of predicted torque based on the FE analysis lay between 14.17% and 25.00%. It is thought that the lack of chip formation and related friction between generated chip and drill are the reason of this difference.

Table 7-2: Experimental and Simulation based Torque in Drilling of Ti-6Al-4V

Feed Rate (mm/min)	Spindle Speed (rpm)	Experimental Torque (N.m)	Predicted Torque (N.m)	Deviation (%)
95	1000	1.00±0.05	1.2	20.00
95	1400	0.85±0.04	1.05	23.53
95	1800	0.70±0.04	0.87	24.29
119	1000	1.10±0.05	1.27	15.45
119	1400	1.00±0.05	1.2	20.00
119	1800	0.85±0.04	1.02	20.00
142	1000	1.20±0.06	1.37	14.17
142	1400	1.10±0.05	1.3	18.18
142	1800	0.95±0.05	1.1	15.79
171	1000	1.30±0.06	1.5	15.38
171	1400	1.15±0.06	1.4	21.74
171	1800	1.00±0.05	1.25	25.00

Torque was estimated to increase with regards to the increase in feed rate and decrease in cutting speed. The higher torque would cause to higher friction, thus increased surface roughness and cutting temperatures. These can be minimised by the choice of moderately low feed rate and average spindle speed. In addition to minimising the possible rejections, the cost of manufacturing could be reduced.

It should be mentioned that the trend predicted by the FE model was in agreement with the experimental values for torque. To achieve more accurate results for prediction of drilling induced torque using finite element analysis, chip formation, deformable cutting tool, extremely fine mesh for tool and workpieces, and more advanced damage and contact models are necessary. However due to the complexity of the geometry and the process moving to very fine mesh would require huge computing resources. Restrictions on the computing resources have limited us in terms of the mesh refinement and other

techniques. Within the resources available the accuracy of the predictions of the torque for different process parameters can be acceptable.

7.3.2 Effects of Tool Geometry on Torque

Various step drill geometries have been utilized in the finite element analysis of drilling process of Ti-6Al-4V. The investigations of the effect of the geometry on torque have been performed with FE analysis. All the torque values reported below are the average values from the steady state drilling stage, and the secondary drilling stage for step drills.

Figure 7-8 shows the numerical predictions of torque in drilling of Ti-6Al-4V at 119 mm/min feed rate and 1400 rpm spindle speed. The FE model estimated torque to be 1.2 N.m in drilling Ti-6Al-4V by 8 mm diameter rigid twist drill. When step drills were utilized in FE analysis of drilling of Ti-6Al-4V, torque values were estimated remarkably lower than the twist drill. The comparison of the estimated torque values for the twist drill and step drills with various stage ratios is shown in Figure 7-8. The greater stage ratio has provided higher reduction in torque. 0.79 N.m was estimated for the step drill with 0.56 stage ratio or 4.5 mm step drill diameter whereas the torque was estimated to reduce to 0.34 N.m for 6.5 mm step drill diameter, or 0.81 stage ratio. The smaller area to be cut by the cutting edges of the step drill required smaller contact between the titanium alloy workpiece and the rigid drill. The smaller contact provides smaller friction between the surfaces of drill and the workpiece. This minimizes the cutting torque and related cutting energy.

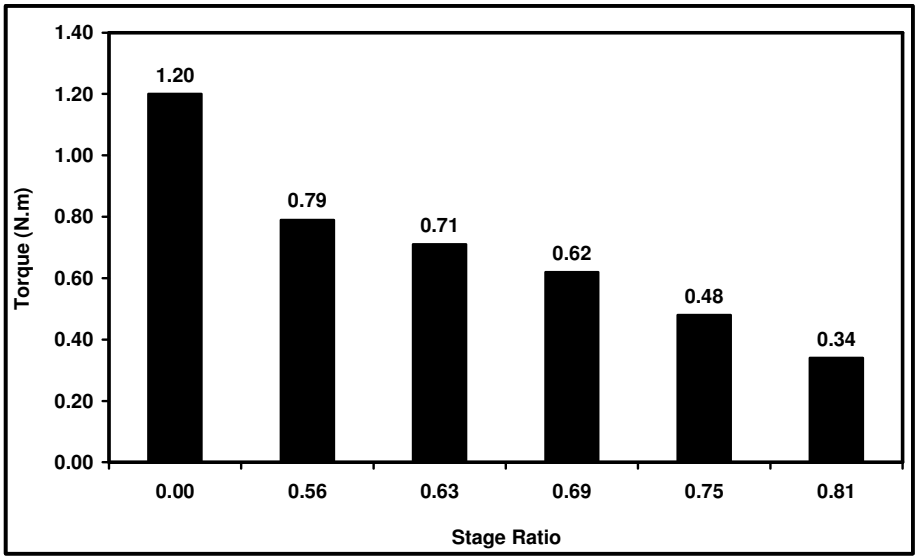

Figure 7-8: Effect of Drill Geometry on Torque in Drilling Ti-6Al-4V (f=119 mm/min, S=1400 rpm)

In summary, drilling induced torque was estimated to reduce significantly due to the provided initial step part of the step drill. The reduced torque would assist to achieve reduced friction, so reduced surface roughness and cutting temperatures. The choice of step drill could help to maintain high structural integrity and provide longer service life for the machined parts. Possible material rejections could be also decreased, so lower cost of manufacturing could be achieved.

7.3.3 Effects of Tool Wear on Torque

The number of holes that can be drilled should be determined to provide quality and economic manufacturing process. Figure 7-9 shows the progress of drilling induced torque versus number of holes drilled in Ti-6Al-4V workpiece at 119 mm/min feed rate and 1400 rpm spindle speed. During drilling experiments of Ti-6Al-4V, torque increased steadily. After drilling 32 holes in Ti-6Al-4V, torque rose by 9.2% from 1.00 N.m to 1.09 N.m.

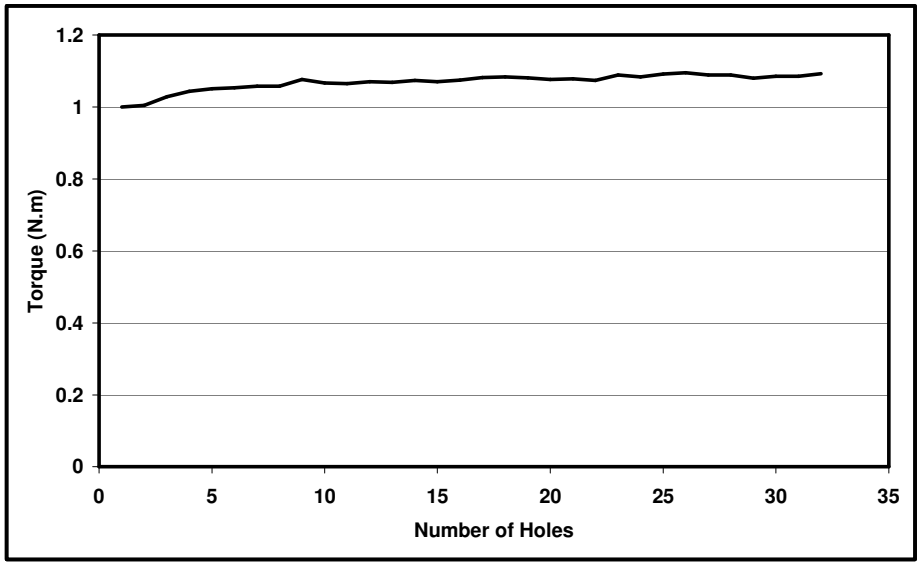

Figure 7-9: Effect of Number of Holes on Torque in Drilling of Ti-6Al-4V (f=119 mm/min, S=1400 rpm)

By drilling 32 holes in Ti-6Al-4V, the flank wear of drill bit has reached the wear criterion which was set to 0.25 mm for 8 mm diameter twist drill according to the industrial experience. The drill was considered to reach its service life, thus cutting action was not suggested beyond this limit since torque might increase significantly due to the loss of sharpness of cutting edges of the drill. In that case it would be difficult to maintain the quality of the drilled holes due to increase in friction between drill and workpiece and higher mechanical and thermal stresses. This would also cause to possible changes in material removal mechanisms which could lead to excessive wear rate and material defects. There could be significant chipping on the margins.

7.4 Analysis of Burr Formation

In terms of hole quality, burr is an important damage to control in drilling of metals. Most of machining processes of titanium and its alloys create burr on both entry and exit sides. In most cases the exit burr is much larger in size compared to the entry burr. It is estimated that up to 30% of the cost of components is due to deburring operations [17]. Thus, influences of process parameters and tool wear on burr formation have been investigated. In order to investigate the influences of process parameters on burr formation in drilling of

Ti-6Al-4V, experiments were performed at the combinations of four feed rates and three spindle speeds, a total of 12 sets of cutting conditions. Effect of tool wear on burr formation was investigated at one set of parameter. All the drilling experiments were conducted with the use of 3 μm TiN/TiAlN multilayer coated 8 mm diameter tungsten carbide twist drill with 140° point angle and 30° helix angle in wet conditions. All experiments were carried out with high pressure cooling through tool coolant holes of drills. 5 percent emulsion of Hocut 795B cutting fluid was applied in wet cutting experiments at a constant 38 bar coolant pressure (equal flow rate of ~2.4 l/min). Each measurement was repeated 5 times.

Figure 7-10 shows typical drilling induced burr formation and the assessment of burr width based on image analysis. These burr formation figures were used to evaluate the effects of process parameters and tool wear on burr height and width after drilling Ti-6Al-4V. Throughout the tests, limited amount of damage in the form of burr formation was observed. All burrs in exit and entry were uniform without caps. The burr height and width extended only several tens of micrometers with regard to process parameters and number of holes drilled. The application of jet cooling was one of the reasons of such low burr formation. There was no other evidence for any other damage around the hole. In FE analysis, burr formation was measured from the ultimate plastic deformation in the vicinity of holes at entry and exit sides.

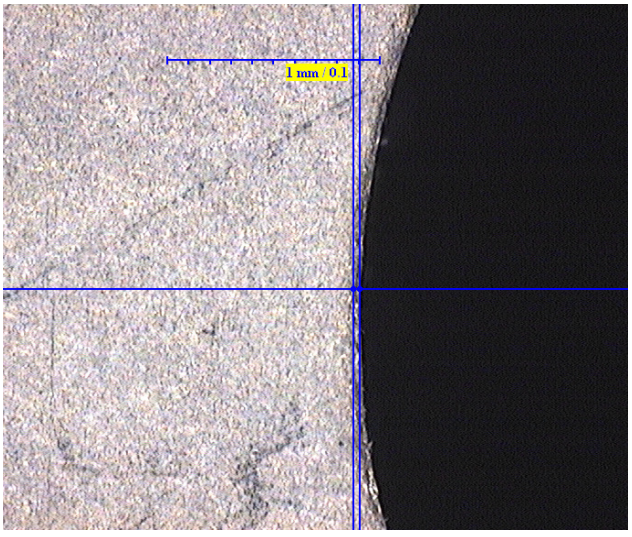

Figure 7-10:Burr Width Measurement in Drilling Ti-6Al-4V

7.4.1 Effects of Process Parameters on Burr Formation

Figure 7-11 (a) and Figure 7-11 (b) show the influences of process parameters on the experimentally obtained and FEA predicted the average burr height in drilling of Ti-6Al-4V at entrance and exit, respectively. As can be observed in plots, greater amount of burr heights were induced and predicted at hole exit comparing to the entrance side in drilling of Ti-6Al-4V at various cutting parameters. It can be seen in Figure 7-11 (a) and Figure 7-11 (b) the average burr height increased with regard to the increase in feed rate whereas it decreased according to the increase in spindle speed in the region tested and simulated at both entrance and exit sides. It could be observed in Figure 7-11 (a) that drilling induced burr height at entrance was between 15.00 μm and 35.65 μm in drilling tests whereas in FE analysis it was predicted between 11.00 μm and 24.60 μm regarding to the cutting condition in drilling of Ti-6Al-4V. The experimentally induced burr height at exit of holes lay between 42.30 μm and 73.20 μm while it altered between 26.00 μm and 47.40 μm in FE analysis as shown in Figure 7-11 (b). The results show that both feed rate and spindle speed have influences on the drilling induced burr formation.

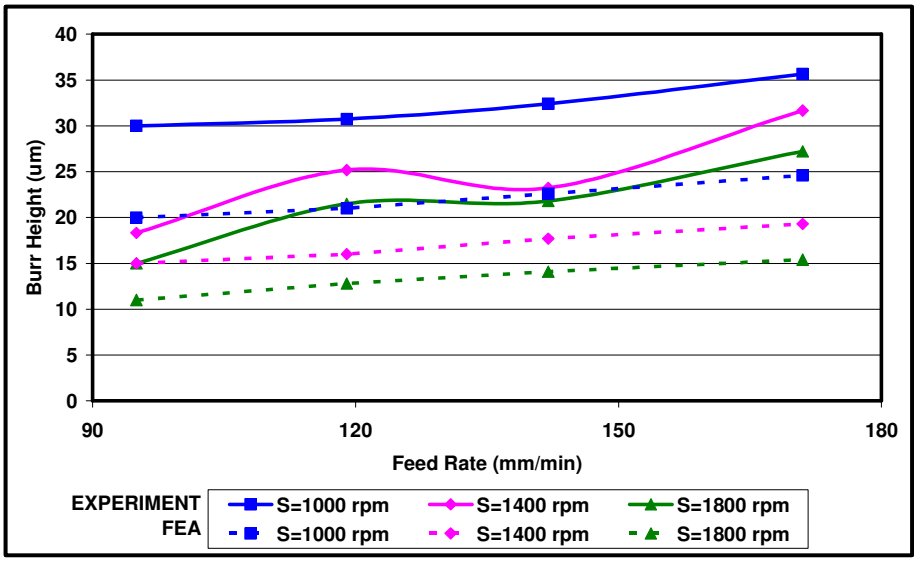

(a)

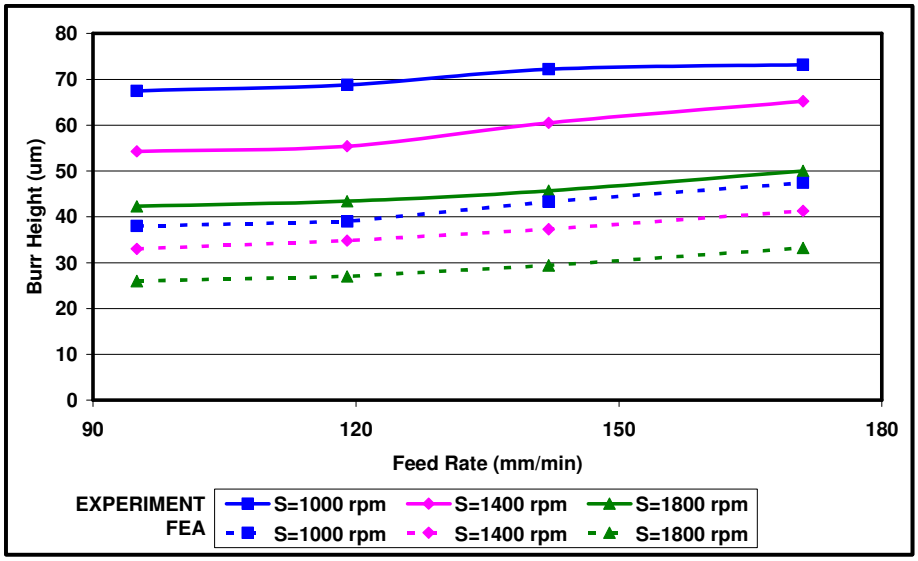

(b)

Figure 7-11: Effects of Cutting Parameters on Burr Height in Drilling of Ti-6Al-4V a) Entrance (b) Exit

Table 7-3 shows the experimental and estimated height of the drilling induced burr formation at the entrance and exit of holes in details for each cutting condition. The experimental results show that the minimum height of induced burr at entrance and exit was measured 15.00 μm and 42.30 μm at 1800 rpm spindle speed and 95 mm/min feed rate, respectively. The maximum burr height was observed 35.65 μm and 73.20 μm at the entrance and exit sides of the holes respectively when drilling Ti-6Al-4V at 1000 rpm spindle speed and 171 mm/min feed rate. As feed rate increased by 80%, height of burr formation at entrance increased between 18.83% and 81.47% whereas increases between 8.44% and 20.07% was observed at exit depending on the spindle speed in drilling tests. Results depict that burr height at entrance of holes was more susceptible to the change in feed rate comparing to burr height at exit. 80% higher spindle speed caused to decreases between 23.65% and 50.00% at hole entry and between 31.69% and 37.33% at hole exit with regard to feed rate in drilling tests. Similar to the effect of feed rate, spindle speed has more influence on the burr height at hole entry than hole exit. However in each cases higher burr height was measured at hole exit than that obtained at hole entry.

The overall trends of drilling induced burr height versus drilling parameters have been shown and discussed above. Table 7-3 shows the estimated burr height at entrance and exit sides for each set of machining parameters in detail for FE analysis. According to the FE results, the minimum burr height was estimated as 11.00 μm at entrance and 26.00 μm at exit side at 1800 rpm and 95 mm/min which was the combination of the maximum spindle speed and the minimum feed rate in drilling Ti-6Al-4V by 8 mm diameter rigid twist drill. The maximum burr height was calculated 24.60 μm and 47.40 μm at 1000 rpm spindle speed and 171 mm/min, which was the combination of the least cutting speed and the largest feed rate at entrance and exit sides of the holes, respectively. The FE results show that 80% higher feed rate caused increases in estimated drilling induced burr height between 23.00% and 40.00% at entrance and between 24.74% and 27.69% at exit side depending on the cutting speed; whereas 80% greater cutting speed led to decreases in burr height between 37.40% and 45.00% at entry side and 29.96% and 31.58% at exit side according to the feed rate in drilling of Ti-6Al-4V. Results depict that the influence of spindle speed on burr height was slightly higher than the effect of feed rate. Similar to experimental results, burr height at the entrance was found to be more affected by the process parameters. However simulated trends of the burr height versus process parameters agreed with the experiments; the deviations of predicted drilling induced burr height lay between 18.17% and 43.42% at hole entry, and between 33.60% and 43.70% at hole exit with underestimation according to the set of process parameters. Application of chip formation and finer mesh on the workpiece would improve the performance of FE model.

Table 7-3: Burr Height in Experimental and Simulation based Drilling of Ti-6Al-4V

Feed Rate (mm/min)	Spindle Speed (rpm)	Burr Height at Entrance			Burr Height at Exit		
		Experimental (μm)	FEA (μm)	Deviation (%)	Experimental (μm)	FEA (μm)	Deviation (%)
95	1000	30.00±1.00	20.00	-33.33	67.50±2.80	38.00	-43.70
95	1400	18.33±0.70	15.00	-18.17	54.30±2.45	33.00	-39.23
95	1800	15.00±0.60	11.00	-26.67	42.30±1.80	26.00	-40.09
119	1000	30.74±1.10	21.00	-31.69	68.80±2.75	39.00	-43.31
119	1400	25.19±0.80	16.00	-36.48	55.40±2.40	34.80	-37.18
119	1800	21.5±0.70	12.80	-40.47	43.40±1.85	27.00	-36.17
142	1000	32.41±1.10	22.60	-30.27	72.20±3.00	43.30	-40.03
142	1400	23.24±0.75	17.70	-23.84	60.50±2.55	37.30	-38.35
142	1800	21.80±0.70	14.10	-35.32	45.70±1.75	29.40	-35.67
171	1000	35.65±1.20	24.60	-31.00	73.20±3.10	47.40	-35.25
171	1400	31.67±1.10	19.30	-39.06	65.20±2.75	41.30	-36.66
171	1800	27.22±0.95	15.40	-43.42	50.00±1.80	33.20	-33.60

Figure 7-12 (a) and Figure 7-12 (b) show the influences of process parameters on the experimentally obtained and FEA predicted the average burr width in drilling of Ti-6Al-4V at entrance and exit, respectively. As can be observed in plots, slightly higher amount of burr width were observed and predicted at hole exit comparing to the entrance side in drilling of Ti-6Al-4V at various cutting parameters. It can be seen in Figure 7-12 (a) and Figure 7-12 (b) that burr width increased with regard to the increase in feed rate whereas it decreased according to the increase in spindle speed in the region tested and simulated at both entrance and exit sides. As shown in Figure 7-12 (a), drilling induced burr width occurred between 37.20 μm and 57.60 μm at entrance in drilling tests whereas it was predicted between 20.00 μm and 33.70 μm in FE

analysis regarding to the cutting condition in drilling of Ti-6Al-4V. The burr width at exit side altered between 43.30 μm and 65.20 μm in drilling experiments while it altered between 22.00 μm and 40.60 μm in FE analysis as shown in Figure 7-12 (b). The results show that both feed rate and spindle speed have influences on the drilling induced burr formation.

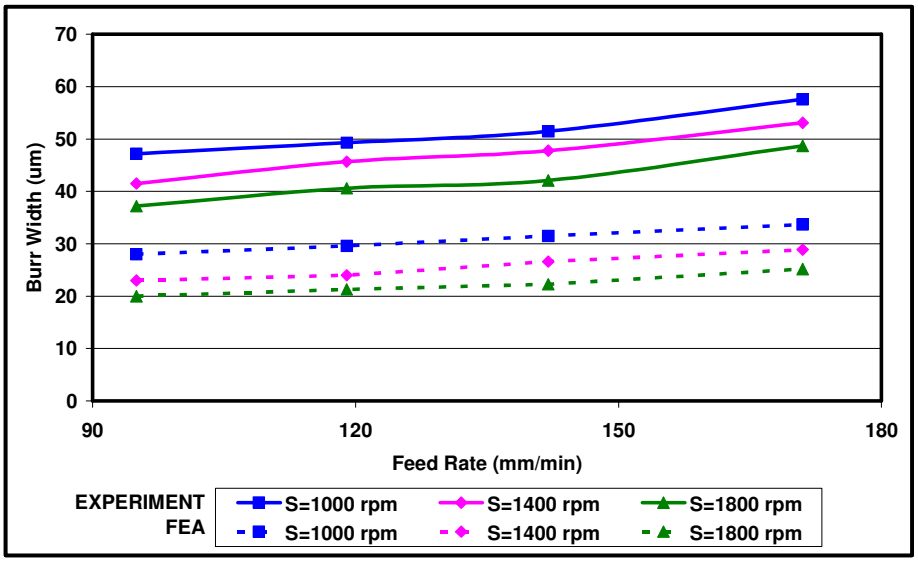

(a)

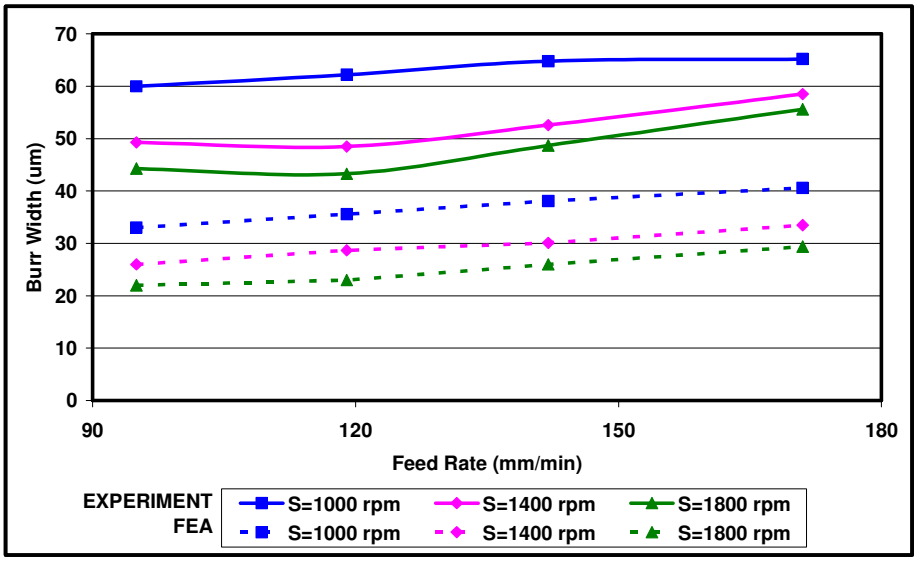

(b)

Figure 7-12: Effects of Cutting Parameters on Burr Width in Drilling of Ti-6Al-4V (a) Entrance (b) Exit

Table 7-4 shows the experimental and estimated burr width at the entrance and exit of holes in details for each cutting condition. The experimental results show that the minimum burr width at the entrance and exit was measured 37.20 μm and 43.30 μm at 1800 rpm spindle speed and 95 mm/min feed rate, respectively. The maximum burr width was observed 57.60 μm and 65.20 μm at the entrance and exit sides of the holes respectively when drilling Ti-6Al-4V at 1000 rpm spindle speed and 171 mm/min feed rate. As feed rate increased by 80%, burr width at entrance increased between 22.03% and 30.91% whereas increased between 8.67% and 28.41% at exit depending on the spindle speed in drilling tests. 80% higher spindle speed caused to decreases in burr width between 15.45% and 21.19% at hole entry and between 14.72% and 28.78% at hole exit with regard to feed rate in drilling tests. The influences of process parameters on burr width were found similar in the tested region. On average, 16.07% larger burr width was measured at hole exit than that obtained at hole entry.

The general progression of drilling induced burr width versus drilling parameters have been shown and discussed above. Table 7-4 shows the estimated burr width at entrance and exit sides for each set of machining parameters in detail for FE analysis. According to the FE results, the minimum burr width was estimated as 20.00 μm at entrance and 22.00 μm at exit side at 1800 rpm and 95 mm/min which was the combination of the maximum spindle speed and the minimum feed rate in drilling Ti-6Al-4V by 8 mm diameter rigid twist drill. The maximum burr width was calculated 33.70 μm and 40.60 μm at 1000 rpm spindle speed and 171 mm/min, which was the combination of the least cutting speed and the largest feed rate at entrance and exit sides of the holes, respectively. The FE results show that 80% higher feed rate caused increases in estimated drilling induced burr width between 20.36% and 26.00% at entrance and between 23.03% and 33.64% at exit side depending on the cutting speed; whereas 80% greater cutting speed led to decreases in burr width between 25.22% and 29.21% at entry side and 27.59% and 35.39% at exit side according to the feed rate in drilling of Ti-6Al-4V. Results depict that the influences of process parameters were slightly greater in the exit side comparing to entrance. The trends of the burr width versus process parameters

agreed with the experiments however the deviations of predicted drilling induced burr width lay between 38.83% and 48.25% at hole entry, and between 37.73% and 49.19% at hole exit with underestimation with regard to process parameters. Utilisation of chip generation and advanced meshing on the workpiece would improve the prediction of burr formation in FE model.

Table 7-4: Burr Width in Experimental and Simulation based Drilling of Ti-6Al-4V

Feed Rate (mm/min)	Spindle Speed (rpm)	Burr Width at Entrance			Burr Width at Exit		
		Experimental (μm)	FEA (μm)	Deviation (%)	Experimental (μm)	FEA (μm)	Deviation (%)
95	1000	47.20±1.60	28.00	-40.68	60.00±2.40	33.00	-49.19
95	1400	41.50±1.45	23.00	-44.58	49.30±1.85	26.00	-47.26
95	1800	37.20±1.40	20.00	-46.24	43.30±1.70	22.00	-50.34
119	1000	49.30±1.70	29.60	-39.96	62.20±2.55	35.60	-42.77
119	1400	45.70±1.55	24.00	-47.48	48.50±1.80	28.70	-40.82
119	1800	40.60±1.40	21.30	-47.54	44.30±1.75	23.00	-48.08
142	1000	51.50±1.75	31.50	-38.83	64.80±2.35	38.10	-41.20
142	1400	47.80±1.65	26.60	-44.35	52.60±1.90	30.10	-42.78
142	1800	42.10±1.50	22.30	-47.03	48.70±1.80	26.00	-46.61
171	1000	57.60±1.75	33.70	-41.49	65.20±2.50	40.60	-37.73
171	1400	53.10±1.70	28.90	-45.57	58.50±2.25	33.50	-42.74
171	1800	48.70±1.65	25.20	-48.25	55.60±2.15	29.40	-47.12

In summary, the height and width of burr formation was observed and estimated to increase with regards to the increase in feed rate and decrease in the spindle speed. Higher burr formation was observed at hole exit by means of height and width. The amount of burr has been decreased significantly comparing to the literature in the drilling of Ti-6Al-4V with the utilisation of the high point angle drill geometry and application of high pressure coolant. The

unwanted material would require extra machining cost therefore these could be minimized by controlling the process parameters. Combination of moderately low feed rate and higher spindle speed could reduce burr formation in drilling of Ti-6Al-4V.

Overall trends predicted by the FE models were in agreement with the experimental values for the burr formation. However, the magnitudes of the estimations were noticeably underestimated. In order to achieve accurate results for prediction of burr formation in drilling of Ti-6Al-4V using finite element analysis, chip formation and extremely fine mesh are suggested to be utilized in models. Limitation in the computing resources and computing time had restricted the FE model in terms of the chip formation and mesh refinement. Within the resources available the predicted trends of chip formation versus process parameters could be acceptable.

7.4.2 Effects of Tool Geometry on Burr Formation

Figure 7-13 (a) and Figure 7-13 (b) show FE predictions of burr height and burr width versus stage ratio after drilling of Ti-6Al-4V by step drill at 119 mm/min feed rate and 1400 rpm spindle speed at both sides, entrance and exit. As shown in Figure 7-13 (a), burr height at the exit was estimated significantly greater than the entrance in drilling of Ti-6Al-4V workpiece. Burr height at entrance and exit sides tended to decrease gradually with the increasing stage diameter of the step drill. When 8 mm twist drill used in drilling simulations, burr heights were calculated as 16.00 μm and 34.80 μm at hole entry and exit, respectively. By the use of step drill with 0.81 stage ratio, the burr height decreased by approximately two thirds to 5.89 μm and 11.84 μm at hole entry and exit, respectively. Similar observations can be made for the burr width with drilling step drill as shown in Figure 7-13 (b). The improvements in burr width can show the advantages of step drill in drilling of Ti-6Al-4V. The higher stage ratio provided lower amount of burr width at entrance and exit sides of the holes. The decreased thrust force and torque by step drill would lead a decrease in the extent of burr formation. Work piece defects could be controlled with the proper selection of step geometry and process parameters.

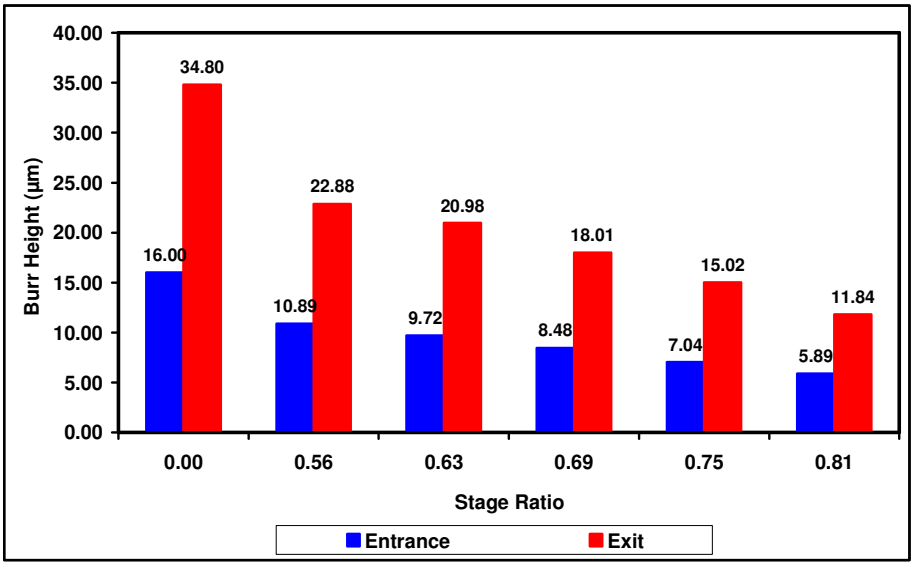

(a)

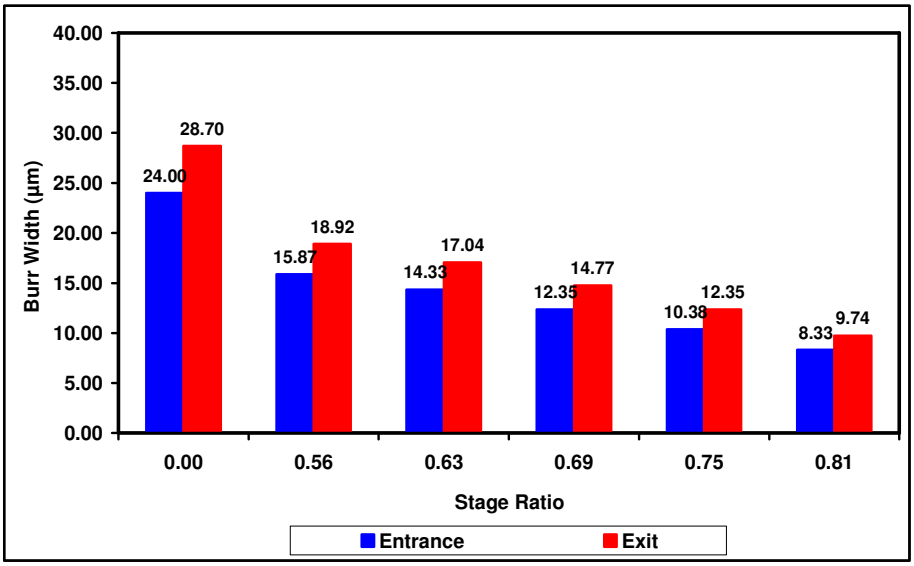

(b)

Figure 7-13: Effect of Drill Geometry on Burr Formation in Drilling of Ti-6Al-4V (a) Burr Height (b) Burr Width (S=1400 rpm, f=119 mm/min)

Predicted burr formation substantially decreased by the disappearance of the effect of chisel edge by the initial step diameter of the step drill. The reduced burr formation would mean that higher structural integrity and possibly longer service life. The use of step drill could assist to reduce possible workpiece rejections owing to tight tolerances, so it could boost the improvements and decrease the manufacturing costs.

In order to obtain more accurate results via finite element analysis, chip formation and deformable cutting tool should be integrated in the model. In addition to that extremely fine mesh should be used in the model. Nevertheless, these features would require substantially increased computing resources.

7.4.3 Effects of Tool Wear on Burr Formation

It is important to determine the effect of tool wear on the extent of burr formation in the workpiece in order to assess the structural integrity of the machined part. This also provides a limit number of holes that can be drilled in the structures before replacing the tool. Figure 7-14 (a) and Figure 7-14 (b) indicate the influence of the number of drilled holes on burr formation in drilling of Ti-6Al-4V at 1400 rpm spindle speed and 119 mm/min feed rate. Figure 7-14 (a) shows drilling induced burr height at hole entry and exit versus number of holes drilled. As it can be observed from Figure 7-14 (a) burr height rose steadily by 65.94% and 28.34% at entrance and exit of holes after drilling 32 holes in Ti-6Al-4V with 8 mm twist drill, respectively. The burr height at entrance was affected more from the change in the tool wear. Similar observations could be made for burr width as shown in Figure 7-14 (b). The burr width increased gradually by 56.92% and 36.94% at hole entry and exit sides at the end of 32 drilled holes. The burr width at the entrance sides of the holes was more susceptible to tool wear than burr width at the exit side.

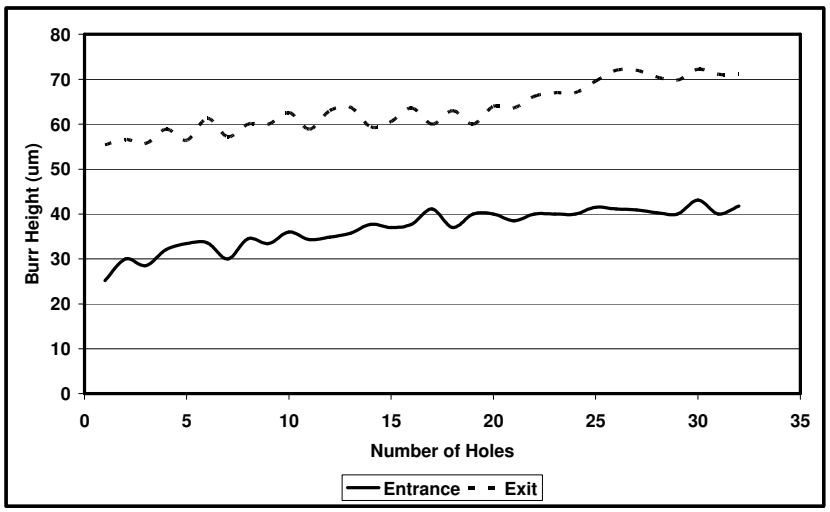

(a)

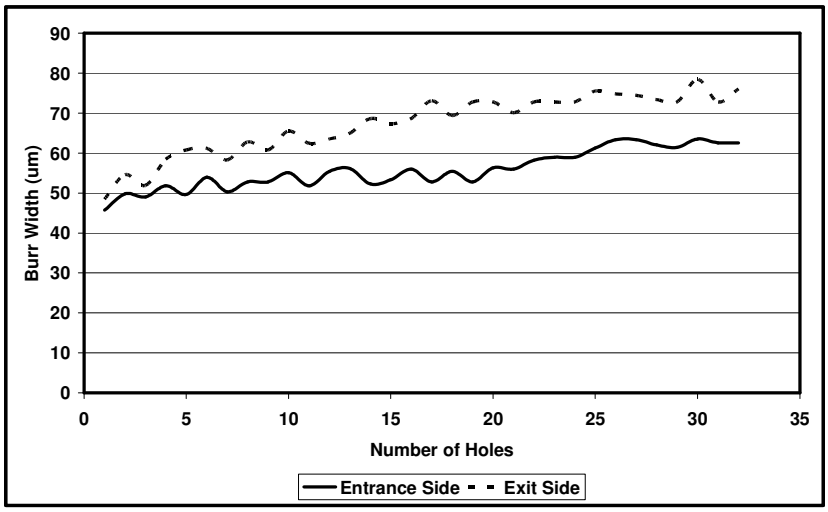

(b)

Figure 7-14: Effect of Number of Holes on Burr Formation in Drilling of Ti-6Al-4V (a) Burr Height (b) Burr Width (S=1400 rpm, f=119 mm/min)

7.5 Analysis of Surface Roughness

In terms of hole quality, surface roughness is another important factor to control in drilling of metals. Influences of process parameters and tool wear on surface roughness have been investigated. In order to investigate the influences of process parameters on drilling of Ti-6Al-4V, experiments were performed at the combinations of four feed rates and three spindle speeds, a total of 12 sets of cutting conditions. Effect of tool wear on surface roughness was investigated at one set of parameters. All the drilling experiments were conducted with the use of 3 μm TiN/TiAlN multilayer coated 8 mm diameter tungsten carbide twist drill with 140° point angle and 30° helix angle in wet conditions. All experiments were carried out with high pressure cooling through tool coolant holes of drills. 5 percent emulsion of Hocut 795B cutting fluid was applied in wet cutting experiments at a constant 38 bar coolant pressure (equal flow rate of ~2.4 l/min). Each surface roughness measurement was repeated 5 times.

7.5.1 Effect of Process Parameters on Surface Roughness

Figure 7-15 shows influences of cutting parameters on the average surface roughness (Ra) when drilling Ti-6Al-4V at different cutting parameters. The

average surface roughness was obtained between 1.09 μm and 3.11 μm in drilling of Ti-6Al-4V workpiece within the range of cutting parameters tested. It was observed that the average surface roughness increased with increased feed rate tremendously. Feed rate was found the dominant factor on the average surface roughness. Spindle speed had a minor influence on the average surface roughness. An increase in spindle speed led to a decrease in the average surface roughness. The trend of the surface roughness also agreed with the literature [20, 131-132].

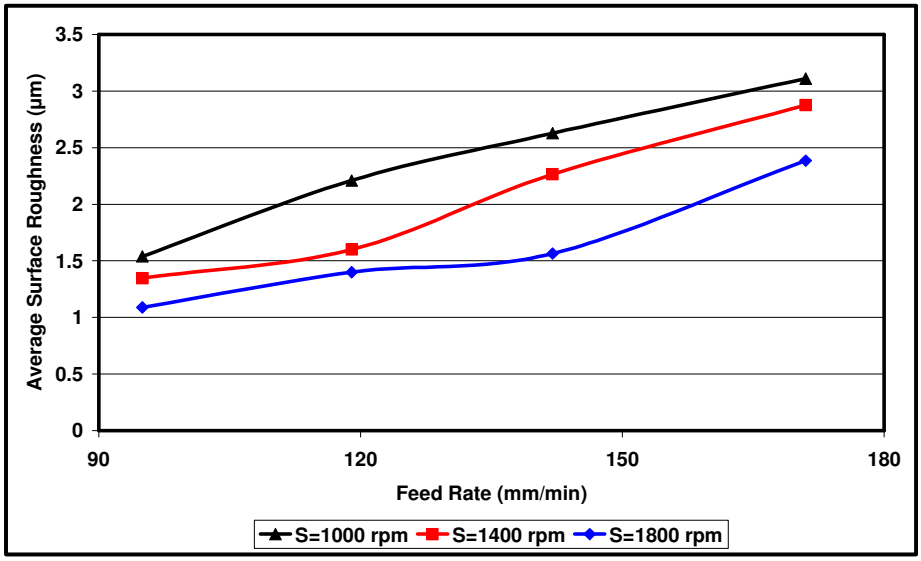

Figure 7-15: Effects of Cutting Parameters on the Average Surface Roughness in Drilling of Ti6Al4V

Table 7-5 shows the experimental average surface roughness in details for each cutting condition. The experimental results show that the minimum average surface roughness was obtained as 1.09 μm in the tests at 1800 rpm spindle speed and 95 mm/min feed rate whereas the maximum average surface roughness was found to be 3.11 μm in test performed at 1000 rpm spindle speed and 171 mm/min feed rate in drilling of Ti-6Al-4V with 8 mm diameter twist drill. 80% higher feed rate resulted in an increase in the average surface roughness between 101.95% and 119.30% depending on the cutting speed; whereas 80% greater cutting speed caused a decrease in the average surface roughness between 23.28% and 40.63% according to the feed rate in drilling of

Ti-6Al-4V. The results clearly indicate that the average surface roughness was more highly susceptible to the change in feed rate rather than spindle speed.

Table 7-5: Experimentally obtained Average Surface Roughness in Drilling of Ti-6Al-4V

Feed Rate (mm/min)	Spindle Speed (rpm)	Average Surface Roughness (μm)
1000	95	1.54±0.2
1400	95	1.35±0.1
1800	95	1.09±0.1
1000	119	2.21±0.2
1400	119	1.60±0.2
1800	119	1.40±0.1
1000	142	2.63±0.3
1400	142	2.27±0.2
1800	142	1.57±0.2
1000	171	3.11±0.3
1400	171	2.88±0.3
1800	171	2.39±0.3

Results show that desired surface roughness in industry which is typically below 1.6 μm R_a can be reached with the selection of medium-high spindle speed and low-medium feed rate in the machining of Ti-6Al-4V by the use of TiAlN/Ti multilayer coated WC drills. By the use if these suggested process parameters, required tolerances can be achieved.

7.5.2 Effect of Tool Wear on Surface Roughness

Surface roughness is another aspect of machining and it is worth to determine the number of holes that can be drilled in Ti-6Al-4V workpiece to maintain hole quality and control manufacturing cost. Development of the average surface roughness by the number of holes can be observed during drilling in addition to the development of the wear regions. Figure 7-16 shows

the average surface roughness versus the number of holes drilled in Ti-6Al-4V at 119 mm/min feed rate and 1400 rpm spindle speed. After drilling 32 holes in Ti-6Al-4V, average surface roughness increased by 294.38 % from 1.6 μm to 6.31 μm. This was due to the developed tool wear and consequently increased thrust force. This clearly indicates the importance of tool wear on the average surface roughness.

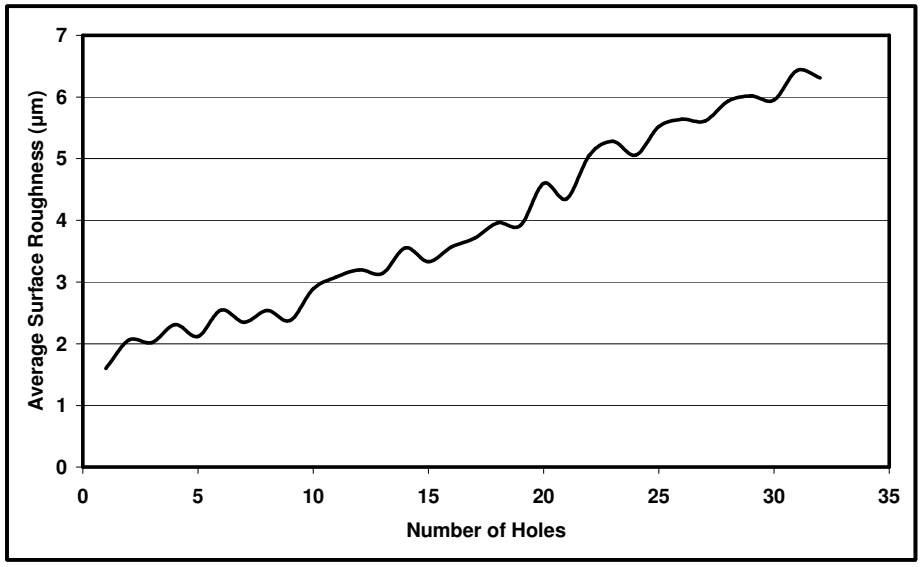

Figure 7-16: Effect of Number of Holes on the Average Surface Roughness in Drilling of Ti-6Al-4V (f=119 mm/min S=1400 rpm)

The life of the drill has been reached with regard to the criteria based on industrial experience. The use of the drill is not suggested beyond this limit. Providing that drilling continues with the same drill, the average surface roughness could suddenly elevate due to increased wear. Chatter could be highly to occur in drilling with the use of an extremely worn drill.

7.6 Analysis of Tool Wear

Severe tool wear in machining of high strength aerospace materials is one of the main reasons for machining cost. In order to maintain quality of the machined workpieces, it is important to replace cutting tools as they reach wear criteria as explained in methodology section. Variation of thrust force, torque, burr formation and surface roughness versus number of holes drilled can be typical indication of tool wear as discussed in previous subsections.

Figure 7-17 shows the tool wear in drilling of Ti6Al4V by multilayer TiAlN/TiN coated WC drill. The tests were performed at process parameters of 1400 rpm spindle speed and 119 mm/min feed rate. It was found that tools exceeded their service life after drilling 32 holes in Ti alloy workpieces. Beyond this number of holes, cutting process would not be stable due to excessive wear of the cutting edges. The gradual loss of sharpness of cutting edges causes a decrease in the capability of tool to cut the material, thus it leads an increase in cutting forces and torques. Thrust force increased gradually from 750.58 N to 867.22 N. The increase in tool wear would degenerate the material removal mechanism progressively. As it can be seen from Figure 7-17 (b), flank wear was the dominant wear mechanism in drilling of titanium alloy alone. This was not a surprise since high cutting forces are generated in the cutting region. The hard phases within titanium alloy workpieces also abraded the flank surfaces of cutting tools. Some significant wear has been also observed on the chisel edges of the drills as shown in Figure 7-17 (d). This could also be an indication of the high forces induced during cutting process. As shown in Figure 7-17 (c), higher crater wear has been inspected on the tools in drilling of Ti6Al4V. The generated chip flows over this region causing rubbing of the surfaces. Adhesion is well known characteristic in machining of titanium and reported by [17], [18] and [218]. High chemical affinity of titanium to most of tool materials leads to material transfer on to cutting tools. Adhesion can cause to build-up-edge (BUE) formation on tool edges or diffusion into tool materials. The accumulation of work material on cutting edges can result in devastation of the cutting edge and consequently tool chipping or fracture on cutting tools; deterioration of quality of the machined surfaces. Diffusion can cause softening of cutting tool and consequently increase the wear rate. However, no significant sign of adhesion was observed on cutting edges or flank surfaces. This was due to the use of high amount of coolant at high pressure and the high performance of coating on the tools.

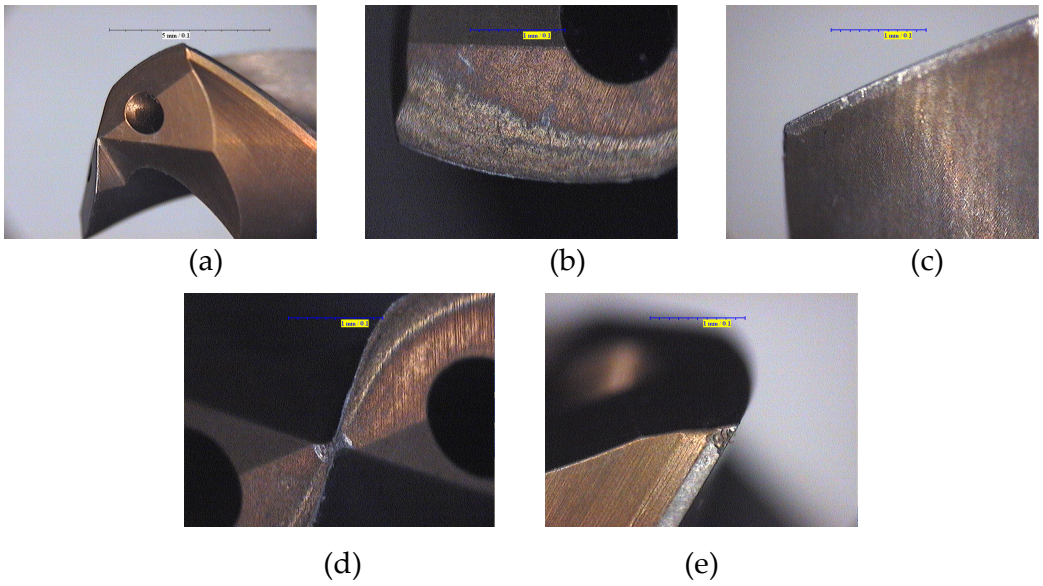

Figure 7-17: Tool Wear in Drilling of Ti-6Al-4V (S=1400 rpm, f=119 mm/min) (a) Overall (b) Flank Wear (c) Crater Wear (d) Chisel Wear (e) Margin Wear

Nevertheless, after making 32 holes, noticeable chipping was observed at the end of major cutting edge near the margin of the drill. This could be clearly observed in Figure 7-17 (e). These findings indicated the end of life for the cutting tool.

Figure 7-18 shows the effects of the number of holes drilled on tool wear of multilayer TiAlN/TiN coated WC drill in drilling of Ti-6Al-4V. Both flank wear and crater wear of drill bit versus number of holes drilled are indicated in drilling at 119 mm/min of feed rate and 1400 rpm of spindle speed. The flank wear passed beyond the 0.25 mm tool wear criterion after 32 holes whereas crater wear reached 0.20 mm. The wear on the clearance surface was more significant compared to the wear on the rake surface. This was due to the high induced cutting forces and hard phases in Ti-6Al-4V. Due to chip formation, noticeable crater wear was observed in drilling of Ti alloy. It should be noted that peck drilling would minimize these wear factors. After drilling 32 holes at 1400 rpm spindle speed and 119 mm/min feed rate, 5.38 min tool life was measured for drilling of Ti-6Al-4V with multilayer TiAlN/TiN coated WC drill.

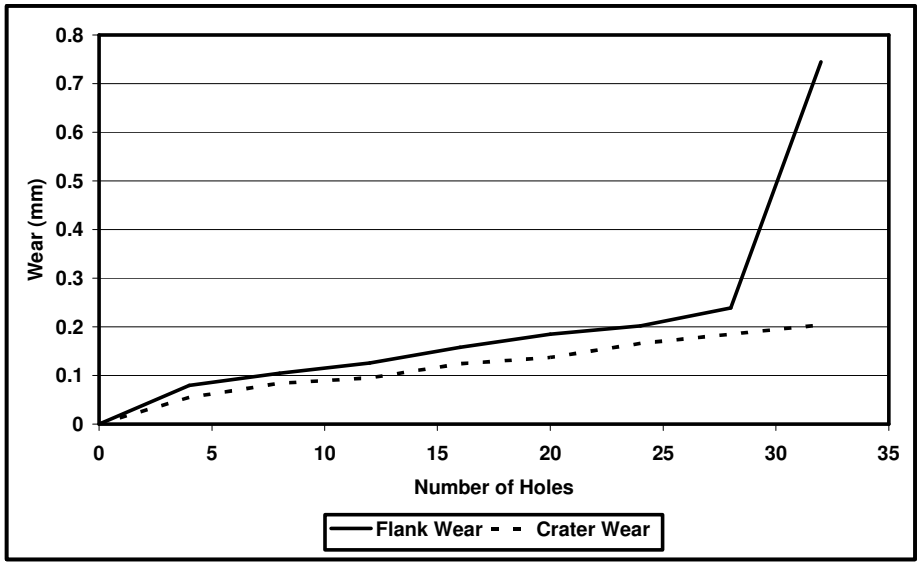

Figure 7-18: Progression of Tool Wear in Drilling of Ti-6Al-4V (S=1400 rpm, f=119 mm/min)

In summary, in drilling of Ti-6Al-4V by multilayer TiAlN/TiN coated WC, significant amount of progressive flank and crater wear occurred due to high cutting forces. Owing to these wear formations the cutting edges have become dull, hence thrust force, torque, burr formation and the average surface roughness have increased gradually. In addition to these, substantial chipping has been observed at the margin and corners of the cutting edges at the end of tool life.

7.7 Analysis of Workpiece Stress Distribution

The progressive damage and the stress distributions of Ti-6Al-4V work piece during drilling process are shown in Figure 7-19 (a) and Figure 7-19 (b) by 8 mm rigid twist drilled at 1400 rpm spindle speed and 119 mm/min feed rate. As the drill bit contacts with the workpiece material, stress was induced with regard to the applied process parameters. It can be observed from Figure 7-19 (a), the highest stresses induced around the centre of the hole where the drill penetrates and cuts the material. The induced Mises stress was estimated up to 1.039 GPa in the FE analysis whereas the residual stress on the workpiece was estimated between 100 and 500 MPa in some very local places and generally up

to 50 MPa in the hole vicinity after the drilling as shown in Figure 7-19 (a) and Figure 7-19 (b), respectively.

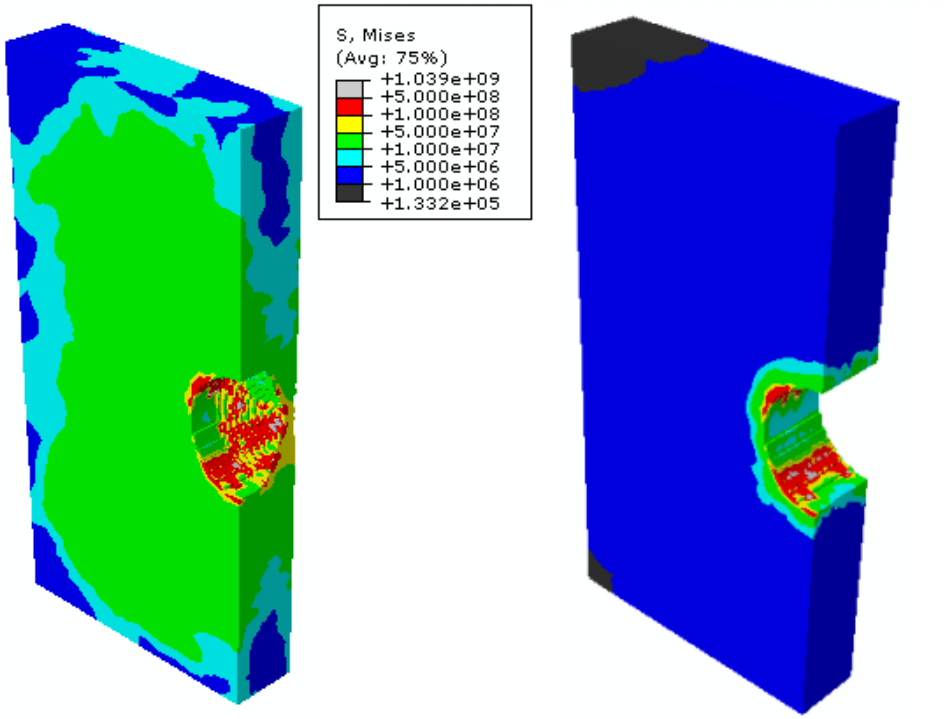

(a) **(b)**

Figure 7-19: Workpiece Stress Distribution in drilling of Ti-6Al-4V (a) at 1.75 s (b) after drilling (S=1400 rpm, f=119 mm/min)

The stress distributions of the Ti-6Al-4V work piece after the drilling process are shown in Figure 7-20 (a) and Figure 7-20 (b) for 8 mm twist drill and 8 mm step drill with a stage ratio of 0.63, respectively. As can be observed in Figure 7-20 (a) and Figure 7-20 (b), the highest stresses were induced in the vicinity of hole where the drill cut the material and gradually reduced until boundary conditions at the edges of the workpiece. Stress distribution shows that drilling induced area in the hole vicinity was estimated lower in drilling of Ti-6Al-4V with 0.63 stage ratio rigid step drill compared to drilling of Ti alloy with 8 mm rigid twist drill at 1400 rpm spindle speed and 119 mm/min feed rate. This was due to the fact that the step drill performs the secondary stage cutting with a lower contact area compared to the twist drill. The decrease in the contact means less material to be cut. The reduced material would require less energy and force hence less induced stress and damage in the workpiece.

The estimated thrust force and torque in the previous subsections can be the sign of the advantage of using step drill.

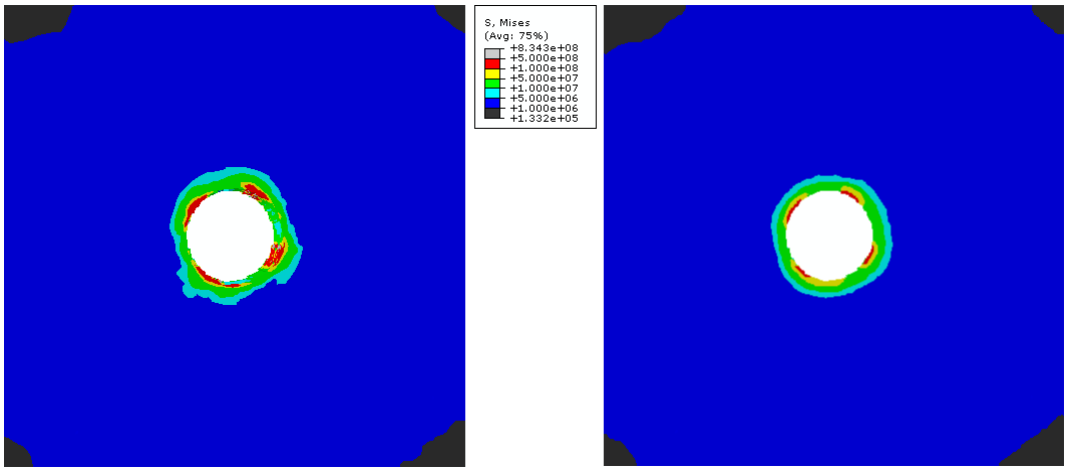

(a) (b)

Figure 7-20: Effect of Drill Geometry on Stress in Drilling of Ti-6Al-4V (a) Twist Drill (b) Step Drill (S=1400 rpm, f=119 mm/min)

7.8 Chip Morphology

The chip morphology indicates a continuous chip formation in all Ti drilling tests in this study. An example of the chip generated by multilayer TiAlN/TiN coated WC drill at 1000 spindle speed and 95 mm/min feed rate in wet drilling is shown in Figure 7-21 (a). The length of spiral chip can be considered to evaluate the difficulty of chip evacuation in drilling. As shown in Figure 7-21 (a), the chip length was about 50-60 mm in drilling with cutting fluid. At higher feed rate, 1000 rpm spindle speed and 171 mm/min feed rate, the chip was generated at a higher material removal rate, the chip ejection was more difficult and the length of spiral chip was short, approximately 10 mm. Under such drilling condition, the thrust force induced was higher than lower material removal rate and chip length indicated more difficult chip ejection as shown in Figure 7-21 (b).

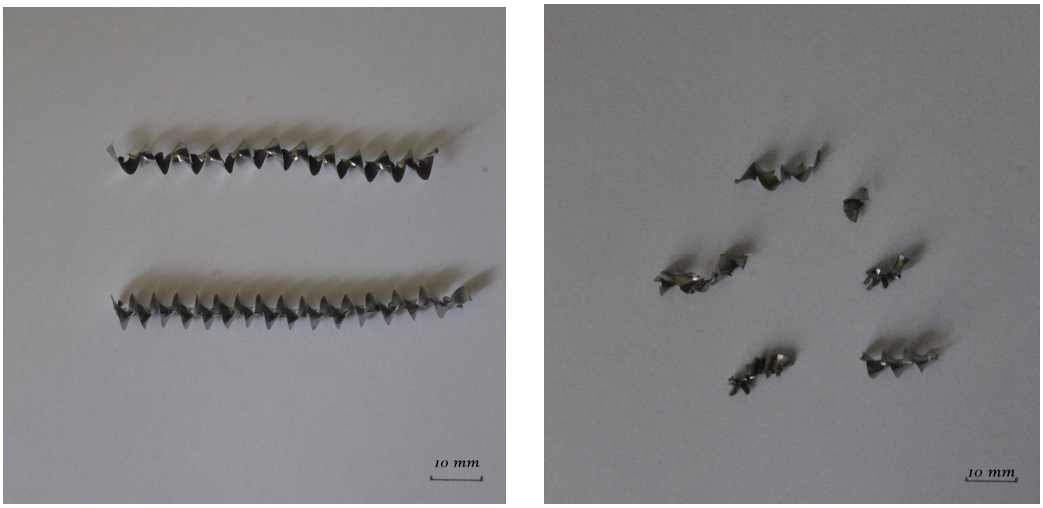

(a) (b)

Figure 7-21: Chip Morphology in Drilling of Ti-6Al-4V (a) S=1000 rpm, f=95 mm/min (b) S=1000 rpm, f=171 mm/min

7.9 Summary of Drilling of Ti-6Al-4V

Experimental analysis and finite element simulations were performed for investigations of drilling of Ti-6Al-4V. The effects of process parameters and complex tool geometry on drilling outputs have been examined in drilling of Ti alloy. All experiments were carried out with the use of coolant.

Experimental results showed that an increase in feed rate led to an increase in thrust force, torque, burr formation and surface roughness in drilling of Ti-6Al-4V with TiN/TiAlN multilayer coated 8 mm diameter tungsten carbide twist drill. The increase in spindle speed caused a decrease in thrust force, torque, burr height, burr width and average surface roughness. The effect of wear on drilling outputs has also been investigated. The effect of process parameters has been observed on drilling induced chip to show machinability.

3D finite element model based on a mechanical Lagrangian formulation has been used to simulate drilling of Ti6Al4V. The effects of cutting parameters, namely spindle speed and feed, on thrust force, torque and burr have been investigated by the proposed FE model. Johnson-Cook constitutive material model was implemented due to continuous form of chip generation. The results

of the comparisons show that cutting parameters have significant influence on thrust force, torque and burr formation in drilling of Ti alloy. The predictions of thrust force using the FE model closely match the experimentally measured values. Drilling induced torque has been simulated in acceptable range by FE model. This shows the applicability of the developed model. Results clearly show that the induced thrust force and torque have increased with the increasing feed and decrease with the increasing spindle speed. Although the extent of burr formation predicted significantly lower than the experimental test results, the correlation between process parameters and burr formation is predicted well. Further improvements with utilisation of chip formation and finer mesh could improve FE results of burr formation. The study has shown that the JC model is accurate for drilling simulation when there is a continuous chip generation whilst drilling with a cutting speed in the test region (25–45 m/min). The model has also shown that incorporation a mechanical model can be sufficient to predict the drilling process provided that sufficient cooling is applied during the drilling operation. Based on the performance of FE model, the effect of drill geometry on drilling of Ti-6Al-4V has been investigated by various step drills. FE results indicated the advantages of step drill over twist drill by several aspects including thrust force, torque and burr formation.

The material respond of Ti-6Al-4V is highly dependant on material data in FE analysis. Although the material data were obtained from an experimental study in which experimental test had been carried out at high speeds, it could still be one of the main reasons of the diversity between the results of FE analysis and experiments. In addition to strain, strain rate and temperature, the material properties are also dependant on the micro structure of the material. This could affect the stress-strain curve under the multi-axial state of loading, consequently the outputs of drilling such as thrust force, torque and burr formation. To obtain higher accuracy and improve the reliability of drilling Ti-6Al-4V, material properties of Ti-6Al-4V should be tested at similar conditions to the drilling operation.

Chapter 8

Results and Discussions of Drilling of CFRP/Ti-6Al-4V Hybrid

Machining of composites materials and metals are quite different, so investigations on the machinability of these materials have been carried out separately as explained in detail in Chapter 6 and Chapter 7 for CFRP and Ti-6Al-4V, respectively. In this chapter, drilling of these distinct materials together is discussed and compared with drilling of individual materials. To understand and provide high machinability of CRRP/Ti-6Al-4V stack, effects of process parameters and tool geometry have been investigated in various aspects of drilling including thrust force, torque, burr formation, delamination, surface roughness, wear and workpiece stress through experiments and finite element analysis.

8.1 Analysis of Thrust Force

Figure 8-1 shows the development of thrust force in drilling of Ti-6Al-4V, CFRP and CFRP/Ti-6Al-4V stack workpieces by 3 μm TiN/TiAlN multilayer coated 8 mm diameter tungsten carbide twist drill with 140° point angle and 30° helix angle. Figure 8-1 (a) shows the development of thrust force in drilling of UD-CFRP at 457 mm/min feed rate and 4500 rpm spindle speed (113 m/min cutting speed). Figure 8-1 (b) presents induced thrust force throughout drilling of Ti-6Al-4V at 119 mm/min and 1400 rpm spindle speed (35.13 m/min cutting speed). The plot of thrust force in drilling of titanium alloy in Figure 8-1 (b) is different compared to drilling of CFRP as shown in Figure 8-1 (a). This is due to the use of peck drilling strategy in drilling of titanium alloy as explained in the experimental methodology section. Figure 8-1 (c) displays thrust force in drilling of CFRP/Ti-6Al-4V stack at 457 mm/min and 119 mm/min feed rates; 4500 rpm and 1400 rpm spindle speeds in CFRP and Ti-6Al-4V, respectively. As

it can be observed in Figure 8-1 (c), thrust force rapidly rose as drill reached to the exit of composite workpiece and entered titanium workpiece. This sudden change in thrust force in the transition region from CFRP to Ti-6Al-4V was approximately three times and it may affect the quality of drilling process and performance of drill as it has been also addressed in the literature [159]. The induced thrust force was measured to be higher in drilling of stack of CFRP and Ti-6Al-4V comparing to the drilling of each materials alone. Higher stiffness of Ti-6Al-4V workpiece under CFRP workpiece provided an increased stiffness in CFRP workpiece particularly against bending in loading in the normal direction, thus thrust force has induced greater in drilling of CFRP part in stack of CFRP and Ti-6Al-4V. Similar to CFRP, higher thrust force has been obtained in Ti-6Al-4V workpiece in drilling of stacked form. The increased thrust force in CFRP workpiece has caused to an increase in wear. This was observed as higher amount of wear in the progression of wear and also higher thrust forces in the progression of thrust force in the both material. In addition to that combinations of the aspects of drilling two distinct materials have also raised the extent of tool wear in drilling of stacked materials and consequently resulted in greater thrust force in Ti-6Al-4V workpiece after drilling CFRP workpiece in stacked form.

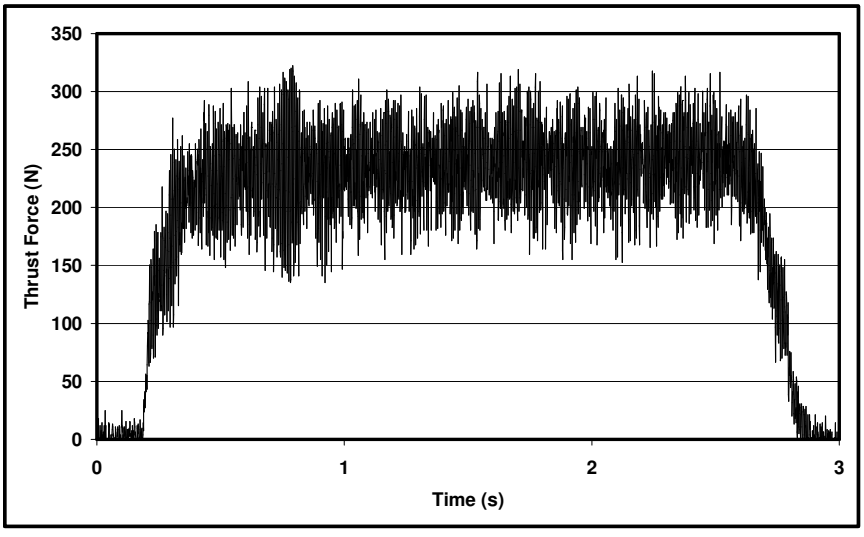

(a)

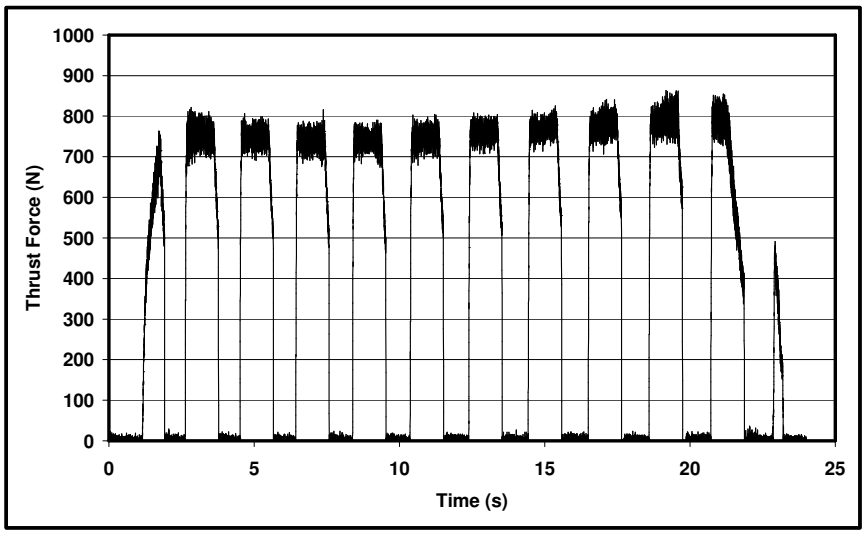

(b)

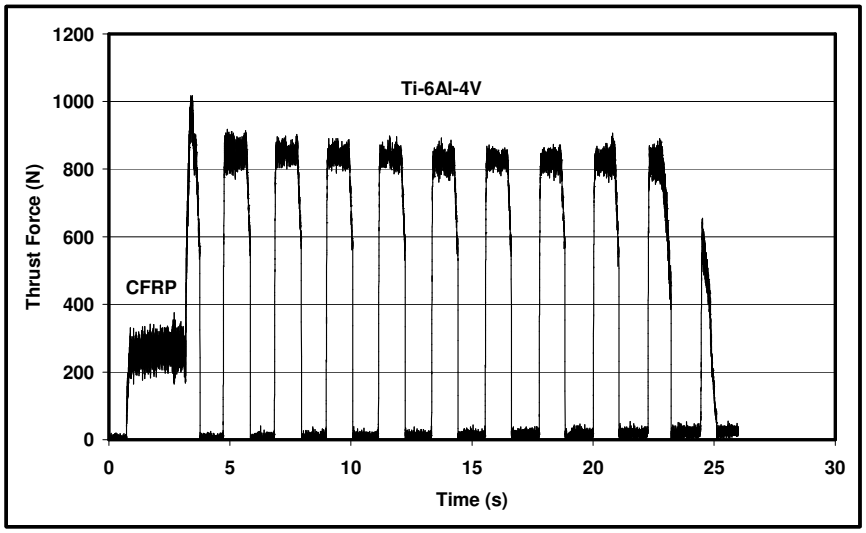

(c)

Figure 8-1: Thrust Force through Hole (a) Drilling of CFRP alone (b) Drilling of Ti-6Al-4V alone (c) Drilling of CFRP/Ti-6Al-4V Hybrid

8.1.1 Effects of Process Parameters on Thrust Force

Analysis of induced thrust force in drilling of CFRP and Ti-6Al-4V separately has been discussed in Chapter 6 and 7, respectively. Since the materials are rather distinct from each other, different machining parameters are required. Thus, drilling of CFRP/Ti-6Al-4V is not as straightforward as drilling of each material separately. The cutting parameters in each zone could

influence drilling. For that purpose, drilling parameters in drilling of stacked materials have been limited with regard to the analysis based on the drilling of each material. In analysis of induced thrust force in drilling of CFRP/Ti-6Al-4V, each scenario has been investigated carefully as shown in Table 8-1 in detail.

Based on the results of drilling of CFRP and Ti-6Al-4V separately, the analysis of thrust force in drilling of stack has focused on combinations of 2 cutting speeds and 2 feed rates in each material which means a total of 16 set of machining condition. Combinations of moderate cutting speeds and low feed rates have been focused to optimise drilling of stacked materials. As can be observed in Table 8-1 experimentally obtained and finite element based induced thrust forces are given for Ti-6Al-4V and CFRP in regard with the machining conditions and related deviations. Thrust force was found to increase with regard to the increase in feed rate in both materials drilled together. Similar to the results of each material drilled separately given in Chapter 6 and 7, thrust force has decreased in titanium zone and increased in CFRP zone of stacked workpieces with regard to spindle speed in the tested region. The possible reason of this in Ti-6Al-4V is the effect of strain rate and softening mechanism. The lack of this mechanism in CFRP led to an increase in drilling of CFRP workpiece. It must be also noted that this has observed in drilling of CFRP with the use of coolant which avoid thermal softening of matrix. Comparing to the drilling of each material separately, relatively higher thrust forces have been obtained. Since stiffer Ti-6Al-4V supported the CFRP workpiece, the stiffness of CFRP has been increased particularly against bending under loading in normal direction. Thus higher thrust forces have been obtained in experiments and predicted in FE simulations. Higher induced thrust force has been observed in Ti-6Al-4V zone as well. In experiments, the cutting tool has been first drilled the CFRP part on top of titanium alloy, thus some amount of wear has been occurred. This would cause an increase in the extent of thrust force comparing to drilling of titanium alloy workpiece alone. This can be clearly observed in Table 8-1. In addition to that very dusty abrasive chips generated in drilling of CFRP workpiece could also influence drilling of titanium zone in stacked condition. The FE analysis with fully 3-D elements has provided close results to the experiments in drilling of CFRP/Ti-6Al-4V. The

deviations of predicted thrust force lay between 3.07% and 14.98% underestimation in Ti-6Al-4V zone, 3.14% and 4.66% underestimation in CFRP zone according to the set of process parameters.

Table 8-1: Experimental and Simulation based Thrust Force in Drilling of CFRP/Ti-6Al-4V

Ti-6Al-4V		CFRP		Ti-6Al-4V Thrust Force (N)			CFRP Thrust Force (N)		
S (rpm)	f (mm/min)	S (rpm)	f (mm/min)	Exp.	FEA	Deviation (%)	Exp.	FEA	Deviation (%)
1400	95	4500	355	738.44±8.2	699.14	-5.32	256.54±2.8	244.59	-4.66
1400	119	4500	355	831.18±7.4	805.65	-3.07	256.54±2.8	244.59	-4.66
1400	95	4500	457	758.82±5.4	699.14	-7.87	265.00±3.2	255.72	-3.50
1400	119	4500	457	851.00±9.5	805.65	-5.33	265.00±3.2	255.72	-3.50
1400	95	6000	355	753.24±6.8	699.14	-7.18	261.33±2.6	253.12	-3.14
1400	119	6000	355	848.45±8.2	805.65	-5.04	261.33±2.6	253.12	-3.14
1400	95	6000	457	778.92±7.3	699.14	-10.24	277.46±3.1	266.85	-3.82
1400	119	6000	457	878.36±8.9	805.65	-8.28	277.46±3.1	266.85	-3.82
1800	95	4500	355	658.49±6.4	594.16	-9.77	256.54±2.8	244.59	-4.66
1800	119	4500	355	751.23±9.4	694.24	-7.59	256.54±2.8	244.59	-4.66
1800	95	4500	457	678.22±9.1	594.16	-12.39	265.00±3.2	255.72	-3.50
1800	119	4500	457	744.08±6.9	694.24	-6.70	265.00±3.2	255.72	-3.50
1800	95	6000	355	671.04±6.5	594.16	-11.46	261.33±2.6	253.12	-3.14
1800	119	6000	355	763.94±8.3	694.24	-9.12	261.33±2.6	253.12	-3.14
1800	95	6000	457	698.88±7.4	594.16	-14.98	277.46±3.1	266.85	-3.82
1800	119	6000	457	778.39±7.2	694.24	-10.81	277.46±3.1	266.85	-3.82

8.1.2 Effect of Geometry on Thrust Force

Similar to drilling of CFRP and Ti-6Al-4V separately as explained in Chapter 6 and 7, effect of tool geometry on thrust force have been investigated in drilling of CFRP/Ti-6Al-4V stacked materials. The estimated thrust forces were found to be 3.50% and 5.33% different than the experiments for CFRP and Ti-6Al-4V respectively in drilling stacked form in the tested region with 8mm diameter coated carbide drill. These deviations showed that the FE model could estimate thrust forces closely in drilling of CFRP/Ti-6Al-4V stack.

Figure 8-2 (a) and Figure 8-2 (b) show the numerical predictions of thrust forces in drilling of CFRP/Ti-6Al-4V stack at 119 mm/min feed rate and 1400 rpm spindle speed for Ti-6Al-4V, 457 mm/min feed rate and 4500 rpm spindle speed for CFRP with twist drill and various step drills. Similar to drilling of CFRP and Ti-6Al-4V separately, the secondary drilling stage by step drill has been the subject of matter in drilling of CFRP/Ti-6Al-4V stack and thrust forces shown in Figure 8-2 (a) and Figure 8-2 (b) are the average estimated values in the secondary drilling stage. The FE model estimated the thrust force to be 255.72 N in drilling CFRP workpiece in stack form by 8 mm diameter twist drill. The estimated thrust force was 12.65% greater in CFRP region in drilling of stack than that estimated in drilling of CFRP alone. When step drills were utilized in FE analysis of drilling of CFRP, thrust forces were estimated significantly lower than that obtained in drilling by twist drill. Comparisons of the estimated thrust forces for the twist drill and step drills with various stage ratios are shown in Figure 8-2 (a) for drilling of CFRP alone and in stack form. Thrust force decreased 38.93% when a step drill with an initial 4.5 mm drill diameter; and 68.76% when a step drill with an initial 6.5 mm drill diameter in drilling of CFRP workpiece in stack with Ti-6Al-4V. As it can be seen the higher stage ratio has provided higher reduction in thrust force. This was due to disappearance of the effects of chisel edge in the second stage cutting of step drill. Moreover, smaller area to be cut required smaller contact between the CFRP workpiece and cutting edges of drill which reduced the need of cutting energy and cutting force. In each drilling scenario with step drill, higher thrust forces has been estimated in drilling of CFRP in stack with Ti-6Al-4V

comparing to drilling of CFRP alone as shown in Figure 8-2 (a). The higher rigidity of titanium alloy workpiece under CFRP workpiece has provided stiffness to the CFRP workpiece.

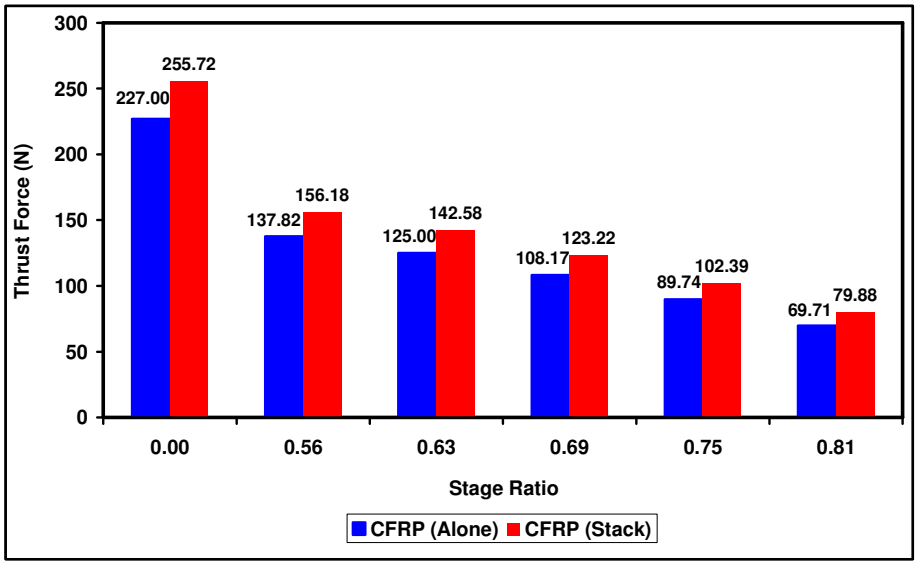

(a)

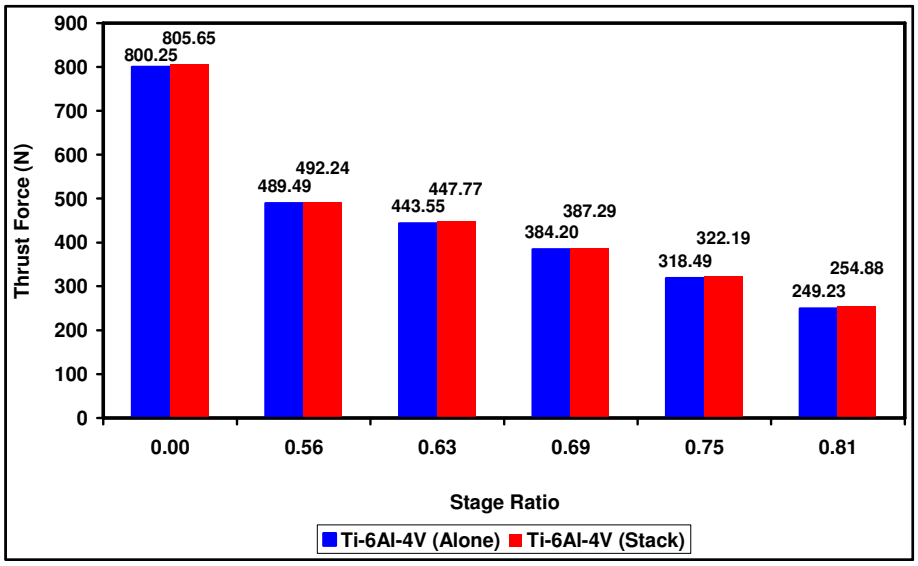

(b)

Figure 8-2: Effect of Drill Geometry on Thrust Force in Drilling of CFRP/Ti-6Al-V Stack

Figure 8-2 (b) shows the effect of drill geometry on thrust force in Ti-6Al-4V region in drilling of CFRP/Ti-6Al-4V stack. Induced thrust force was estimated as 805.65 N in drilling of Ti-6Al-4V workpiece in stack with CFRP by 8 mm diameter twist drill. The estimated thrust force was slightly greater in Ti-

6Al-4V region in drilling of stack than that estimated in drilling of Ti-6Al-4V alone. Significantly lower thrust forces were estimated by the use of step drill in drilling of CFRP/Ti-6Al-4V stack. Comparisons of the estimated thrust forces for the twist drill and step drills with various stage ratios are shown in Figure 8-2 (b) for drilling of Ti-6Al-4V alone and in stack form. In each drilling scenario with step drill, slightly higher thrust forces has been estimated in drilling of Ti-6Al-4V in stack with CFRP comparing to drilling of Ti-6Al-4V alone. This was due to the existence of CFRP worpkiece on Ti-6Al-4V workpiece as a constraint. Thrust force decreased 38.90% when a step drill with an initial 4.5 mm drill diameter; and 68.36% when a step drill with an initial 6.5 mm drill diameter in drilling of Ti-6Al-4V workpiece in stack with CFRP. As it was seen previously, the higher stage ratio has provided higher reduction in thrust force.

In summary, drilling induced thrust force was predicted to reduce noticeably comparing to twist drill. The reduced thrust force would assist to minimise burr height and burr width; and other drilling induced defects. This could provide high structural integrity and long service life. The use of step drill could decrease possible rejections thus cost of manufacturing.

8.1.3 Effect of Tool Wear on Thrust Force

Figure 8-3 shows thrust force versus number of holes drilled in CFRP, Ti-6Al-4V and CFRP/Ti-6Al-4V stack. Drilling of CFRP alone and in stack was performed at 457 mm/min feed rate and 4500 rpm spindle speed whereas drilling of Ti-6Al-4V was conducted at 119 mm/min feed rate and 1400 rpm spindle speed. In drilling of CFRP and Ti-6Al-4V alone, drill bits worn after drilling 56 and 32 holes, respectively. Thrust force increased by 163% in drilling of CFRP and 15.6% in drilling of Ti-6Al-4V. However, drill bits worn faster in drilling of CFRP/Ti-6Al-4V stack when the same cutting parameters were used in experiments for each material. It was observed that after drilling 15 holes in stack, thrust force rose by 37.8% and 56.6% in Ti-6Al-4V and CFRP workpieces, respectively. The reason for that would be the combination of two different cutting mechanisms, thus existence of different wear mechanisms together in drilling of stacked form. CFRP is very abrasive material therefore abrasive wear

was expected whereas titanium alloy is an elastoplastic material with the requirement of very high cutting force which would result in high deformation and sudden fracture in the drill. It is believed that the existence of these two different cutting mechanisms whist drilling of materials in stacked form accelerated the tool wear as it can be observed from the number of holes drilled. The increased impact resistance of CFRP by the addition of a Ti-6Al-4V workpiece as a back-up plate has led to an increase in thrust force in drilling of CFRP zone of stack. Due to accelerated wear, thrust force of each material has risen significantly with the number of drilled holes in drilling of stack comparing to drilling of each material separately.

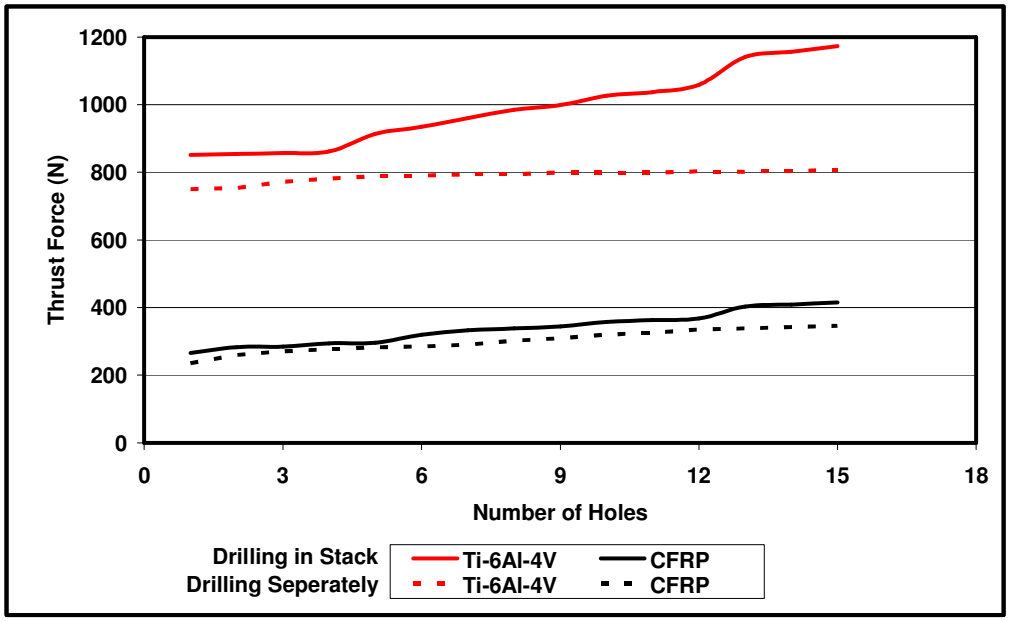

Figure 8-3: Effect of Number of Holes on Thrust Force

As it could be found in Figure 8-3, thrust force has increased significantly after drilling 15 holes, particularly in drilling of Ti-6Al-4V part of stack form. Thus it is not suggested to continue drilling after this number of holes with the given cutting parameters since the outputs would be difficult to be controlled. Increased cutting forces could elevate cutting stresses, cutting temperatures and friction between drill and workpiece. This would likely to affect material removal mechanism which can accelerate wear rate. Consequently it could be finalized with chipping and sudden tool breakage, unacceptable material defects including excessive burr and surface roughness, thus possible rejections and increased manufacturing costs.

8.2 Analysis of Torque

Figure 8-4 shows the progression of induced torque in drilling of Ti-6Al-4V, CFRP and CFRP/Ti-6Al-4V stack workpieces by 3 μm TiN/TiAlN multilayer coated 8 mm diameter tungsten carbide twist drill with 140° point angle and 30° helix angle. Figure 8-4 (a) shows the development of torque in drilling of CFRP at 457 mm/min feed rate and 4500 rpm spindle speed whereas Figure 8-4 (b) presents induced torque throughout drilling of Ti-6Al-4V at 119 mm/min and 1400 rpm spindle speed. The plot of torque is similar to thrust force in drilling of the materials. Figure 8-4 (c) displays torque in drilling of CFRP/Ti-6Al-4V stack at 457 mm/min and 119 mm/min feed rates; 4500 rpm and 1400 rpm spindle speeds in CFRP and Ti-6Al-4V, respectively. As it can be observed in Figure 8-4 (c), torque jumped significantly as drill reached to the exit of composite workpiece and entered titanium workpiece. This sudden change was similar to the progression of thrust force as plotted earlier. The induced torque was measured to be higher in drilling of stack of CFRP and Ti-6Al-4V comparing to the drilling of each materials alone. Higher stiffness of Ti-6Al-4V workpiece under CFRP workpiece provided an increased stiffness in CFRP workpiece. In addition to that higher torque has been obtained in Ti-6Al-4V workpiece in drilling of stacked form owing to increased wear at the entrance region of stacked materials.

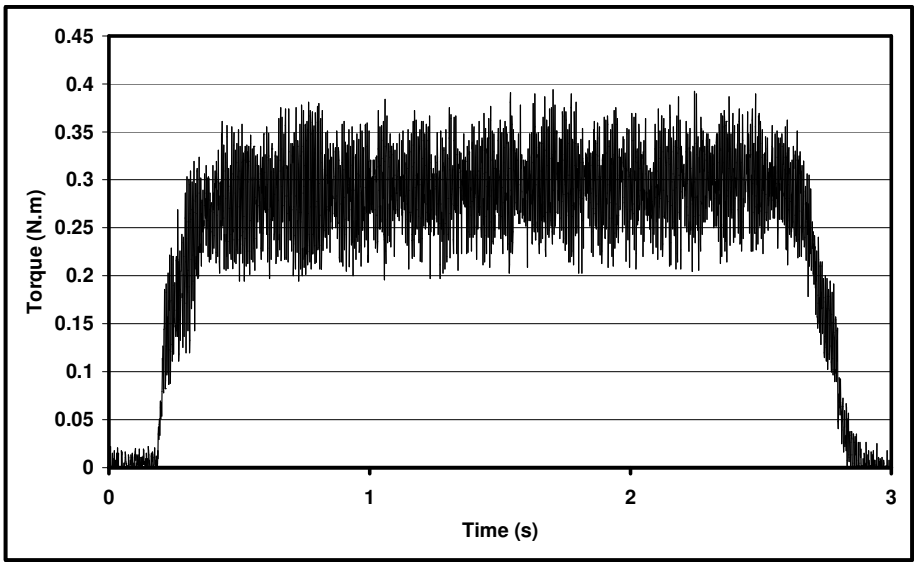

(a)

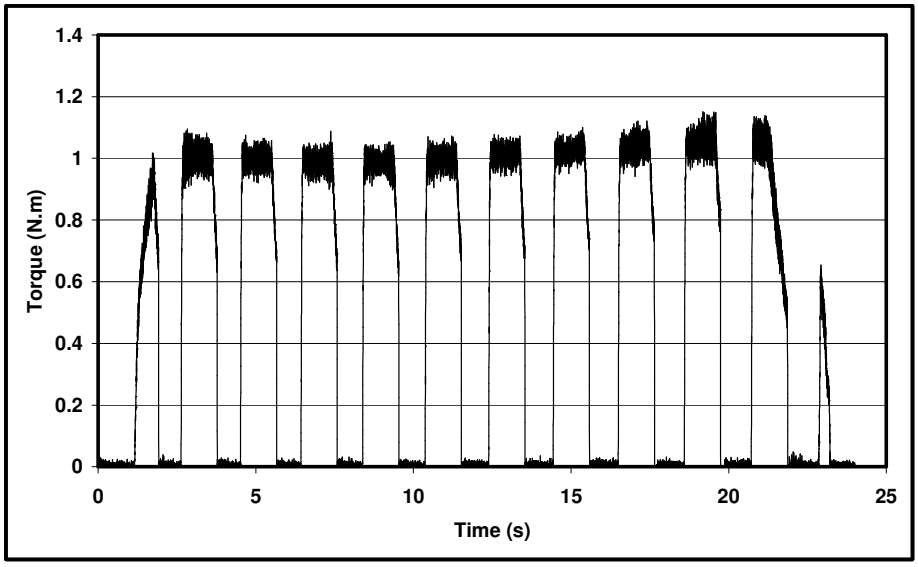

(b)

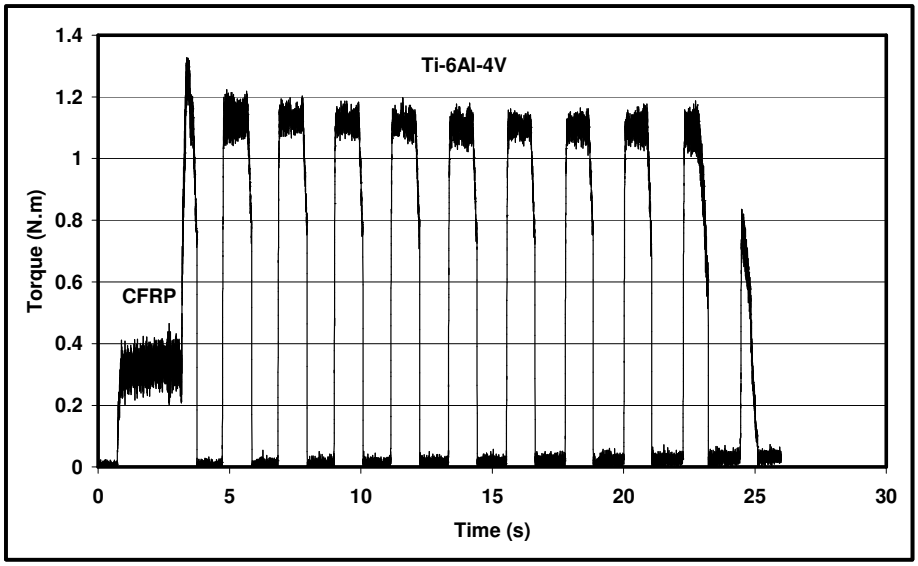

(c)

Figure 8-4: Torque through Hole (a) Drilling of CFRP alone, (b) Drilling of Ti-6Al-4V alone (c) Drilling of CFRP/Ti-6Al-4V

8.2.1 Effects of Process Parameters on Torque

Analysis of induced torque in drilling of CFRP and Ti-6Al-4V separately has been discussed in the previous results chapters 6 and 7, respectively. Owing to being very different materials, different machining parameters have been used in each material. The influences of these parameters have been shown clearly for each material. However, effects of cutting parameters in drilling of

stacked materials would be more complicated because of the fact that different machining mechanisms take place in each section and combined effects could affect drilling of each material. For optimisation purpose, machining parameters in drilling of stacked materials have been limited with regard to the analysis based on the drilling of each material.

Based on the results of drilling of CFRP and Ti-6Al-4V separately, investigations of torque in drilling of CFRP/Ti-6Al-4V stack have been focused on combinations of 2 cutting speeds and 2 feed rates in each material which means a total of 16 set of machining condition. Combinations of moderate cutting speeds and low feed rates have been chosen in the optimisation of drilling of stacked materials and given in Table 8-2. As it can be observed from the table, experimentally obtained and finite element based induced torque values are given in each material section with regard to the machining conditions. Drilling induced torque increased with the increased feed rate in drilling of both materials together. As it was observed in drilling of each material separately, as cutting speed has been increased torque decreased in drilling of titanium alloy whereas it increased in CFRP zone of stacked workpieces. Similar to the findings in thrust force, higher torque values have been measured in each material in drilling of CFRP/Ti-6Al-4V comparing to drilling of these materials separately. Titanium alloy workpiece has supported CFRP plate in stacked form, thus the resistance of the laminated composite has increased under multi-axial loading. Similar to CFRP, higher induced torque has been measured in drilling of Ti-6Al-4V zone in stacked form. As the tool has worn in the entrance part of stack, CFRP workpiece, an increase has been found in torque in drilling of titanium alloy workpiece comparing to drilling of titanium alloy workpiece alone. Furthermore, dusty abrasive composite particles could also deteriorate drilling and would result in increased torque in drilling of titanium zone in stacked situation. The FE analysis of drilling of CFRP/Ti-6Al-4V stack has reflected these changes in torque successfully. The diversions between the FE predicted torque and experimentally measured torque have been found between 0.15% and 14.44% in Ti-6Al-4V workpiece; 6.9% and 11.84% in CFRP workpiece with regard to set of machining parameters.

Table 8-2: Experimental and Simulation based Torque in Drilling of CFRP/Ti-6Al-4V

Ti-6Al-4V		CFRP		Ti-6Al-4V Torque (N.m)			CFRP Torque (N.m)		
S (rpm)	f (mm/min)	S (rpm)	f (mm/min)	Exp.	FEA	Deviation (%)	Exp.	FEA	Deviation (%)
1400	95	4500	355	0.93±0.06	1.03	10.59	0.29±0.03	0.31	6.90
1400	119	4500	355	1.08±0.07	1.21	12.04	0.29±0.03	0.31	6.90
1400	95	4500	457	0.96±0.05	1.03	7.14	0.30±0.02	0.34	11.84
1400	119	4500	457	1.13±0.06	1.21	7.08	0.30±0.03	0.34	11.84
1400	95	6000	355	0.96±0.06	1.03	7.14	0.32±0.03	0.35	9.37
1400	119	6000	355	1.12±0.07	1.21	8.04	0.32±0.04	0.35	9.37
1400	95	6000	457	1.03±0.06	1.03	-0.15	0.35±0.04	0.38	8.57
1400	119	6000	457	1.17±0.07	1.21	3.42	0.35±0.05	0.38	8.57
1800	95	4500	355	0.89±0.06	0.85	-4.83	0.29±0.03	0.31	6.90
1800	119	4500	355	1.04±0.05	1.03	-1.11	0.29±0.03	0.31	6.90
1800	95	4500	457	0.92±0.05	0.85	-7.93	0.30±0.02	0.34	11.84
1800	119	4500	457	1.09±0.06	1.03	-5.64	0.30±0.03	0.34	11.84
1800	95	6000	355	0.91±0.05	0.85	-6.92	0.32±0.03	0.35	9.37
1800	119	6000	355	1.08±0.07	1.03	-4.77	0.32±0.04	0.35	9.37
1800	95	6000	457	0.99±0.06	0.85	-14.44	0.35±0.04	0.38	8.57
1800	119	6000	457	1.12±0.07	1.03	-8.17	0.35±0.05	0.38	8.57

8.2.2 Effects of Tool Geometry on Torque

Effect of tool geometry on torque has been investigated in drilling of CFRP/Ti-6Al-4V stacked materials by the comparison with drilling of CFRP and Ti-6Al-4V separately. The estimated torque values were found to be 11.85% and 7.08% different comparing to the drilling experiments for CFRP and Ti-6Al-4V

respectively as stacked form by 8 mm diameter coated carbide drill. These deviations showed that the FE model could estimate drilling induced torque closely in drilling of CFRP/Ti-6Al-4V stack.

Figure 8-5 (a) and Figure 8-5 (b) show the finite element predictions of drilling induced torque in drilling of CFRP/Ti-6Al-4V stack at 119 mm/min feed rate and 1400 rpm spindle speed for Ti-6Al-4V, 457 mm/min feed rate and 4500 rpm spindle speed for CFRP with twist drill and various step drills. The FE model estimated the torque as 0.34 N.m in drilling CFRP workpiece in stack form by 8 mm diameter twist drill. The estimated drilling induced torque was 13.33% greater in CFRP region of stack than that estimated in drilling of CFRP alone. Torque was estimated significantly lower with regard to the stage ratio of step drill comparing to that obtained in drilling by twist drill. Comparisons of the estimated torque are shown in Figure 8-5 (a) for drilling of CFRP alone and in stack form with regard to the drill geometry. Torque decreased 32.35% when a step drill with an initial 4.5 mm drill diameter; and 73.53% when a step drill with an initial 6.5 mm drill diameter in drilling of CFRP region of stacked materials. As it can be seen the higher stage ratio has provided higher reduction in torque. Smaller area to be cut needed smaller contact between the CFRP workpiece and cutting edges of drill. This provided less friction between the drill and workpiece and minimizes the cutting energy and cutting torque. In each drilling scenario with step drill, higher drilling induced torque has been estimated in drilling of CFRP region of stacked materials comparing to drilling of CFRP alone as shown in Figure 8-5 (a).

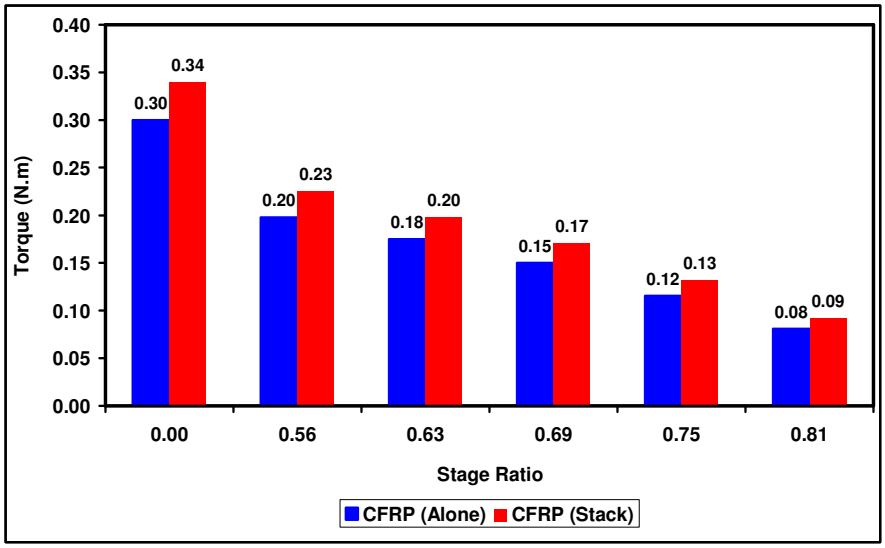

(a)

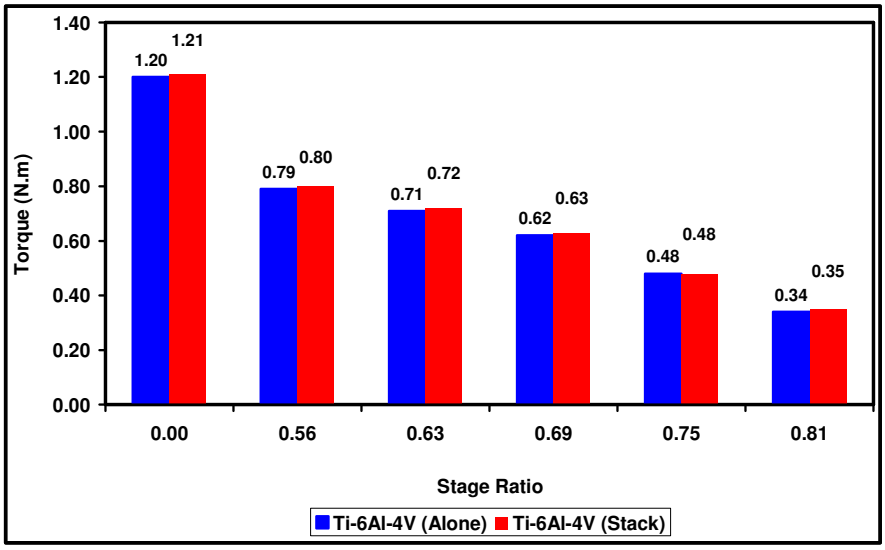

(b)

Figure 8-5: Effect of Drill Geometry on Torque in Drilling Ti-6Al-4V

Figure 8-5 (b) shows the effect of drill geometry on torque in Ti-6Al-4V region in drilling of CFRP/Ti-6Al-4V stack. Induced torque was estimated as 1.21 N.m in drilling of Ti-6Al-4V workpiece in stack with CFRP by 8 mm diameter twist drill. The estimated torque was slightly greater in Ti-6Al-4V region in drilling of stack than that estimated in drilling of Ti-6Al-4V alone. Significantly lower torque was estimated by the use of step drill in drilling of CFRP/Ti-6Al-4V stack. Comparisons of the estimated torque with regard to drill geometry are shown in Figure 8-5 (b) for drilling of Ti-6Al-4V alone and in stack

form. In each drilling scenario with step drill, slightly higher torque has been estimated in drilling of Ti-6Al-4V in stack with CFRP comparing to drilling of Ti-6Al-4V alone. This was due to the existence of CFRP worpkiece on Ti-6Al-4V workpiece as a constraint. Drilling induced torque decreased 33.88% when a step drill with an initial 4.5 mm drill diameter; and 71.07% when a step drill with an initial 6.5 mm drill diameter in drilling of Ti-6Al-4V workpiece in stack with CFRP. As it was seen previously, the higher stage ratio has provided higher reduction in torque.

To summarise, drilling induced torque was estimated significantly lower in drilling of CFRP/Ti-6Al-4V with step drill than drilling with twist drill. The reduced torque would lead to minimise friction and improve surface roughness. The use of step drill could provide better machinability with less part rejections and low cost of manufacturing.

8.2.3 Effects of Tool Wear on Torque

Figure 8-6 displays the progression of torque through number of holes in drilling of CFRP, Ti-6Al-4V and CFRP/Ti-6Al-4V stack. Due to different machining requirements, different process parameters have been used in drilling of CFRP and Ti-6Al-4V separately and stacked. In drilling of CFRP, 457 mm/min feed rate and 4500 rpm spindle speed have been used whereas in drilling of Ti-6Al-4V, 119 mm/min feed rate and 1400 rpm spindle speed has been set. In drilling of CFRP and Ti-6Al-4V separately, the life of cutting tools found to be 56 and 32 holes, with other words 2.45 and 5.38 minutes, respectively. However in drilling of CFRP/Ti-6Al-4V, drill bits have worn after 15 holes or 3.36 minute cutting time with the given parameters. After drilling 15 holes in CFRP, torque rose from 0.29 N.m. to 0.426 N.m. by 47% rise. After reaching tool life by drilling 56 holes in CFRP, torque reached to 0.767 N.m with 164% increase. In titanium alloy, torque increased only by 7% from 1 N.m to 1.07 N.m after 15 holes. After drilling 32 holes, torque reached to 1.09 N.m indicating a 9% growth. Drill bits have faced with higher wear rates in drilling of CFRP/Ti-6Al-4V stack. It was observed that after drilling 15 holes in CFRP/Ti-6Al-4V stack torque rose by 44.5% and 83.5% in Ti-6Al-4V and CFRP

workpieces, respectively. It is believed that the combination of two different cutting mechanisms has ended with combined wear mechanisms and consequently accelerated tool wear. This is proved by our wear inspection discussed in later sections.

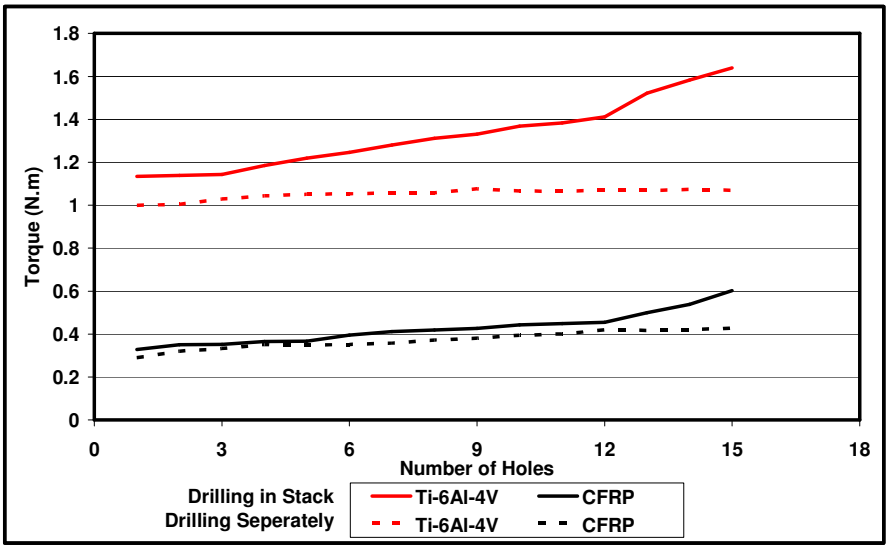

Figure 8-6: Effect of Number of Holes on Torque

8.3 Analysis of Delamination

8.3.1 Effects of Process Parameters on Delamination

Table 8-3 illustrates the influences of process parameters on delamination in laminated composite workpiece in drilling of CFRP/Ti-6Al-4V. As can be found in the table, experimentally obtained and simulation based drilling induced delamination at hole entrance and exit sides are given with regard to the drilling condition and related deviations between the experimental and FE analysis of drilling of CFRP work piece.

According to the results, it was found that delamination at both sides increased with the increase in feed rate and decreased with the growth in spindle speed. In experiments and FE analysis, it was observed that delamination at entrance was affected by the cutting parameters used for CFRP. However, delamination at exit side was found to be influenced by the machining parameters used for titanium alloy. This could be attributed to the drilling strategy in stack. Since titanium alloy was much strong and required

significantly different cutting parameters, the cutting parameters were set to the ones used for titanium alloy. This was mainly due to the conical geometry of the drill tip and to avoid a sudden breakage at the entrance of titanium workpiece. Although thrust force found to increase in drilling of CFRP in stack with titanium alloy; the extent of delamination at both sides has decreased noticeably due to the increased impact resistance by stiffer titanium alloy workpiece under CFRP.

Table 8-3: Alternative Delamination Factor in CFRP in Drilling of CFRP/Ti-6Al-4V Stack

Ti-6Al-4V		CFRP		Delamination Factor (Entrance)			Delamination Factor Exit		
S (rpm)	f (mm/min)	S (rpm)	f (mm/min)	Exp. (μm)	FEA (μm)	Deviation (%)	Exp. (μm)	FEA (μm)	Deviation (%)
1400	95	4500	355	1.035±0.002	1.055	1.93	1.07±0.004	1.085	1.40
1400	119	4500	355	1.035±0.002	1.055	1.93	1.09±0.005	1.1	0.92
1400	95	4500	457	1.05±0.003	1.06	0.95	1.07±0.004	1.085	1.40
1400	119	4500	457	1.05±0.003	1.06	0.95	1.09±0.005	1.1	0.92
1400	95	6000	355	1.03±0.002	1.045	1.46	1.07±0.005	1.085	1.40
1400	119	6000	355	1.03±0.002	1.045	1.46	1.09±0.005	1.1	0.92
1400	95	6000	457	1.04±0.003	1.053	1.25	1.07±0.004	1.085	1.40
1400	119	6000	457	1.04±0.003	1.053	1.25	1.09±0.005	1.1	0.92
1800	95	4500	355	1.035±0.002	1.055	1.93	1.055±0.003	1.08	2.37
1800	119	4500	355	1.035±0.002	1.055	1.93	1.07±0.004	1.09	1.87
1800	95	4500	457	1.05±0.003	1.06	0.95	1.055±0.003	1.08	2.37
1800	119	4500	457	1.05±0.003	1.06	0.95	1.07±0.004	1.09	1.87
1800	95	6000	355	1.03±0.003	1.045	1.46	1.055±0.003	1.08	2.37
1800	119	6000	355	1.03±0.003	1.045	1.46	1.07±0.004	1.09	1.87
1800	95	6000	457	1.04±0.003	1.053	1.25	1.055±0.003	1.08	2.37
1800	119	6000	457	1.04±0.003	1.053	1.25	1.07±0.004	1.09	1.87

As can be found in the table, FE analysis with the use of fully 3D elements in drilling of CFRP/Ti-6Al-4V has predicted drilling induced delamination factor quite satisfactory. The deviations between the predicted and experimentally obtained drilling induced delamination factor lay between 0.92% and 2.37% according to the set of process parameters. It is thought that this could be improved by addition of modelling of tool wear to the current FE model.

8.3.2 Effect of Tool Geometry on Delamination

Figure 8-7 shows FE estimations of entrance and exit delamination plots in drilling of CFRP with Ti-6Al-4V by step drills at 457 mm/min feed rate and 4500 rpm spindle speed for CFRP, 119 mm/min feed rate and 1400 rpm spindle speed for Ti-6Al-4V. As shown in Figure 8-7, white areas symbolize the drilled area due to fracture whereas red coloured area show delaminated zone at the interface of two adjacent plies which can cause to strength degradation of the structure. FE simulations show that the damaged area which is the combination of white and red colour zones reduced with regard to the increase in the stage ratio of step drill. This was mainly due to the fact that the smaller contact between drill bit and workpiece, and the chisel edge effect. Due to the smaller cutting edge reduced contact take place between drill bit and workpiece to drill. This required less thrust force and cutting energy. Due to the lack of chisel edge, penetration action is avoided thus cutting force is minimized. Greater stage ratio of the step drill requires less energy and force. Induced thrust force and torque estimations in drilling of CFRP in stack with Ti-6Al-4V shown in Figure 8-2 and Figure 8-5 can be indicators of this.

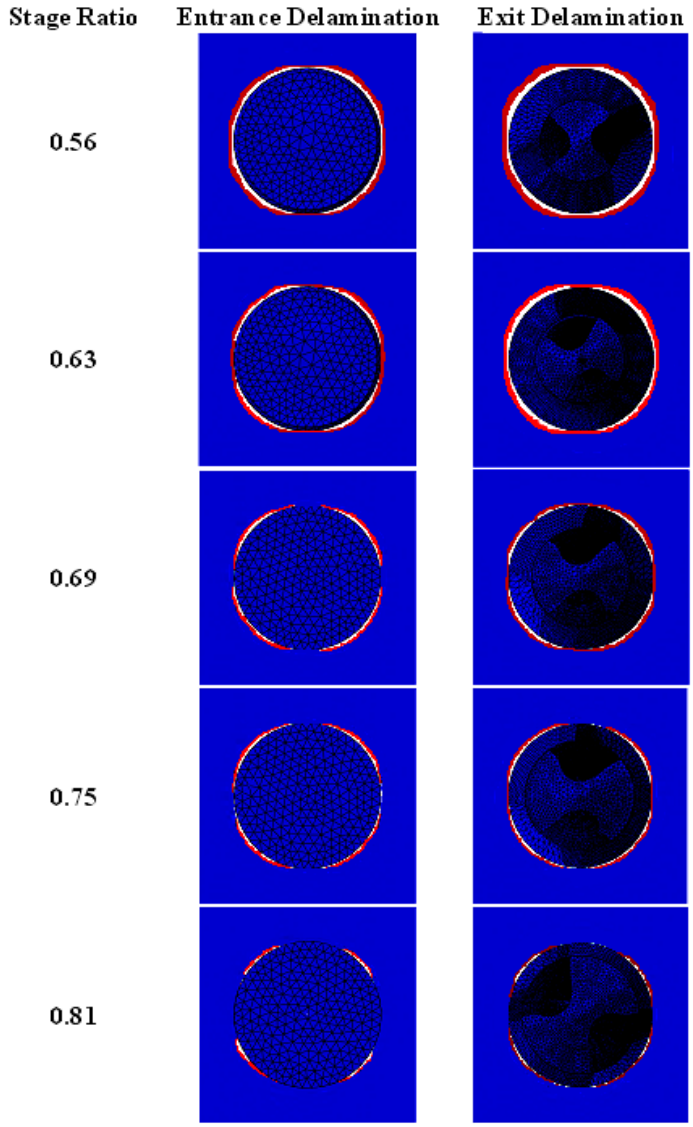

Figure 8-7: Effect of tool geometry on delamination patterns in CFRP in Drilling of CFRP/Ti-6Al-4V stack

Figure 8-8 shows FE predictions of delamination factors versus stage ratio after drilling of CFRP without back-up and in stack with Ti-6Al-4V by step drill at 457 mm/min feed rate and 4500 rpm spindle speed for CFRP, 119 mm/min feed rate and 1400 rpm spindle speed for Ti-6Al-4V. As could be seen from the comparison of Figure 8-8 (a) and Figure 8-8 (b), delamination factors has reduced significantly in drilling of CFRP in stack with Ti-6Al-4V. The main reason of that was the existence of Ti-6Al-4V as a support plate under CFRP workpiece. This would improve the impact resistance of CFRP particularly against bending in a loading in the normal direction, thus better workpiece

quality has been estimated after drilling. In addition to that, exit delamination factor has been simulated greater than the entrance delamination factor in drilling of CFRP in stack with Ti-6Al-4V similar to drilling of CFRP alone. Due to the number of plies for support, last plies at the exit side were more susceptible against thrust force and related bending. As shown in Figure 8-8 (b), induced delamination factor has been reduced with the increase in stage ratio of step drill in both sides of the holes. The use of step drill has provided significant advantage to reduce delamination factors in drilling of CFRP/Ti-6Al-4V stack. Increased stage diameter of step drill would have smaller contact with the workpiece, hence less thrust force and cutting energy is required. This would minimize drilling induced workpiece defects.

Drilling induced delamination predicted substantially lower owing to initial step part and disappearance of the chisel edge of the drill bit. The minimized delamination would mean higher structural integrity and possibly longer service life. The use of step drill could avoid the possible rejections owing to tight tolerances, so it could boost the improvements in manufacturing costs.

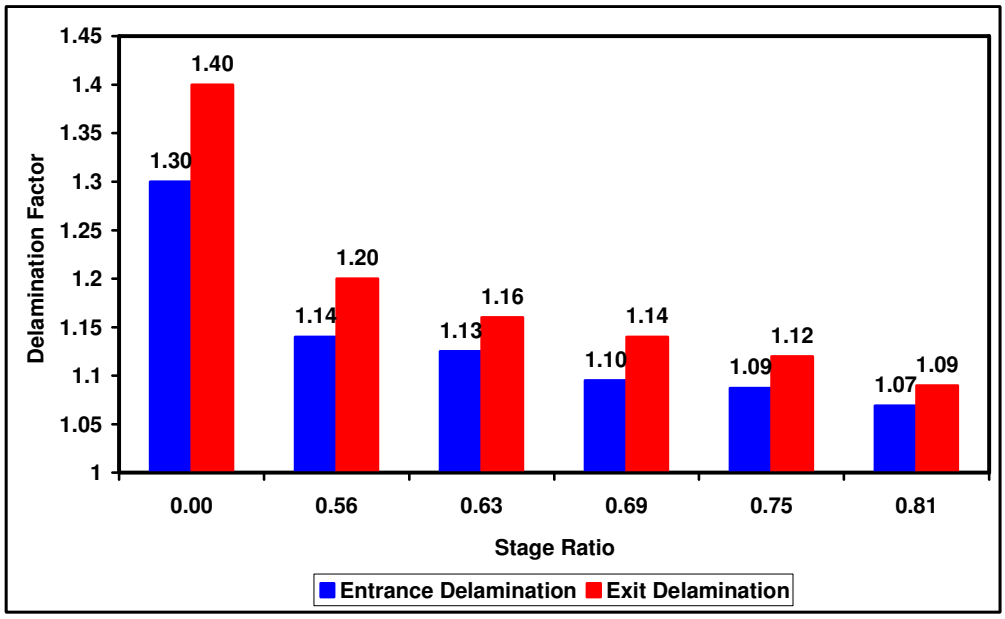

(a)

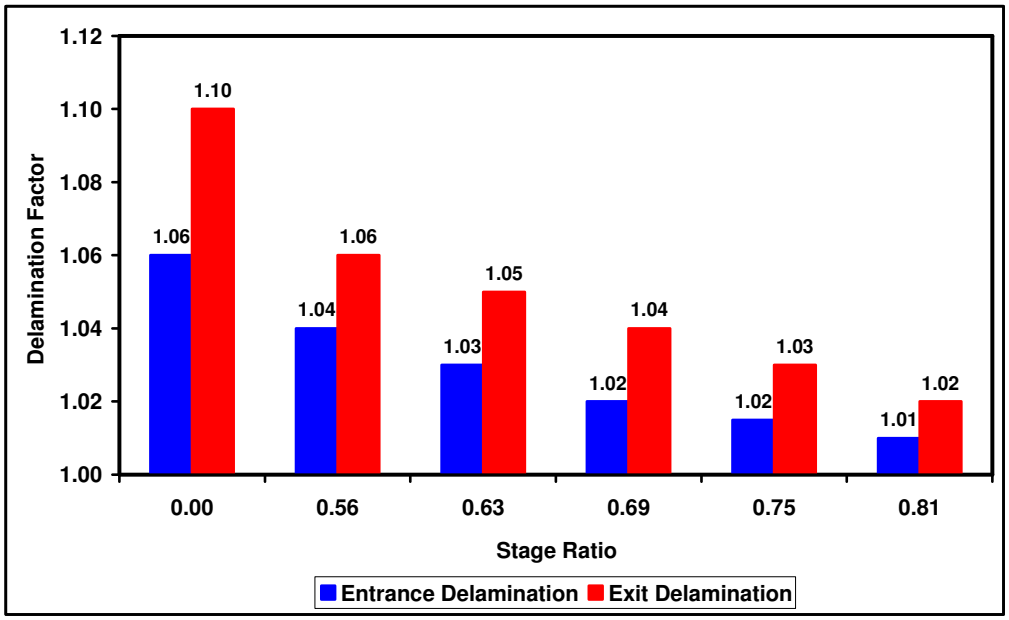

(b)

Figure 8-8: Effect of Drill Geometry on Delamination (a) Drilling of CFRP (b) Drilling of CFRP/Ti-6Al-4V Stack

8.3.3 Effect of Tool Wear on Delamination

Figure 8-9 present delamination patterns observed at the entrance of drilled holes after drilling of CFRP and CFRP in stack with Ti-6Al-4V. As can be observed from the images, delamination at the entrance has been reduced significantly in drilling of CFRP with Ti-6Al-4V comparing to drilling CFRP alone. Figure 8-9 (c) and Figure 8-9 (d) show the state of the entry of the first and last hole after drilling of CFRP with Ti-6Al-4V. Even after drilling 15 holes, very good hole quality has been obtained at the entrance side of the CFRP workpieces in stacked form. Ti-6Al-4V workpiece under the CFRP sample has supported the composite under the multi-axis loading condition and would increase the stiffness of the laminated composite. Reinforced composites are strong in fibre direction however they are very weak in the normal direction. Stiffer support under composite sample, Ti-6Al-4V workpiece, could improve bending behaviour of the composite under loading in normal direction. Even with the increased wear and thrust force, delamination has been reduced at the entrance of the holes in drilling of CFRP with Ti-6Al-4V.

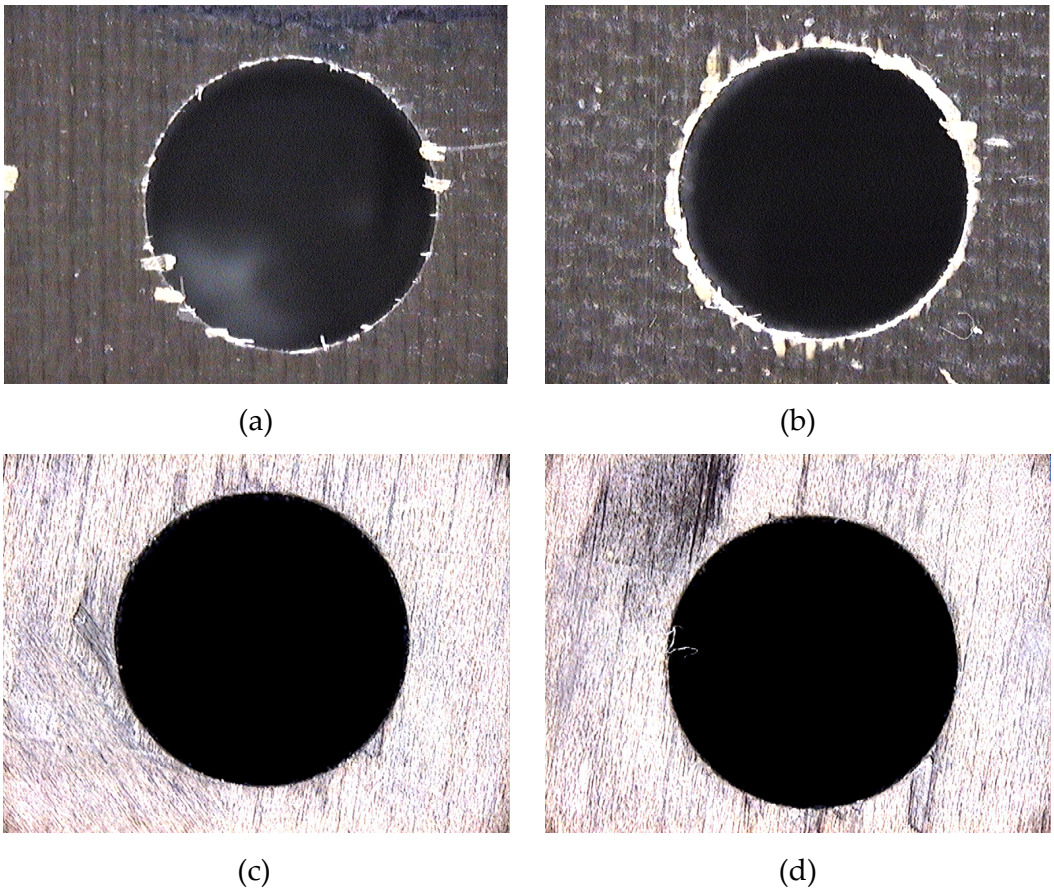

(a) (b)

(c) (d)

Figure 8-9: Delamination at Hole Entry (a) Drilling of CFRP-1st Hole (b) Drilling of CFRP-56th Hole (c) Drilling of CFRP/Ti-6Al-4V Stack-1st Hole (d) Drilling of CFRP/Ti-6Al-4V Stack-15th Hole

Figure 8-10 shows the state of the holes at the exit side after drilling in CFRP alone and in stack with Ti-6Al-4V. As can be clearly noticed from the plots, delamination at the exit side has been improved significantly. Figure 8-10 (a) and Figure 8-10 (b) shows fibre pull outs in the first and last hole in drilling of CFRP alone. In drilling of CFRP without a support, buckled fibres could be observed significantly due to last plies which cannot withstand thrust force. The hole surface quality at the exit side has been improved substantially in drilling of CFRP in stack with Ti-6Al-4V.

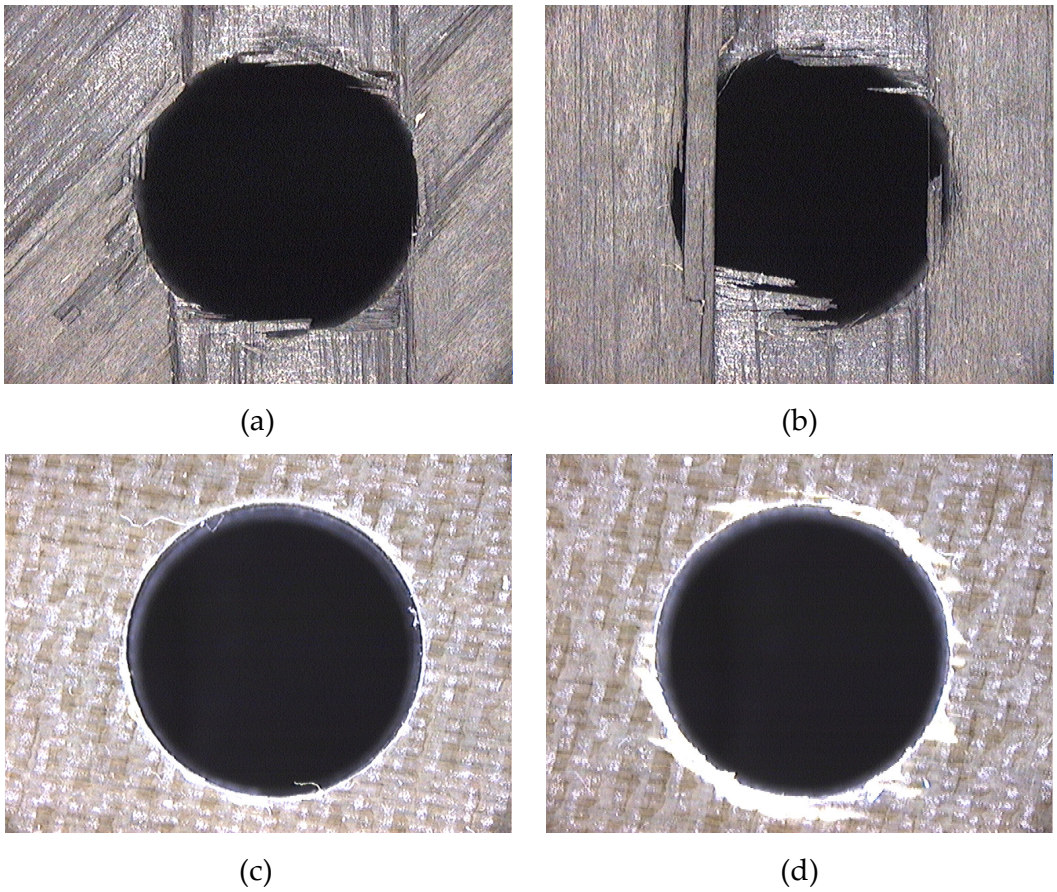

Figure 8-10: Delamination at Hole Exit (a) Drilling of CFRP-1st Hole (b) Drilling of CFRP-56th Hole (c) Drilling of CFRP-Ti-6Al-4V Stack-1st Hole (d) Drilling of CFRP/Ti-6Al-4V Stack-15th Hole

Figure 8-11 indicates the influence of the number of drilled holes on delamination factors in CFRP workpiece in drilling of CFRP/Ti-6Al-4V at 4500 rpm spindle speed and 457 mm/min feed rate for CFRP, 1400 rpm spindle speed and 119 mm/min feed rate for titanium alloy. As can be observed from Fig. 8.11 both delamination factors rose gradually with the number of holes drilled due to the wear of cutting tool and increased thrust force. After drilling 15 holes in stacked materials, entrance and exit delamination factors have increased by 4.76% and 6.76%, respectively. Although the delamination factors have been reduced significantly in drilling of CFRP/Ti-6Al-4V, dependency of delamination factor to tool wear has seemed to be increased when it was compared to the drilling of CFRP separately. This could be attributed to the increased tool wear rate due to the combination of different cutting and wear mechanisms in machining of stacked materials.

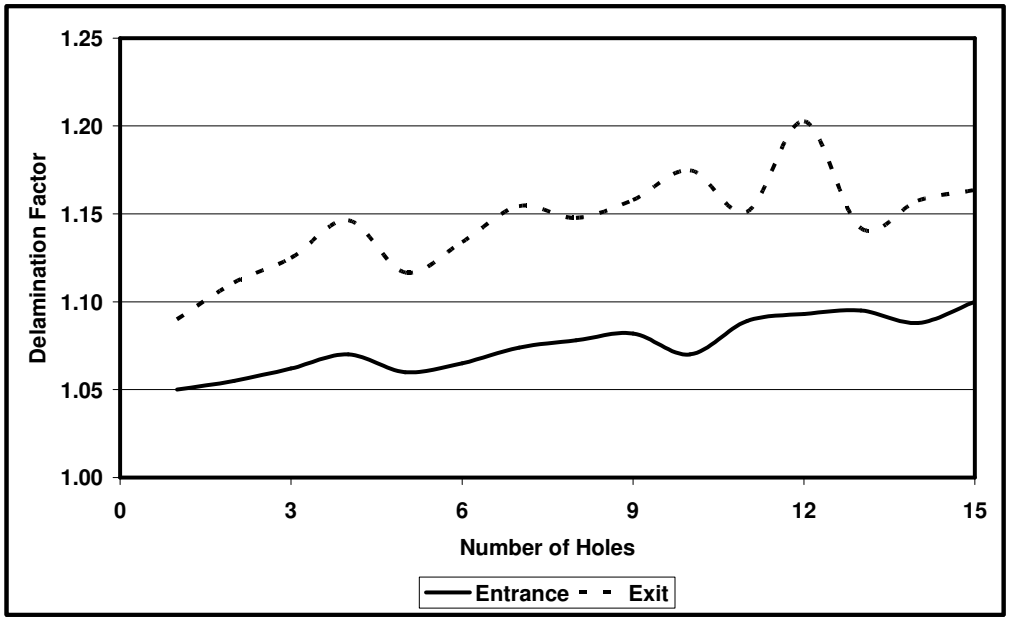

Figure 8-11: Effect of Number of Holes on Delamination Factors in Drilling of CFRP/Ti-6Al-4V Stack

8.4 Analysis of Burr Formation

Analysis of drilling induced burr formation in drilling of Ti-6Al-4V has been discussed in Chapter 7 in detail. Since the materials are rather distinct from each other, different machining parameters are required. Drilling of CFRP/Ti-6Al-4V is not as straightforward as drilling of each material separately. Different cutting mechanisms and wear types induced in machining of these materials could influence machining of each other. Burr formation could be also affected, thus analysis of drilling induced burr formation in drilling of CFRP/Ti-6Al-4V has been carried out carefully.

8.4.1 Effects of Process Parameters on Burr Formation

Table 8-4 shows the effects of process parameters on burr height in titanium alloy workpieces in drilling of CFRP/Ti-6Al-4V stack. Experimentally obtained and finite element based drilling induced burr height at entrance and exit sides of holes are given in regard with the machining conditions and related deviations. Burr height at both sides was found to increase with increasing feed rate whereas decreased with increased cutting speed in drilling of Ti-6Al-4V. The tendency was observed similar to the drilling of Ti-6Al-4V

separately as discussed in Chapter 7. However, it must be noted that the machining parameters in CFRP zone was found to affect burr height of Ti-6Al-4V workpiece. As can be observed in Table 8-4, higher burr height was measured in experimental tests carried out at the same cutting parameters in Ti-6Al-4V, but higher feed rate and cutting speed in CFRP workpiece. It is that fact that cutting tool has worn in drilling of the entrance part of stack, CFRP workpiece. The tool wear is dependant on cutting parameters and it showed higher wear at higher cutting speed and feed rate, thus higher burr height has been induced in drilling of the bottom part of stack, Ti-6Al-4V. In addition to that, higher burr height was found at both sides in drilling of stacked form comparing to drilling of titanium alloy separately. Furthermore, increased thrust force and dusty abrasive fibre chips could also affect the extent of burr height.

However simulated trends of the burr height versus process parameters agreed with the experimental results; the deviations of predicted drilling induced burr height lay between 38.09% and 56.99 with underestimation according to the set of process machining condition in drilling of CFRP/Ti-6Al-4V. It is thought that this could be significantly improved by addition of modelling of tool wear and chip formation to the current FE model.

Table 8-4: Burr Height in Ti-6Al-4V in Drilling of CFRP/Ti-6Al-4V Stack

Ti-6Al-4V		CFRP		Burr Height at Entrance			Burr Height at Exit		
S (rpm)	f (mm/min)	S (rpm)	f (mm/min)	Exp. (μm)	FEA (μm)	Deviation (%)	Exp. (μm)	FEA (μm)	Deviation (%)
1400	95	4500	355	35.10±1.2	17.90	-49.00	54.30±1.6	33.50	-38.31
1400	119	4500	355	36.20±1.2	19.80	-45.30	56.15±1.6	34.90	-37.85
1400	95	4500	457	37.15±1.3	17.90	-51.82	57.20±1.6	33.50	-41.43
1400	119	4500	457	38.90±1.3	19.80	-49.10	60.30±1.8	34.90	-42.12
1400	95	6000	355	38.10±1.3	17.90	-53.02	57.20±1.6	33.50	-41.43
1400	119	6000	355	39.60±1.4	19.80	-50.00	60.20±1.6	34.90	-42.03
1400	95	6000	457	40.55±1.4	17.90	-55.86	61.05±1.7	33.50	-45.13
1400	119	6000	457	42.15±1.4	19.80	-53.02	63.35±1.7	34.90	-44.91
1800	95	4500	355	31.90±1.1	16.00	-49.84	52.20±1.6	30.40	-41.76
1800	119	4500	355	33.05±1.2	17.40	-47.35	53.30±1.6	33.00	-38.09
1800	95	4500	457	34.05±1.2	16.00	-53.01	55.15±1.5	30.40	-44.88
1800	119	4500	457	35.65±1.3	17.40	-51.19	57.25±1.6	33.00	-42.36
1800	95	6000	355	35.15±1.2	16.00	-54.48	53.85±1.5	30.40	-43.55
1800	119	6000	355	36.65±1.3	17.40	-52.52	56.20±1.6	33.00	-41.28
1800	95	6000	457	37.20±1.4	16.00	-56.99	57.30±1.7	30.40	-46.95
1800	119	6000	457	39.10±1.4	17.40	-55.50	58.70±1.6	33.00	-43.78

Table 8-5 shows the influences of cutting parameters on burr width in Ti-6Al-4V workpiece in drilling of CFRP/Ti-6Al-4V stack based on experimental and FE results. Burr width at entrance and exit sides increased slightly with the increasing feed rate, but reductions in burr width has been measured as spindle speed increased in drilling of Ti-6Al-4V in stack with CFRP. A similar trend between machining parameters and burr width was found in drilling of Ti-6Al-

4V with CFRP comparing to drilling of Ti-6Al-4V separately. Nevertheless, it was also observed that machining of CFRP has influenced on drilling of Ti-6Al-4V as both materials machined together. Similar to the observations made in burr height above, burr width was found greater in experiments where CFRP workpiece was machined at higher feed rate and spindle speed. This could be attributed to tool wear induced in drilling of CFRP. As wear rate accelerates at higher feed rates and cutting speeds, cutting forces could also increases. This has been shown in analysis of thrust force earlier. Increased thrust force and degenerated geometry would cause to an increase in the extent of defects in the workpiece. Thus, higher burr width has been found on both sides of drilled holes in titanium alloy. Moreover it should be also mentioned that very tiny abrasive fibre chips could go between workpiece and cutting tool, which could end up degenerated workpiece hole quality.

Although predicting smaller amount of burr width, trends of the burr height versus process parameters were agreed with the experimental results in FE simulations. The deviations between predicted and experimentally obtained burr width altered between 42.63% and 56.90 with underestimation with regard to machining parameters in drilling of CFRP/Ti-6Al-4V. Addition of tool wear and chip formation would improve the predictions of the model significantly.

Table 8-5: Burr Width in Ti-6Al-4V in Drilling of CFRP/Ti-6Al-4V Stack

Ti-6Al-4V		CFRP		Burr Width at Entrance			Burr Width at Exit		
S (rpm)	f (mm/min)	S (rpm)	f (mm/min)	Exp. (μm)	FEA (μm)	Deviation (%)	Exp. (μm)	FEA (μm)	Deviation (%)
1400	95	4500	355	48.20±1.5	24.80	-48.55	59.50±1.6	31.60	-46.89
1400	119	4500	355	50.25±1.6	26.80	-46.67	61.85±2.2	32.90	-46.81
1400	95	4500	457	50.40±1.5	24.80	-50.79	62.50±2.3	31.60	-49.44
1400	119	4500	457	52.80±1.6	26.80	-49.24	64.60±2.0	32.90	-49.07
1400	95	6000	355	50.50±1.4	24.80	-50.89	62.40±2.1	31.60	-49.36
1400	119	6000	355	53.15±1.6	26.80	-49.58	64.40±2.2	32.90	-48.91
1400	95	6000	457	54.10±1.5	24.80	-54.16	64.80±2.2	31.60	-51.23
1400	119	6000	457	56.20±1.6	26.80	-52.31	66.70±2.1	32.90	-50.67
1800	95	4500	355	44.70±1.4	22.50	-49.66	57.40±1.7	29.20	-49.13
1800	119	4500	355	47.70±1.4	24.00	-49.69	59.50±1.8	31.00	-47.90
1800	95	4500	457	49.20±1.6	22.50	-54.27	50.90±1.7	29.20	-42.63
1800	119	4500	457	50.40±1.5	24.00	-52.38	62.40±1.9	31.00	-50.32
1800	95	6000	355	49.80±1.6	22.50	-54.82	59.85±1.8	29.20	-51.21
1800	119	6000	355	51.40±1.7	24.00	-53.31	61.60±1.7	31.00	-49.68
1800	95	6000	457	52.20±1.5	22.50	-56.90	63.10±187	29.20	-53.72
1800	119	6000	457	54.15±1.6	24.00	-55.68	64.80±1.8	31.00	-52.16

In summary, the height and width of burr formation was observed and estimated to increase with regards to the increase in feed rate and decrease in the spindle speed in drilling of Ti-6Al-4V with CFRP. Higher burr formation was observed at hole exit by means of height and width. It was also observed that burr formation affected by the machining parameters of CFRP due to its effect on tool wear. The amount of burr in titanium alloy has been increased

with increased cutting speed and feed rate in drilling of CFRP part in stacked form. In overall, trends predicted by the FE models were in agreement with the experimental values for the burr formation. However, the magnitudes of the estimations were noticeably underestimated. In order to achieve accurate results for prediction of burr formation in drilling of Ti-6Al-4V in stack with CFRP using finite element analysis, utilisation of tool wear and chip formation to the current model are suggested. Limitation in the computing resources and computing time had restricted the FE model in terms of the chip formation and mesh refinement.

8.4.2 Effects of Tool Geometry on Burr Formation

Figure 8-12 (a) and Figure 8-12 (b) show predicted burr heights in drilling of Ti-6Al-4V alone and in CFRP/Ti-6Al-4V stack with respect to the stage ratio. Drilling simulations has performed at 1400 rpm spindle speed and 119 mm/min feed rate in titanium alloy; 4500 rpm spindle speed and 457 mm/min feed rate in CFRP workpiece. As shown in Fig. 8.12 (b), the use of step drill has estimated significant advantage to minimize burr formation in drilling of CFRP/Ti-6Al-4V. An increase in the stage diameter of step drill provided a considerable decrease in burr height at both sides of the holes in titanium alloy workpiece. Burr height at the exit was estimated significantly greater than the entrance in drilling of Ti-6Al-4V workpiece in stack with CFRP as it was simulated in drilling of titanium alloy alone shown in Figure 8-12 (a). When 8 mm twist drill used in drilling simulations of Ti-6Al-4V with CFRP, burr heights were predicted as 19.80 μm and 34.90 μm at hole entry and exit, respectively. By the use of step drill with 0.81 stage ratio, the burr height decreased by approximately two thirds to 6.05 μm and 12.15 μm at hole entry and exit, respectively. When drilling of titanium alloy with CFRP is compared to titanium alloy alone, it can be seen that burr height is slightly affected. As it can be observed in Figure 8-12 (a) and Figure 8-12 (b), the burr height has increased at entrance and exit sides of the drilled holes. The increase in the thrust force has cause to an increase in burr height between 2.00% and 3.41% at hole entrance, between 0.29% and 2.73% at hole exit with regard to stage ration in drilling of Ti-6Al-4V in stack with CFRP. Figure 8-12 (a) and (b) clearly show that the use of step drill would minimize

the burr height in drillings of Ti-6Al-4V alone and CFRP/Ti-6Al-4V stack, respectively.

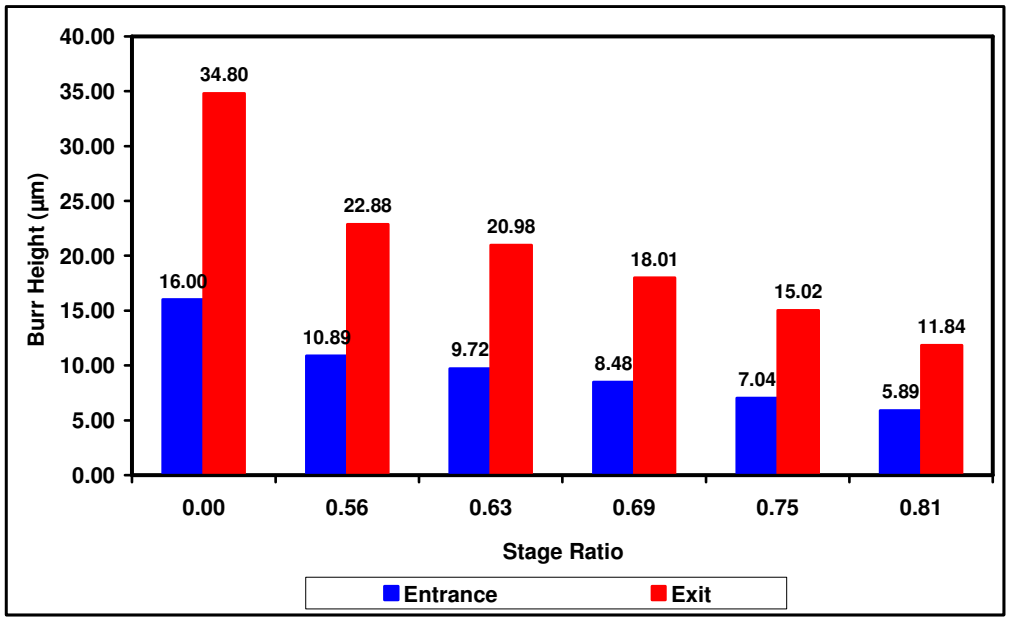

(a)

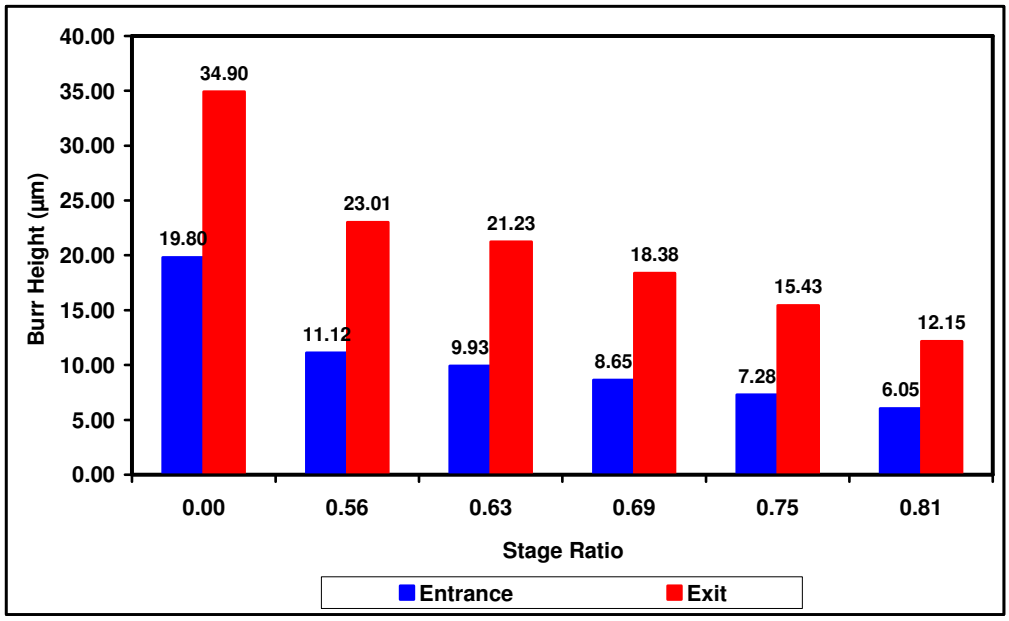

(b)

Figure 8-12: Effect of Drill Geometry on Burr Height (a) Drilling of Ti-6Al-4V (b) Drilling of CFRP/Ti-6Al-4V Stack

Figure 8-13 (a) and Figure 8-13 (b) show estimated burr width induced in drilling of Ti-6Al-4V alone and in CFRP/Ti-6Al-4V stack with regard to stage

ratio of step drill. As shown in Figure 8-13 (b), the use of step drill has brought significant advantage to reduce burr width in drilling of CFRP/Ti-6Al-4V stack. Increased stage diameter of step drill has enabled to have reduced burr height at both sides of the holes in titanium alloy workpiece comparing to drilling with twist drill. The smaller contact between the drill bit and workpiece is required less thrust force, thus smaller amount of workpiece defect is formed. Burr width at the exit side was simulated considerably greater than the entrance side in drilling of Ti-6Al-4V with CFRP which has predicted in similar trend in drilling of titanium alloy alone as shown in Figure 8-13 (a). Burr width were measured to be 26.80 μm and 32.90 μm with 8 mm twist drill in FE analysis of drilling of Ti-6Al-4V in stack with CFRP at hole entry and exit, respectively. This workpiece defect has been reduced by approximately two thirds to 8.48 μm at the entrance and 9.94 μm at the exit with the use of 8 mm diameter step drill with 6.5 mm diameter stage diameter. The burr width at entrance and exit sides were slightly greater in drilling of Ti-6Al-4V in stack with CFRP than drilling of Ti-6Al-4V alone as shown in Figure 8-13 (a) and Figure 8-13 (b). The defect has increased due to the increase in thrust force in drilling of CFRP/Ti-6Al-4V.

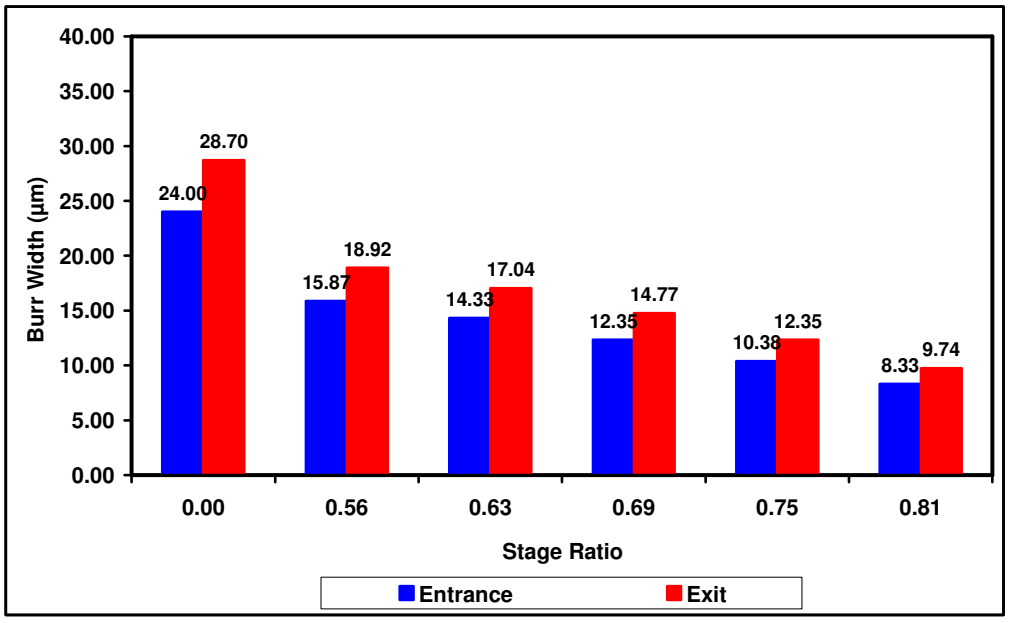

(a)

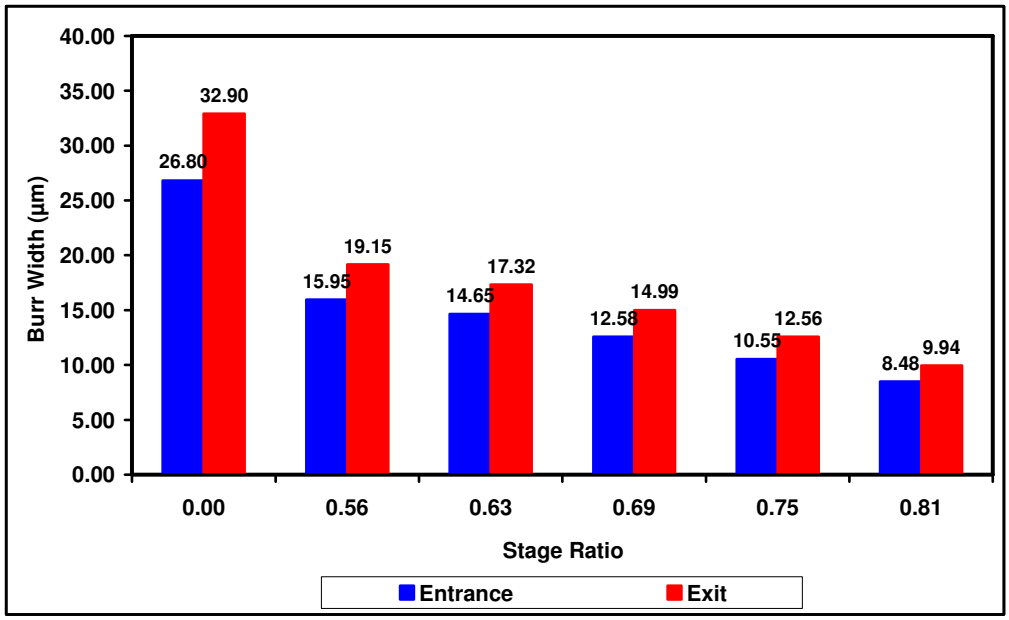

(b)

Figure 8-13: Effect of Drill Geometry on Burr Width (a) Drilling of Ti-6Al-4V (b) Drilling of CFRP/Ti-6Al-4V Stack

Figure 8-12 and Figure 8-13 indicate the advantages of step drill over twist drill in drilling of Ti-6Al-4V in stack with CFRP. The reduction in the contact between drill bit and workpiece has been simulated to provide substantial reduction in the burr formation in the finite element analysis of drilling of Ti-6Al-4V with CFRP. Although the burr could form greater particularly at the exit side of hole in drilling of stack than drilling of titanium alloy itself, the extent of workpiece defects could be minimized with the proper selection of geometry and possibly parameters. The reduced burr formation would mean that higher structural integrity and possibly longer service life. The use of step drill could assist to avoid rejections due to excessive burr, so it could improve machining of structural parts and decrease the manufacturing costs.

8.4.3 Effects of Tool Wear on Burr Formation

Figure 8-14 (a) and Figure 8-14 (b) report the effect of the tool wear on burr height versus the number of holes drilled in Ti-6Al-4V workpieces alone and in stack with CFRP, respectively. Experiments were carried out at 1400 rpm spindle speed and 119 mm/min feed rate in titanium alloy; 4500 rpm spindle speed and 457 mm/min feed rate in CFRP workpiece. Burr height increases with

the number of drilled holes. This is mainly due to the increased wear and consequently higher thrust force in drilling of the workpiece. In terms of the hole quality in titanium alloy workpiece, there is a significant rise in the extent of burr height with the number of holes drilled in both surfaces. The trends of burr height has been found similar in drilling of titanium alone and in stack form, however the burr height has been measured much larger in titanium workpiece drilled in the stack form compared to alone. The burr height measured for stack has reached almost twice the values obtained for titanium on its own. This could be justified by the high tool wear rate and increased wear in stack drilling.

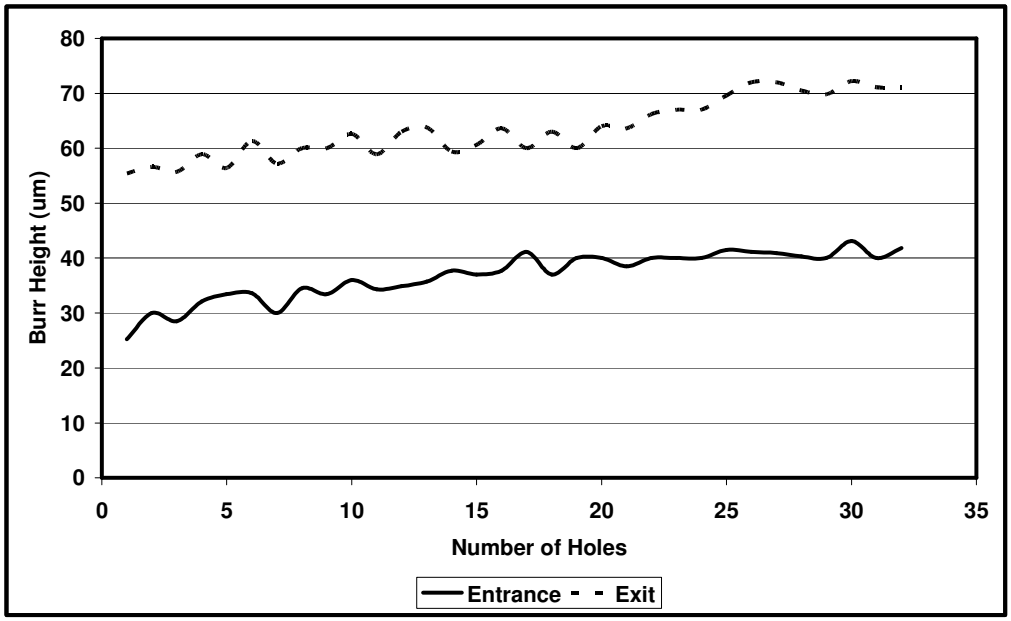

(a)

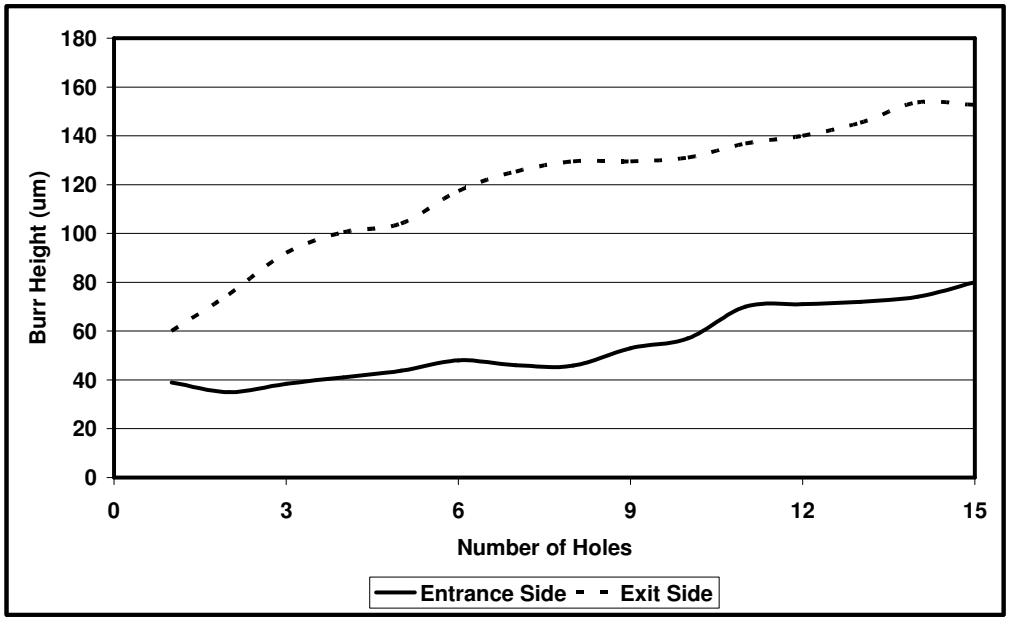

(b)

Figure 8-14: Effect of Number of Holes on Burr Height (a) Drilling of Ti-6Al-4V (b) Drilling of CFRP/Ti-6Al-4V Stack

Figure 8-15 (a) and Figure 8-15 (b) show the influence of the number of drilled holes on burr width in Ti-6Al-4V alone and stack with CFRP, respectively. Burr width has increased with the number of holes drilled. An increase in the tool wear has led to an increase in thrust force and consequently resulted in grater workpiece defect around the drilled holes. Increased burr width with the number of holes drilled could be observed at the both sides. In addition to observed similar trends between burr width and tool wear in drilling of titanium alone and in stack form, the growth of burr width has been found more rapidly in titanium workpiece drilled in the stack form compared to alone. The measured burr width has been found approximately doubled in drilling of titanium in stack form than drilled alone. This can be due to increased cutting tool wear rate and higher tool wear in stack drilling.

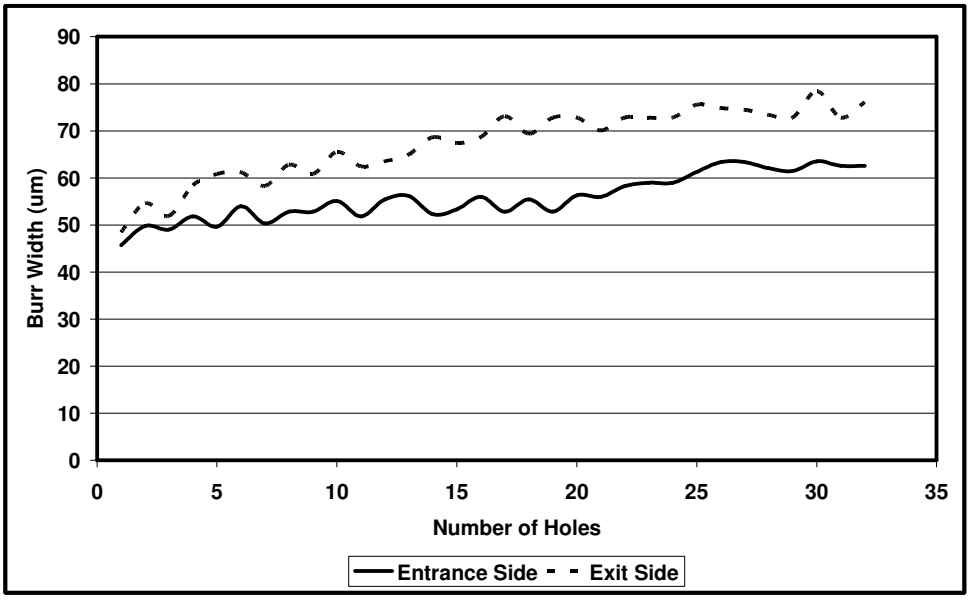

(a)

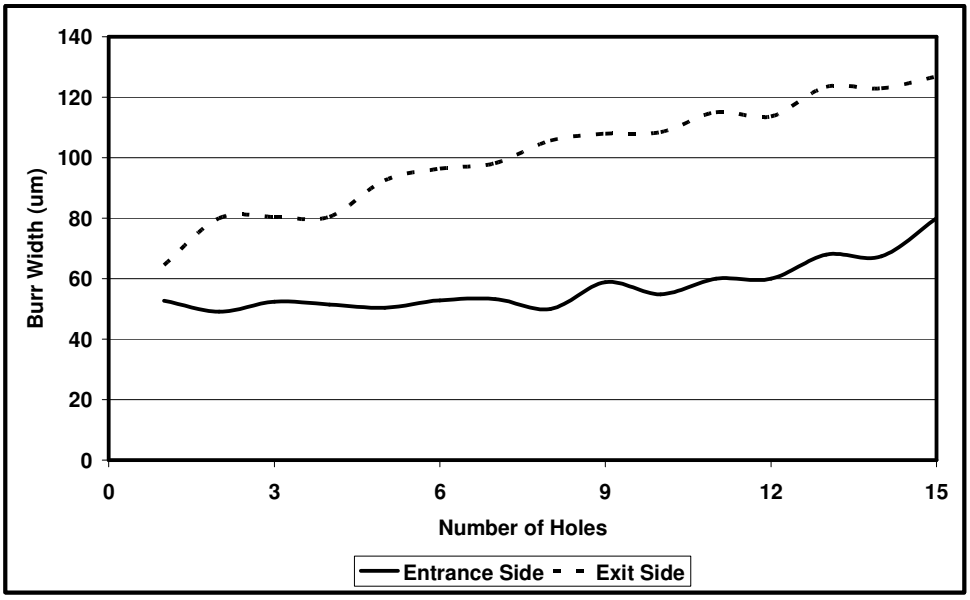

(b)

Figure 8-15: Effect of Number of Holes on Burr Width (a) Drilling of Ti-6Al-4V (b) Drilling of Ti-6Al-4V in Stack

8.5 Analysis of Surface Roughness

Since machining of aerospace materials is difficult and a challenge, quality of machined surfaces is significantly important to provide acceptable products and long service life. In order to maintain quality of the machined workpieces,

it is important to investigate surface roughness of machined surfaces with regard to cutting parameters and number of drilled holes, with other words tool wear. Owing to having distinct physical and mechanical properties in CFRP and Ti-6Al-4V, different machining characteristics are presented in drilling of them. Based on this fact drilling of these materials are required distinct machining conditions. Thus drilling of these materials and related analysis have been carried out separately as explained in Chapter 6 and 7. In the following lines, analysis of surface roughness is carried out in drilling of CFRP/Ti6Al4V stack with the comparison of drilling of both materials separately.

8.5.1 Effects of Process Parameters on Surface Roughness

Table 8-6 shows the effects of process parameters on average surface roughness (Ra) of drilled holes in CFRP and titanium alloy workpieces in drilling of CFRP/Ti-6Al-4V stack. First of all it should be noted that in drilling of CFRP/Ti-6Al-4V stack, the analysis of surface roughness would not as straightforward as in drilling of each material separately due to the fact that machining of each section could affect each other.

As it could be noticed in Table 8-6 average surface roughness increased with the increasing feed rate whereas decreased with the increasing spindle speed in both materials drilled together. This was similar to the findings in drilling of each material separately as explained in Chapter 6 and 7. It was also observed that the average surface roughness has slightly affected from machining parameters used in each sections. The main reason of this was higher induced forces in drilling of stacked material. Greater thrust force could increase vibration and tool wear; consequently these would lead to increased surface roughness in machined holes. In addition to that, when cutting tool started to drill titanium alloy part, the cutting parameters were shifted from the ones set for CFRP to titanium alloy. At this transition region, both materials were machined together with the process parameters set for Ti-6Al-4V. This could also affect surface roughness of CFRP workpieces as the machining parameters were significantly different for titanium alloy. Dusty and abrasive chips generated in drilling of CFRP could high likely to influence the surface

roughness of titanium alloy. The combination of tool wear and existence of dust chips could be attributed to the increase in the surface roughness of titanium alloy workpieces. When the average surface roughness of each material compared with ones drilled separately, noticeably higher values were obtained in drilling of stack. This could show the complexity of drilling of CFRP/Ti-6Al-4V stack.

Table 8-6: Average Surface Roughness in Drilling of CFRP/Ti-6Al-4V Stack

Ti-6Al-4V		CFRP		Surface Roughness Ti-6Al-4V (μm)	Surface Roughness CFRP (μm)
S (rpm)	F (mm/min)	S (rpm)	F (mm/min)		
1400	95	4500	355	3.67±0.14	2.83±0.12
1400	119	4500	355	4.01±0.15	2.95±0.13
1400	95	4500	457	3.78±0.16	3.35±0.12
1400	119	4500	457	4.07±0.15	3.41±0.15
1400	95	6000	355	3.78±0.14	2.48±0.11
1400	119	6000	355	4.15±0.15	2.65±0.13
1400	95	6000	457	3.92±0.16	3.14±0.14
1400	119	6000	457	4.33±0.14	3.22±0.13
1800	95	4500	355	3.53±0.15	2.72±0.12
1800	119	4500	355	3.89±0.16	2.81±0.14
1800	95	4500	457	3.66±0.15	3.22±0.13
1800	119	4500	457	3.88±0.15	3.33±0.14
1800	95	6000	355	3.61±0.14	2.38±0.12
1800	119	6000	355	4.02±0.17	2.52±0.14
1800	95	6000	457	3.81±0.18	3.01±0.12
1800	119	6000	457	4.13±0.16	3.13±0.16

8.5.2 Effect of Tool Wear on Surface Roughness

Figure 8-16 shows the influence of the number of holes drilled on average surface roughness (Ra) in drilling of CFRP and Ti-6Al-4V separately and together at 4500 rpm spindle speed and 457 mm/min feed rate for CFRP, 1400 rpm spindle speed and 119 mm/min feed rate for Ti-6Al-4V. As shown in Figure 8-16, the average surface roughness increased from 3.3 μm to 3.42 μm after drilling 15 holes and reached to 6.4 μm by drilling 56 holes in drilling CFRP workpiece alone. Although machining at the same cutting parameters, the average surface roughness in CFRP holes measured greater than the ones drilled separately. As it could be noticed, the progression of surface roughness with the number of drilled holes was much steeper due to more aggressive cutting condition. The average surface roughness has increased from 3.41 μm to 7.27 μm with a 113% increase after drilling 15 holes in CFRP in stacked with titanium alloy. Similar findings could be found in drilling of titanium alloy workpiece. As shown in Figure 8-16, the average surface roughness gradually rose from 1.6 μm to 3.33 μm after drilling 15 holes and reached to 6.31μm at the end of tool life by drilling 32 holes in drilling Ti-6Al-4V separately. The analysis of titanium alloy in stack depicts higher amount of surface roughness, particularly at the beginning. The average surface roughness altered between 4 μm and 11.3 μm for the holes drilled in Ti-6Al-4V in stack. The tool wear occurred at the beginning of stack would cause to this noticeably increase. In addition to that the fine abrasive chips could deteriorate the quality of the titanium holes. It is believed that the combination of different cutting mechanism and wear mechanisms caused to poorer surface finish in drilling stacks compared to separate materials.

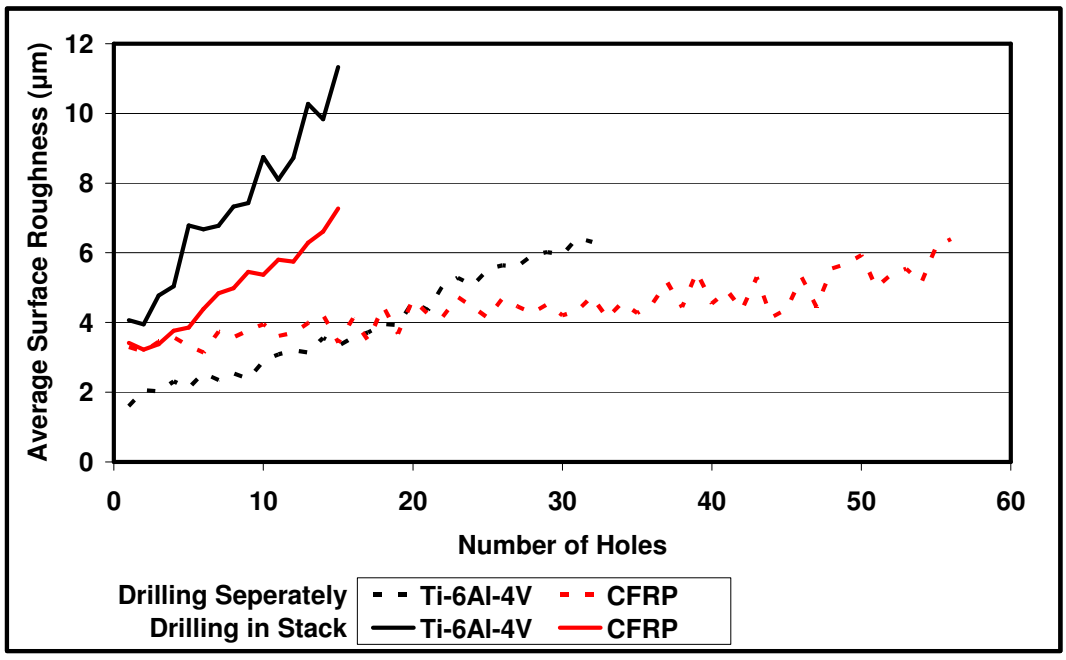

Figure 8-16: Effect of Number of Holes on the Average Surface Roughness

8.6 Analysis of Tool Wear

Since machining of aerospace materials is difficult and a challenge, tool wear is significantly important to provide quality and low cost. In order to maintain quality of the machined workpieces, it is important to replace cutting tools as they reach wear criteria as explained in the methodology section. Variation of thrust forces, torques and surface roughness versus number of holes drilled can be typical indication of tool wear as discussed in previous subsections. CFRP and Ti-6Al-4V have distinct properties, thus shows different machining characteristics. Based on this fact they are required different machining requirement, so that initially drilling of these materials and related analysis have been carried out separately as explained in detail in Chapter 6 and 7.

In drilling of CFRP alone by multilayer TiAlN/TiN coated WC drill, abrasive wear was observed on flank and crater surfaces of the drill bit owing to the very abrasive fibres. These two wear creates edge wear which grinded the cutting edge gradually. Due to wear thrust force, torque, delamination and the average surface roughness increased gradually. There was no sign of plastic deformation and chipping on tool surfaces. Tool life was found 56 holes in

drilling of CFRP alone. Whereas in drilling of Ti-6Al-4V alone, significant amount of flank and crater wear was observed due to high cutting forces. Owing to these wear formations the cutting edges have become dull, hence thrust force, torque, burr formation and the average surface roughness have increased gradually. In addition to these, substantial chipping has been observed at the margin and corners of the cutting edges at the end of tool life. Tool life was found 32 holes in drilling of Ti-6Al-4V alone.

Drilling of two unique materials together makes the process even more complicated. Different wear mechanisms took place together and could have affected each other. Figure 8-17 shows the tool wear in drilling of CFRP/Ti-6Al-4V stack after drilling 15 holes. First of all, a shortened tool life has been found after the tests. The total machined volume was 56300 mm^3 and 32170 mm^3 for drilling of CFRP and Ti respectively. Whereas the machined volume was reduced to 30160 (each workpiece 15080) mm^3 in drilling of CFRP/Ti-6Al-4V in stack form developed after drilling 15 holes. Providing that the same machining parameters have been used for drilling of materials separately or in stacked form, the machinability has considerably reduced. It is believed that the combination of the different wear mechanisms have resulted in poor performance of the drill in the stacked form.

As can be observed in Figure 8-17, more aggressive wear could be induced in drilling of composite/metal stack. This must be due to interaction of the two wear mechanism in the dissimilar materials in the stacked structure. As shown in Figure 8-17 (b), significant amount of wear has been observed in the flank surface of the drills. This abrasion mechanism was due to the hard phases in titanium alloy as explained above. Moreover, obvious crater wear could also be noticed on the cutting tool in Figure 8-17 (c). The combination of these two wear mechanisms accelerated the progression of the wear and shortened the tool life.

In addition to these failure mechanisms, noticeable chipping has been found on the flank surface. The chipping occurs near the region of maximum cutting speed on the cutting edges of the tool. This macro chipping which is clearly shown in Figure 8-17 (b) and Figure 8-17 (e) indicate much more aggressive wear. Abrasive dust particles between the surfaces of cutting tool

and workpiece would cause scratching and locally higher contact stresses. As a result of the degenerated contact surfaces, cutting forces and the wear rates would increase. As shown in Table 8-1, Table 8-2 and Table 8-6, higher amount of thrust force, torque and the average surface roughness were obtained in drilling of stack respectively compared to drilling of Ti and CFRP separately. Similar to drilling of titanium alloy alone, significant wear has also been observed on the chisel edge due to high thrust force (Figure 8-17 (d)). There was no sign of built-up-edge on drills. Some chipping has also been identified on the margin as shown in Figure 8-17 (f).

In summary, combinations of dissimilar wear mechanisms were observed in drilling of CFRP/Ti-6Al-4V stack. Although separate process parameters used for each material in stack, a shortened tool life has been observed due to the different mechanical and physical properties. The combination of diverse wear mechanisms has accelerated the tool wear in drilling of CFRP/Ti-6Al-4V stack.

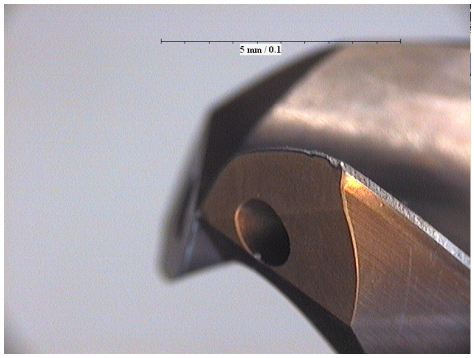

(a)

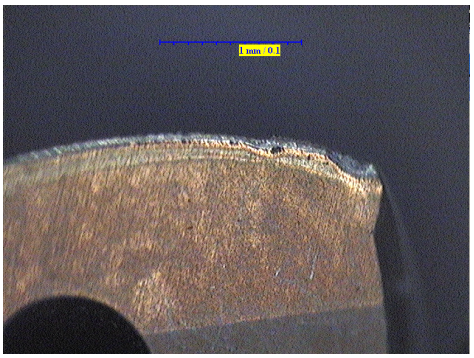

(b)

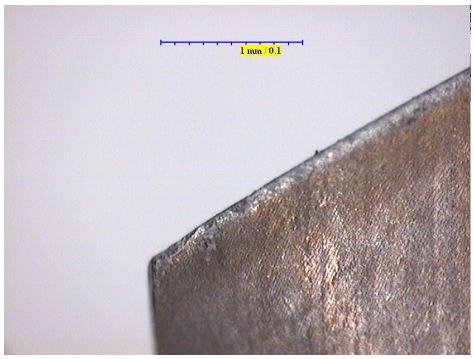

(c)

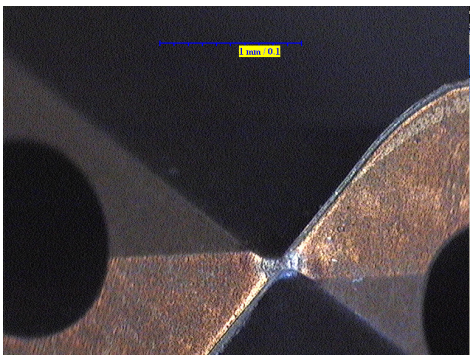

(d)

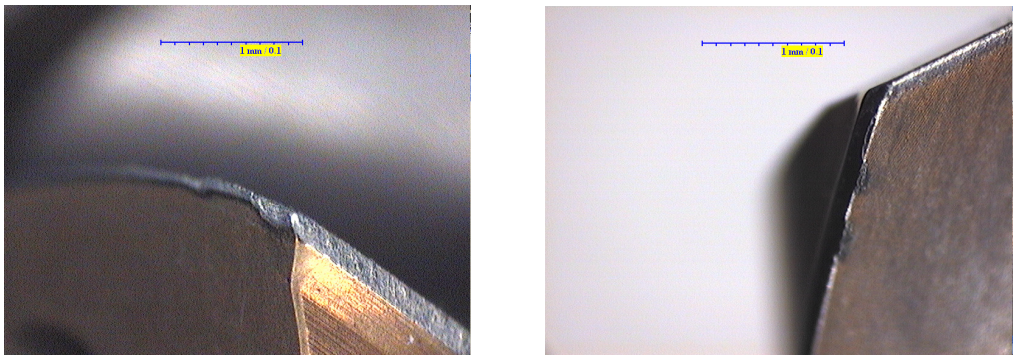

(e) (f)

Figure 8-17: Tool Wear in Drilling of CFRP/Ti6Al4V Stack (a) Overall (b) Flank Wear (c) Crater Wear (d) Chisel Wear (e) Chipping (f) Margin Wear

8.7 Analysis of Workpiece Stress Distribution

The stress distributions of the workpieces after the drilling of CFRP/Ti-6Al-4V are shown in Figure 8-18 and Figure 8-19. Figure 8-18 demonstrated the predicted stress plots in CFRP workpiece simulated at 4500 rpm spindle speed and 457 mm/min feed rate with twist drill and step drill. As can be observed in Figure 8-18 (a) and Figure 8-18 (b), higher stresses were predicted than drilling of CFRP separately due to the support under CFRP workpiece. The existence of titanium alloy workpiece has increased the impact resistance of CFRP workpiece, therefore laminated composite work plate could able to carry higher load. The higher thrust force could also support this. The highest stresses were induced around the centre of the hole where the drill cut the material. As could be observed in Fig (b), Mises stress was estimated lower in drilling of CFRP region by the step drill with 0.63 stage ratio compared to 8 mm rigid twist drill. This was due to the fact that the step drill had a smaller contact area with the composite workpiece than twist drill had. The decrease in the contact means less material to be cut. The reduced material would require less cutting energy and cutting forces. The estimated thrust force, torque and delamination in the previous sections could be the sign of this reduction.

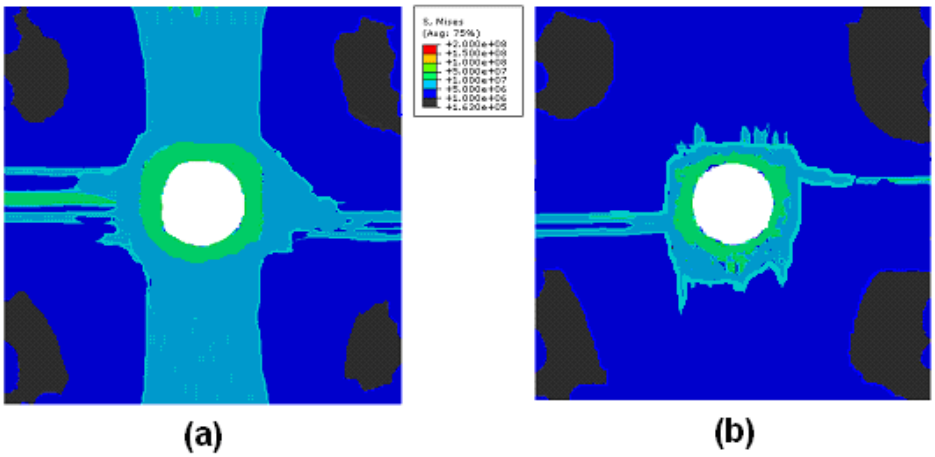

Figure 8-18: Stress Distribution of CFRP Workpiece in Drilling of CFRP/Ti-6Al-4V Stavk (a) Twist Drill (b) Step Drill

Figure 8-19 demonstrated the stress distributions of titanium alloy work plate in drilling of CFRP/Ti-6Al-4V hybrid structure at 4500 rpm spindle speed and 457 mm/min feed rate with twist drill and step drill. As can be observed in Figure 8-19 (a) and Figure 8-19 (b), slightly higher stresses were predicted than drilling of Ti-6Al-4V separately. The existence of CFRP workpiece constrained the titanium alloy work plate from the top which should cause to this increase. The highest stresses were induced at the vicinity of drilled hole. As could be observed in Figure 8-19 (b), the step drill with 0.63 stage ratio decreased the predicted Mises stress in drilling of titanium alloy comparing to 8 mm rigid twist drill. The reduced contact would decrease the cutting forces, required energy and workpiece defects as well. The estimated thrust force, torque and burr formation in the previous sections could be the sign of this reduction.

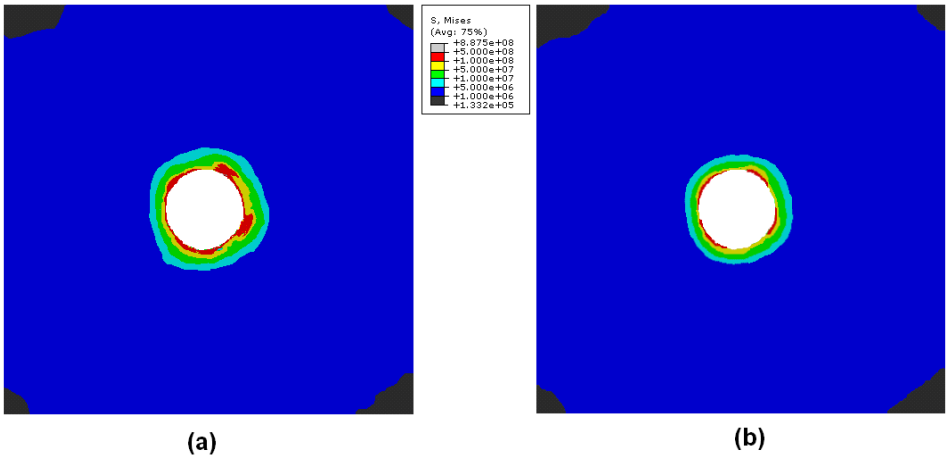

Figure 8-19: Stress Distribution of Ti-6Al-4V Workpiece in Drilling of CFRP/Ti-6Al-4V Stavk (a) Twist Drill (b) Step Drill

8.8 Summary

Experimental and numerical investigations were carried out in drilling of CFRP/Ti-6Al-4V hybrid structure. The results of the analysis were compared with the results of drilling of CFRP and Ti-6Al-4V.

Experimental results showed that an increase in feed rate led to an increase in thrust force, torque, surface roughness and workpiece defects in both work plates with 8 mm twist drill. The increase in spindle speed caused an increase in thrust force and torque whereas a decrease in delamination and average surface roughness in CFRP workpiece. The increase in cutting speed reduced thrust force, torque, burr formation and surface roughness in titanium alloy. One of the most significant observations was all the drilling outputs except delamination was higher in drilling of hybrid structure than drilling work plates separately. This was due to the combination of different cutting mechanisms and increased wear rate. More aggressive tool wear was observed thus tool life has shortened. As was expected, it was found that drilling of each section influenced drilling of whole hybrid structure.

Two finite element models used in for drilling of CFRP and titanium alloy have been combined in a model to simulate drilling process of CFRP/Ti-6Al-4V hybrid structure. Due to its success in drilling of CFRP, the FE approach with fully 3-D solid elements and zero-thickness cohesive surfaces was utilized for

the composite section. Finite element analysis of drilling of CFRP/Ti-6Al-4V generally demonstrated good performances. Positive correlations were acquired for between the process parameters and drilling outputs. Thrust force, torque and drilling induced delamination were predicted closely. The effect of tool geometry was investigated and the advantages of step drill have been indicated to minimize workpiece defects in both material.

Chapter 9

Conclusions and Future Work

This research is a contribution to on-going research area on drilling of aerospace materials; laminated carbon fibre reinforced composites and titanium alloys. The drilling of CFRP, Ti-6Al-4V and CFRP/Ti-6Al-4V were investigated through experimental exploration and finite element analysis.

9.1 Major Contributions

This research consisted of the following major contributions.

The high throughput drilling of laminated carbon fibre reinforced composites was investigated in feasibly technical range, by drilling in a wide range of cutting parameters, using high point angle drill geometry, multilayer TiAlN/TiN PVD coated fine-grained tungsten carbide tool material and internal cutting fluid supply at high pressure.

The effects of process parameters on thrust force, torque, delamination and surface roughness were demonstrated. At a moderate material removal rate, tool life was investigated and the effect of tool wear on thrust force, torque, delamination and surface roughness was studied. A delamination measurement algorithm was developed based on digital image analysis.

A first research attempt to investigate a fully three-dimensional drilling of CFRP with the 3-D complex drill geometry was developed by finite element tools. Two different modeling approaches were generated for CFRP. The material and damage models were developed to model material behaviour and drilling induced workpiece defects. Hashin's failure model was utilized.

Finite elements analysis of drilling of CFRP was validated. The effects of process parameters on drilling outputs were demonstrated and compared with results of experimental study.

Based on the capability of FE analysis and gained confidence, the effect of tool geometry on drilling of CFRP was investigated numerically. The optimisations of tool geometry and process parameters were discussed.

Drilling of titanium alloy was investigated in feasibly technical range, by selecting of suitable cutting parameters, high point angle drill geometry, multilayer TiAlN/TiN PVD coated fine-grained tungsten carbide tool material and internal cutting fluid supply at high pressure.

The effects of process parameters on thrust force, torque, burr formation and surface roughness were demonstrated in drilling of titanium alloy. At a moderate material removal rate, tool life was investigated and the effect of tool wear on thrust force, torque, burr formation and surface roughness was studied.

A novel 3-D finite element model of drilling of Ti-6Al-4V with the 3-D complex drill geometry was developed. Johnson-Cook material and failure models were utilized for titanium alloy workpiece. The effects of process parameters on drilling outputs were demonstrated and compared with results of experimental study.

Based on the capability of FE analysis and gained experience, the effect of tool geometry on drilling of Ti-6Al-4V was investigated numerically. The optimisations of tool geometry and process parameters were discussed.

Drilling of CFRP/Ti-6Al-4V stack was investigated in feasibly technical range, by selecting of suitable cutting parameters based on the analysis of drilling of CFRP and titanium alloy separately, high point angle drill geometry which was used in drilling of both material separately, multilayer TiAlN/TiN PVD coated fine-grained tungsten carbide tool material and internal cutting fluid supply at high pressure.

The effects of process parameters on thrust force, torque, burr formation, delamination and surface roughness were demonstrated in drilling of CFRP/Titanium alloy. At a moderate material removal rate, tool life was investigated and the effect of tool wear on thrust force, torque, delamination, burr formation and surface roughness was studied. The results of investigations were compared with drilling of each material separately.

A novel 3-D finite element model of drilling of CFRP/Ti-6Al-4V with the 3-D complex drill geometry was developed and validated. The effects of process parameters on drilling outputs were demonstrated and compared with results of experimental study and results of FE analysis of drilling each material separately.

The effect of tool geometry on drilling of CFRP/Ti-6Al-4V was investigated in finite element analysis. The optimisations of tool geometry and process parameters were discussed to minimize workpiece defects and cost of manufacturing, to increase productivity.

Highlights of Drilling of Ti-6Al-4V

Through complete experimental analysis, moderate to high material removal rate (80-143 mm3/s) was achieved with the use of feed rate between 95 mm/min and 171 mm/min, spindle speed between 1000 rpm and 1800 rpm (equal cutting speed between 25 and 45 m/min), and a commercially available 8 mm diameter multilayer TiN/TiAlN coated tungsten carbide drill. The internal cutting fluid through the coolant holes of drill bit was applied at high pressures to improve chip removal and to avoid thermal effects. The influences of feed rate and cutting speed were demonstrated. Experimental results showed that thrust force, torque, burr formation and surface roughness were increased with feed rate and decreased with the spindle speed. As the workpiece surface quality is extremely important, the progression of drilling outputs was shown with regard to tool wear by means of number of drilled holes.

A novel 3-D finite element model based on Lagrangian formulation was developed to simulate drilling of Ti6Al4V. The effects of cutting parameters on thrust force, torque and burr were investigated numerically and compared to the experimental results. The predictions of the FE model generally matched the experimentally measured values closely and showed the applicability in drilling process. Although the extent of burr formation was predicted significantly lower than the experimental test results, the correlation between process parameters and burr formation was good. Possible suggestions were made to improve the performance of finite element model. The diversity between the results of FE analysis and experiments were lower at lower speeds

and increased with the machining rate. This showed the importance of the material model parameters and the need of material properties at higher rates. The effect of drill geometry on drilling of Ti-6Al-4V was investigated by various step drills numerically. FE results indicated the advantages of step drill over twist drill by several aspects including thrust force, torque and burr formation. Drilling outputs were predicted to decrease with the increasing stage ratio of step drill. The developed 3-D finite element model demonstrated the effect of process parameters and complex tool geometry and showed the advantage for process and tool design.

Highlights of Drilling of CFRP

Complete drilling experiments of laminated carbon fibre reinforced composites were conducted at high material removal rates (297-574 mm3/s) which were achieved with the use of feed rate between 355 mm/min and 685 mm/min, and spindle speed between 3000 rpm and 9000 rpm (equal cutting speed between 75 and 225 m/min); with the use of commercially available 8 mm diameter multilayer TiN/TiAlN coated tungsten carbide drills. The cutting fluid was employed at high pressure through the coolant holes of drill bits to improve of removal of dusty chips and to avoid effect of temperature. A delamination measurement algorithm was developed through digital image analysis. The influences of feed rate and cutting speed were exhibited. Thrust force and torque was found to increase with feed rate and cutting speed. Delamination and surface roughness increased with the feed rate, but decreased with the cutting speed. Due to the tolerances, the progression of drilling outputs was observed with regard to tool wear by means of number of drilled holes in the workpiece.

A novel 3-D finite element model based on Lagrangian formulation was developed to simulate drilling of CFRP. The effects of cutting parameters on thrust force, torque and delamination were investigated numerically and compared to the experimental results. The FE model based on 3-D solid elements predicted close results to experiments. Material behaviour of composite and induced drilling workpiece defects were modeled successfully. The diversity between the results of FE analysis and experiments was found

lower at lower speeds and increased with the machining rate. This showed the importance of the material model parameters with regard to the test rate and the need of material properties at higher rates. Other possible improvements to the performance of finite element model were suggested for the future researchers. The effect of drill geometry on drilling of CFRP was investigated by various step drills numerically. FE results demonstrated the possible advantages of step drill over twist drill in drilling of CFRP.

Highlights of Drilling of CFRP/Ti-6Al-4V Hybrid Structure

After gaining information and experience based on the investigations of distinct materials separately, drilling experiments and related analysis of CFFRP/Ti-6Al-4V hybrid structure were carried out under the same cutting condition, but within a limited cutting parameter region. The combination of different attributes of these materials was found to affect drilling process. Greater thrust force, torque, burr formation, surface roughness and tool wear induced in drilling of hybrid structure. Delamination decreased significantly due to the increased impact resistance of composite workpiece in hybrid structure. Similar trends were observed between process parameters and drilling outputs, however it was also found that the process parameters used in each section influenced the drilling outputs in the other section. Due to accelerated tool wear rate, tool life was found to be shorter in drilling of hybrid structures.

A novel 3-D finite element model based on Lagrangian formulation was developed to simulate drilling of CFRP/Ti-6Al-4V hybrid structure. The different attributes and requirements were taken into account in the numerical analysis. The FE model generally predicted close results compared to the experiments. The effect of drill geometry on drilling of CFRP/Ti-6Al-4V hybrid structure was investigated numerically. FE results showed the possible advantages of step drill in drilling of the hybrid structure. The possible improvements to the performance of finite element model were discussed.

9.2 Recommendations for Future Study

This research has identified several directions for the further explorations in machining of composite/metal hybrid structures. Modeling of the drilling process based on the finite element method is an important research direction to understand the deformation of workpiece, deformation of cutting tool, workpiece defects, tool wear, and thermal effects in drilling; to increase productivity with reduced costs.

Several key assumptions were made in this study. First, mechanical analysis assumed the stress solution was not dependent on temperature due to the use of high amount of coolant. To simulate the drilling process more accurately, a thermo-mechanical model would be a good option to solve stress and temperature simultaneously. Secondly, a rigid cutting tool was assumed in the finite element models due to the limited computational facilities. Utilisation of a deformable cutting tool would improve the results but the computational cost must be balanced. Another further step to that would be the employment of the tool wear model in FE analysis.

Another key point could be the addition of the chip formation into the FE model. It could increase the complexity of the model substantially, but it would improve the modeling of burr formation in drilling of metals. This would require high computational facilities due to required accuracy and it must be balanced.

The 3-D FE analysis of drilling neglected the interaction between adjacent segments. To improve the modeling accuracy further, more complex contact mechanics including stress, strain rate, temperature and fibre orientation dependant friction model is required to simulate the drilling process. This would require further mechanical and tribological analysis.

An important point of the FE model is the material and failure models. It is thought that the material properties should be one of the reasons of the diversity between the results of FE and experiments due to the material test conditions. The stress-strain curves of the workpiece material would be different at different cutting speeds, thus material respond and related drilling

outputs would induce different. The material data for CFRP in the literature is generally based on the tests carried out very slow rates, however the respond of matrix could be affected due to the strain rate. The progression of failure and delamination could be affected significantly. Similar to that, Ti-Al-4V is highly dependant on the strain rate, temperature and micro structure. Thus, it is worthwhile to investigate the material respond of these materials at higher strain rates and temperatures.

Each of these suggested topics could be future Ph.D. research topics to enhance the understanding of drilling of composite/metal hybrid structures and contribute to minimizing the workpiece defects, providing better solutions, reducing cost of machining and increasing the productivity.

References

[1] W. D. Brewer, *et al.*, "Titanium alloys and processing for high speed aircraft," *Materials Science and Engineering: A,* vol. 243, pp. 299-304, 1998.

[2] E. O. Ezugwu and Z. M. Wang, "Titanium alloys and their machinability--a review," *Journal of Materials Processing Technology,* vol. 68, pp. 262-274, 1997.

[3] A. R. Machado and J. Wallbank, "Machining of Titanium and its Alloys-a Review," *Proceedings of the Institution of Mechanical Engineers, Part B: Journal of Engineering Manufacture,* vol. 204, pp. 53-60, 1990.

[4] http://www.airforce-technology.com/projects/f22/. 15/09/2011).

[5] E. Brinksmeier, *et al.*, "High Speed Machining of Multilayer Composite Materials by Orbital Drilling," in *Proceedings of the Sixth International Conference on High Speed Machining*, San Sebastian, 2007.

[6] W. Koenig, *et al.*, "Developments in drilling, contouring composites containing Kevlar," *Production Engineer* vol. 63, pp. 56-61, 1984.

[7] V. Tagliaferri, *et al.*, "Effect of drilling parameters on the finish and mechanical properties of GFRP composites," *International Journal of Machine Tools and Manufacture,* vol. 30, pp. 77-84, 1990.

[8] E. Persson, *et al.*, "Propagation of hole machining defects in pin-loaded composite laminates," *Journal of Composite Materials,* vol. 31, pp. 383-408, 1997.

[9] J. Ramkumar, *et al.*, "An enhancement of the machining performance of GFRP by oscillatory assisted drilling," *The International Journal of Advanced Manufacturing Technology,* vol. 23, pp. 240-244, 2004.

[10] X. D. Xu, *et al.*, "The structural intensities of composite plates with a hole," *Composite Structures,* vol. 65, pp. 493-498, 2004.

[11] W. Koenig, *et al.*, "Machining of New Materials," *CIRP Annals - Manufacturing Technology,* vol. 39, pp. 673-681, 1990.

[12] R. Komanduri, "Machining of Fiber-Reinforced Composites," *Machining Science and Technology,* vol. 1, pp. 113-152, 2011/10/13 1997.

[13] J. P. Davim, *et al.*, "Experimental study of drilling glass fiber reinforced plastics (GFRP) manufactured by hand lay-up," *Composites Science and Technology,* vol. 64, pp. 289-297, 2004.

[14] R. Zitoune and F. Collombet, "Experimental and analytical study of the influence of HexFit® glass fibre composite manufacturing process on delamination during drilling," *International Journal of Machining and Machinability of Materials,* vol. 3, pp. 326-342, 2008.

[15] R. Zitoune, Collombet, F., "Influence of machining quality on composite part manufacturing," in *Drilling of composite materials (Materials and*

Manufacturing Technology Series), D. J. P., Ed., ed: Nova Publishers, 2009, pp. 83-96.

[16] R. Boyer, *et al.*, *Materials properties handbook: Titanium alloys*: The materials information society, ASM International, Materials Park., 1994.

[17] D. A. Dornfeld, *et al.*, "Drilling burr formation in titanium alloy, Ti-6Al-4V," *CIRP Annals - Manufacturing Technology,* vol. 48, pp. 73-76, 1999.

[18] P. F. Zhang, *et al.*, "Mechanical Drilling Processes for Titanium Alloys: A Literature Review," *Machining Science and Technology,* vol. 12, pp. 417-444, 2011/10/13 2008.

[19] X. Yang and R. C. Liu, "Machining Titanium and Its Alloys," *Machining Science and Technology,* vol. 3, pp. 107-139, 1999.

[20] M. Ramulu, *et al.*, "A study on the drilling of composite and titanium stacks," *Composite Structures,* vol. 54, pp. 67-77, 2001.

[21] D. Kim and M. Ramulu, "Drilling process optimization for graphite/bismaleimidetitanium alloy stacks," *Composite Structures,* vol. 63, pp. 101-114, 2004.

[22] C. Soutis, "Fibre reinforced composites in aircraft construction," *Progress in Aerospace Sciences,* vol. 41, pp. 143-151, 2005.

[23] T. Sinmazçelik, *et al.*, "A review: Fibre metal laminates, background, bonding types and applied test methods," *Materials and Design,* vol. 32, pp. 3671-3685, 2011.

[24] A. M. Abrão, *et al.*, "Drilling of fiber reinforced plastics: A review," *Journal of Materials Processing Technology,* vol. 186, pp. 1-7, 2007.

[25] J. Y. Sheikh-Ahmad, *Machining of Polymer Composites*: Springer, 2009.

[26] E. C. Botelho, *et al.*, "A review on the development and properties of continuous fiber/epoxy/aluminum hybrid composites for aircraft structures," *Materials Research,* vol. 9, pp. 247–256, 2006.

[27] D. Gay, *et al.*, *Composite materials design and applications*. New York: CRC Press, 2003.

[28] I. Shyha, *et al.*, "Effect of laminate configuration and feed rate on cutting performance when drilling holes in carbon fibre reinforced plastic composites," *Journal of Materials Processing Technology,* vol. 210, pp. 1023-1034, 2010.

[29] Y. Fan and L. Zhang, "New development of extra large composite aircraft components application technology - Advance of aircraft manufacture technology," *Hangkong Xuebao/Acta Aeronautica et Astronautica Sinica,* vol. 30, pp. 534-543, 2009.

[30] ASM, *ASM Handbook, Volume 2: Properties and Selection: Nonferrous Alloys and Special-Purpose Materials* vol. 2: ASM, 1992.

[31] T. Farthing, "Application of titanium in the chemical industry," *Chemical Age of India,* vol. 30, pp. 151–166, 1979.

[32] K. V. Kumar, "Grinding titanium," *Aerospace Engineering,* vol. 11, pp. 17-19, 1991.
[33] http://www.airforce-technology.com/projects/f22/.
[34] D. K. Peacock, "Aerospace applications for titanium," *Sheet Metal Industries,* vol. 65, pp. 406-408, 1988.
[35] M. M. Salama, *et al.*, "Titanium drilling risers-application and qualification," *Journal of Offshore Mechanics and Arctic Engineering,* vol. 122, pp. 47-51, 2000.
[36] I. Abdullin, *et al.*, "Improving surface finish for titanium alloy medical instruments," *Biomedical Engineering,* vol. 22, pp. 48-50, 1988.
[37] F. Froes, "Titanium sport and medical application focus," *Materials Technology,* vol. 17, pp. 4-7, 2002.
[38] S. R. Ravishankar and C. R. L. Murthy, "Ultrasonic imaging for evaluation of drill induced delaminations in composite laminates," in *14th Conference on Non-Destructive Testing*, 1996, pp. 8-13.
[39] C. A. Friend, *et al.*, "Machining graphite composite materials," in *Composite Materials in Engineering Design*, B. B. Noton, Ed., ed: ASM Press, 1973, pp. 217-224.
[40] V. Tagliaferri, *et al.*, "Laser cutting of fibre-reinforced polyesters," *Composites,* vol. 16, pp. 317-325, 1985.
[41] A. Di Ilio and V. Tagliaferri, "Thermal damage in laser cutting of (0/90)2s aramid/epoxy laminates," *Composites,* vol. 20, pp. 115-119, 1989.
[42] G. Caprino and V. Tagliaferri, "Maximum cutting speed in laser cutting of fiber reinforced plastics," *International Journal of Machine Tool Design and Research,* vol. 28, pp. 389-398, 1988.
[43] H. Ho-Cheng, "A failure analysis of water jet drilling in composite laminates," *International Journal of Machine Tools and Manufacture,* vol. 30, pp. 423-429, 1990.
[44] M. Hashish, "Machining of advanced composites with abrasive-waterjets," *Manufacturing Review,* vol. 2, pp. 142-150, 1989.
[45] G. E. Miller, "Special theory of ultrasonic machining," *Journal of Applied Physics,* vol. 28, pp. 149-156, 1957.
[46] V. Soundararajan and V. Radhakrishnan, "An experimental investigation on the basic mechanisms involved in ultrasonic machining," *International Journal of Machine Tool Design and Research,* vol. 26, pp. 307-321, 1986.
[47] H. Hocheng and C. C. Hsu, "Preliminary study of ultrasonic drilling of fiber-reinforced plastics," *Journal of Materials Processing Technology,* vol. 48, pp. 255-266, 1995.
[48] W. S. Lau, *et al.*, "Electrical discharge machining of carbon fibre composite materials," *International Journal of Machine Tools and Manufacture,* vol. 30, pp. 297-308, 1990.

[49] R. Teti, "Machining of composite materials," *CIRP Annals - Manufacturing Technology,* vol. 51, pp. 611-634, 2002.

[50] C. Wern*, et al.*, "Investigation of stresses in he orthogonal cutting of fiber-reinforced plastics," *Experimental Mechanics,* vol. 36, pp. 33-41, 1996.

[51] G. V. G. Rao*, et al.*, "Micro-mechanical modeling of machining of FRP composites – Cutting force analysis," *Composites Science and Technology,* vol. 67, pp. 579-593, 2007.

[52] F. Lachaud*, et al.*, "Drilling of composite structures," *Composite Structures,* vol. 52, pp. 511-516, 2001/6// 2001.

[53] E. Persson*, et al.*, "Effects of hole machining defects on strength and fatigue life of composite laminates," *Composites Part A: Applied Science and Manufacturing,* vol. 28, pp. 141-151, 1997.

[54] R. Mishra*, et al.*, "Neural network approach for estimating the residual tensile strength after drilling in uni-directional glass fiber reinforced plastic laminates," *Materials and Design,* vol. 31, pp. 2790-2795, 2010.

[55] S. Abrate, "Machining of composite materials," in *Composites engineering handbook*, P. K. Mallick, Ed., ed New York: Marcel Dekker, 1997, pp. 777–809.

[56] W. C. Chen, "Some experimental investigations in the drilling of carbon fiber-reinforced plastic (CFRP) composite laminates," *International Journal of Machine Tools and Manufacture,* vol. 37, pp. 1097-1108, 1997.

[57] I. El-Sonbaty*, et al.*, "Factors affecting the machinability of GFR/epoxy composites," *Composite Structures,* vol. 63, pp. 329-338, 2004.

[58] U. A. Khashaba, "Delamination in drilling GFR-thermoset composites," *Composite Structures,* vol. 63, pp. 313-327, 2004.

[59] N. S. Mohan*, et al.*, "Machining of Fiber-reinforced Thermoplastics: Influence of Feed and Drill Size on Thrust Force and Torque during Drilling," *Journal of Reinforced Plastics and Composites,* vol. 24, pp. 1247-1257, 2005.

[60] I. Singh*, et al.*, "Drilling of uni-directional glass fiber reinforced plastics: Experimental and finite element study," *Materials and Design,* vol. 29, pp. 546-553, 2008.

[61] L. M. P. Durão*, et al.*, "Drilling tool geometry evaluation for reinforced composite laminates," *Composite Structures,* vol. 92, pp. 1545-1550, 2010.

[62] Abrão AM*, et al.*, "The Effect of cutting tool geometry on thrust force and delamination when drilling glass fibre reinforced plastic composite," *Materials & Design,* vol. 29, pp. 508–513., 2008.

[63] C. Murphy*, et al.*, "The performance of coated tungsten carbide drills when machining carbon fibre-reinforced epoxy composite materials," *Proceedings of the Institution of Mechanical Engineers. Part B: Journal of Engineering Manufacture,* vol. 216, pp. 143–152, 2002.

[64] S. Rawat and H. Attia, "Wear mechanisms and tool life management of WC-Co drill during dry high speed drilling of woven carbon fibre composites," *Wear*, vol. 267, pp. 1022–1030, 2009.

[65] A. Faraz, *et al.*, "Cutting edge rounding: an innovative tool wear criterion in drilling CFRP composite laminates," *International Journal of Machine Tools and Manufacture*, vol. 49, pp. 1185–1196, 2009.

[66] U. A. Khashaba, *et al.*, "Machinability analysis in drilling woven GFR/epoxy composites: part II – effect of drill wear," *Composites Part A: Applied Science and Manufacturing*, vol. 41, pp. 1130–1137, 2010.

[67] A. Velayudham, *et al.*, "Evaluation of drilling characteristics of high volume fraction fibre glass reinforced polymeric composite," *International Journal of Machine Tools and Manufacture*, vol. 45, pp. 399–406, 2005.

[68] M. Fernandes and C. Cook, "Drilling of carbon composites using a one shot drill bit. Part I: Five stage representation of drilling and factors affecting maximum force and torque," *International Journal of Machine Tools and Manufacture*, vol. 46, pp. 70-75, 2006.

[69] U. A. Khashaba, *et al.*, "Machinability analysis in drilling woven GFR/epoxy composites: part I - effect of machining parameters," *Composites Part A: Applied Science and Manufacturing*, vol. 41, pp. 391-400, 2010.

[70] R. Stone and K. Krishnamurthy, "A neural network thrust force controller to minimize delamination during drilling of graphite-epoxy laminates," *International Journal of Machine Tools and Manufacture*, vol. 36, pp. 985-1003, 1996.

[71] K. Ogawa, *et al.*, "Investigation on cutting mechanism in small diameter drilling for GFRP (thrust force and surface roughness at drilled hole wall)," *Composite Structures*, vol. 38, pp. 343-350, 1997.

[72] V. N. Gaitonde, *et al.*, "Analysis of parametric influence on delamination in high-speed drilling of carbon fiber reinforced plastic composites," *Journal of Materials Processing Technology*, vol. 203, pp. 431-438, 2008.

[73] S. Jain and D. C. H. Yang, "Delamination-free drilling of composite laminates," *Journal of engineering for industry*, vol. 116, pp. 475-481, 1994.

[74] H. Hocheng and C. K. H. Dharan, "Delamination during drilling in composite laminates," *Journal of Engineering for Industry*, vol. 112, pp. 236–239, 1990.

[75] K. Y. Park, *et al.*, "Delamination-free and high efficiency drilling of carbon fiber reinforced plastics," *Journal of Composite Materials*, vol. 29, pp. 1988–2002, 1995.

[76] S. D. Andrews, *et al.*, "The effect of fastener hole defects," *Journal of Composite Materials*, vol. 27, pp. 3-20, 1993.

[77] J. P. Davim and P. Reis, "Drilling carbon fiber reinforced plastics manufactured by autoclave-experimental and statistical study," *Materials and Design,* vol. 24, pp. 315-324, 2003.

[78] J. P. Davim, *et al.*, "A novel approach based on digital image analysis to evaluate the delamination factor after drilling composite laminates," *Composite Science and Technology,* vol. 67, pp. 1939–1945, 2007.

[79] C. C. Tsao and H. Hocheng, "Effect of tool wear on delamination in drilling composite materials," *International Journal of Mechanical Sciences,* vol. 49, pp. 983–988, 2007.

[80] E. Capello, "Workpiece damping and its effect on delamination damage in drilling thin composite laminates," *Journal of Materials Processing Technology,* vol. 148, pp. 186–195, 2004.

[81] G. W. Kim and K. Y. Lee, "Critical thrust at propagation of delamination zone due to drilling of FRP/metallic strips," *Composite Structures,* vol. 69, pp. 137–141, 2005.

[82] H. Hocheng and C. C. Tsao, "Comprehensive analysis of delamination in drilling of composite materials with various drill bits," *Journal of Materials Processing Technology,* vol. 140, pp. 335-339, 2003.

[83] H. Hocheng and C. C. Tsao, "Effects of special drill bits on drilling-induced delamination of composite materials," *International Journal of Machine Tools and Manufacture,* vol. 46, pp. 1403–1416, 2006.

[84] L. B. Zhang, *et al.*, "Mechanical model for predicting thrust and torque in vibration drilling fibre-reinforced composite materials," *International Journal of Machine Tools and Manufacture,* vol. 41, pp. 641–657, 2001.

[85] S. Abrate and D. A. Walton, "Machining of composite material. Part I: traditional methods," *Composites Manufacturing,* vol. 3, pp. 75–83, 1992.

[86] P. C. Upadhyay and J. S. Lyons, "On the evaluation of critical thrust for delamination-free drilling of composite laminates," *Journal of Reinforced Plastics and Composites,* vol. 18, pp. 1287–1303, 1999.

[87] G. Caprino and V. Tagliaferri, "Damage development in drilling glass fiber reinforced plastics," *International Journal of Machine Tools and Manufacture,* vol. 35, pp. 817–829, 1995.

[88] R. Q. Sardiñas, *et al.*, "Multi-objective optimization of cutting parameters for drilling laminate composite materials by using genetic algorithms," *Composites Science and Technology,* vol. 66, pp. 3083-3088, 2006.

[89] S. Rawat and H. Attia, "Characterization of the dry high speed drilling process of woven composites using machinability maps approach," *CIRP Annals – Manufacturing Technology,* vol. 58, pp. 105–108, 2009.

[90] J. P. Davim and P. Reis, "Study of delamination in drilling carbon fiber reinforced plastics (CFRP) using design experiments," *Composite Structures,* vol. 59, pp. 481-487, 2003.

[91] C. C. Tsao and H. Hocheng, "Computerized tomography and C-Scan for measuring delamination in the drilling of composite materials using various drills," *International Journal of Machine Tools and Manufacture,* vol. 45, pp. 1282-1287, 2005.

[92] S. R. Karnik, *et al.*, "Delamination analysis in high speed drilling of carbon fiber reinforced plastics (CFRP) using artificial neural network model," *Materials and Design,* vol. 29, pp. 1768-1776, 2008.

[93] E. Kilickap, "Optimization of cutting parameters on delamination based on Taguchi method during drilling of GFRP composite," *Expert Systems with Applications,* vol. 37, pp. 6116-6122, 2010.

[94] S. Arul, *et al.*, "The effect of vibratory drilling on hole quality in polymeric composites," *International Journal of Machine Tools and Manufacture,* vol. 46, pp. 252–259, 2006.

[95] J. C. Rubio, *et al.*, "Effects of high speed in the drilling of glass fibre reinforced plastic: evaluation of delamination factor," *International Journal of Machine Tools and Manufacture,* vol. 48, pp. 715–720, 2008.

[96] E. Aoyama, *et al.*, "Drilled hole damage of small diameter drilling in printed wiring board," *Journal of Materials Processing Technology,* vol. 118, pp. 436–441, 2001.

[97] C. C. Tsao and H. Hocheng, "Taguchi analysis of delamination associated with various drill bits in drilling of composite material," *International Journal of Machine Tools and Manufacture,* vol. 44, pp. 1085-1090, 2004.

[98] H. Hocheng and C. C. Tsao, "The path towards delamination-free drilling of composite materials," *Journal of Materials Processing Technology,* vol. 167, pp. 251-264, 2005.

[99] C. C. Tsao, "Prediction of thrust force of step drill in drilling composite material by Taguchi method and radial basis function network," *International Journal of Advanced Manufacturing Technology,* vol. 36, pp. 11-18, 2008.

[100] C. C. Tsao, "Effect of induced bending moment (IBM) on critical thrust force for delamination in step drilling of composites," *International Journal of Machine Tools and Manufacture,* vol. 59, pp. 1-5, 2012.

[101] C. C. Tsao and H. Hocheng, "Parametric study on thrust force of core drill," *Journal of Materials Processing Technology,* vol. 192-193, pp. 37-40, 2007.

[102] H. Zhang, *et al.*, "Assessment of the exit defects in carbon fibre-reinforced plastic plates caused by drilling," *Key Engineering Materials,* vol. 196, pp. 43–52, 2001.

[103] A. M. Abrão, *et al.*, "The Effect of cutting tool geometry on thrust force and delamination when drilling glass fibre reinforced plastic composite," *Materials and Design,* vol. 29, pp. 508–513, 2008.

[104] R. Piquet, *et al.*, "Experimental analysis of drilling damage in thin carbon/epoxy plate using special drills," *Composites Part A: Applied Science and Manufacturing,* vol. 31, pp. 1107-1115, 2000.

[105] M. Fernandes and C. Cook, "Drilling of carbon composites using a one shot drill bit. Part II: Empirical modeling of maximum thrust force," *International Journal of Machine Tools and Manufacture,* vol. 46, pp. 76-79, 2006.

[106] C. C. Tsao, "Experimental study of drilling composite materials with step-core drill," *Materials and Design,* vol. 29, pp. 1740–1744, 2008.

[107] C. C. Tsao and H. Hocheng, "The effect of chisel length and associated pilot hole on delamination when drilling composite materials," *International Journal of Machine Tools and Manufacture,* vol. 43, pp. 1087-1092, 2003.

[108] C. C. Tsao and H. Hocheng, "Effect of eccentricity of twist drill and candle stick drill on delamination in drilling composite materials," *International Journal of Machine Tools and Manufacture,* vol. 45, pp. 125-130, 2005.

[109] C. C. Tsao and H. Hocheng, "Effects of exit back-up on delamination in drilling composite materials using a saw drill and a core drill," *International Journal of Machine Tools and Manufacture,* vol. 45, pp. 1261-1270, 2005.

[110] C. C. Tsao, "The effect of pilot hole on delamination when core drill drilling composite materials," *International Journal of Machine Tools and Manufacture,* vol. 46, pp. 1653-1661, 2006.

[111] M. S. Won and C. K. H. Dharan, "Chisel edge and pilot hole effects in drilling composite laminates," *Journal of Manufacturing Science and Engineering, Transactions of the ASME,* vol. 124, pp. 242-247, 2002.

[112] A. Chambers and G. Bishop, "The drilling of carbon fibre polymer matrix composites," in *Proceedings of the Tenth International Conference on Composite Materials: Processing and manufacturing*, Canada, 1995, pp. 565–572.

[113] M. C. Shaw, *Metal Cutting Principles*, 2nd ed. New York: Oxford University Press, 2005.

[114] D. Iliescu, *et al.*, "Modeling and tool wear in drilling of CFRP," *International Journal of Machine Tools and Manufacture,* vol. 50, pp. 204–213, 2010.

[115] S. C. Lin and I. K. Chen, "Drilling carbon fiber-reinforced composite material at high speed," *Wear,* vol. 194, pp. 156-162, 1996.

[116] ASM, *ASM Handbook, Volume 16: Machining* vol. 16: ASM International, 1995.

[117] M. Mahdi and L. Zhang, "A finite element model for the orthogonal cutting of fiber-reinforced composite materials," *Journal of Materials Processing Technology,* vol. 113, pp. 373-377, 2001.
[118] M. Mahdi and L. Zhang, "An adaptive three-dimensional finite element algorithm for the orthogonal cutting of composite materials," *Journal of Materials Processing Technology,* vol. 113, pp. 368-372, 2001.
[119] D. Arola, *et al.*, "Finite element modelling of edge trimming fiber reinforced plastics," *Journal of Manufacturing Science and Engineering,* vol. 124, pp. 32–41, 2002.
[120] D. Arola and M. Ramulu, "Orthogonal cutting of fiber-reinforced composites: A finite element analysis," *International Journal of Mechanical Sciences*, vol. 39, pp. 597-613, 1997.
[121] R. Zitoune, *et al.*, "Experiment-calculation comparison of the cutting conditions representative of the long fiber composite drilling phase," *Composites Science and Technology*, vol. 65, pp. 455-466, 2005.
[122] L. M. P. Durão, *et al.*, "Numerical simulation of the drilling process on carbon/epoxy composite laminates," *Composites Part A: Applied Science and Manufacturing,* vol. 37, pp. 1325-1333, 2006.
[123] L. M. P. Durão, *et al.*, "Numerical prediction of delamination onset in carbon/epoxy composites drilling," *Engineering Fracture Mechanics,* vol. 75, pp. 2767-2778, 2008.
[124] R. Zitoune and F. Collombet, "Numerical prediction of the thrust force responsible of delamination during the drilling of the long-fibre composite structures," *Composites Part A: Applied Science and Manufacturing,* vol. 38, pp. 858-866, 2007.
[125] P. T. Schroeder. (1998) Widening interest in twist drill. *Modern Machining Shop*. 106–113.
[126] H. K. Tonshoff, *et al.*, "Machining of holes developments in drilling technology," *CIRP Annals - Manufacturing Technology,* vol. 43, pp. 551-561, 1994.
[127] D. Kim, *et al.*, "Machinability of titanium/graphite hybrid composites in drilling," in *Transactions of the North American Manufacturing Research Institute of SME*, 2005, pp. 445-452.
[128] K. Colligan, "New tool drills both titanium and carbon composites," *American Machinist,* vol. 138, pp. 56-58, 1994.
[129] D. Kim and M. Ramulu, "Cutting and drilling characteristics of hybrid Titanium Composite Laminate (HTCL)," in *International SAMPE Technical Conference*, 2005, pp. 1-8.
[130] D. Kim and M. Ramulu, "Study on the Drilling of Titanium/Graphite Hybrid Composites," *Journal of Engineering Materials and Technology,* vol. 129, pp. 390-396, 2007.

[131] R. Li, *et al.*, "High-throughput drilling of titanium alloys," *International Journal of Machine Tools and Manufacture,* vol. 47, pp. 63-74, 2007.

[132] E. A. Rahim and S. Sharif, "Investigation on Tool Life and Surface Integrity when Drilling Ti-6Al-4V and Ti-5Al-4V-Mo/Fe," *JSME International Journal Series C Mechanical Systems, Machine Elements and Manufacturing,* vol. 49, pp. 340-345, 2006.

[133] J. F. Kahles, *et al.*, "Machining of titanium alloys," *Journal of Metals,* vol. 37, pp. 27-35, 1985.

[134] W. Konig, "Applied research on the machinability of titanium and its alloys," in *47th Meeting of AGARD Structures and Materials* Italy, 1978, pp. 1-10.

[135] C. S. P. Rao, *et al.*, "Drilling of titanium cladded steel plate," *Journal of the Institution of Engineers (India), Part PR: Production Engineering Division,* vol. 71, pp. 1-3, 1990.

[136] D. Kim, *et al.*, "Hole quality in drilling of graphite/bismalemide-titanium stacks," in *33rd. International SAMPE Technical Conference*, Seattle, USA, 2001, pp. 1315-1326.

[137] A. E. Bayoumi and J. Q. Xie, "Some metallurgical aspects of chip formation in cutting Ti-6Al-4V alloy," *Materials Science and Engineering: A,* vol. 190, pp. 173-178, 1995.

[138] A. R. Shahan and A. K. Taheri, "Adiabatic shear bands in titanium and titanium alloys: a critical review," *Materials and Design,* vol. 14, pp. 243-250, 1993.

[139] H. C. Child and A. L. Dalton, "Machining of titanium alloys-metallurgical factors affecting machinability," in *Conference on Machinability*, London, 1965, pp. 139-142.

[140] P. A. Dearnley and A. N. Grearson, "Evaluation of principal wear mechanisms of cemented carbides and ceramics used for machining titanium alloy IMI 318," *Materials Science and Technology,* vol. 2, pp. 47-58, 1986.

[141] S. Motonishi, *et al.*, "Study on machining of titanium and its alloys," *Kobelco Technology Review,* vol. 2, pp. 28-31, 1987.

[142] N. Narutaki, *et al.*, "Study on Machining of Titanium Alloys," *CIRP Annals - Manufacturing Technology,* vol. 32, pp. 65-69, 1983.

[143] E. F. Smart and E. M. Trent, "Temperature distribution in tools used for cutting iron, titanium and nickel," *International Journal of Production Research,* vol. 13, pp. 265-290, 1975.

[144] W. Konig and K. W. Schroder, "Face milling and drilling of titanium alloys," in *the Influence of Metallurgy on Machinability*, 1975, pp. 308-323.

[145] S. Sharif and E. A. Rahim, "Performance of coated- and uncoated-carbide tools when drilling titanium alloy-Ti-6Al4V," *Journal of Materials Processing Technology,* vol. 185, pp. 72-76, 2007.

[146] H. Barish, "Quality drills contribute to successful titanium tooling," *Journals of Cutting Tool Engineering,* vol. 40, pp. 38-39, 1988.
[147] E. Aust and H. Niemann, "Machining of γ-TiAl," *Advanced Engineering Materials,* vol. 1, pp. 53-57, 1999.
[148] L. Zhu and J. Wang, "A Study on Titanium Alloys Deep-hole Drilling Technique," *Material Science Forum,* vol. 532-533, pp. 945-948, 2006.
[149] R. Komanduri and W. R. Reed, "Evaluation of carbide grades and a new cutting geometry for machining titanium alloys," *Wear,* vol. 92, pp. R. Komanduri, W.R. Reed, Wear 92 (1983) 113-123., 1983.
[150] P. A. Dearnley, *et al.*, "Wear Mechanisms of Cemented Carbides and Ceramics Used for Machining Titanium Alloys," *High-Tech Ceramics,* vol. 38, pp. 2699-2712, 1987.
[151] P. D. Hartung, *et al.*, "Tool Wear in Titanium Machining," *CIRP Annals - Manufacturing Technology,* vol. 31, pp. 75-80, 1982.
[152] D. Eylon, *et al.*, "High-Temperature Titanium Alloys - a Review," *J. Met,* vol. 36, pp. 55-62, 1984.
[153] K. Kertesz, *et al.*, "Machining Titanium Alloys with Ceramic Tools," *Journal of Materials,* vol. 40, pp. 50-51, 1988.
[154] R. Li and A. J. Shih, "Spiral point drill temperature and stress in high-throughput drilling of titanium," *International Journal of Machine Tools & Manufacture,* vol. 47, pp. 2005-2017, 2007.
[155] D. Umbrello, "Finite element simulation of conventional and high speed machining of Ti6Al4V alloy," *Journal of Materials Processing Technology,* vol. 196, pp. 79-87, 2008.
[156] M. Calamaz, *et al.*, "A new material model for 2D numerical simulation of serrated chip formation when machining titanium alloy Ti-6Al-4V," *International Journal of Machine Tools and Manufacture,* vol. 48, pp. 275–288, 2008.
[157] M. Sima and T. Ozel, "Modified material constitutive models for serrated chip formation simulations and experimental validation in machining of titanium alloy Ti-6Al-4V," *International Journal of Machine Tools and Manufacture,* vol. 50, pp. 943–960, 2010.
[158] E. Brinksmeier and R. Janssen, "Drilling of Multi-Layer Composite Materials consisting of Carbon Fiber Reinforced Plastics (CFRP), Titanium and Aluminum Alloys," *CIRP Annals - Manufacturing Technology,* vol. 51, pp. 87-90, 2002.
[159] R. Zitoune, *et al.*, "Study of drilling of composite material and aluminium stack," *Composite Structures,* vol. 92, pp. 1246-1255, 2010.
[160] I. S. Shyha, *et al.*, "Hole quality assessment following drilling of metallic-composite stacks " *International Journal of Machine Tools & Manufacture,* vol. 51, pp. 569–578, 2011.

[161] K. H. Park, *et al.*, "Tool wear in drilling of composite/titanium stacks using carbide and polycrystalline diamond tools," *Wear,* vol. 271, pp. 2826–2835, 2011.

[162] Hexcel. (2009, 10/01/2009). *Hexcel Product Datasheet*. Available: http://www.hexcel.com/NR/rdonlyres/A4AE89BC-0EA6-473A-A3CA-F2F98C13D033/0/HexPly_M21_eu.pdf

[163] F.-X. Irisarri, *et al.*, "Multiobjective stacking sequence optimization for laminated composite structures," *Composites Science and Technology,* vol. 69, pp. 983-990, 2009.

[164] L. Aihua, *et al.*, "Friction and wear properties of TiN, TiAlN, AlTiN and CrAlN PVD nitride coatings," *International Journal of Refractory Metals and Hard Materials,* vol. 31, pp. 82-88, 2012.

[165] J. H. Hsieh, *et al.*, "Deposition and characterization of TiAlN and multi-layered TiN/TiAlN coatings using unbalanced magnetron sputtering," *Surface and Coatings Technology,* vol. 108–109, pp. 132-137, 1998.

[166] H. C. Barshilia, *et al.*, "Structure, hardness and thermal stability of TiAlN and nanolayered TiAlN/CrN multilayer films," *Vacuum,* vol. 77, pp. 169-179, 2005.

[167] C. Edoardo, "Workpiece damping and its effect on delamination damage in drilling thin composite laminates," *Journal of Materials Processing Technology,* vol. 148, pp. 186-195, 2004.

[168] G. Dini, "On-Line Prediction of Delamination in Drilling of GFRP by Using a Neural Network Approach," *Machining Science and Technology,* vol. 7, pp. 295-314, 2003/01/11 2003.

[169] P. L. B. Oxley, *Mechanics of Machining: An Analytical Approach to Assessing Machinability*. Chichester: Ellis Horwood Limited, 1989.

[170] K. Maekawa, *et al.*, "Flow Stress of Low Carbon Steel at High Temperature and Strain Rate (Part 2) - Flow Stress under Variable Temperature and Variable Strain Rate," *Bulletin of the Japan Society of Precision Engineering,* vol. 17, pp. 167-172, 1983.

[171] G. R. Johnson and W. H. Cook, "A Constitutive Model and Data for Metals Subjected to Large Strains, High Strain Rates and High Temperatures," in *Proceedings of the 7th International Symposium on Ballistics*, The Hague, The Netherlands, 1983, pp. 541-547.

[172] F. J. Zerilli and R. W. Armstrong, "Dislocation Mechanics Based Constitutive Relations for Material Dynamics Calculations," *Journal of Applied Physics,* vol. 61, pp. 1816-1825, 1987.

[173] S. W. Tsai, "Strength theories of filamentary structures. ," in *Fundamental Aspects of Fiber Reinforced Plastic Composites*, R. Schwartz, T. and H. Schwartz, S., Eds., ed New York: Wiley Interscience, 1968, pp. 3-11.

[174] R. Hill, *The mathematical theory of plasticity*. London: Oxford University Press, 1950.

[175] S. W. Tsai and V. D. Azzi, "Strength of Laminated Composite Materials," *American Institute of Aeronautics and Astronautics Journal,* vol. 4, pp. 296–301, 1966.
[176] O. Hoffman, "The Brittle Strength of Orthotropic Materials," *Journal of Composite Materials,* vol. 1, pp. 200-206, January 1, 1967 1967.
[177] S. W. Tsai and E. M. Wu, "A General Theory of Strength for Anisotropic Materials," *Journal of Composite Materials,* vol. 5, pp. 58-80, January 1, 1971 1971.
[178] Z. Hashin and A. Rotem, "Fatigue failure criterion for fiber reinforced materials," *Journal of Composite Materials,* vol. 7, pp. 448-464, 1973.
[179] Z. Hashin, "Failure criteria for unidirectional fiber composites," *Journal of Applied Mechanics,* vol. 47, pp. 329-334, 1980.
[180] P. D. Soden, Kaddour, A.S., Hinton, M.J., *Failure Criteria in Fibre-Reinforced-Polymer Composites*: Elsevier, 2004.
[181] Z. Zou, *et al.*, "Mode separation of energy release rate for delamination in composite laminates using sublaminates," *International Journal of Solids and Structures,* vol. 28, pp. 2597-2613, 2001.
[182] R. Krueger, "The virtual crack closure technique: history, approach and applications," vol. R. Krueger, The virtual crack closure technique: history, approach and applications, NASA/CR-2002-211628 (2002). NASA, Ed., ed, 2002.
[183] J. R. Rice, "A path independent integral and the approximate analysis of strain concentration by notches and cracks," *Journal of Applied Mechanics,* vol. 35, pp. 379-386, 1968.
[184] T. K. Hellen, "On the method of the virtual crack extension," *International Journal for Numerical Methods in Engineering,* vol. 9, pp. 187-207, 1975.
[185] D. M. Parks, "A stiffness derivative finite element technique for determination of crack tip stress intensity factors," *International Journal of Fracture,* vol. 10, pp. 487-502, 1974.
[186] S. Liu, "Quasi-impact damage initiation and growth of thick-section and toughened composite material," *International Journal of Solids and Structures*, vol. 31, pp. 3079-3098, 1999.
[187] Z. Zou, *et al.*, "Modelling interlaminar and intralaminar damage in filament wound pipes under quasi-static indentation," *Journal of Composite Materials,* vol. 36, pp. 477-499, 2002.
[188] W. Cui and M. Wisnom, "A combined stress-based and fracture-mechanics-based model for predicting delamination in composites," *Composites,* vol. 24, pp. 467-474, 1993.
[189] J. Schellekens and R. d. Borst, "A nonlinear finite-element approach for the analysis of mode-I free edge delamination in composites," *International Journal of Solids and Structures,* vol. 30, pp. 1239-1253, 1993.

[190] X. Xu and A. Needleman, "Numerical simulations of fast crack growth in brittle solids," *Journal of Mechanics and Physics of Solids,* vol. 42, pp. 1397-1434, 1994.

[191] O. Allix, *et al.*, "Damage analysis of interlaminar fracture specimens," *Composite Structures,* vol. 31, pp. 66-74, 1995.

[192] O. Allix and A. Corigliano, "Modelling and simulation of crack propagation in mixed-mode interlaminar fracture specimens," *International Journal of Fracture,* vol. 77, pp. 111-140, 1996.

[193] G. T. Camacho and M. Ortiz, "Computational modelling of impact damage in brittle materials," *International Journal of Solids and Structures,* vol. 33, pp. 2899-2938, 1996.

[194] J. L. Chaboche, *et al.*, "Numerical analysis of composite systems by using interphase/interface models," *Composite Mechanics,* vol. 20, pp. 3-11, 1997.

[195] U. Mi, *et al.*, "Progressive delamination using interface elements," *Journal of Composite Materials,* vol. 32, pp. 1246-1272, 1998.

[196] J. Chen, *et al.*, "Predicting progressive delamination of composite material specimens via interface elements," *Mechanics of Composite Materials and Structures,* vol. 6, pp. 301-317, 1999.

[197] G. Alfano and M. Crisfield, "Finite element interface models for the delamination analysis of laminated composites: mechanical and computational issues," *International Journal for Numerical Methods in Engineering,* vol. 77, pp. 111-170, 2001.

[198] P. P. Camanho, Davila, C.G., "Mixed-Mode Decohesion Finite Elements for the Simulation of Delamination in Composite Materials, ," NASA, Ed., ed, 2002, pp. 1-37.

[199] P. P. Camanho, *et al.*, "Numerical simulation of mixed-mode progressive delamination in composite materials," *Journal of Composite Materials,* vol. 37, pp. 1415-1438, 2003.

[200] J. Segurado and J. Llorca, "A new three-dimensional interface finite element to simulate fracture in composites," *International Journal of Solids and Structures,* vol. 41, pp. 2977-2993, 2004.

[201] A. Turon, *et al.*, "A damage model for the simulation of delamination in advanced composites under variable-mode loading," *Mechanics of Materials,* vol. 38, pp. 1072-1089, 2006.

[202] P. Prombut, *et al.*, "Delamination of multidirectional composite laminates at 0_/ θ°_ ply interfaces," *Engineering Fracture Mechanics,* vol. 73, pp. 2427–2442, 2006.

[203] J. C. Simo, *et al.*, "An analysis of strong discontinuities induced by strain-softening in rate-independent inelastic solids," *Computational Mechanics,* vol. 12, pp. 277-296, 1993.

[204] J. C. Simo and J. Oliver, "A new approach to the analysis and simulation of strong discontinuities," in *Proceedings of the US-Europe Workshop on*

Fracture and Damage in Quasibrittle Structures, Prague, Czech Republic, 1994, pp. 25-39.

[205] J. Oliver, "Continuum modelling of strong discontinuities in solid mechanics using damage models," *Computational Mechanics,* vol. 17, pp. 49-61, 1995.

[206] F. Armero and K. Garikipati, "An analysis of strong discontinuities in multiplicative finite strain plasticity and their relation with the numerical simulation of strain localization in solids," *International Journal of Solids and Structures,* vol. 33, pp. 2863-2885, 1996.

[207] T. Belytschko and T. Black, "Elastic crack growth in finite elements with minimal remeshing," *International Journal for Numerical Methods in Engineering,* vol. 45, pp. 601-620, 1999.

[208] N. Maoes, *et al.*, "A finite element method for crack growth without remeshing," *International Journal for Numerical Methods in Engineering,* vol. 46, pp. 131-150, 1999.

[209] N. Moes and T. Belytschko, "Extended finite element method for cohesive crack growth," *Engineering Fracture Mechanics,* vol. 69, pp. 813-833, 2002.

[210] G. Alfano and M. A. Crisfield, "Finite element interface models for the delamination analysis of laminated composites," *International Journal of Numerical Methods in Engineering,* vol. 50, pp. 1701–1736., 2001.

[211] L. Ye, "Role of Matrix Resin in Delamination Onset and Growth in Composite Laminates," *Composites Science and Technology,* vol. 33, pp. 257-277, 1988.

[212] J. Bertolini, *et al.*, "Multi-level experimental and numerical analysis of composite stiffener debonding. Part 1: Non-specific specimen level," *Composite Structures,* vol. 90, pp. 381-391, 2009.

[213] D. R. Lesuer, "Experimental investigations of material models for Ti–6Al–4V Titanium and 2024-T3 Aluminium," O. o. A. Research, Ed., ed. Washington, 2000.

[214] J. D. Gardner and D. Dornfeld, "Finite Element Modeling of Drilling Using DEFORM," ed, 2006.

[215] J. P. Davim, *et al.*, "Experimental study of drilling glass fiber reinforced plastics (GFRP) manufactured by hand lay-up," *Composites Science and Technology,* vol. 64, pp. 289-297, 2004.

[216] I. Singh, *et al.*, "Drilling of uni-directional glass fiber reinforced plastics: Experimental and finite element study," *Materials & Design,* vol. 29, pp. 546-553, 2008.

[217] D. Kim and M. Ramulu, "Cutting and drilling characteristics of hybrid Titanium Composite Laminate (HTCL)," in *International SAMPE Technical Conference*, 2005.

[218] M. Arai and M. Ogawa, "Effects of high pressure supply of coolant in drilling of titanium alloy," *Keikinzoku/Journal of Japan Institute of Light Metals,* vol. 47, pp. 139-144, 1997.

Appendix A

User Defined Subroutine for CFRP

The user defined subroutine is developed to model the material behaviour of unidirectional fibre reinforced composites under multi-axis stress for use in Abaqus/Explicit. Unidirectional fibre reinforced composites are modelled with linear elastic material with orthotropic behaviour prior to failure. The initiation of failure is modelled with Hashin's failure criteria for unidirectional fibre composites in any mode as expressed in detail in Chapter 4. The model can be implemented as a VUMAT user subroutine and can be used with three-dimensional stress-displacement continuum elements.

Note: The subroutine is developed for Abaqus/Explicit version 6.9. It requires Intel Fortran Compiler version 9.1.

```
subroutine vumat(
1  nblock, ndir, nshr, nstatev, nfieldv, nprops, lanneal,
2  stepTime, totalTime, dt, cmname, coordMp, charLength,
3  props, density, strainInc, relSpinInc,
4  tempOld, stretchOld, defgradOld, fieldOld,
5  stressOld, stateOld, enerInternOld, enerInelasOld,
6  tempNew, stretchNew, defgradNew, fieldNew,
7  stressNew, stateNew, enerInternNew, enerInelasNew )
include 'vaba_param.inc'
dimension props(nprops), density(nblock),
1  coordMp(nblock,*),
2  charLength(*), strainInc(nblock,ndir+nshr),
3  relSpinInc(nblock,nshr), tempOld(nblock),
4  stretchOld(nblock,ndir+nshr), defgradOld(nblock,ndir+nshr+nshr),
5  fieldOld(nblock,nfieldv), stressOld(nblock,ndir+nshr),
6  stateOld(nblock,nstatev), enerInternOld(nblock),
7  enerInelasOld(nblock), tempNew(*),
8  stretchNew(nblock,ndir+nshr), defgradNew(nblock,ndir+nshr+nshr),
9  fieldNew(nblock,nfieldv), stressNew(nblock,ndir+nshr),
1  stateNew(nblock,nstatev),
2  enerInternNew(nblock), enerInelasNew(nblock)
character*80 cmname
dimension eigen(maxblk*3)
E1 = props(i_pro_E1)
E2 = props(i_pro_E2)
E3 = props(i_pro_E3)
xnu12 = props(i_pro_nu12)
xnu13 = props(i_pro_nu13)
xnu23 = props(i_pro_nu23)
G12 = props(i_pro_G12)
G13 = props(i_pro_G13)
G23 = props(i_pro_G23)
xnu21 = xnu12 * E2 / E1
xnu31 = xnu13 * E3 / E1
xnu32 = xnu23 * E3 / E2
gg = one / ( one - xnu12*xnu21 - xnu23*xnu32 - xnu31*xnu13 -
two*xnu21*xnu32*xnu13 )
C11  = E1 * ( one - xnu23*xnu32 ) * gg
C22  = E2 * ( one - xnu13*xnu31 ) * gg
C33  = E3 * ( one - xnu12*xnu21 ) * gg
C12  = E1 * ( xnu21 + xnu31*xnu23 ) * gg
C13  = E1 * ( xnu31 + xnu21*xnu32 ) * gg
C23  = E2 * ( xnu32 + xnu12*xnu31 ) * gg
f1t = props(i_pro_sigu1t)
f1c = props(i_pro_sigu1c)
f2t = props(i_pro_sigu2t)
f2c = props(i_pro_sigu2c)
f3t = props(i_pro_sigu3t)
f3c = props(i_pro_sigu3c)
f12 = props(i_pro_sigu12)
f13 = props(i_pro_sigu13)
f23 = props(i_pro_sigu23)
beta = props(i_pro_beta)
alfa = props(i_pro_alfa)
end if
call OrthoEla3dExp (
nblock,stateOld(1,i_svd_DmgFiberT),stateOld(1,i_svd_DmgFiberC),stateOl
d(1,i_svd_DmgMatrixT),stateOld(1,i_svd_DmgMatrixC),C11, C22, C33, C12,
C23, C13, G12, G23, G13,strainInc,stressNew )
return
```

```
end if
call strainUpdate ( nblock, strainInc,stateOld(1,i_svd_strain),
stateNew(1,i_svd_strain) )
call OrthoEla3dExp (
nblock,stateOld(1,i_svd_D_FiberT),stateOld(1,i_svd_D_FiberC),stateOld(
1,i_svd_D_MatrixT),stateOld(1,i_svd_D_MatrixC),C11, C22, C33, C12,
C23, C13, G12, G23, G13,stateNew(1,i_svd_strain),stressNew )
call copyr ( nblock, stateOld(1,i_svd_DmgFiberT),
stateNew(1,i_svd_DmgFiberT) )
call copyr ( nblock, stateOld(1,i_svd_DmgFiberC),
stateNew(1,i_svd_DmgFiberC) )
call copyr ( nblock, stateOld(1,i_svd_DmgMatrixT),
stateNew(1,i_svd_DmgMatrixT) )
call copyr ( nblock, stateOld(1,i_svd_DmgMatrixC),
stateNew(1,i_svd_DmgMatrixC) )
call copyr ( nblock, stateOld(1,i_svd_D_FiberT),
stateNew(1,i_svd_D_FiberT) )
call copyr ( nblock, stateOld(1,i_svd_D_FiberC),
stateNew(1,i_svd_D_FiberC) )
call copyr ( nblock, stateOld(1,i_svd_D_MatrixT),
stateNew(1,i_svd_D_MatrixT) )
call copyr ( nblock, stateOld(1,i_svd_D_MatrixC),
stateNew(1,i_svd_D_MatrixC) )
call Hashin3d  ( nblock, nDmg, f1t, f2t, f3t, f1c, f2c, f3c, f12, f23,
f13,stateNew(1,i_svd_DmgFiberT),stateNew(1,i_svd_DmgFiberC),stateNew(1
,i_svd_DmgMatrixT),stateNew(1,i_svd_DmgMatrixC),stateNew(1,i_svd_D_Fib
erT),stateNew(1,i_svd_D_FiberC),stateNew(1,i_svd_D_MatrixT),stateNew(1
,i_svd_D_MatrixC),stateNew(1,i_svd_statusMp), stressNew, alfa )
if ( nDmg .gt. 0 ) then
call OrthoEla3dExp (
nblock,stateNew(1,i_svd_D_FiberT),stateNew(1,i_svd_D_FiberC),stateNew(
1,i_svd_D_MatrixT),stateNew(1,i_svd_D_MatrixC),C11, C22, C33, C12,
C23, C13, G12, G23, G13,stateNew(1,i_svd_strain),stressNew )
end if
call EnergyInternal3d ( nblock, stressOld, stressNew,strainInc,
density, enerInternOld, enerInternNew )
return
end
subroutine OrthoEla3dExp ( nblock,d_FiberT, d_FiberC, d_MatrixT,
d_MatrixC,C11, C22, C33, C12, C23, C13, G12, G23, G13,strain, stress )
include 'vaba_param.inc'
dimension  strain(nblock,n_s33_Car), d_FiberT(nblock),
d_FiberC(nblock), d_MatrixT(nblock),
d_MatrixC(nblock),stress(nblock,n_s33_Car)
do k = 1, nblock
dft = d_FiberT(k)
dfc = d_FiberC(k)
dmt = d_MatrixT(k)
dmc = d_MatrixC(k)
df = one - ( one - dft ) * ( one - dfc )
dC11 = ( one - df ) * C11
dC22 = ( one - df ) * ( one - dmt ) * ( one - dmc ) * C22
dC33 = ( one - df ) * ( one - dmt ) * ( one - dmc ) * C33
dC12 = ( one - df ) * ( one - dmt ) * ( one - dmc ) * C12
dC23 = ( one - df ) * ( one - dmt ) * ( one - dmc ) * C23
dC13 = ( one - df ) * ( one - dmt ) * ( one - dmc ) * C13
dG12 = ( one - df ) * ( one - smt*dmt ) * ( one - smc*dmc ) * G12
dG23 = ( one - df ) * ( one - smt*dmt ) * ( one - smc*dmc ) * G23
dG13 = ( one - df ) * ( one - smt*dmt ) * ( one - smc*dmc ) * G13
```

```
stress(k,i_s33_Xx) = dC11 * strain(k,i_s33_Xx)+ dC12 *
strain(k,i_s33_Yy)+ dC13 * strain(k,i_s33_Zz)
stress(k,i_s33_Yy) = dC12 * strain(k,i_s33_Xx)+ dC22 *
strain(k,i_s33_Yy)+ dC23 * strain(k,i_s33_Zz)
stress(k,i_s33_Zz) = dC13 * strain(k,i_s33_Xx)+ dC23 *
strain(k,i_s33_Yy)+ dC33 * strain(k,i_s33_Zz)
stress(k,i_s33_Xy) = two * dG12 * strain(k,i_s33_Xy)
stress(k,i_s33_Yz) = two * dG23 * strain(k,i_s33_Yz)
stress(k,i_s33_Zx) = two * dG13 * strain(k,i_s33_Zx)
end do
return
end
subroutine strainUpdate ( nblock, strainInc, strainOld, strainNew )
include 'vaba_param.inc'
parameter(
dimension strainInc(nblock,n_s33_Car),
strainOld(nblock,n_s33_Car),strainNew(nblock,n_s33_Car)
do k = 1, nblock
strainNew(k,i_s33_Xx)= strainOld(k,i_s33_Xx) + strainInc(k,i_s33_Xx)
strainNew(k,i_s33_Yy)= strainOld(k,i_s33_Yy)+ strainInc(k,i_s33_Yy)
strainNew(k,i_s33_Zz)= strainOld(k,i_s33_Zz)+ strainInc(k,i_s33_Zz)
strainNew(k,i_s33_Xy)= strainOld(k,i_s33_Xy)+ strainInc(k,i_s33_Xy)
strainNew(k,i_s33_Yz)= strainOld(k,i_s33_Yz)+ strainInc(k,i_s33_Yz)
strainNew(k,i_s33_Zx)= strainOld(k,i_s33_Zx)+ strainInc(k,i_s33_Zx)
end do
return
end
subroutine Hashin3d ( nblock, nDmg,f1t, f2t, f3t, f1c, f2c, f3c, f12,
f23, f13,dmgFiberT, dmgFiberC, dmgMatrixT, dmgMatrixC,d_FiberT,
d_FiberC, d_MatrixT, d_MatrixC,statusMp, stress, alfa )
include 'vaba_param.inc'
dimension  dmgFiberT(nblock), dmgFiberC(nblock), dmgMatrixT(nblock),
dmgMatrixC(nblock),d_FiberT(nblock),
d_FiberC(nblock),d_MatrixT(nblock),
d_MatrixC(nblock),stress(nblock,n_s33_Car),eigen(nblock,n_v3d_Car),sta
tusMp(nblock)
if ( f1t .gt. zero ) f1tInv = one / f1t
if( f2t .gt. zero ) f2tInv = one / f2t
if ( f3t .gt. zero ) f3tInv = one / f3t
if ( f1c .gt. zero ) f1cInv = one / f1c
if ( f2c .gt. zero ) f2cInv = one / f2c
if ( f3c .gt. zero ) f3cInv = one / f3c
if ( f12 .gt. zero ) f12Inv = one / f12
if ( f23 .gt. zero ) f23Inv = one / f23
if ( f13 .gt. zero ) f13Inv = one / f13
do k = 1, nblock
if ( statusMp(k) .eq. one ) then
s11 = stress(k,i_s33_Xx)
s22 = stress(k,i_s33_Yy)
s33 = stress(k,i_s33_Zz)
s12 = stress(k,i_s33_Xy)
s23 = stress(k,i_s33_Yz)
s13 = stress(k,i_s33_Zx)
if ( s11 .gt. zero ) then
dmgFiberT(k) = (s11*f1tInv )**2 + alfa*((s12*f12Inv )**2) +
alfa*((s13*f13Inv )**2 )
if ( dmgFiberT(k) .ge. one ) then
d_FiberT(k) = one
else
d_FiberT(k) = zero
```

```
end if
else if ( s11 .lt. zero ) then
dmgFiberC(k) = abs(s11) * f1cInv
if ( dmgFiberC(k) .ge. one ) then
d_FiberC(k) = one
else
d_FiberC(k) = zero
end if
end if
if ( ( s22 + s33 ) .gt. zero ) then
dmgMatrixT(k) = ((s22+s33)**2)*(f2tInv**2) + ((s23**2)-
(s22*s33))*(f23Inv**2) + ((s12**2)+(s13**2))*(f12Inv**2)
if ( dmgMatrixT(k) .ge. one ) then
d_MatrixT(k) = one
else
d_MatrixT(k) = zero
end if
else if ( ( s22 + s33 ) .lt. zero ) then
dmgMatrixC(k) = (((f2c*f23Inv*half)**2)-one)*(f2cInv)*abs(s22+s33) +
((f23Inv*half)**2)*((s22 + s33)**2) + (f23Inv**2)*((s23**2) -
(s22*s33)) + (f12Inv**2)*((s12**2) + (s13**2))
if ( dmgMatrixC(k) .ge. one ) then
d_MatrixC(k) = one
else
d_MatrixC(k) = zero
end if
end if
if ( d_FiberT(k) .eq. one .or. d_FiberC(k) .eq. one ) then
statusMp(k) = zero
end if
end if
end do
return
end
subroutine EnergyInternal3d(nblock, sigOld, sigNew ,strainInc,
curDensity, enerInternOld, enerInternNew)
include 'vaba_param.inc'
dimension sigOld (nblock,n_s33_Car), sigNew
(nblock,n_s33_Car),strainInc (nblock,n_s33_Car), curDensity
(nblock),enerInternOld(nblock), enerInternNew(nblock)
do k = 1, nblock
stressPower  = half * ( ( sigOld(k,i_s33_Xx) + sigNew(k,i_s33_Xx) ) *
( strainInc(k,i_s33_Xx) ) + ( sigOld(k,i_s33_Yy) + sigNew(k,i_s33_Yy)
) * ( strainInc(k,i_s33_Yy)) +       ( sigOld(k,i_s33_Zz) +
sigNew(k,i_s33_Zz) ) * ( strainInc(k,i_s33_Zz)) + two * (
sigOld(k,i_s33_Xy) + sigNew(k,i_s33_Xy) ) * strainInc(k,i_s33_Xy) +
two * ( sigOld(k,i_s33_Yz) + sigNew(k,i_s33_Yz) ) *
strainInc(k,i_s33_Yz) + two * ( sigOld(k,i_s33_Zx) +
sigNew(k,i_s33_Zx) ) * strainInc(k,i_s33_Zx) )
enerInternNew(k) = enerInternOld(k) + stressPower/curDensity(k)
end do
return
end
subroutine CopyR(nCopy, old, new )
include 'vaba_param.inc'
dimension old(nCopy), new(nCopy)
do k = 1, nCopy
new(k) = old(k)
end do
return
```

```
end
```

Appendix B

Delamination Algorithm

The user defined delamination algorithm is developed to define delamination factor based on diameter and arbitrary delaminated area around the drilled holes in unidirectional fibre reinforced composite workpiece for use in Matlab software. The images of drilling induced damage around hole are used as input to the developed codes. The images are treated for digital image processing. Thresholding and noise suppression are applied to the images. After the application of edge detection module, the images are divided into areas to obtain quantitative data on the image. Finally, the maximum diameter and damaged area are obtained and delamination factors are calculated as explained in Chapter 3.

Note: The user defined delamination algorithm is developed for Matlab version R12.

Delamination.m

```
clear;
for sample=1:n
Sample_Name = sprintf('%d',sample);
Ornek_uzantisi= sprintf('bmp');
Resim_adi = strcat(Sample_Name, '.', Ornek_uzantisi);
Raw_Image = strcat(Sample_Name, '\', Sample_Name, '_RAW', '.', 'bmp');
a=imread(Resim_adi);
I=rgb2gray(a);
satir=0;
for th=1:20
   thresh = th/20;
thr = sprintf('%g', thresh);
bw=im2bw(I,thresh);
mkdir(Sample_Name);
imwrite(a, Raw_Image, 'bmp');
mkdir(Sample_Name,'Threshold');
Threshed_Image = strcat(Sample_Name, '\Threshold\', Sample_Name, '_th_',
thr, '.', 'bmp');
imwrite(bw, Threshed_Image, 'bmp');
for x = 1:5
   for y = 1:4
AO = x*50;
ST = y;
ao = sprintf('%d', AO);
st = sprintf('%d', ST);
bw1=bwareaopen(bw,AO);
se=strel('disk', ST);
BW=imclose(bw1,se);
[B,L,N,A] = bwboundaries(BW,'holes');
imageL=label2rgb(L, 'gray', [1 1 1]);
mkdir(Sample_Name,'NR')
NR_Image = strcat(Sample_Name, '\NR\',  Sample_Name, '_th_', thr, '_AO_',
ao, '_ST_', st, '.', 'bmp');
f1 = figure('visible','off'), imshow(imageL, 'Border', 'tight');
print(f1, '-r96', '-dbmp', NR_Image);
title('DELAMINATION ANALYSIS','FontWeight','bold')
f2 = figure('visible','off'), imshow(imageL, 'Border', 'tight');
```

```
s = regionprops(L, I, 'Eccentricity', 'EquivDiameter', 'Perimeter', 'Area',
'Centroid', 'WeightedCentroid');
title1 = {'Image Number', 'Coef. Threshold', 'Coef. bwareaopen', 'coef. strel',
'method strel', 'Object Number', 'Area', 'Perimeter', 'Eccentricity', 'Equivalent
Diameter', 'Max Delamination', 'Real Hole Area', 'Real Hole Radius', 'Area Calbr
Coef', 'Radius Calbr Coef', 'Delamination Area', 'Max Delamination Radius',
'Delamination Coef (by area)','Delamination Coef(by radius)'};
Results_Location= strcat(Sample_Name, '\', 'Delamination_', Sample_Name,
'.xls');
sheet = sprintf('Results');
xlswrite(Results_Location,title1,sheet)
hold on
for k = 1:length(B)
  boundary = B[192];
  [d,e]=size(boundary);
  plot(boundary(:,2), boundary(:,1), 'r', 'LineWidth', 2);
  maxpoint=0;
  pointX=0;
  pointY=0;
  for i=1:d
     contour_row=sprintf('E%d', i);
     if(i==1)
     m=boundary(i:i,2)*boundary(i:i,2)-s(k).Centroid(2)*s(k).Centroid(2);
     n=boundary(i:i,1)*boundary(i:i,1)-s(k).Centroid(1)*s(k).Centroid(1);
     p=sqrt(abs(m)+abs(n));
     if (p > maxpoint)
        maxpoint = p;
        pointX = boundary(i:i,2);
        pointY = boundary(i:i,1);
     end
     end
  end
Name = strcat(Sample_Name, '_th_', thr, '_ao_', ao, '_st_', st, '.', 'bmp');
obje = sprintf('%d',k);
text(boundary(1,2)-10, boundary(1,1)-10, obje, 'Color', 'g',
'FontSize',14,'FontWeight','bold');
plot(pointX, pointY, 'g+', 'MarkerSize',100);
plot(s(k).WeightedCentroid(1), s(k).WeightedCentroid(2), 'g+', 'MarkerSize',30);
plot(s(k).Centroid(1), s(k).Centroid(2), 'r+','MarkerSize',30);
data = {Name thresh AO ST 'disk' k s(k).Area s(k).Perimeter s(k).Eccentricity
s(k).EquivDiameter maxpoint};
satir = satir+1;
```

```
cell = sprintf('A%d', satir+1);
xlswrite(Results_Location, data, sheet, cell)
end
mkdir(Sample_Name,'Analysis\Points')
Analysed_Image = strcat(Sample_Name, '\Analysis\Points\', Sample_Name,
'_th_', thr, '_ao_', ao, '_st_', st, '.', 'bmp');
print(f2, '-r96', '-dbmp', Analysed_Image);
%
for kk = 1:length(B)
  boundary1 = B{kk};
  [dd,ee]=size(boundary1);
  maxpoint1=0;
  pointXX=0;
  pointYY=0;
  for ii=1:dd
    if(ii==1)
    mm=boundary1(ii:ii,2)*boundary1(ii:ii,2)-
s(kk).Centroid(2)*s(kk).Centroid(2);
    nn=boundary1(ii:ii,1)*boundary1(ii:ii,1)-s(kk).Centroid(1)*s(kk).Centroid(1);
    pp=sqrt(abs(mm)+abs(nn));
    if (pp > maxpoint1)
      maxpoint1 = pp;
      pointXX = boundary1(ii:ii,2);
      pointYY = boundary1(ii:ii,1);
    end
    end

  end
plot([s(kk).Centroid(1), pointXX], [s(kk).Centroid(2), pointYY], 'LineWidth',5,
'MarkerEdgeColor','k', 'MarkerFaceColor','g', 'MarkerSize',30);
end
mkdir(Sample_Name,'Analysis\Radius')
Delamination = strcat(Sample_Name, '\Analysis\Radius\', Sample_Name,
'_DL_th_', thr, '_ao_', ao, '_st_', st, '.', 'bmp');
print(f2, '-r96', '-dbmp', Delamination);
hold off
end
end
end
end
```

Appendix C

Optimisation of Finite Element Analysis

Finite element analysis is highly dependent on the size of elements and significant differences can be observed in the response of material behaviour. In order to find an optimum element size, several simulations have been carried out. For this reason, 2 mm, 1mm, 0.5 mm and 0.26 mm element sizes used in the finite element analysis of drilling process. Due to the large stress gradients and potential damage at the boundary of the hole, the mesh was refined only in the hole vicinity with an aspect ratio of 1.0 in the latest model. The density of mesh was reduced outside of the hole vicinity in the workpieces to reduce solution time as the outside region was less critical in the analysis. A maximum aspect ratio of 4.0 was used away from the hole region. The meshed FE models of the workpieces are shown in Figure C-1.

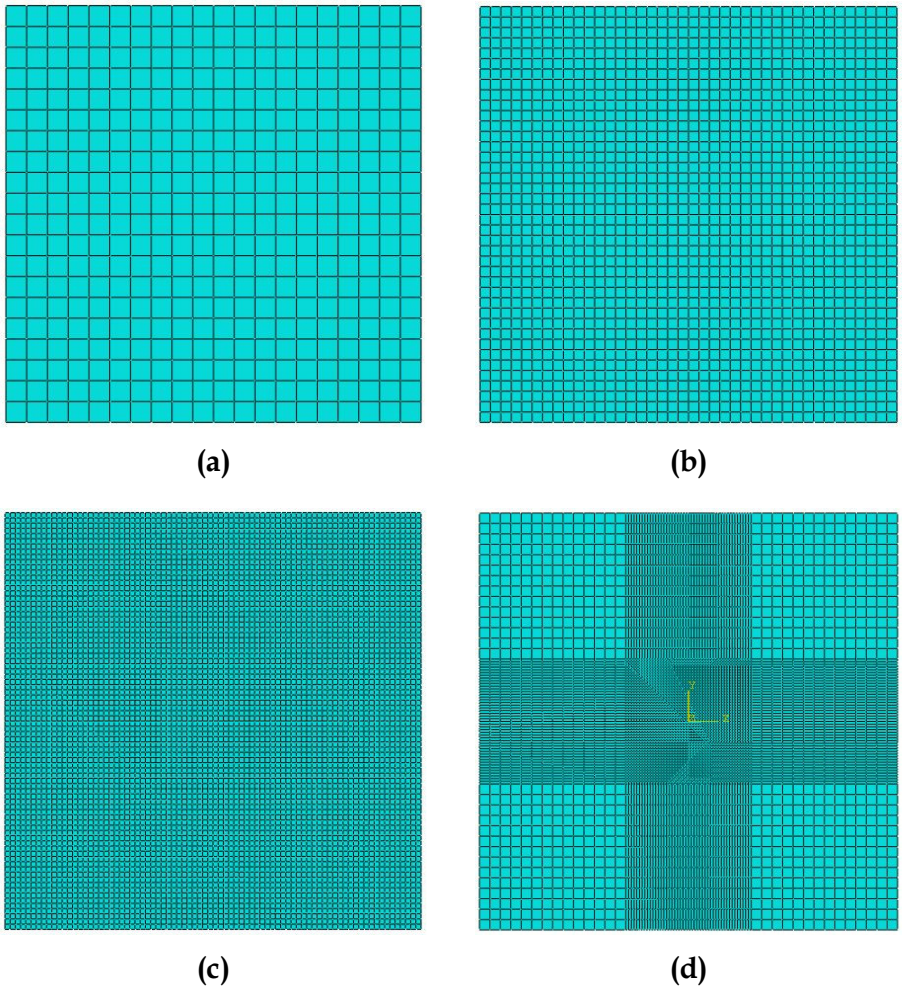

Figure C-1: Mesh Size of Workpieces (a) 2 mm (b) 1 mm (c) 0.5 mm (d) Graded (0.26 mm & 1 mm)

Figure C-2 plots the estimated thrust force versus element size in drilling of CFRP and Ti-6Al-4V separately. Drilling of CFRP was performed at 4500 rpm spindle speed and 457 mm/min feed rate, drilling of Ti-6Al-4V was simulated at 1400 rpm spindle speed and 119 mm/min feed rate with 8 mm twist drill. The best results were obtained from the simulation with 0.26 mm where the aspect ratio is 1 in the hole vicinity. As it can be seen from the figure, the performance of FE analysis is significantly dependant on the element size. Within the computational facilities, further mesh size improvements are not suggested due to the long computational time requirements.

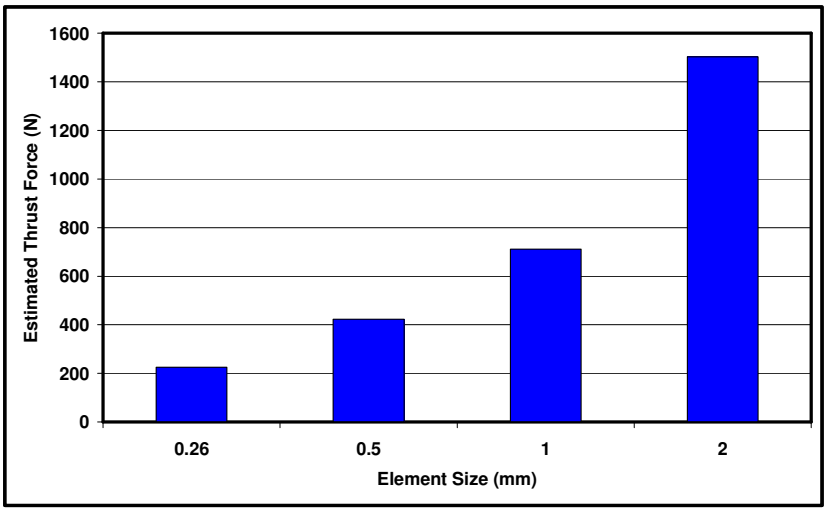

(a)

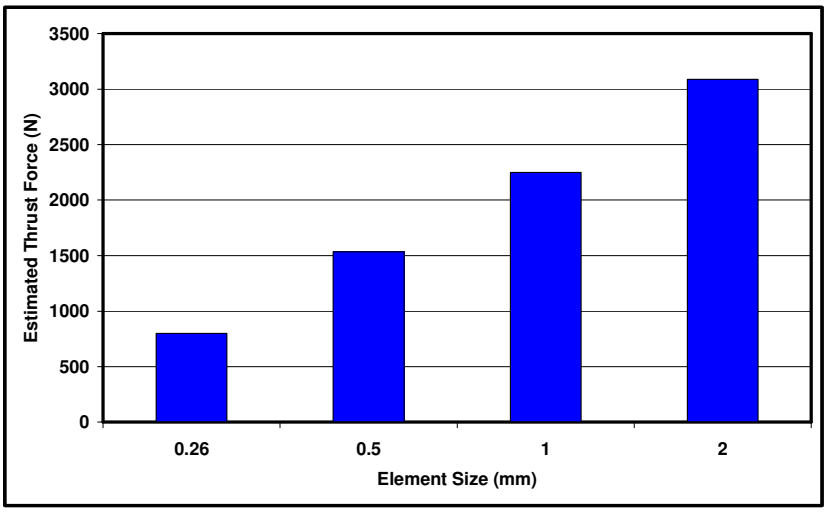

(b)

Figure C-2: Effect of Mesh size on Estimated Thrust Force (a) Drilling of CFRP (b) Drilling of Ti-6Al-4V